

Investigating early age thermal cracking of concrete

Author:

Ghareh Chaei, Maryam

Publication Date:

2019

DOI:

<https://doi.org/10.26190/unsworks/21534>

License:

<https://creativecommons.org/licenses/by-nc-nd/3.0/au/>

Link to license to see what you are allowed to do with this resource.

Downloaded from <http://hdl.handle.net/1959.4/64570> in <https://unsworks.unsw.edu.au> on 2024-05-05

Investigating Early Age Thermal Cracking of Concrete

Maryam Ghareh chaei

A thesis in fulfilment of the requirements for the degree of

Doctor of Philosophy



UNSW
A U S T R A L I A

School of Civil and Environmental Engineering

Faculty of Engineering

May 2019

ORIGINALITY STATEMENT

'I hereby declare that this submission is my own work and to the best of my knowledge it contains no materials previously published or written by another person, or substantial proportions of material which have been accepted for the award of any other degree or diploma at UNSW or any other educational institution, except where due acknowledgement is made in the thesis. Any contribution made to the research by others, with whom I have worked at UNSW or elsewhere, is explicitly acknowledged in the thesis. I also declare that the intellectual content of this thesis is the product of my own work, except to the extent that assistance from others in the project's design and conception or in style, presentation and linguistic expression is acknowledged.'

Signed

Date

COPYRIGHT STATEMENT

'I hereby grant the University of New South Wales or its agents the right to archive and to make available my thesis or dissertation in whole or part in the University libraries in all forms of media, now or here after known, subject to the provisions of the Copyright Act 1968. I retain all proprietary rights, such as patent rights. I also retain the right to use in future works (such as articles or books) all or part of this thesis or dissertation.

I also authorise University Microfilms to use the 350 word abstract of my thesis in Dissertation Abstract International (this is applicable to doctoral theses only).

I have either used no substantial portions of copyright material in my thesis or I have obtained permission to use copyright material; where permission has not been granted I have applied/will apply for a partial restriction of the digital copy of my thesis or dissertation.'

Signed

Date

AUTHENTICITY STATEMENT

'I certify that the Library deposit digital copy is a direct equivalent of the final officially approved version of my thesis. No emendation of content has occurred and if there are any minor variations in formatting, they are the result of the conversion to digital format.'

Signed

Date

INCLUSION OF PUBLICATIONS STATEMENT

UNSW is supportive of candidates publishing their research results during their candidature as detailed in the UNSW Thesis Examination Procedure.

Publications can be used in their thesis in lieu of a Chapter if:

- The student contributed greater than 50% of the content in the publication and is the “primary author”, ie. the student was responsible primarily for the planning, execution and preparation of the work for publication
- The student has approval to include the publication in their thesis in lieu of a Chapter from their supervisor and Postgraduate Coordinator.
- The publication is not subject to any obligations or contractual agreements with a third party that would constrain its inclusion in the thesis

Please indicate whether this thesis contains published material or not.

This thesis contains no publications, either published or submitted for publication

Some of the work described in this thesis has been published and it has been documented in the relevant Chapters with acknowledgement

This thesis has publications (either published or submitted for publication) incorporated into it in lieu of a chapter and the details are presented below

CANDIDATE'S DECLARATION

I declare that:

- I have complied with the Thesis Examination Procedure
- where I have used a publication in lieu of a Chapter, the listed publication(s) below meet(s) the requirements to be included in the thesis.

Name	Signature	Date (dd/mm/yy)
Maryam Ghareh chaei		14/05/2019

ABSTRACT

This thesis presents the results of a comprehensive study conducted to develop a practical tool to assist concrete specialists in i) evaluating the risk of early age thermal cracking of concrete for a particular concrete element, ii) identifying the optimal concrete mix design to reduce the risk of early age thermal cracking, iii) evaluating the effectiveness of construction strategies, including sequential placement and internal cooling using embedded pipes, in reducing the risk of early age thermal cracking. This thesis addresses the gaps in the available literature regarding early age thermal cracking including evaluating the accuracy of the available hydration models for Australian concrete, a lack of existence of a comprehensive numerical simulation for evaluating early age thermal cracking and mix design optimisation with the aim of minimizing the risk of early age thermal cracking. A comprehensive experimental study was conducted to address the first gap by evaluating the precision of existing hydration heat models through extensive calorimetry tests. To address the second gap, an advanced three-dimensional numerical simulation model was developed and verified by real-world site measurements using COMSOL Multiphysics. This model allows direct use of calorimetry data as well as existing hydration models as the heat source and is capable of modelling the effect of reinforcement, thermal and mechanical boundary conditions, etc. This model is also modified to numerically analyze common construction methodologies for reducing early age thermal cracking such as sequential concrete pouring and using of embedded cooling pipes in concrete. While the proposed numerical simulation model makes available a means of evaluating the effect of different mixes on early age thermal cracking, try and error to identify an optimal mix design which minimizes the risk of early age thermal cracking is highly time-

consuming. To address this issue, a genetic algorithm multi-objective mix design optimisation method was developed to mathematically identify the optimal mix design that minimizes the risk of early age thermal cracking in a particular element, while considering the practical constraints. The proposed optimisation algorithm was developed in MATLAB and was designed to include an embedded finite difference model to allow its use as a stand-alone tool.

PREFACE

This thesis is submitted in partial fulfillment of the requirements for the degree of Doctor of Philosophy at The University of New South Wales (UNSW), Sydney, Australia. The work described herein was performed by the candidate in the School of Civil and Environmental Engineering, UNSW. The candidate was supervised by Dr. Ali Akbarnezhad and Dr. Arnaud Castel during a period from August 2015 to May 2019. The thesis has been supported by papers that have been written, submitted for consideration, accepted or published in renowned journals and conferences. These papers are listed as follows.

- 1- Maryam Gharehchaei, Ali Akbarnezhad, Arnaud Castel, Redmond Lloyd, Louise Keyte, Stephen Foster, “Precision of cement hydration heat models in capturing the effects of SCMs and retarders”, Magazine of Concrete Research, Volume 70, Issue 23, December, 2018, pp. 1217-1231 (**Content of Chapter 3**)
- 2- Maryam Gharehchaei, Ali Akbarnezhad, Arnaud Castel, Farzad Moghaddam, and Stephen Foster, “A Genetic Algorithm Mix Optimisation Model to Minimize the Risk of Early Age Thermal Cracking of Concrete”, Submitted to Magazine of Concrete Research (**Content of Chapters 4 and 5**)
- 3- Maryam Gharehchaei, Ali Akbarnezhad, Masuzyo Chilwesa, Arnaud Castel, Redmond Lloyd and Stephen Foster, “A genetic algorithm method to identify the optimal concrete mix for the elements subject to risk of early age thermal cracking”, The International Federation for Structural Concrete 5th International fib Congress 2018, Melbourne, October 2018 (**Content of Chapter 4 and 5**)
- 4- Maryam Gharehchaei, Ali Akbarnezhad, Alireza Akbarzadeh Chiniforoush, Arnaud Castel, Louise Keyte, and Stephen Foster, “Numerical Simulation of Risk

Mitigation Methods for Early Age Thermal Cracking of Concrete” Accepted by the 29th Biennial National Conference of the Concrete Institute of Australia in Sydney, Australia, September 2019 (**Content of Chapter 4 and 6**)

- 5- Maryam Gharehchae, Ali Akbarnezhad, Arnaud Castel, Louise Keyte, and Stephen Foster, “Numerical Simulation of Practical Methods for Reducing the Risk of Early Age Thermal Cracking of Concrete, In Preparation for Journal Submission (**Content of Chapter 4 and 6**)

Acknowledgement

I would like to express my sincere gratitude to my supervisor Dr. Ali Akbarnezhad for all the patient guidance, inspiration, advice and comments he has provided throughout my study which made the completion of this work possible. I could not ask for a more supportive supervisor and I was extremely lucky to have a caring and kind supervisor like him. I also would like to acknowledge the University of New South Wales and BORAL Ltd. for providing my scholarship and the required funding for my research. My sincere thanks also go to Professor Stephen Foster and Dr. Arnaud Castel for their insightful comments and help during my study.

Finally, I would like to dedicate this thesis to the love of my life, Milad, who has been a constant source of unconditional love, support, encouragement and inspiration to me every single day no matter what; and to my beloved parents, Maria and Bagher, who have always loved me unconditionally, believed in me and supported me to achieve my goals in life and to my lovely siblings, Arezoo and Afshin, for always being there for me. I feel so blessed to have you all in my life.

Table of Contents

Investigating Early Age Thermal Cracking of Concrete	1
Chapter 1: Introduction	1
1.1 Background	1
1.2 Research Motivation and Objective	6
1.3 Research Methodology	8
1.4 Thesis Outline	10
Chapter 2: Literature Review	12
2.1 Introduction.....	12
2.2 Heat of Hydration Prediction Models	13
2.2.1 Concrete hydration and hydration products	13
2.2.2 Heat of hydration	16
2.2.3 Factors influencing the heat of hydration.....	16
2.2.4 Measuring heat of hydration	21
2.2.5 Heat of hydration prediction models.....	23
2.2.6 Maturity functions.....	23
2.2.7 Strength- maturity relationships.....	26
2.3 Numerical models of concrete temperature development.....	28
2.4 Mix design Optimisation.....	33
2.4.1 Mix design optimisation methods	33
2.4.2 Genetic algorithm optimisation.....	39
2.5 Construction strategies to mitigate early age thermal cracking	47
2.6 Conclusions.....	54
Chapter 3: Precision of cement hydration heat models in capturing the effects of SCMs and retarders	56
3.1 Introduction.....	56
3.2 Existing Models for Hydration Heat Prediction.....	57
3.2.1 Schindler and Folliard model	57
3.2.2 Original and modified Bogue models	59
3.3 Methodology	61
3.3.1 Materials.....	61

3.3.2	Calorimetry measurements.....	61
3.4	Results and discussion	62
3.4.1	The effect of SCMs and retarders on hydration curves.....	62
3.4.2	The effect of curing temperature on hydration curves.....	68
3.4.3	Comparing the experimental results with hydration heat prediction models 72	
3.5	Conclusions.....	88
Chapter 4: A Three-Dimensional Customizable Model to Simulate Thermal Cracking of Concrete at Early Ages		
90		
4.1	Introduction.....	90
4.2	Features of proposed model	93
4.2.1	Heat Transfer model.....	96
4.2.2	Solid Mechanics model.....	105
4.2.3	Numerical simulation of reinforcement	111
4.2.4	Coupling Heat transfer and Solid mechanics models	112
4.2.5	Ordinary Differential Equation (ODEs).....	114
4.3	Case study	115
4.4	Conclusions.....	135
Chapter 5: A mix design optimisation algorithm method to minimize risk of early age thermal cracking of concrete		
137		
5.1	Introduction.....	137
5.2	Proposed Framework	138
5.2.1	Genetic algorithm optimisation.....	138
5.2.2	Numerical heat prediction model.....	143
5.3	Case study	147
5.3.1	General information	147
5.3.2	Constraints	153
5.3.3	Results and discussion	153
5.4	Conclusions.....	162
Chapter 6: Numerical investigation of construction strategies for mitigating the risk of early age thermal cracking.....		
165		
6.1	Introduction.....	165

6.2	Sequential concrete placement.....	166
6.2.1	Numerical modelling methodology	167
6.2.2	Case study	169
6.2.3	Results and discussion	173
6.3	Lowering placement temperature.....	180
6.3.1	Case study	181
6.3.2	Results and discussion	183
6.4	Using aggregates with lower thermal expansion coefficient	187
6.4.1	Thermal Expansion of aggregates- Case study	187
6.4.2	Results and discussion	188
6.5	Internal water cooling	190
6.5.1	Numerical modelling.....	191
6.5.2	Embedded water-cooling pipes- Case study	192
6.5.3	Results and discussion	194
6.6	Conclusions.....	198
Chapter 7: Conclusions		199
7.1	Concluding remarks	199
7.2	Limitations and Future Work Recommendations	205
References		208

LIST OF TABLES

Table 2- 1 Main chemical components of Portland cement.....	14
Table 2- 2 main chemical components of Portland cement [56, 57].....	28
Table 3- 1 Chemical compositions for OPC, Class F FA and GGBFS (%).....	63
Table 3- 2 Technical data for retarders	64
Table 3- 3 Comparison of peak heat flow for OPC at various curing temperatures	71
Table 3- 4 Comparison of selected hydration curve parameters for cement pastes with 40% FA or 40% GGBFS at various curing temperatures.....	76
Table 3- 5 Input parameters for existing hydration models	77
Table 3- 6 Output parameters of existing hydration models.....	77
Table 3- 7 Comparison of peak heat flow time and magnitude between test results and Schindler and Folliard’s Model.....	80
Table 3- 8 Comparison of peak heat flow between test results and Bogue’s Model for a 100% OPC system.....	83
Table 3- 9 Comparison of peak heat flow between test results and Bogue's model for 100% OPC with chemical retarders	85
Table 4- 1 properties of structural steel	112
Table 4- 2 Mix design of the concrete wall	115
Table 4- 3 Composition of Portland cement	116
Table 4- 4 Heat parameters for the concrete mix design based on Bogue model	116
Table 4- 5 Input parameters	117
Table 4- 6 Comparing the numerical model results and temperature sensor measurements	123
Table 4- 7 Comparing the numerical model results when using the direct calorimetry results and heat prediction model with temperature sensor measurements.....	125
Table 5- 1 Originally planned mix design	150
Table 5- 2 Composition of Portland cement	150
Table 5- 3 Heat parameters for the original mix design based on Bogue model	151
Table 5- 4 Sensor coordinates.....	152
Table 5- 5 Comparing the numerical model results and temperature sensor measurements	154

Table 5- 6 Optimised mix design.....	157
Table 6- 1 Mix design of the dam base.....	172
Table 6- 2 Composition of Portland cement.....	172
Table 6- 3 Heat parameters for the concrete mix design based on Bogue model.....	173
Table 6- 4 Mix design for the concrete pile.....	182
Table 6- 5 Heat parameters for the concrete mix design based on Bogue model.....	183
Table 6- 6 Coefficient of thermal expansion of different aggregate types.....	188
Table 6- 7 Thermal properties of the pipes.....	194

List of Figures

Figure 1- 1 factors affecting early age cracking [10].....	3
Figure 2- 1 Rate of heat generation during the hydration of Portland cement [27]	15
Figure 2- 2 The influence of cement fineness of the hydration rate of cement [36].....	18
Figure 2- 3 Schematic view of a typical adiabatic calorimeter [47]	21
Figure 2- 4 Schematic view of a typical semi-adiabatic calorimeter using a commercial thermos vessel [47].....	22
Figure 2- 5 Schematic view of an isothermal calorimeter (Tam Air calorimeter) [49]	23
Figure 2- 6 Concrete maturity diagram using Nurse-Saul maturity function [52].....	25
Figure 2- 7 Strength- Maturity curve [52]	27
Figure 2- 8 Basin with mounted cooling pipe (strand tube) [11].....	52
Figure 2- 9 Cylindrical model: water flux Q at temperature T_0 through a pipe cools an insulated concrete cylinder [90]	53
Figure 3- 1 Heat evolution for OPC pastes with different levels of a. Class F FA and b. GGBFS	66
Figure 3- 2 Heat evolution for OPC pastes with different dosages of a. Retarder N, b. Citrate and c. Sucrose	68
Figure 3- 3 Heat evolution for OPC at various curing temperatures	69
Figure 3- 4 Relationship between curing	70
Figure 3- 5 Normalized cumulative heat for	70
Figure 3- 6 Heat evolution for OPC pastes at various temperatures with a. 40% FA and b. 40% GGBFS.....	74
Figure 3- 7 Comparison of heat evolution for cement pastes with 40% FA or GGBFS at a) 10 °C, b) 23°C and c) 30°C.....	75
Figure 3- 8 Relationship between curing temperature and peak heat flow for 40% replacement	76
Figure 3- 9 Comparison of heat evolution between test results and Schindler and Folliard's model for an OPC system containing a. FA and b. GGBFS.....	78
Figure 3- 10 Heat evolution of test results and Schindler and Folliard's Model for a 100% OPC system at varying curing temperatures.....	79

Figure 3- 11 Comparison of heat evolution between test results and Bogue’s model for an OPC system containing a. FA and b. GGBFS	82
Figure 3- 12 Heat evolution of test results and Bogue’s Model for a 100% OPC system at varying curing temperatures	82
Figure 3- 13 Comparison of heat evolution between test results and Bogue’s Model for a General-Purpose cement system containing retarders.	87
Figure 4- 1 the framework of the numerical model	95
Figure 4- 2 Truss interface	113
Figure 4- 3 Cracking probability density [122]	114
Figure 4- 4 Measured heat data under three different curing temperatures	118
Figure 4- 5 Embedded sensor locations (in meter)	118
Figure 4- 6 Sensor Installation and data collection.....	120
Figure 4- 7 Numerical model of the concrete wall	120
Figure 4- 8 Reinforced element simulation.....	121
Figure 4- 9 Recorded ambient temperature.....	122
Figure 4- 10 Comparison between numerical results and site measurements for point U3	123
Figure 4- 11 Comparison between numerical results and site measurements for point C3	124
Figure 4- 12 Comparison between numerical results and site measurements for point L1	124
Figure 4- 13 Comparing the numerical model results when using the direct calorimetry results and heat prediction model with temperature sensor measurements for point C3	126
Figure 4- 14 2D presentation of temperature results at t=0 (hr)	127
Figure 4- 15 2D presentation of temperature results s at t=10 (hr).....	127
Figure 4- 16 2D presentation of temperature results at t=25 (hr)	128
Figure 4- 17 2D presentation of temperature results at t=50 (hr)	128
Figure 4- 18 2D presentation of temperature results at t=100 (hr)	129
Figure 4- 19 The studied points on the raft.....	129
Figure 4- 20 Thermal (compressive) stress development	130
Figure 4- 21 Thermal (tensile) stress development.....	130
Figure 4- 22 Cracking ratio development	131
Figure 4- 23 Cracking ratio pattern at t=0 (hr).....	131

Figure 4- 24 Cracking ratio pattern at t=20 (hr).....	132
Figure 4- 25 Cracking ratio pattern at t=50 (hr).....	132
Figure 4- 26 Cracking ratio pattern at t=100 (hr).....	133
Figure 4- 27 Temperature development pattern at t=100 (hr).....	134
Figure 4- 28 Temperature development of Point A for the wall with or without reinforcement	134
Figure 4- 29 Cracking ratio pattern at t=100 (hr).....	135
Figure 5- 1 Flowchart of the proposed framework	140
Figure 5- 2 2D control volume.....	144
Figure 5- 3 Foundation plan view	148
Figure 5- 4 Numerical model of the raft in COMSOL Multiphysics.....	149
Figure 5- 5 Embedded sensor locations (in meters).....	151
Figure 5- 6 Sensor installation	152
Figure 5- 7 Comparison between numerical results and site measurements for point 1.....	154
Figure 5- 8 Pareto front curve	155
Figure 5- 9 Comparing the original and optimised mix designs	158
Figure 5- 10 The studied points on the raft.....	158
Figure 5- 11 Temperature development of points A and B for both mix designs.....	159
Figure 5- 12 Thermal (tensile) stress development using the originally planned mix design...	160
Figure 5- 13 Thermal (tensile) stress development using the optimised mix design	161
Figure 5- 14 Cracking ratios using the originally planned mix design	161
Figure 5- 15 Cracking ratios using the optimised mix design	162
Figure 5- 16 Compressive strength development for both mixes	162
Figure 6- 1 Plan view of the dam base.....	170
Figure 6- 2 Section view of the dam base.....	171
Figure 6- 3 Numerical model of the dam base.....	171
Figure 6- 4 Temperature curves for different points of the foundation for the time interval of 1 day.....	175

Figure 6- 5 Temperature curves for different points of the foundation for the time interval of 2 days	176
Figure 6- 6 Temperature curves for different points of the foundation for the time interval of 3 days	176
Figure 6- 7 Maximum temperature within the foundation.....	177
Figure 6- 8 Maximum temperature gradient within the foundation.....	177
Figure 6- 9 Heat transfer in the foundation after pouring the first layer at time= 30 hrs.....	178
Figure 6- 10 Heat transfer in the foundation after pouring the 2nd layer at time= 85 hrs	178
Figure 6- 11 Heat transfer in the foundation at time= 350 hrs.....	179
Figure 6- 12 Heat transfer in the foundation at time= 600 hrs.....	179
Figure 6- 13 Heat transfer in the foundation at time= 700 hrs.....	179
Figure 6- 14 Heat transfer in the foundation at time= 1100 hrs.....	179
Figure 6- 15 Maximum crack ratio within the foundation.....	180
Figure 6- 16 The effect of placing temperature on the temperature rise in a 500 mm thick wall using concrete with 350 kg/m ³ CEM I cast in steel formwork [3].....	181
Figure 6- 17 Numerical model of the concrete pile	182
Figure 6- 18 Temperature development of point A for different initial temperatures	184
Figure 6- 19 Maximum temperature gradient within the pile	184
Figure 6- 20 Compressive strength development of point A for different initial temperatures	185
Figure 6- 21 Maximum Cracking ratio development within the concrete pile	186
Figure 6- 22 Maximum Cracking ratio within the concrete pile for different placement temperatures.....	186
Figure 6- 23 Maximum temperature development within the concrete pile using different aggregate types in the mix design.....	189
Figure 6- 24 Maximum tensile stress within the concrete pile using different aggregate types in the mix design.....	189
Figure 6- 25 Maximum cracking ratio development within the concrete pile using different aggregate types in the mix design with placement temperature of 32 °C.....	190
Figure 6- 26 Numerical model of the embedded water piping system	192
Figure 6- 27 Pile containing 2 embedded water pipes and the points under study	193

Figure 6- 28 Pile containing 4 embedded water pipes	194
Figure 6- 29 Temperature distribution of the pile with piping system at t=0 hours	195
Figure 6- 30 Temperature distribution of the pile with piping system at t=10 hours	195
Figure 6- 31 Temperature distribution of the pile with piping system at t=50 hours	196
Figure 6- 32 Temperature distribution of the pile with piping system at t=100 hours	196
Figure 6- 33 Maximum temperature of the piles with and without water piping system	196
Figure 6- 34 Cracking ratio of point A for the pile with and without internal cooling system .	197
Figure 6- 35 Cracking ratio of point B for the pile with and without internal cooling system .	197

Chapter 1: Introduction

1.1 Background

Concrete is the most used manmade material and is widely used in construction sites all around the world [1]. Concrete is used predominantly in construction of various types of structures and critical infrastructures. This infrastructure comprises the structures needed for the provision of transport, energy, water and communication, with significant social and economic impacts. Therefore, concrete performance is vital in providing essential services and maintaining their economic activities. Concrete is generally considered as a durable and long-lasting material [1]. The key performance requirements for the design, construction and maintenance of concrete structures relate to safety, serviceability and durability [2,3]. The two latter features however can be compromised significantly due to volumetric cracking that provides a path for harmful materials to ingress into the concrete. One of the dominant causes of cracking, especially in mass and high performance concrete, is early-age differential thermal stresses due to hydration induced internal heating of concrete and subsequent cooling [2]. Dale et al. (2008) reported an informal estimation of an annual \$500 million costs associated with the required rework and rehabilitation due to early age cracking encountered by major ready-mix companies in the U.S. [1].

The early age cracking problem originates from the exothermic nature of cement hydration reaction and low thermal diffusivity of concrete [4]. Because of the relatively low thermal diffusivity of concrete, the released heat due to hydration of a cementitious system may cause a considerable temperature rise at early ages after casting [3]. The increase in the temperature and subsequent cooling leads to volume changes and/or considerable temperature differential in concrete elements [3]. Since

concrete elements are generally internally and externally restrained, volume changes result in considerable thermal stresses [3]. In addition, due to low thermal conductivity of concrete, considerable temperature differences may be developed between the cooler exterior and hotter interior of concrete elements, leading to the development of differential thermal stresses in the concrete [5]. The thermal stresses developed due to heat of hydration may consequently lead to initiation of early age thermal cracking in concrete when the concrete's tensile strength is exceeded [6]. This is undesirable from the point of view of aesthetics, durability and structural performance [7,8]. Cracking increases the permeability and diffusivity of concrete and thus the kinetics of concrete deterioration due to steel corrosion, chloride ions penetration, leaching, etc. [7, 8]. In addition, another source of deterioration is delayed ettringite formation (DEF) which may happen as a result of significant temperatures reached in the core of massive structures due to heat of hydration [9].

The issue of thermal cracking due to hydration heat is significant especially in mass concrete in which huge dimensions and the low thermal conductivity of the concrete element tends to result in higher internal temperature gradients [10]. It is also significant in high strength concrete that usually contains higher amounts of Portland cement compared to other types of concrete. Apart from the cement content and dimensions of the concrete elements, the risk of early age cracking is affected by numerous other factors that determine the rate of heat generation as well as the rates of internal and external heat flow. These factors have been summarized by Safiuddin et al. as shown in Figure 1-1 and will be discussed in details in Chapter 2 [10].

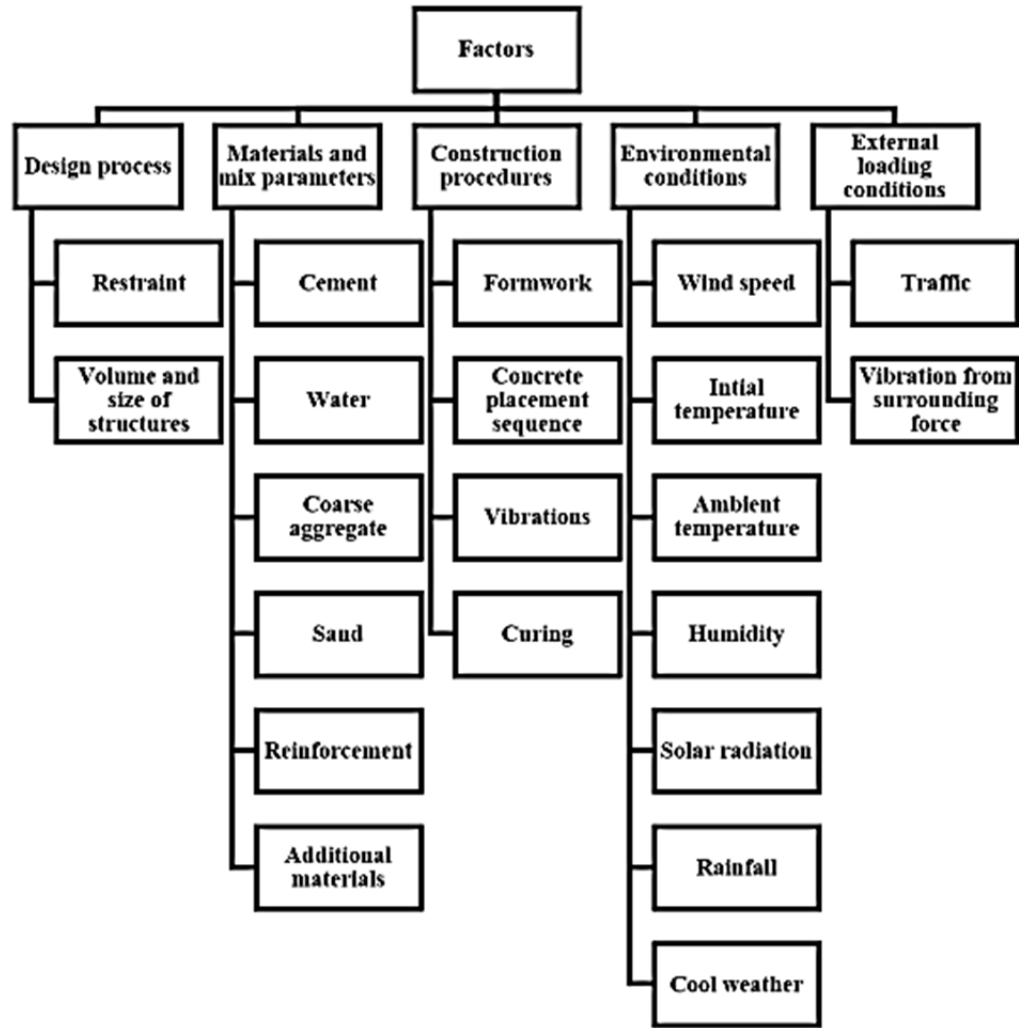


Figure 1- 1 factors affecting early age cracking [10]

Various techniques to reduce the maximum temperature in mass concrete have been investigated in the literature. These methods are mostly based on lowering the internal heat release through adopting concrete mixtures with lower cement contents or use of supplementary cementing materials such as fly ash and slag, exhausting the generated heat through cooling of water and/or aggregates before mixing operations or introducing internal cooling pipes in concrete, delaying the peak heat using retarders, and adopting concrete construction schedules that maintain temperature gradients in concrete below prescribed limits [11]. Among such techniques, modifying the concrete mixes and the use of supplementary materials are usually favoured by the industry,

mainly because these methods do not require changes to the construction method and plan. However, using other mentioned techniques in conjunction with mix design-based methods may be required in severe cases with very high hydration heat generation.

Optimising the concrete mix, on the other hand, requires the ability to predict the effect of a particular mix on temperature rise and development of thermal stresses in concrete. Numerical simulation of concrete elements is commonly used to estimate the temperature gradient, and thereby the risk of early age thermal cracking of the concrete elements [12, 13]. Reaching an acceptably precise numerical prediction, however, depends on both precision of analytical and empirical models used in numerical simulation and the precision of input data provided to the numerical simulation model. The main models used in numerical simulation of early age temperature development and potential cracking of concrete include models that estimate of heat generation over time (heat function) and models that estimate of maturity development rate and thus development rate of mechanical properties of concrete, which are themselves functions of temperature and thus, the heat generated [14, 15]. A number of commonly used empirical hydration heat models are reported in the literature [16–18]. These equations are a function of chemical composition of cement, supplementary cementitious material, curing temperature, and time [16–18]. The current state-of-the-art numerical simulation however faces considerable challenges with regards to inadequate precision of such models for new classes of concrete used in practice in which different types of admixtures and supplementary cementitious are commonly used to regulate fresh and hardened concrete properties and reduce the total amount of cement [6]. Furthermore, the existing numerical simulation models suffer from a number of technical limitations including the inability

to provide a three-dimensional representation of elements, account for the effects of reinforcement, etc., which will be discussed further in Chapter 3.

While numerical simulation can provide a good understanding of effect of a particular mix on risk of early age thermal cracking, identifying the optimal mix design through blind try and error in numerical simulation can be cumbersome and highly time consuming. Therefore, a smart methodology to guide the mix optimisation process is generally required to identify the optimal concrete mix among many alternative combinations of different concrete mix proportions. The same issue also applies to conventional mix optimisation approaches to identify the optimal concrete mix that meets the required mechanical and fresh concrete properties of concrete. With this in mind, improving concrete properties by optimising the concrete mix design has been under study for a long time [19–21]. The available concrete mix design-based methods focus mainly on achieving target mechanical properties of concrete and generally overlook the effect concrete composition has on internal hydration heat generation and transfer [19–21]. In fact, such methods have been developed based on empirical relationships between basic concrete properties and quantities and properties of conventional concrete constituents and lack a scientific basis relating the hydration kinetics to development of concrete properties.

Overlooking the important effects that concrete mix proportioning has on the internal temperature profile of concrete at early ages in the design stage over the years has led engineers to adopt conservative, worst case, approaches in design of structures and use non-conventional construction methods when dealing with mass concrete and relatively large high strength concrete elements [3, 22, 23]. In addition, in many cases, this has led to a considerable amount of re-work at significant cost to the public [1].

With the increasing awareness about the importance of this challenge, however, the availability of the models that assist practitioners in i) identifying the risk of early age cracking associated with the use of a particular concrete mix for a given element, and ii) identifying the optimal concrete mix that minimizes the risk of early age cracking in a concrete element, are among the well-emphasized needs of the concrete industry [3].

The present study aims to contribute to efforts towards developing methods for estimating and reducing the risk of early age thermal cracking by addressing some of the major gaps, partly highlighted above, in the available literature on numerical simulation of early age thermal cracking and mix optimisation to reduce the risk of the latter. The significance of the present study and its objectives are further elaborated in the following sections.

1.2 Research Motivation and Objective

Concrete is predominantly used for the construction of Australia's critical infrastructure and therefore, its performance is crucial to provide the nation's essential services and maintain its economic activities. Ensuring the durability of concrete is vital to ensure the designed infrastructure can reach the planned service life without putting undue pressure on future generations to maintain and retrofit this infrastructure. Safety, durability and serviceability of concrete infrastructures can be compromised significantly due to volumetric early age cracking, which provides a path for harmful materials to ingress into the concrete. Early age thermal cracking is a major concern especially in construction of mass and high-performance concrete elements. Many critical elements of concrete infrastructure such as footings and retaining walls can be classified as high risk with respect to early age thermal cracking.

By making available improved prediction models to numerically estimate the risk of early age thermal cracking as well as making available an effective mix optimisation model to provide practical mix design solutions to reduce the risk of early age thermal cracking at design stage, costly over design and disrupting repair and retrofitting could be avoided. However, developing effective early age cracking prediction numerical simulation models and mix optimisation models to reduce the risk of early age thermal cracking faces a number of technical challenges including i) difficulties in precisely predicting the internal heat generation and transfer in a particular concrete mix given the outdated nature of existing heat generation estimation models and a lack of update numerical models to account for the effects of different types of supplementary cementitious materials and admixtures on hydration kinetics; ii) a gap in the knowledge about relationships between heat of hydration and development of concrete properties, including strength, elasticity, heat capacity, thermal expansion coefficient, thermal conductivity, etc., as well as variations in such relationships with changes in the mix; iii) difficulties in modelling the effects of variations in internal temperature at early ages on hydration kinetics; iv) difficulties in modelling realistic boundary conditions at air-concrete, formwork-concrete and soil-concrete interfaces; v) difficulties in modelling the internal constraints caused by hardening of concrete and the presence of reinforcing bars; and vi) difficulties in capturing the impacts of changing the construction plans such as sequence concrete pouring and using an internal cooling system on temperature development [9, 11, 24, 25].

The components of this study are:

- A systematic approach is adopted to address the above challenges to meet the key objectives which are outlined in the following: Verifying the accuracy of the

existing hydration heat prediction models in capturing the effects of SCMs and admixtures using local concrete compounds in Australia through calorimetry tests

- Develop a three-dimensional time-dependent numerical simulation method for prediction heat of hydration, early age thermal stresses and strains as well as thermal and mechanical properties of concrete.

- Eliminate the sensitivity of thermal modelling of concrete to accuracy of hydration heat models by allowing the model to accept direct calorimetry measurements as input.

- Develop a multi-objective mix design optimisation model that minimizes the risk of early age thermal cracking of concrete elements while meeting also meeting the strength development requirements.

- Numerically investigate the effectiveness of various construction strategies for mitigating the risk of early age thermal cracking of concrete including sequence concrete pouring, pre-cooling of concrete to change the placement temperature, using of aggregates with lower thermal expansion and using of embedded cooling pipes to capture their efficiency.

1.3 Research Methodology

To achieve the objectives, a four-step methodology is followed in this thesis. The methodology adopted in each step is briefly described in the following.

1- Due to the importance of the accuracy of the input heat of hydration data for numerical models, a comprehensive series of isothermal calorimetry measurements is conducted to investigate the impacts of using supplementary cementitious materials including class F fly ash and ground granulated blast-furnace slag (GGBFS) and the

three most used chemical retarders in Australia (Retarder N, Sucrose and Citrate) on the heat of hydration development of cementitious materials, as well as the ability of existing heat of hydration models in capturing these effects. Furthermore, the calorimetry measurements will be carried out at three different curing temperatures of 10, 23 and 30 °C to evaluate the effect of temperature on the rate of hydration.

2- A comprehensive three-dimensional numerical model is developed in COMSOL Multiphysics to predict the temperature development, temperature gradient, and thermal stresses and strains within the concrete, as well as the resulting early age thermal cracking ratio as an indicator of risk of early age thermal cracking of concrete. Coupled finite element analysis of heat transfer and solid mechanics modelling for concrete elements subject to thermal loads allows the user to investigate how various mix designs, cement types, structural boundary conditions, thermal boundary conditions, steel reinforcement and curing methods can affect the magnitude and pattern of differential thermal stresses developed due to hydration heat. Moreover, the model is developed with an interpolation algorithm to allow for the use of direct calorimetry measurements as the heat source in place of prediction of hydration heat models.

3- A genetic algorithm-based optimisation method is proposed to identify the optimal mix design for concrete elements subject to the risk of early age thermal cracking. The method is a multi-objective optimisation method which aims to reduce the temperature gradient within the concrete section while maximizing the tensile strength development rate. Bogue's heat of hydration model and finite difference simulation method are used to account for temperature and tensile strength calculation

of different points of the concrete element. The mechanical properties of the element under study are controlled to be in a pre-defined acceptable range.

4- While optimising mix design is an effective method to control the risk of early age thermal cracking, there may be a need to use other complementary methods to decrease the possibility of the occurrence of the early age thermal cracking in cases with very high chance of early age cracking. The numerical model explained earlier is modified to enable investigating the effectiveness of other common strategies adopted in practice to reduce the risk of other early age thermal cracking of concrete. These strategies include sequential concrete pouring, use of embedded water-cooling pipes, lowering concrete's placement temperature and using aggregates with lower thermal expansion coefficient on early age thermal cracking.

1.4 Thesis Outline

The present thesis is organized into seven chapters. A brief illustration of each chapter is presented below:

Chapter 1 discusses the importance of studying early age thermal cracking of concrete, the gaps in the previous researches which motivated this study, the goals and objectives of this research and the thesis outline.

Chapter 2 provides a review of the literature on heat of hydration of concrete and different factors influencing it, methods for measuring hydration heat, available heat of hydration prediction methods, numerical models for analysing hydration heat of concrete, mix design optimisation methods and different construction strategies used in practice to reduce the risk of early age thermal cracking of concrete.

Chapter 3 investigates the precision of available hydration heat models in capturing such effects of supplementary cementitious materials and retarders on heat of hydration through a comprehensive series of calorimetry measurements.

Chapter 4 presents a finite element-based simulation method to estimate the temperature development and evaluate the risk of early age thermal cracking using COMSOL Multiphysics. The accuracy of the obtained results is verified through using real world in-situ measurements.

Chapter 5 proposes a genetic algorithm-based optimisation method for optimising concrete mix designs with the objective of minimizing temperature gradient within the concrete section while maximizing the tensile strength of concrete. The method is applied on a real-world case study and the element is modelled using the numerical model introduced in Chapter 4 to investigate the effects of the mix design optimisation on reducing the risk of early age thermal cracking.

Chapter 6 presents a modified version of the numerical model developed in Chapter 4 for considering the effect of sequence concrete pour and using embedded water-cooling pipes. Moreover, these methods alongside two other early age thermal cracking mitigation methods including using lower thermal expansion aggregates and lowering the initial temperature of concrete are applied to real life case studies and their impact on reducing the risk of early age thermal cracking is investigated.

Chapter 7 discusses the contributions of this research and future research recommendations.

Chapter 2: Literature Review

2.1 Introduction

Concrete is the most used material in construction sites around the world. One of the major issues affecting the structural performance and serviceability of concrete elements is cracking, which allows the harmful materials to ingress into concrete, thereby causing numerous durability issues. One of the dominant causes of cracking especially in mass and high-performance concrete, is early age thermal cracking, that is due to hydration induced internal heating of concrete and subsequent cooling [1]. Several studies have been conducted on different aspects related to early age thermal cracking of concrete including methods to estimate the development of temperature and thermal stresses in concrete, and strategies to reduce the risk of early age thermal cracking. Furthermore, each of these areas rely on an extensive body of knowledge related to cement hydration and hydration heat estimation, modelling of concrete's maturity development and modelling the development of mechanical and thermal properties of concrete that provide the scientific backbone to discussions and studies in the field.

The focus of this chapter is current methods for evaluating the heat of hydration and maturity of concrete at early ages, which are the underlying concepts of this study. The available studies on mix design optimisation of concrete, numerical simulations of concrete elements subject to early age thermal cracking and construction strategies to reduce the risk of early age thermal cracking are also reviewed.

2.2 Heat of Hydration Prediction Models

2.2.1 Concrete hydration and hydration products

The exothermic chemical reaction between cementitious materials, and other concrete mix components, with water leads solidification of the concrete, this is known as hydration. The products formed as a result of this reaction are called hydration products and have varying impacts on the thermal and mechanical properties of the concrete.

Portland cement consists of five main compounds which are presented in Table 2-1. In the presence of water, silicates in cementitious materials powder create Calcium-Silicate-Hydrate (C-S-H) gel, which gives strength to the system and has the greatest effect on the mechanical properties of the cement paste. C-S-H replaces C_3S and C_2S minerals, which are the most plentiful minerals, and is the most abundant hydration product, constituting approximately 50% of the paste volume. The second most common hydration product, which forms mainly from C_3S and less from C_2S , is Calcium Hydroxide (CH), also known as Portlandite, and occupies about 15% of Portland cement paste volume. The shape and size of the CH crystals varies depending on the available space for their growth. CH and C-S-H gel form a cohesive mixture.

CH decreases the total pore volume of the mix, which leads to a moderate increase in concrete strength. However, CH is the most soluble hydration product and it dissolves when exposed to water which results in more porosity. Therefore, it is not the best concrete binder in terms of durability. There are several additional hydration products such as Calcium Sulfoaluminate, Hydrogarnet, Brucite, and Syngenite but their impact on the engineering properties of concrete is negligible [26].

Table 2- 1 Main chemical components of Portland cement

Cement Compound	Weight Percentage	Chemical Formula
Tricalcium silicate (C ₃ S)	50 %	Ca ₃ SiO ₅ or 3CaO·SiO ₂
Dicalcium silicate (C ₂ S)	25 %	Ca ₂ SiO ₄ or 2CaO·SiO ₂
Tricalcium aluminate (C ₃ A)	10 %	Ca ₃ Al ₂ O ₆ or 3CaO·Al ₂ O ₃
Tetracalcium aluminoferrite (C ₄ AF)	10 %	Ca ₄ Al ₂ Fe ₂ O ₁₀ or 4CaO·Al ₂ O ₃ ·Fe ₂ O ₃
Gypsum	5 %	CaSO ₄ ·2H ₂ O

Figure 2-1 shows the rate of heat evolution during hydration, which noticeably impacts the heat liberation [27]. As shown, there are five phases associated with the hydration of Portland cement [28]:

- Stage one: Dissolution stage (<15mins)
 - Aluminate rich C-S-H gel is produced from the (C₃A) phase reacting with water
 - Rapid heat generation
 - Dissolution of ions and initial hydration

- Stage Two: Dormant period (2-4 hours)
 - Ettringite is formed from the reaction of the C-S-H gel with sulphate
 - Cement remains plastic and reaction slows

- Stage three: Acceleration phase (2-4 hours)
 - Greatest rate of heat evolution, initial and final set occur
 - Initiation of silicate hydration, Alite(C_3S) and Belite (C_2S) react to form calcium silicate hydrate and calcium hydroxide. (C_3A) reaction continues
 - Concrete strength development increases
- Stage 4: Deceleration stage
 - Reaction slows, heat peaks and begins to drop, concrete cools and contracts
 - Depletion of sulphate
- Stage 5: Steady state stage
 - Constant reaction rate that can continue for years

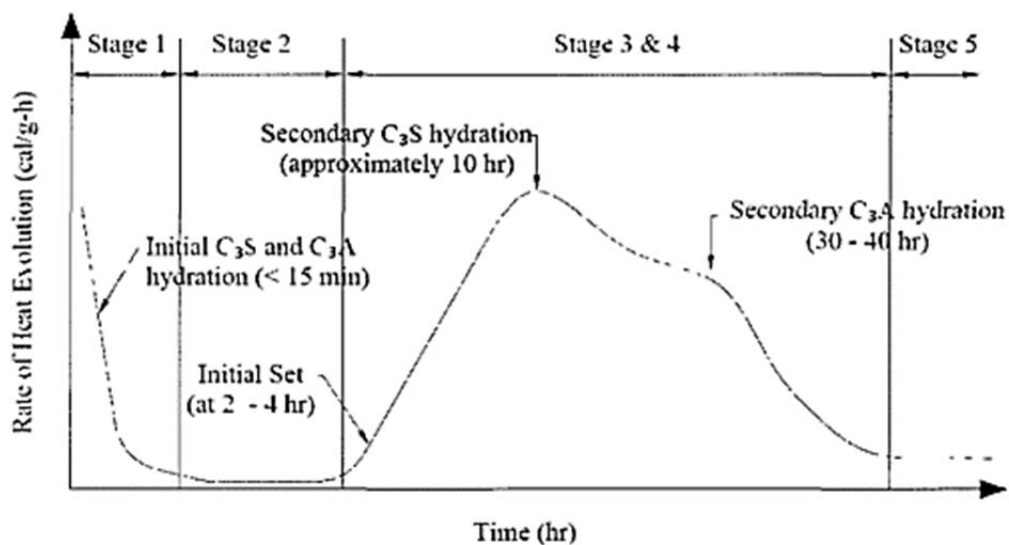


Figure 2- 1 Rate of heat generation during the hydration of Portland cement [27]

The layers of the C-S-H gel expand around the cement particles and cause the cement paste to harden. There are two varying types of C-S-H gels that are formed in stages three and four of the hydration process as shown in Figure 2-1. Low-density C-S-H gels are formed rapidly in stage three which is the acceleration phase and high-

density C-S-H gels start to generate in stage four of the hydration process which is known as the deceleration stage. However, the order of formation of these two gel types may vary in some cases. This means that it is possible to witness low-density gel formation in stage four and high-density gel formation prior to it in stage three [26].

2.2.2 Heat of hydration

Hydration is an exothermic chemical reaction. The total heat liberation in the hydration process consists of two parts; the heat released by a solution of the anhydrous materials and the heat liberated by the precipitation of hydrates from solution [29]. The total heat of hydration and the heat evolution rate are mostly influenced by concrete composition, especially the amount and fineness of cementitious materials and the water to cementitious materials ratio. However, several external factors such as placement temperature and ambient temperature are mentioned in the literature to impact the heat of hydration as well [29]. The influence of these factors is discussed in detail in the following section.

2.2.3 Factors influencing the heat of hydration

- **Chemical composition of cementitious materials**

Understanding how the chemical components of cementitious materials hydrate is vital to investigate the hydration process. The hydration heats of four Bogue compounds introduced in section 2-2-1 are investigated in several studies. Tricalcium silicate (Alite), C_3S , has a noticeable influence on early age strength of concrete since it hydrates and hardens quickly [30]. Rapid hydration of Alite is associated with high heat of hydration and increased hydration rate. Dicalcium silicate (Belite), C_2S , has the least hydration rate leading to less participation in hydration heat and early age strength. Tricalcium aluminate, C_3A , generates heat instantly upon exposure to water and a

notable amount of heat generation continues within the first few days. Tetra-calcium aluminoferrite (Ferite), C_4AF , hydrates rapidly, however it contributes minimally to concrete strength and the heat liberation of C_4AF during hydration is lower than C_3A . Adding gypsum to the concrete mix slows the hydration rate of C_3A and prevents rapid setting leading to optimum strength being obtained. Generally, about 2.5-8% of gypsum is required in the cement mix to control the setting [31]. Moreover, the amount of sulphate, SO_3 , can significantly affect the degree of hydration of concrete by increasing the rate of hydration at early ages. Several studies confirmed that the most significant components of Portland cement influencing the amount and rate of heat of hydration and, therefore, early age strength of concrete are C_3A and C_3S [29, 31, 32]. Bogue also noted here that approximately half of the total generated heat is liberated at the age of 1 to 3 days after casting. This value reaches to about three quarters in 7 days and to 83-91% in 6 months. He also mentioned that “*the total quantity and the rate of heat liberation are greatest with those cements high in tricalcium aluminate and tricalcium silicate*” [29].

- **Fineness of cementitious materials**

Several studies in the literature mentioned the cement fineness as an effective factor on the kinetics of cement hydration [29, 31, 33, 34]. Finer cement particles provide more surface area to react with water, which leads to a faster rate of hydration, higher heat generation and greater early age strength [30]. However, Bentz and Haecker [35] stated that the influence of cement fineness fades for high cement to water ratios. Fineness of cement is quantified using the total specific surface area, that is, the surface area available for hydration. Generally, the Blaine method is used for calculations of specific surface and Blaine values of cement range from 2,600 to 5,000

(cm^2/g). It should be noted that while cement fineness has considerable impact on the rate of heat development at early ages, it does not noticeably affect the total heat of hydration [30]. Figure 2-2 demonstrates how the rate of hydration is impacted by the fineness of cement.

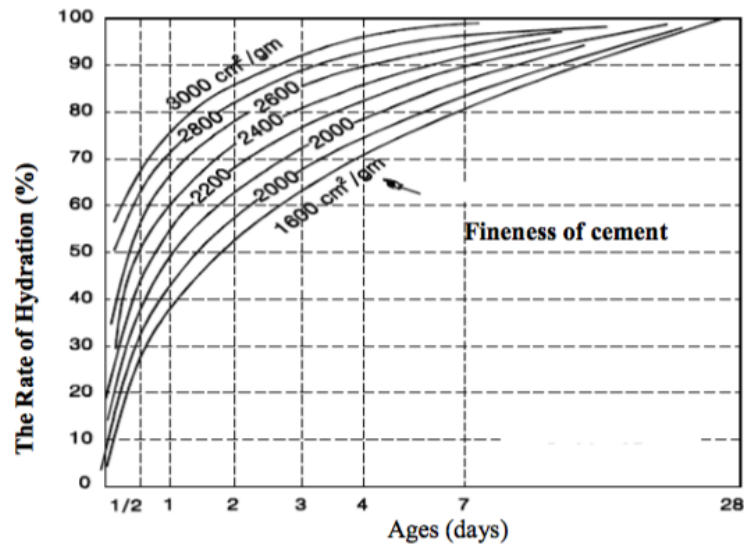


Figure 2- 2 The influence of cement fineness of the hydration rate of cement [36]

- **Water to binder ratio**

A higher water content provides cement grains with more microstructure space available for hydration, forcing the hydration reaction to occur at an increased pace. More specifically, the water to binder ratio has the greatest impact on rising the rate of hydration during the acceleration phase. The Portland Cement Association [37] stated that for Type I cement, equivalent to Australian General Purpose (GP) cement [30], the heat of hydration at the age of 7 days is increased about 11% when altering the w/b ratio from 0.4 to 0.6. It should be noted that for moderate and low heat cements, variations of the hydration heat due to changing w/b ratio is not significant [38].

- **Curing temperature**

The effects of curing temperature on the process of hydration have been shown to be significant, both experimentally and theoretically. Several studies concur that specimens with higher curing temperatures have a higher rate of hydration [31, 33, 39]. Termkhajornkit et al. also showed that increasing the curing temperature decreased the long-term compressive strength of concrete [33]. This understanding suggests that the hydration kinetics decelerate succeeding the initial acceleration phase [33,39]. Bogue confirmed these results experimentally expressing that the heat evolution at the curing temperature of 35°C are higher than those evolved at the curing temperature of 25°C, however the amount of the difference is not significant [29].

- **Supplementary cementitious material**

Supplementary cementitious materials such as Fly Ash, Ground Granulated Blast Furnace Slag (GGBFS), Silica Fume, etc. are added to mix design as a sustainable and efficient addition to the cementitious system. It is commonly accepted that these mineral admixtures enhance the performance and durability of hardened concrete [39]. Moreover, the total heat release and the intensity of heat development is lower for mixes with mineral admixtures [40]. Also, as mineral admixtures are finer compared to Portland cement, they make the concrete mix less porous which results in more durability [41]. Siler et al. showed that increasing replacement levels of Fly Ash delays the hydration process and setting time while decreasing the peak heat of hydration [40]. A similar impact on hydration was shown when using Ground Granulated Blast Furnace Slag (GGBFS) in concrete mix design. Furthermore, Bamforth expressed that the temperature rise was reduced by about 40% in mass concrete when 65-80% of GGBFS was replaced with Portland cement [42]. However, high replacement levels of

GGBFS adversely affects the mechanical properties of fresh concrete. Moreover, increasing the proportion of GGBFS decreases workability [43]. It is important to note that the results were based on cementitious systems produced in the United Kingdom and cannot be directly imposed to Australian cementitious mixes.

- **Chemical Admixtures**

Chemical admixtures are added to cementitious systems in order to enhance the performance of fresh and hardened concrete. There are various types of chemical admixtures such as retarders, accelerators, super plasticizers, water reducer, etc. [44]. Retarders are commonly used for mass concreting and are the most common admixture used in concrete elements subject to heat of hydration issues; thus, they are of particular interest in this study due to their direct significant effect on hydration heat [27]. The benefits of using retarders include controlling setting and hardening of concrete, improving workability, improving mechanical properties resistance against frost and sulphate. Retarders also impact the hydration process due to their influence on the tricalcium silicate and tricalcium aluminate constitutes of Portland cement. Since retarders delay the initial set of concrete, the rate of heat generation is reduced [45].

- **Mix design**

Based on what has been discussed earlier, concrete mix design which determines the quantity of different components in the concrete, directly influences the rate and amount of heat generation and temperature rise in concrete elements [29, 31].

2.2.4 Measuring heat of hydration

The heat of hydration of concrete can be measured experimentally by means of a calorimeter [46]. There are three different methods for calorimetry testing to be conducted as explained below.

✓ **Adiabatic calorimeter:** In this method, there is no change in heat through the system and any heat generated causes the temperature of the sample to increase. However, this definition is the ideal and in the real world no adiabatic calorimeter is fully adiabatic. Where the maximum heat loss in a calorimeter is less than $0.02 \text{ J}/(\text{h.K})$, it is considered as an adiabatic calorimetry [47]. A schematic view of an adiabatic calorimeter is shown in Figure 2-2.

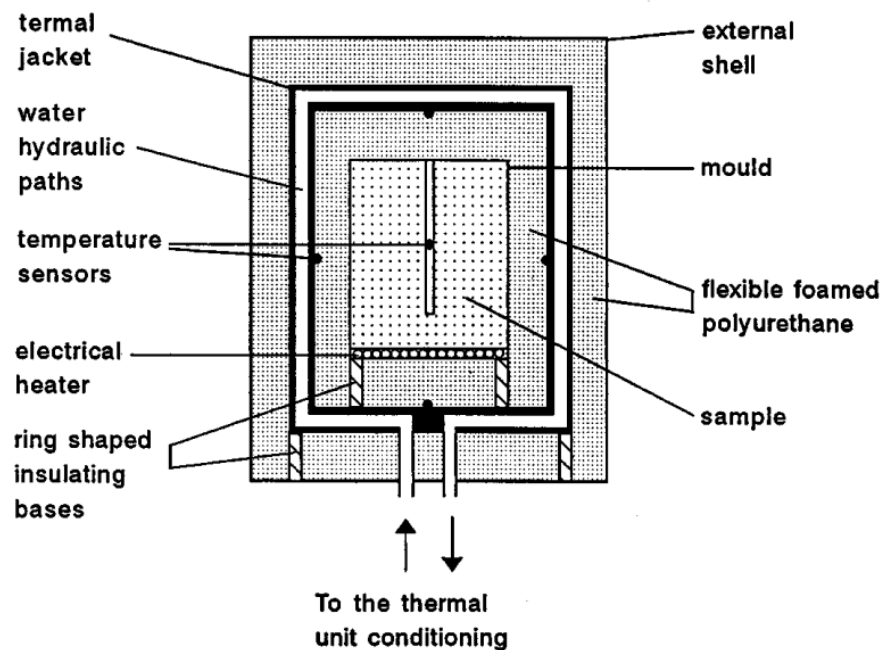


Figure 2- 3 Schematic view of a typical adiabatic calorimeter [47]

✓ **Semi-adiabatic calorimeter:** A schematic view of a typical semi adiabatic calorimeter is shown in Figure 2-3. The principles of a semi-adiabatic calorimeter are

similar to adiabatic calorimeters [48]. The difference is that in the semi-adiabatic calorimeters the heat loss is allowed up to 100 J/(h.K) [47].

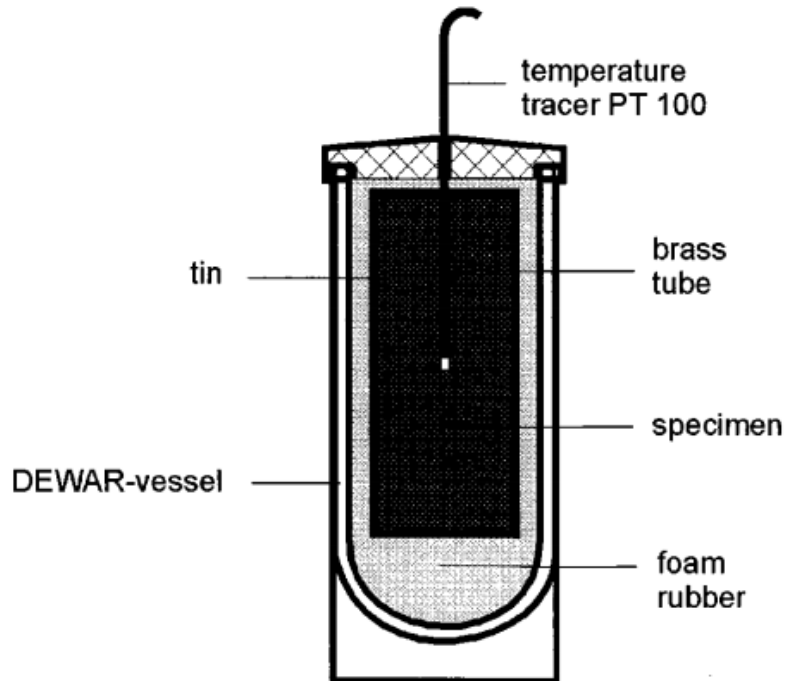


Figure 2- 4 Schematic view of a typical semi-adiabatic calorimeter using a commercial thermos vessel [47]

✓ **Isothermal calorimeter:** In isothermal calorimeters the temperature through the system is constant and can be set [46, 49]. The heat evolution of the sample is measured with the help of a reference sample. A cutaway view of an eight-channel isothermal calorimeter (TAM-Air calorimeter) is presented in Figure 2-3 [49]. The test method for isothermal calorimetry is presented in ASTM C1702 [50].

The isothermal calorimeters directly measure the rate of heat flow, which is continually related to the rate of reaction, whereas adiabatic and semi-adiabatic calorimeters measure temperature change and convert it to heat development. Considering the focus of this study, isothermal calorimetry is the preferred method for quantifying the heat of hydration for this thesis based on ASTM C1702 [47, 49]. The

isothermal calorimeter used in this study is the eight-channel TAM-AIR calorimeter. The mechanism of this device will be explained in section 3-3-2.

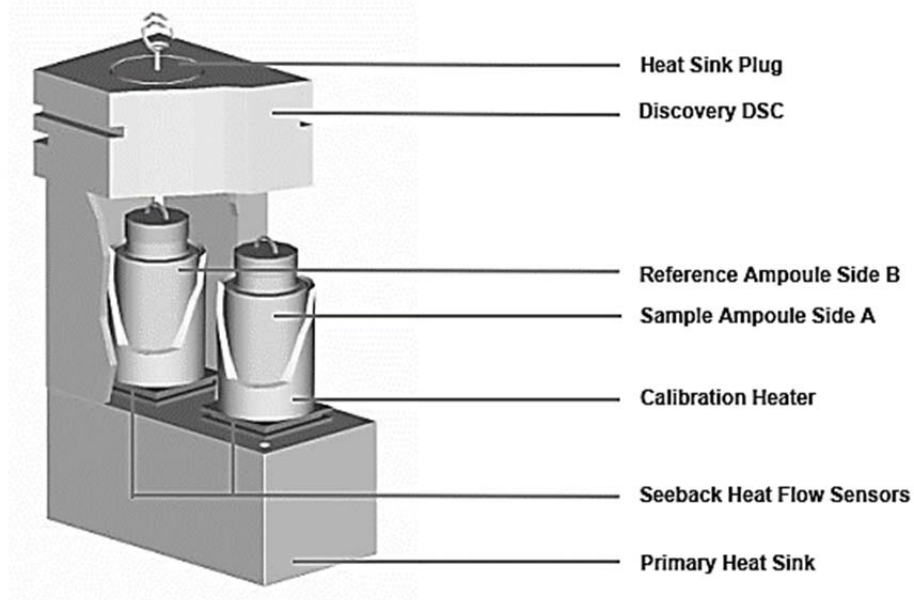


Figure 2- 5 Schematic view of an isothermal calorimeter (Tam Air calorimeter) [49]

2.2.5 Heat of hydration prediction models

A number of commonly used empirical hydration heat models are reported in the literature. These equations are typically a function chemical composition of cement, supplementary cementitious material, curing temperature, and time [16–18]. Two of the most commonly used models for heat of hydration prediction are the Schindler and Folliard model [16] and the Bogue model [18]. These models will be described in detail in Section 3-2 in Chapter 3.

2.2.6 Maturity functions

The urge to have a method for calculating the combined effect of time and temperature on strength development of concrete for different temperature curing methods has been felt for a long time. There are several methods available in the literature in this regard [51].

Nurse-Saul Function: In 1949, Nurse and Saul developed a method to relate concrete strength and maturity, known as the Nurse-Saul Function. The function attempts to predict concrete strength by introducing a maturity index called the “temperature-time factor” (TTF). The maturity index is the quantitative amount of temperature and time a concrete mixture has accumulated. The function is based on the temperature history of the concrete and the assumption that the rate of strength gained during the accelerator period behaves linearly with temperature [52]. The Nurse-Saul function is defined in ASTM C1074- 98 [53]:

$$M(t) = \sum_0^t (T_c - T_0) \cdot \Delta t \quad \text{Equation 2- 1}$$

where, M is the maturity index at age t ($^{\circ}\text{F}\cdot\text{hr}$ or $^{\circ}\text{C}\cdot\text{hr}$), T_c is the average concrete temperature during time interval ($^{\circ}\text{F}$ or $^{\circ}\text{C}$), T_0 is the datum temperature ($^{\circ}\text{F}$ or $^{\circ}\text{C}$) and Δt is a time interval (hr). The Nurse-Saul function is governed by the following maturity rule “Concrete of the same mix at the same maturity (reckoned in temperature-time) has approximately the same strength whatever combination of temperature and time go to make up that maturity.” [52]. To calculate the maturity index, it is important to define a correct datum temperature for the specific concrete mix and curing conditions. Computation of the Nurse-Saul maturity function can be explained by Figure 2-4. The selection of the datum temperature is based on several factors including the type of cement, the usage of chemical admixtures and the water to binder ratio. It should be noted that there are limitations to the Nurse-Saul function. One of the most important ones is that the results of this method are not accurate enough for varying curing temperatures [52].

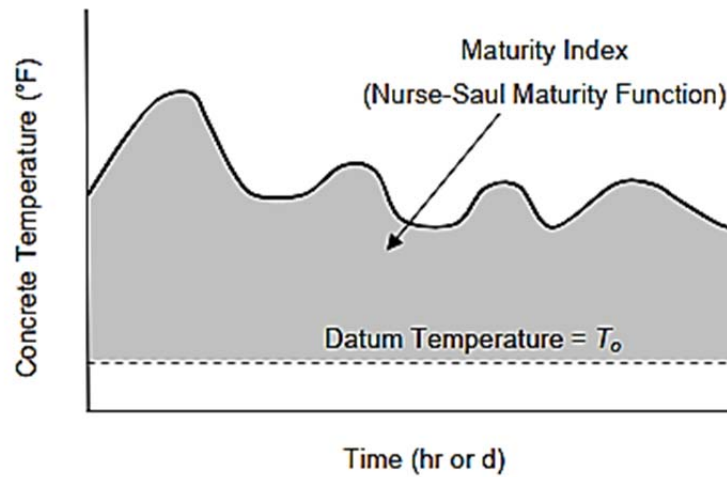


Figure 2- 6 Concrete maturity diagram using Nurse-Saul maturity function [52]

Arrhenius maturity function: The limitations of the Nurse-Saul function led researchers to look for a more accurate maturity function. In 1977, Freiesleben Hansen and Pedersen proposed a new function that basically converts the actual age of the concrete to an equivalent age at a specified reference temperature. The equivalent age defined as Equation 2-2 assumes that the rate of strength development follows Arrhenius's equation.

$$t_e = \sum_0^t e^{\frac{-E}{R} \left[\frac{1}{273+T_c} - \frac{1}{273+T_r} \right]} \cdot \Delta t \quad \text{Equation 2- 2}$$

where, t_e is the equivalent age at a specified temperature (hr), E is the activation energy (J/mol), R is the universal gas constant equal to 8.314 J/(mol.K), T_r is the reference temperature of concrete during time interval (°C) (usually considered as 20 °C or 23 °C), T_c is the average concrete temperature for the time interval, Δt , (°C) and Δt is the time interval (hr). Activation energy is a new parameter in this equation which shows the dependency of the curing temperature on strength development. Computation of activation energy depends on the type of the cement used, the presence and dosage of admixtures and w/b ratio.

2.2.7 Strength- maturity relationships

Concrete strength can be predicted at any age using the strength-maturity curve of the concrete. The strength-maturity curve for a concrete mix is presented in Figure 2-5. Several researches have been conducted on modelling strength- maturity relationships. Some of the most typical ones are proposed below [52].

- **Exponential Function:**

Freiesleben-Hansen and Peterson developed a revised exponential function based on the research of Nykanen in 1956. The original exponential function was predominately dependent on the w/c ratio of the concrete mixture, and as such it did not fit the actual strength data very accurately. The modified exponential function has proven to be a reasonable fit for the actual strength data of many researchers. This function was accepted by ASTM C 1074 as an appropriate model for the strength-maturity relationship. Freiesleben-Hansen and Pederson's modified exponential function is as follows [52, 53]:

$$S = S_u e^{-\left(\frac{\tau}{M}\right)^\alpha} \quad \text{Equation 2- 3}$$

where S is the compressive strength at age t , S_u is the limiting compressive strength, M is the maturity index (hr), α is the shaper parameter and τ is the time constant.

- **Logarithmic function:**

In 1956, Plowman [54] proposed a logarithmic relationship between strength and maturity presented in Equation 2-4. Due to the simplicity of the calculation of this function, it gained popularity. However, since no limiting strength is considered in the function, this function has a limitation in plotting high and low maturity indexes accurately. Plowman's equation is given as:

$$S = a + b \log(M)$$

Equation 2- 4

where a and b are constants related to the used mix design and M is the maturity index.

• **Modified hyperbolic function:**

Carino [53] developed a modified hyperbolic strength- maturity function which can be found in Equation 2-5 [54]. The hyperbolic introduced an offset time, t_0 , which accounts for the assumption that strength gains begin after some time, t_0 . Carino's function is recommended in ASTM C 1074 as an acceptable function to model strength gain.

$$S = S_u \frac{k(t-t_0)}{(1+k(t-t_0))}$$

Equation 2- 5

where, k is the rate constant (1/day) and t_0 is the age that strength development starts (hr).

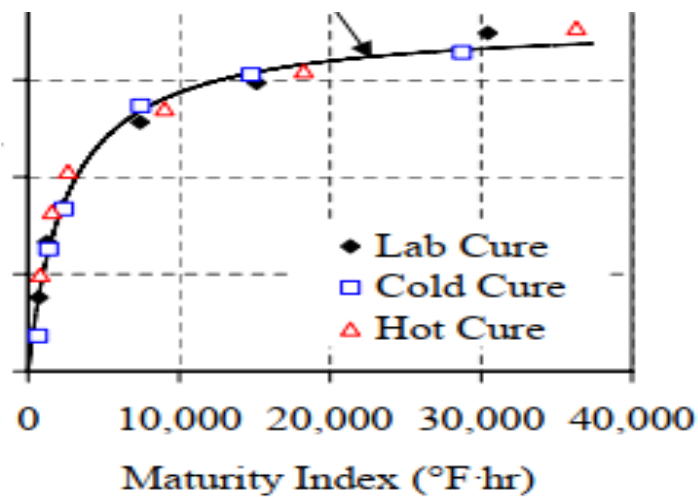


Figure 2- 7 Strength- Maturity curve [52]

Since the exponential function is introduced as the most accurate method for calculating the maturity- strength relationship, it is used in this study [52, 53].

Since no studies have been conducted using the Australian materials and admixtures, in this study the heat of hydration of mixes including concrete compounds and common chemical admixtures from Australia are utilized.

2.3 Numerical models of concrete temperature development

Numerical modelling of heat transfer in concrete by considering cement hydration as the heat source allows the designers and contractors to estimate the development of temperature and temperature gradient and consequently the risk of early age thermal cracking of concrete. Several studies have been conducted in the literature to numerically model the heat generation and transfer phenomena in concrete.

Ye [55] proposed a 2-D numerical simulation to analyse the temperature and moisture development in early age concrete pavements (TMAC2) to assist curing effectiveness evaluation. He used the conservation of energy concept and law of conservation of moisture mass to calculate heat transfer and moisture diffusion in concrete and synthesized these models. To consider water movement because of relative humidity he used moisture capacity concept and modelled relative humidity drop due to self-desiccation using this. He measured the actual temperature and moisture gradients at National Airport Pavement Test Facility (NAPTF) and used the results to characterize the concrete thermal conductivity and moisture diffusivity.

Folliard et al. [56, 57] developed a 2-D software package called ConcreteWorks to conduct thermal analysis and chloride diffusion service life. The software is capable of analysing the member types presented in Table 2-2.

Table 2- 2 main chemical components of Portland cement [56, 57]

Mass Concrete	Rectangular Column Rectangular Footing Partially Submerged Rectangular Footing Rectangular Bent Cap T-Shaped Bent Cap Circular Column Drilled Shaft
Precast Concrete Members	Box Beam (Type 5B40) Type IV I-Beam U40 Beam U54 Beam Precast 1/2 Depth Panels
Bridge Deck Types	Permanent Metal Decking Removable Forms User-Defined
Pavements	User-Selected Layers

ConcreteWorks allows the users to define different mix designs including supplementary cementitious materials and chemical admixtures. Also, the cement compositions can be defined by the user. The boundary conditions are imposed on concrete members to model the effects of ambient temperature, different types of curing methods, form liners, and cure blankets. ConcreteWorks uses the conservation of energy concept to predict the temperature development of several predefined points in a concrete section. It also informs the user of the time to corrosion initiation and damage expected in the concrete element. Moreover, this software gives the cracking probability classification. A low cracking probability category does not guarantee that the structural member will be free of cracks. It only indicates that the probability of cracking is lower

than if the concrete cracking probability classification were moderate, high, or very high. It is expressed that any classification, including the low cracking probability includes some chance that cracking will occur. ConcreteWorks, which is one of the most comprehensive models for investigating early age thermal cracking, however, has a number of important limitations. These include i) the 2-D nature of the analysis which limits the applicability of the model solely to cases that can be simplified to 2-D; ii) the limited number of pre-defined geometries and the inability to add new customized element geometries; iii) the limited postprocessing ability which limits the analysis output to a simplified range of cracking probabilities; iv) inability to account for the effect of reinforcement on heat transfer; v) inability to accept direct calorimetry measurements as heat source which limits the precision of the model to the precision of the hydration heat estimates.

Cervera et al. [58] used hydration degree to model the hydration and aging phenomena of hardening concrete by implementing finite element spatial discretization and a time integration based on the explicit Euler scheme. They used a thermo-chemical model to consider the hydration process. This method was applied to normal and high-performance concrete and showed that the predictions are accurate during the curing process. Moreover, to describe the compressive strength development during the hydration process, a novel concept of ageing degree (κ) was defined by linking it to hydration degree and curing temperature. The calculation for compressive strength was defined as:

$$f(\kappa) = \kappa f_{\infty} \quad \text{Equation 2-6}$$

where f and f_{∞} are the current and final compressive strength and reference temperature and κ is a normalized strength. The rate of ageing degree was defined as Equation 2-7.

$$\dot{\kappa} = \lambda_T(T)\lambda_{\xi}(\xi)\dot{\xi} \quad \text{Equation 2-7}$$

where $\lambda_T\lambda_{\xi} \geq 0$. They assumed λ_{ξ} to be defined as a linear equation as defined by:

$$\lambda_{\xi} = A\xi + B \quad \text{Equation 2-8}$$

where A and B are material parameters and λ_T introduced the influence of curing temperature as:

$$\lambda_T = \left(\frac{100-T}{100-T_r}\right)^a \quad \text{Equation 2-9}$$

where T_r was the reference temperature for determination of f_{∞} and a regulated the impact of temperature on the ageing degree development. The results of the proposed method were verified through applying the method to several case studies which showed its success in accurately predicting the temperature profile. Some major limitations of the proposed method include i) the 2-D nature of the analysis which makes the model unable to analyse the cases which can-not be simplified to 2-D, ii) The inability of the method to consider different thermal and mechanical boundary conditions, and iii) the inability of the model to calculate thermal stresses and strains.

Martinelli et al. [15] proposed a 1-D theoretical model to simulate the hydration heat of concrete based on the Fourier equation of heat flow. They used finite difference scheme integration in time and space for analysing the concrete element and analysing the evolution of mechanical properties of concrete such as compressive strength, tensile strength and elastic modulus using the proposed method. They claimed to present a

novel technique to correlate the development of the mechanical properties of concrete to the actual hydration process. To do this, they measured the temperature development as an indication of the hydration reaction progress. Martinelli et al. validated their model by measuring the temperature curves under adiabatic and semi-adiabatic conditions. Although, the 1-D nature of this method narrows down the cases that can be analysed using it since all elements can-not be simplified to 1-D. also, different types of thermal and mechanical boundary conditions are not considered in this method.

Kuriakose et al. [59] developed a 1D finite element formulation to predict the temperature evolution of concrete floor slabs during the construction phase. They also extended the developed model to a 2-D prediction model to calculate the temperature profile of thick strip footings and considered wind speed, ambient temperature and radiation as thermal boundary conditions to simulate the environment condition of the concrete element. When accurate data was not available, the ambient temperature in this study was calculated by:

$$T_{air} = -\sin\left(\frac{2\pi(t_d+t_m)}{24}\right) \left(\frac{t_{max}-t_{min}}{2}\right) + \left(\frac{t_{max}+t_{min}}{2}\right) \quad \text{Equation 2-10}$$

where t_d is the clock time of day at which the prediction is being made (0 to 24 hours) and t_m is the time at which the minimum overnight temperature occurs (usually at sun rise) and t_{max} and t_{min} are maximum and minimum daily ambient temperatures. The 1-D and 2-D nature of this method is one of the limitations of the proposed method. Also, the focus of the study is on heat prediction rather than thermal cracking, so the mechanical properties of concrete is not considered. Moreover, the method could not consider the presence of reinforcements in the element under study.

2.4 Mix design Optimisation

2.4.1 Mix design optimisation methods

Mix design optimisation tends to be one of the most preferred solutions for modifying concrete properties. Traditional mix design methods are mostly empirical and tend to focus mainly on achieving targeted mechanical properties, without explicitly targeting durability objectives [19, 76]. The increasing complexity of the mix design process due to the increasing requirements for serviceability and durability, including minimizing the risk of early age thermal cracking, alongside the mechanical performance objectives, call for development of systematic concrete mix multi-objective optimisation methods. Given the complex and non-linear nature of the concrete mix optimisation problem, revolutionary algorithms have been adopted widely as effective solution methods [77]. A number of researches have been conducted focusing on the concrete mix design optimisation. Some of them are briefly explained below.

Lim et al. [68] utilized a Genetic algorithm for designing high performance concrete mix proportions. They set compressive strength and slump of HPC as their objectives and categorized their mix designs based on the desired strength into two ranges: 40-80 MPa and 80-120 MPa. They used multiple regression modelling and fitness function to obtain the optimisation functions. In order to find the fitness functions of compressive strength and slump by multiple regression modelling, in all 181 sets of mixtures were used. Authors assumed that the factors affecting compressive strength are water to binder ratio, water content, fine aggregate ratio, replacement ratio of fly ash, replacement ratio of silica fume, and content of an air-entraining agent; while the factors affecting slump are water to binder ratio, water content, fine aggregate

ratio, replacement ratio of fly ash, replacement ratio of silica fume, an air-entraining agent and content of superplasticizer. Verification of the method indicates 5-35% error for both strength ranges.

Ji et al. [78] proposed a concrete mix proportion design method based on an aggregate to paste approach, Modified Tourfar's Model and artificial neural networks (ANNs). They assumed all concrete characteristics such as strength, slump, average paste thickness and equivalent water-cement ratio to be functions of five mix design parameters including nominal water to cement ratio, equivalent water to cement ratio, average paste thickness, fly ash to binder ratio, grain volume fraction of fine aggregates which can be transformed into each other using the Modified Tourfar's Model. Authors generated the prediction models of strength and slump based on artificial neural networks and calculated the other two mentioned characteristics by reversal deduction of these prediction models. As test data is needed to update the connection weights and biases of ANNs, they used eighteen groups of concrete mix proportions of which half was normal concrete and the other half was fly ash concrete mixed with fly ash and superplasticizer and then verified their method by one mix design example.

Jayaram et al. [77] developed elitist Genetic Algorithm (GA) models for optimising 28 days compressive strength of high-volume fly ash concrete (HVFAC) mix designs. Their methodology consisted of two main stages: firstly, to find the range values for functional parameters and constraint ratios, they performed statistical analysis on 350 mix designs available on standard research publications. Secondly, they optimised the proportions of concrete constituents for maximum strength incorporating the constraints extracted from the first stage. Their analytical method considers three constraints of available range, rational ratio and absolute volume. They used a strength

estimation equation of concrete which reflects the impact of large volumes of fly ash and ran five GA models for optimising HPC mixture proportions corresponding to five different strength ranges. The inputs are the bounds of variables and the constraints and the outputs are optimised quantities of cement, fly ash, and water content. Low MSE values of results are reported in this work compared to those in the literature.

Chaboki-Khiabani et al. [20] presented a method to optimise the mix proportions of high strength concrete after exposure to high temperature. Their goal was to maximize compressive and splitting tensile strength. In order to investigate the effect of mix proportions such as water to binder material, the ratio of fine aggregate to total aggregate, silica fume percentage and the superplasticizer on the remained mechanical properties, they tested 400 cylindrical specimens with sixteen different mix proportions and assessed the results by the Taguchi approach. According to the results, the most effective parameter on the retaining strength is the water to binder ratio. Also, the effect of fine aggregate ratio is significant on compressive strength while the other parameters do not affect the compressive strength. Moreover, the results indicate that superplasticizer has a considerable impact on tensile strength although the other parameters do not affect it much.

Ozbay et al. [79] performed a multi-objective mix proportioning optimisation of high-performance concrete. They evaluated the effect of five parameters consisting of water to binder ratio, total binder content, silica fume replacement ratio, fine to total aggregate ratio and amount of superplasticizer on HPC properties such as slump, compressive strength, splitting tensile strength, modulus of elasticity, ultrasonic pulse velocity, water absorption, water penetration, and chloride ion penetration of mixtures by performing a general linear model analysis of variance (GLM-ANOVA). The

authors utilized mix proportion variables to formulate slump, mechanical and permeation properties via regression technique. The full linear or quadratic regression models are simplified by using a backward stepwise technique. Through multi-objective optimisation, 42 optimum mix proportions were obtained and the ones with highest desirability were produced experimentally. Due to the experimental results, they stated that this method can be used to minimize permeation properties of HPCs.

Xie et al. [21] developed a method for optimising HPC mix designs based on the Genetic algorithm toolbox of MATLAB. They defined the objective function for per cubic meter cost of concrete which implies the amount of cement, water, mineral mixtures, fine aggregate, coarse aggregate and FDN. They also put constraints on the range of mixing parameters such as: water to binder ratio, the volume content of coarse aggregate, the maximum diameter of aggregate, the sand ratio, the amount of binding material, the ratio of water-reducing agent to binding material and expressed them in the form of a series of mathematical programming constraints. The authors then used a Genetic algorithm and direct search toolbox of MATLAB for optimising the functions and applied the method to a certain engineering framework column. The results of applying the method to this case study show a reduction in cement content, increase in fly ash amount and decrease in cost. The rate of reduction is 20.5% while the performance of the concrete is constant.

Ahmadi Nedushan [80] introduced an instance- based machine leaning algorithm called *K* nearest neighbor algorithm (KNNNA) for optimising the compressive strength of high strength concrete mix designs. He used five different models (Standard kNNA, kNNA with inverse distance weighting, kNNA with optimised Minkowski metric, kNNA with attribute selection and kNNA with attribute weighting) to

investigate the effects of the number of neighbors, the distance function and the attribute weights on the performance of the models. The author also developed two different models based on generalized regression neural network (GRNN) and stepwise regression model. He stated that kNNA with attribute weighting has the optimal weights. Therefore, this model performs estimating the compressive strength more precisely compared to other KNNA, GRNN and stepwise regression models. The author proposed the RMS error value of 1.1739 MPa for compressive strengths ranging from 38 to 76 MPa.

Park [81] developed a new genetic algorithm method based on Pareto optimality to optimise the mix design of recycled aggregate concrete. The fitness functions for this multi-objective optimisation were considered as slump, strength, carbonation speed coefficient, price and emission of CO₂. He applied this method to several case studies and reported an increase of the average fitness value indicating that better mixes were obtained.

Ahmad and Alghamdi [19] suggested a statistical method for optimising the concrete mix proportioning based on a statistically planned experimental program. They considered three values as the key factors affecting compressive strength of the concrete including water to cementitious materials ratio, cementitious materials content and fine to total aggregate ratio. The methodology used in their work can be summarized in 5 steps: (i) specifying the characteristic performance of concrete, (ii) selection of the levels of key factors, (iii) experimental work considering trial mixtures using full factorial experiment design for generating data to obtain statistical model for optimisation, (iv) statistical analysis of experimental data and fitting of the strength model, and (v) optimisation of mixture proportions using the fitted strength model. A total of 81 specimens (27 concrete mixtures with three replicates) were tested and the

results were used for generating a polynomial regression model for compressive strength in terms of the mentioned key factors and conducting analysis of variance (ANOVA). The authors concluded that the optimum values of the key factors resulted in a higher compressive strength at a lower cementitious materials content which means significant cost saving in the concrete production.

Rahmani [82] expressed that the main part of concrete mix optimisation is optimising aggregate proportions. He generated a new Sequential Packing Algorithm (SPA) to densify arrangement of arbitrary circles. In order to reach his goal, he optimised the porosity packed circle assemblies utilizing GA. He employed a 2-D boundless space to investigate the packing degree of circles. The main goal of his research is the arrangement of circles with different radii in the densest state. He claimed that the developed model can virtually represent and calculate the packing degree of any particle size distribution of aggregates. Results indicate that the ideal grading curve was proposed based on sand data.

Wang et al. [83] modified Brouwers particle packing mix design method for designing self-consolidating concrete (SCC) mix designs. The target of the proposed method is improving particle packing and reducing paste content while maintaining concrete quality and performance. They designed a large matrix of SCC mixes made of different aggregate types, sizes and supplementary cementitious material (SCMs) types to have a particle distribution modulus (q) ranging from 0.23 to 0.29 and assessed fresh properties (such as flowability, passing ability, segregation resistance, yield stress, viscosity, setting time and formwork pressure) and hardened properties (such as compressive strength, surface resistance, shrinkage, and air structure) of these concrete mixes experimentally. The authors claimed that the proposed method was able to

decrease the binder content by up to 20%, when compared to existing SCC mix proportioning methods, while maintaining good performance at the same time.

Despite the significant achievements in adoption of mix optimisation models to meet several key performance objectives of concrete, there is to date no report on mix optimisation with the objective of minimizing the risk of early age thermal cracking of concrete.

2.4.2 Genetic algorithm optimisation

The nature of concrete mix design optimisation problems is highly non-linear and complex. Thus, among different available optimization methods, revolutionary algorithms such as Genetic Algorithms are one of the best solutions for this type of problems. Genetic Algorithms (GA) are heuristic problem-solving methods that are able to consider different constraints based on natural selection and natural genetics [60]. In general, GAs use a population of individuals each representing a possible solution to a studied problem. Each individual consists of a set of variables called Genes [61]. In each generation of a population, the fitter individuals are able to pass their genes to the next generation. To identify the fitter individuals, the fitness function is calculated for each individual and the next generation is selected based on that. Generally forming the next generation is composed of three operations: Selection, Crossover, Mutation [62]. There are several different methods available for each.

2.4.2.1 Initial population

A Genetic algorithm starts with an assortment of chromosomes as the first generation (initial population). Then, each chromosome in the population is checked to satisfy the constraints and is evaluated by the fitness function to see how well it solves

the problem. Following this, the best chromosomes are selected for reproduction [63]. Several methods are suggested in the literature to select the chromosomes to participate in the production of the next generations. Some will be explained in the next part.

2.4.2.2 Selection

Selection is the process of choosing individuals from the current population to be the parents that participate in producing the next generation. The selection process is based on Darwin's evolution theory which expresses that the best individuals survive and engage in creating new offspring. The aim of the selection process is to keep and emphasize on fitter individuals which leads to generating fitter offspring. Although, strong focus on the fitter individual leads to less diversity needed for the progress, yet weak selections make the evolution too slow. Some of the most common selection methods are Roulette Wheel Selection, Rank Selection and Tournament Selection.

- **Roulette Wheel Selection**

This method includes creating the basis of the next generation based on the stochastic selection from one generation. In this technique for each individual i , a proportional probability $p(i)$ to its fitness $f(i)$ is considered (Eq.5.1). In other words, the fitter individuals are more likely to be selected. The Roulette wheel selection is represented by:

$$p(i) = \frac{f(i)}{\sum_{j=1}^n f(j)} \quad \text{Equation 2-11}$$

where n is the population size. Although the Roulette Wheel Selection is simple and time saving, a main drawback of this method is the probability of premature convergence to a local optimum as the dominant individuals have the greater chance to be selected as a parent.

- **Rank Selection**

In order to escape the premature convergence in the Roulette Wheel Selection method, Rank Selection is generated. In this method, the individuals are ranked after being sorted based on their fitness. The rank of the fittest individual is N , while the rank of the worst individual is 1. The probability of the selection of each individual is calculated by Equation 2-12.

$$P(i) = \frac{rank(i)}{n \times (n-1)} \quad \text{Equation 2-12}$$

Although this strategy is robust, due to almost similar participation of all individuals it may lead to slower convergence.

- **Tournament Selection**

Tournament Selection is an advanced form of Rank Selection. In this method a set of individuals are selected randomly from the population. These individuals are then ranked based on their fitness values and compete to survive. The number of the selected individuals is called tournament size. The fittest individuals are chosen for participation in reproduction [64]. This process is repeated n times for the entire population and the probability for selection of each individual is defined:

$$P(i) = \begin{cases} \frac{c(k-1, n-1)}{c(k, n)} & \text{if } i \in [1, n - k - 1] \\ 0 & \text{if } i \in [n - k, n] \end{cases} \quad \text{Equation 2-13}$$

All individuals have the same chance to enter the selection competition. Therefore, the diversity is guaranteed. However, due to this equal chance the convergence might take a longer time. In general, this method is one of the most popular selection methods due to its efficiency and simple implementation [65]. The

selected chromosomes will undergo crossover and mutation process for reproduction. These two operations are explained in the next sections.

2.4.2.3 Crossover

Crossover is an operation which mixes the genetic information of two parents to produce the new offspring. Crossover picks some parts of the bit strings of both parents and combines them in the child. This is how to generate new offspring stochastically from the current population. In order to control the number of individuals which undergo the crossover operation, crossover rate is defined. Crossover rate is the ratio of the number of the children generated in each generation by crossover to the population size. By considering higher crossover ratios, the operator will be able to find the solution in a larger space which leads to reduction in the possibility of finding a false optimum. However, this may increase the computation time noticeably. Some of the most common crossover methods are single-point crossover, N -point crossover, uniform crossover, intermediate crossover, heuristic crossover and arithmetic crossover.

- **Single-point crossover**

Single-point crossover is one of the most used crossover methods. In this method a random spot is selected in both parental chromosomes, and both chromosomes are split at this point. Then, the two parts of the chromosomes next to the cross location are swapped and generate new offspring (Figure 5-2). In single-point crossover, if both parts of the chromosome have good genetic material, the generated offspring will not get good features directly [66–69].

- **N -point crossover**

The general rule of N -point crossover is similar to single-point crossover. In these methods, there are N cutting points instead of one. Two-point crossover is more common among all as adding more crossing points increases the probability of the disruptions of building blocks and may reduce the performance of Genetic algorithm. However, an advantage of having more crossover points is that the problem space may be searched more thoroughly [66–69].

- **Uniform crossover**

Uniform crossover does not split parental chromosomes for generating the next generation. This method exchanges individual bits instead of segments of the bit array and uses a binary crossover mask to choose the offspring bits from. The length of this mask is the same as the length of the parental chromosomes. The bit will be copied from the first parent if the bit in crossover mask is equal to 1, and the bit will be taken from the second parent if the crossover mask is 0. Therefore, the new offspring is a random mixture of genes from both parents [66–69].

- **Intermediate crossover**

Intermediate crossover uses a weighted average of the parents for recombination. This method uses a parameter *Ratio*:

$$offspring = parent1 + rand * Ratio * (parent2 - parent1)$$

Equation 2-14

where the *ratio* can be a scalar or a vector of scalars. If *Ratio* has a value between 0 and 1, the offspring are within the hypercube by the parent's locations at opposite vertices [70].

- **Heuristic crossover**

Heuristic crossover uses the fitness values of two parental chromosomes to generate new offspring. It starts from the worst parent and moves towards parents with better fitness value. Equation 2-15 and Equation 2-16 are used to generate the new offspring:

$$\text{Offspring } A = \text{BestParent} + \beta * (\text{BestParent} - \text{WorstParent})$$

Equation 2-15

$$\text{Offspring } B = \text{BestParent}$$

Equation 2-16

where β is a random number between 0 and 1 [69,71].

- **Arithmetic crossover**

In this technique, new offspring are the weighted arithmetic mean of two parents. Two chromosomes are selected randomly for crossover and the children are a linear combination of the parents. The offspring is calculated using:

$$\text{Offspring} = \alpha \times \text{BestParent} + (1 - \alpha) \times (\text{WorstParent}) \quad \text{Equation 2-17}$$

2.4.2.4 Mutation

Mutation is a genetic operator that aims to preserve diversity between different generations. By preventing the new individuals from becoming similar, mutation helps the algorithm to avoid local optimum. It is the random change of one or more bits of the parents' chromosomes. This operator protects the Genetic algorithm process from premature loss of potentially useful genetic material. Each gene is likely to change with a pre-defined probability (typically 0.001). Mutation may change the chromosomes entirely. Therefore, in order to avoid a primitive random search, the mutation

probability should be set low. In order to control mutation, mutation rate is defined. Mutation rate is the percentages of the number of the genes that are altered by mutation to the total number of the genes in the population. If the mutation rate is set relatively high, the individuals of the next generation lose their resemblance to their parents and this causes the algorithm to lose the ability to learn from the previous generations. If the rate is too low, the useful genes will never have the chance to be tried out. Some of the most common mutation methods are Inversion Mutation, Flip Mutation, Reversing Mutation, Uniform Mutation, Gaussian Mutation, Adaptive Feasible Mutation, [63, 72–74].

- **Inversion Mutation**

In this method two bits are selected randomly and the bits between them are inverted. Although it keeps most of the genetic information and only breaks two links, it causes the disruption of order information [63, 74].

- **Flip Mutation**

Flip mutation is mostly used in binary encoding. Flipping a bit of a chromosomes means changing 0 to 1 and 1 to 0. In this technique, a random bit of the parental chromosome flips and the new generation produces [63].

- **Reversing Mutation**

This method is used for binary encoding as well. In Reversing mutation, a random spot is selected in the chromosome and the bits next to this spot are reversed [63].

- **Uniform Mutation**

In this method, the user specifies a lower and an upper bound and a uniform random value is selected in this range and this value is added to a random gene [74].

- **Gaussian Mutation**

In Gaussian mutation, a random number from a Gaussian distribution with mean 0 is added to the bits of parental chromosomes [72].

- **Adaptive Feasible Mutation**

This method considers the previous successful or unsuccessful generations and generates a random direction accordingly that satisfies the constraints. This method is one of the best for constrained problems [63, 74].

2.4.2.5 Constraints

If there are special specifications of decision variables in the problem, the Genetic algorithm does not optimise the fitness function in a random space, and this is called a constrained optimisation problem. These constraints can be equality or inequality relations. The parameters that are generated by Genetic algorithm will be tested under consideration, objective function (to be minimized or maximized) and the constraints. If the constraints are violated, the set of parameters are considered to be infeasible and have no fitness. If there are no violations, the objective function gives the parameter set a fitness value [75].

2.4.2.6 Fitness function

Fitness functions are calculated based on the chromosome which is a set of decision variables. Decision variables are the numerical quantities that are to be selected in an optimisation problem [63].

2.5 Construction strategies to mitigate early age thermal cracking

Several strategies have been proposed in the literature to reduce the risk of early age thermal cracking. These methods aim mainly to reduce internal heat generation by specifying a lower cement content or partial replacement of cement with supplementary cementitious materials (SCMs), exhausting the generated heat by cooling the mixing water and/or the aggregates before mixing operations or using cooling pipes in concrete, postponing the peak of heat utilizing retarders, adopting concrete construction schedules such as sequence concrete pouring, lowering the placement temperature, using lower thermal expansion aggregates, etc. that maintain temperature gradients in concrete below the prescribed limits [3, 11]. Although, altering mix design for achieving lower risks of early age thermal cracking is favoured since it needs less effort and is more economic, sometimes changing the mix design alone cannot reduce the heat of hydration enough and several complementary techniques must be applied in the construction stage.

- **Sequential construction**

CIRI C660 guidelines on early age thermal cracking [3] specify that lowering the degree of restraint is one of the most economic methods for reducing the risk of early age thermal cracking [3]. This can be achieved through planning the sequence and timing of concrete placement and involves usually dividing a large pour into multiple smaller pours. For huge concrete elements, concrete casting happens in several bays or

lifts and is called “alternate bay” or “sequential” construction. Several studies have investigated the impacts of sequence casting and some of them will be briefly explained.

Mari [84] proposed a numerical simulation method for the nonlinear and time dependent three-dimensional analysis of segmentally cast reinforced and prestressed concrete. They investigated the structural impacts of the load and temperature development, nonlinear behaviour of the materials, shrinkage, concrete ageing, relaxation of prestressed steel, and nonlinear geometry. As changing geometry, loading and boundary conditions were possible in this method, the author claimed that this was a suitable method for simulating current construction strategies. They applied this method on a numerical example and used the proposed method to predict the behaviour of the concrete during the construction stage. The results proved that the method was able to accurately capture the development of stresses, strains, deflections, reactions and internal forces along the time, including the interaction between concrete cracking and time dependent materials behaviour.

Kwak et al. [85] studied the effect of sequent casting a slab deck on the short-term and long-term behaviour of steel box girder bridges. They considered continuous casting and three sequence casting strategies for comparison. They claimed that the impacts of slab casting sequence were negligible for short-term and long-term behaviour of the bridge and resulting moments; and therefore, continuous casting was recommended for closed box sections used in South Korea.

Dezi et al. [86] developed a finite element model to analyse the construction of continuous composite steel-concrete decks in which slab segments were cast in situ by using travelling formworks leaning on un-propped steel beams. This model considered

thermal shrinkage, creep, loading phases during different construction stages and deformability of the shear connectors. They modelled the materials as linear materials and assumed that when the optimised sequence of casting was used; no cracking was observed. This causes limitations in reliably predicting the behaviour of concrete. They used the finite element method to simulate the model and applied the proposed method to a real bridge deck. Two different construction strategies were considered including continuous pour from one end to the other end of the deck and the optimised scheme. Dezi et al. concluded that optimising sequent casting is an important factor in limiting tensile stresses of the slab during the construction stage and optimised sequence pour led to much lower tensile stress.

- **Lowering placement temperature**

Reducing the initial temperature of concrete is used commonly as an effective method to reduce the risk of early age thermal cracking in the literature [2, 3, 87, 88]. Bamford mentioned that lower placement temperatures causes slower rate of heat development and lower temperature rise within the concrete section, longer stiffening time and lower rate of workability loss. This can be achieved by several different strategies including cooling the mix constituents before mixing, use of ice in the mix water, use of liquid nitrogen to cool the mix right before concrete placement, cooling the formwork by spraying cold water before concrete placement, and casting in the late afternoon. These methods are briefly explained below [3].

- **Pre-cooling the concrete components**

Cooling one or all of the concrete components before mixing is the most common method of reducing the initial temperature of concrete. This can be achieved by storing aggregates in shade to avoid direct sun exposure, controlled water sprinkling

of the aggregates, painting all exposed pipes and tanks in white, cooling mix water using ice, utilizing liquid nitrogen to cool the aggregates, blowing chilled air through the aggregate stockpiles, and spraying water on aggregates on a slow-moving belt. It is mentioned that since aggregates have the largest portion in a concrete mix, cooling the aggregates significantly affects the concrete temperature. Bamford expressed that while aggregates have the greatest mass in concrete, water has the most heat capacity. Therefore, cooling the mix water is an effective method of cooling the concrete mix as well [3].

- **Cooling of the fresh concrete before placing**

Liquid nitrogen makes it feasible to cool the concrete mix on site. The method for using the liquid nitrogen is to spray a mist of liquid nitrogen into the mixer at a controlled rate. The heat for boiling of the liquid nitrogen is about 60% of that for melting ice and the efficiency of this method is about 100% in practice [3].

- **Using aggregates with lower thermal expansion aggregates**

Coefficient of thermal expansion (CTE) defines how the size of an object changes with a change in temperature. CTE of concrete is an important factor affecting the risk of early age thermal cracking. Because of the dominancy of the aggregates in a concrete mixture, the CTE of concrete is mainly dependent on the CTE of the used aggregates in the mix design [3]. Therefore, using the aggregates with a lower thermal expansion coefficient reduces the thermal expansion of concrete in total. Since the concrete elements are mostly restrained and restricted, lower thermal expansion coefficient leads to lower expansion because of the heat of hydration and successive reduction in thermal cracking [89]. The coefficient of thermal expansion of different

aggregate types can be found in the literature or defined using the experimental test results [3].

- **Internal water-cooling system**

Cooling concrete after casting can be conducted using two methods: using an embedded cooling system such as a network of water pipes within the core of the pour and surface cooling with water. Using the former method is preferred as it can be used for any mix design. Pumping chilled water or air through a network of pipes absorbs the heat of hydration of the materials and reduces the temperature rise in concrete. When designing this system, it should be noted that it must remove heat at a certain rate without inducing an excessive internal temperature gradient. Designing the embedded cooling systems can be undertaken using ACI Report 207.IR-35. Several researches have been conducted focusing on cooling systems.

Hedlund and Growth [11] developed an easy-to-use experimental method to establish the relationship between the heat transfer coefficient and the flow in cooling pipes. They determined heat transfer coefficients for two different cooling pipes for different pipe flows in combination with various temperature levels experimentally. They used the piping system shown in Figure 2-6.

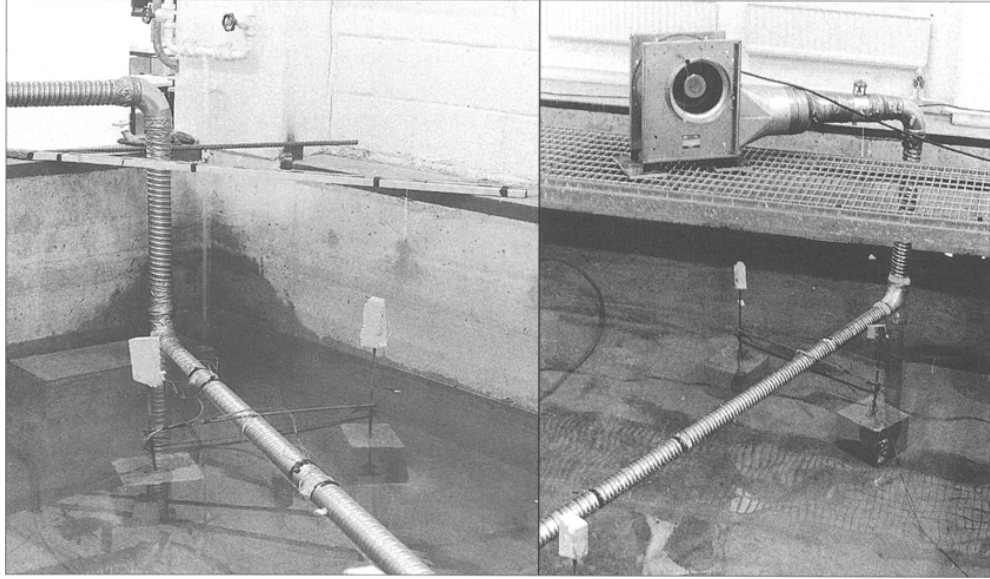


Figure 2- 8 Basin with mounted cooling pipe (strand tube) [11]

Charpin et al. [90] proposed explicit expressions for the peak temperature of concrete as a function of the driving parameters for a simple cylindrical model shown in Figure 2-7. They also determined expressions for the required pipe length and the separation distance to limit the peak temperature to a prescribed amount. The heat equations for concrete and water were evaluated as below.

$$\rho_c c_c \frac{\partial T_c}{\partial t} = \kappa_c \nabla^2 T_c + q \quad \text{Equation 2-18}$$

$$\rho_w c_w \left(\frac{\partial T_w}{\partial t} + u \cdot \nabla T_w \right) = \kappa_w \nabla^2 T_w \quad \text{Equation 2-19}$$

where T_c , T_w are the temperature of the concrete and the water in the pipe, q is the rate of heat production per unit volume in the concrete, and (ρ_c, c_c, κ_c) , (ρ_w, c_w, κ_w) are the density, specific heat and conductivity of concrete and water respectively. The boundary condition at all boundaries was defined as:

$$\kappa_w \frac{\partial T_w}{\partial r} = H(T_c - T_w) \quad \text{Equation 2-20}$$

where r is the radius of the cylinder. The temperature distribution in the concrete slab was locally defined as:

$$T_c(s, r) = T_w(s) + \frac{1}{4}(1 - r^2) + \frac{1}{2}[\ln r + \sum_{i,j} \ln r_{ij}] \quad \text{Equation 2-21}$$

where $T_w(s) = T_0 + \frac{s}{2\epsilon\xi}$ is the temperature of the pipe water at a distance s measured along the pipe from the inlet.

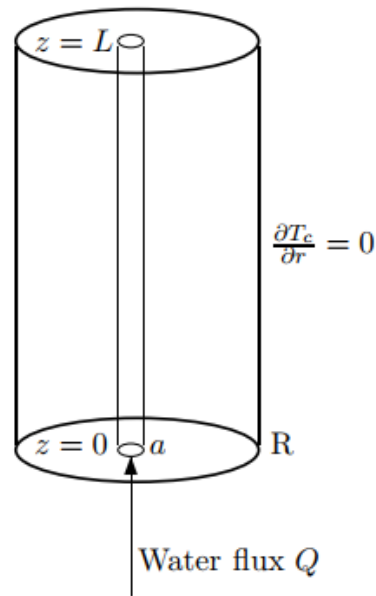


Figure 2- 9 Cylindrical model: water flux Q at temperature T_0 through a pipe cools an insulated concrete cylinder [90]

Qiang et al. [91] used a p -version self-adaption method into the improved embedded simulation of concrete temperature history for elements containing water pipes. They defined the temperature field function as:

$$T_p = \sum_{i=1}^{f_e(p)} \phi_i T_i \quad \text{Equation 2-22}$$

where ϕ_i is the i^{th} base function in an element, T_i is the corresponding temperature, and $f_e(p)$ is the number of base functions in the element, including the point base function,

line base function, face base function, and volume base function. Qiang et al. claimed that the proposed technique performed better in pre-processing of the finite element model since more than one pipe segment can be arranged in one element and complicated geometries could be modelled. They applied the developed method on four different numerical case studies and showed the ability of the model to reach higher accuracy and efficiency.

Hong et al. [92] proposed a semi-analytical singular boundary method formulation for modelling the thermal field in a concrete element including a water pipe cooling system. They simplified the problem into a two-dimensional problem considering Dirichlet boundary conditions. They used two case studies for verifying the method and showed that their methodology can be used as an alternative tool for analysing the heat conduction problem in concrete structures with embedded water pipes.

2.6 Conclusions

A review of available literature on factor affecting the risk of early age thermal cracking as well as strategies and methods available to estimate and minimize the risk of early age thermal cracking was presented. Several gaps in the available literature were identified which provide directions for the research conducted in this thesis and future research in the field. These include: i) a lack of evidence on applicability of existing models for heat of hydration to Australian cement and the ability of such models in capturing the effect of admixtures and SCMs, ii) a lack of a comprehensive three-dimensional numerical simulation model for early age thermal cracking of concrete that allows customization of element geometry, materials properties and the models adopted in performing the analysis, iii) a lack of a mix design optimisation

method to reduce the risk of early age thermal cracking and iv) a lack of numerical simulation model to evaluate the effective of different strategies to reduce the risk of early age thermal cracking of concrete.

Chapter 3: Precision of cement hydration heat models in capturing the effects of SCMs and retarders

3.1 Introduction

Chemical reaction of cementitious materials is an exothermic reaction and the heat generated due to cement hydration causes the internal temperature of concrete to increase. This hydration induced internal heating and the subsequent cooling is main cause of early age thermal cracking especially in high performance and mass concrete. Accordingly, estimating the hydration heat generated in a particular concrete element is a key input to predicting the temperature rise and therefore the risk of early age thermal cracking of the concrete element. In order to predict the risk several hydration heat prediction models have been developed in previous studies and applied extensively in numerical simulation of temperature rise in concrete [28, 29, 31]. Furthermore, given the direct effect of precision of hydration heat models on precision of temperature rise and thermal cracking risk predictions, previous studies have extensively investigated and verified the predictions of the existing hydration heat estimation models for different cement compositions [4, 31, 93]. However, in addition to composition of cement, the amount of hydration heat can be affected significantly by presence and quantity of other supplementary cementitious materials (SCMs) as well as admixtures including retarders [4, 31, 93]. However, despite the already high and growing use of SCMs and retarders in the concrete industry, little effort has been made to investigate the accuracy of existing hydration heat models in capturing the effect of SCMs and retarders on heat of hydration. This chapter presents the results of a series of isothermal calorimetry tests conducted i) to investigate the effects of Class F fly ash, GGBFS and three commonly used retarders (viz. Retarder N, Sucrose and Citrate) on the heat of

hydration profile of Australian general-purpose cement. The choice of SCMs and retarders considered in this study is supported by their widespread use in high performance and mass concrete mixes which are commonly prone to risk of early age thermal cracking [2,3]; and ii) to evaluate the precision of the two most commonly used hydration heat models in capturing the effects of fly ash, GGBFS, retarders and curing temperature on the hydration profile. The measurements are performed under different curing temperatures of 10, 23 and 30 °C to evaluate the effect of the curing temperature on the results.

3.2 Existing Models for Hydration Heat Prediction

The focus of this study is placed on evaluating the precision of the Schindler and Folliard model [16] and the Bogue model [18] as most commonly used models for heat of hydration (as described in detail in Chapter 2). These models are briefly described in the following.

3.2.1 Schindler and Folliard model

In this model, the total heat of hydration of Portland cement is estimated based on the composition of cement as [16]:

$$H_{cem} = 500p_{C_3S} + 260p_{C_2S} + 866p_{C_3A} + 420p_{C_4AF} + 624p_{SO_3} + 1186p_{FreeCaO} + 850p_{MgO} \quad \text{Equation 3-1}$$

where, H_{cem} is the total heat of hydration of the cement (J/g), and p_i is the weight percentage of cement component i . Furthermore, given total cementitious materials content (Cc) (g/m³) and the total heat of hydration of cementitious materials at 100% hydration (Hu) (J/g), the ultimate heat of hydration of the concrete (H_T) is estimated as follows:

$$H_T = H_u \cdot C_c \quad \text{Equation 3-2}$$

where,

$$H_u = H_{cem} \cdot p_{cem} + \sum h_i \cdot p_i \quad \text{Equation 3-3}$$

In this equation, p_{cem} is the weight ratio of cement content in the total cementitious content, H_{cem} is the total heat of hydration of cement, p_i is the weight ratio of SCM i in terms of the total cementitious materials, and h_i is the heat of hydration of SCMs (J/g). The rate of heat generation ($Q_H(t)$) is defined as a function of degree of hydration, $\alpha(t_e)$, which is itself a function of time and temperature [17]:

$$Q_H(t) = H_u \cdot C_c \cdot \left[\frac{\tau}{t_e}\right]^\beta \cdot \left(\frac{\beta}{t_e}\right) \cdot \alpha(t_e) \cdot \frac{E}{R} \left(\frac{1}{273+T_r} - \frac{1}{273+T_c}\right) \quad \text{Equation 3-4}$$

where, $\alpha(t_e)$ is the degree of hydration at equivalent age t_e ; τ , β , E and R are the hydration time parameter (hours), hydration shape parameter, activation energy (J/mol) and universal gas constant (8.3144 J/mol/K), respectively, and α_u , T_c and T_r are the ultimate degree of hydration, average concrete temperature ($^{\circ}\text{C}$) and reference temperature ($^{\circ}\text{C}$), respectively. The following s-shape model is used by Schindler and Folliard [16] to estimate $\alpha(t_e)$:

$$\alpha(t_e) = \alpha_u \cdot \exp\left(-\left[\frac{\tau}{t_e}\right]^\beta\right) \quad \text{Equation 3-5}$$

where t_e is the equivalent age at the reference curing temperature (hours or days), and can be estimated by:

$$t_e(T_r) = \sum_0^t \exp\left(\frac{E}{R} \left(\frac{1}{273+T_r} - \frac{1}{273+T_c}\right)\right) \cdot \Delta t \quad \text{Equation 3-6}$$

In addition, τ , β and α_u can be estimated using the following best-fit multivariate regression models:

$$\tau = 66.78 \cdot p_{C_3A}^{-0.154} \cdot p_{C_3S}^{-0.401} \cdot Blaine^{-0.804} \cdot p_{SO_3}^{-0.758} \cdot \exp(2.187 \cdot p_{SLAG} + 9.5 \cdot p_{FA} \cdot p_{FA-CaO}) \quad \text{Equation 3-7}$$

$$\beta = 181.4 \cdot p_{C_3A}^{-0.146} \cdot p_{C_3S}^{-0.227} \cdot Blaine^{-0.535} \cdot p_{SO_3}^{-0.558} \cdot \exp(-0.647 \cdot p_{SLAG}) \quad \text{Equation 3-8}$$

$$\alpha_u = \frac{1.031 \cdot \frac{w}{c}}{0.194 + \frac{w}{c}} + 0.5 \cdot p_{FA} + 0.3 \cdot p_{SLAG} \leq 1.0 \quad \text{Equation 3-9}$$

where, p_{C_3S} , p_{C_3A} , p_{C_2S} , p_{SO_3} , are the weight ratios of C_3S , C_3A , C_2S and SO_3 compounds in Portland cement, respectively and p_{GGBFS} , p_{FA} and p_{FA-CaO} are the percentages of slag, fly ash and CaO content of cementing materials, respectively. $Blaine$ [m²/kg] is the Blaine value of cement and w/c is the water to cementitious material ratio.

3.2.2 Original and modified Bogue models

The model developed by Bogue [18] to quantify the total heat of hydration is the same as Equation 1. For the purpose of simulating the effect of a blended cementitious system, Maekawa et al. (2009) developed and tested a multi-component hydration heat model based on the Bogue model, which considers the addition of blast furnace slag, fly ash and silica fume as follows:

$$H_{cem} = \sum P_i H_i = p_{C_3A}(H_{C_3AET} + H_{C_3A}) + p_{C_4AF}(H_{C_4AFET} + H_{C_4AF}) + p_{C_3S}H_{C_3S} + p_{C_2S}H_{C_2S} + p_{SG}H_{SG} + p_{FA}H_{FA} + p_{SF}H_{SF} \quad \text{Equation 3-10}$$

where, H_i is the heat generation rate of mineral i per unit weight; p_{SG} , p_{FA} and p_{SF} are the weight percentages of slag, fly ash and silica fume of total cementing materials, respectively. H_{C_3AET} and H_{C_4AFET} are the heat components associated with the formation of ettringite. The heat generation rate of mineral i can be estimated by [94]:

$$H_i = \gamma_i \cdot \beta_i \cdot \lambda_i \cdot \mu_i \cdot H_{i,T_0}(Q_i) \exp\left(-\frac{E}{R}\left(\frac{1}{T} - \frac{1}{T_0}\right)\right) \quad \text{Equation 3-11}$$

accounts for reduction in heat generation rate due to reduced availability of free water, λ_i is a coefficient that accounts for the change in heat-generation rate of the powder admixtures (slag, silica fume), and μ_i is a coefficient that accounts for the change in the heat-generation rate in terms of interdependence between alite and belite in Portland cement. Consequently, the total heat generation of component i over a given time period can be estimated as:

$$Q_i = \int H_i dt \quad \text{Equation 3-12}$$

The hydration parameters used in the Bogue Method considering the usage of retarders are:

$$\tau = \exp(2.68 - 0.386 \cdot p_{C3S} \cdot p_{cem} + 105 \cdot p_{Na2O} \cdot p_{cem} + 1.75 \cdot p_{GGBFS} - 5.33 \cdot p_{FA} \cdot p_{FA-CaO} - 12.6 \cdot ACCL + 97.3 \cdot WRRET) \quad \text{Equation 3-13}$$

$$\beta = \exp(-0.494 - 3.80 \cdot p_{C3A} \cdot p_{cem} - 0.594 \cdot p_{GGBFS} + 96.8 \cdot WRRET + 39.4 \cdot LRWR + 23.2 \cdot MRWR + 38.3 \cdot PCHRWR + 9.07 \cdot NHRWR) \quad \text{Equation 3-14}$$

$$\alpha_u = \frac{1.031 \cdot \frac{w}{cm}}{0.194 + \frac{w}{cm}} + \exp(-0.885 - 13.7 \cdot p_{C4AF} \cdot p_{cem} - 283 \cdot p_{Na2Oeq} \cdot p_{cem} - 9.90 \cdot p_{FA} \cdot p_{FA-CaO} - 339 \cdot WRRET - 98.4 \cdot PCHRWR) \quad \text{Equation 3-15}$$

$$E_a = 41230 + 8330 \cdot (p_{C3S} + p_{C4AF}) \cdot p_{cem} + 8330 \cdot Gypsum \cdot p_{cem} - 3470 \cdot Na_2O_{eq} - 19.8 \cdot Blaine + 2.96 \cdot p_{FA} \cdot p_{FA-CaO} + 162 \cdot p_{GGBFS} - 516 \cdot p_{SF} - 30900 \cdot WRRET - 1450 \cdot ACCL \quad \text{Equation 3-16}$$

where, *Gypsum* is the weight ratio of gypsum in Portland cement and *WRRET*, *PCHRWR*, *LRWR*, *MRWR*, *NHRWR* and *ACCL* are dosages of type B and type D water

reducer/retarder, type F Polycarbocylate based high range water reducer, type A water reducer, midrange water reducer, type F naphthalene high range water reducer, and type C accelerator, respectively. All chemical admixture dosages are in percent solids by weight of cementing material. The execution of both models implemented a reference temperature of 21° C.

3.3 Methodology

3.3.1 Materials

The materials and the isothermal calorimetry methodology used in this study are described in the following.

The chemical composition of General Purpose cement (AS 3972-2010 [95]), Class F fly ash (FA), and GGBFS used in this chapter are summarized in Table 3-1. Cement replacement percentages of 0%, 20%, 40% and 50% were investigated for Fly ash and GGBFS. These replacement percentages were selected by considering the minimum and maximum recommended fly ash and GGBFS contents highlighted in previous studies [96–98]. Furthermore, three common types of retarding admixtures, namely Retarder N (Sika®), Sucrose and citrate (Table 3-2), are used. Retarder N is tested at dosages of 0, 2.5, 5, and 10 mL/kg, while Sucrose and Citrate are tested at dosages of 0, 0.05, 0.1, and 0.2% by weight [99–101]. To ensure that the chemical composition of water is consistent between all samples, purified ultra-pure Milli-Q (MQ), water is used.

3.3.2 Calorimetry measurements

A TAM-AIR isothermal calorimeter is used to measure the heat of hydration of different mixes investigated in this chapter. The instrument comprises eight-channels housed in an air-based thermostat as a single heat-sink block which conducts the heat

away from the sample and effectively minimizes outside temperature effects. The principal mechanics behind this instrument are defined by measuring the fluctuation in heat flow between the active sample and a reference sample. The eight-channel calorimeter used in this study has a reported precision of $\pm 20 \mu\text{W}$. Furthermore, the thermostat uses circulating air and an advanced regulating system to keep the temperature stable within $\pm 0.02 \text{ }^\circ\text{C}$ which makes the measurements accurate and stable over time [102]. The heat liberated from the active sample creates a heat flow and a temperature gradient that is converted into a voltage signal proportional to the heat flow. The heat flow from the active sample is then compared to that of the inert reference. The voltage difference is representative of the heat generated within the active sample. The TAM Assistant Software monitors the heat liberation throughout the entirety of each experiment and records the heat flux of the active samples almost continuously (every 1-2 seconds). The water to binder ratio was 0.45 for all the experiments. According to ASTM C1702 [50], the difference between sample's temperature and test temperature should not exceed $1 \text{ }^\circ\text{C}$. Therefore, the use of smaller samples ($< 6 \text{ g}$ dry cement) is generally recommended to ensure isothermal condition throughout the test [102]. The total weight of the samples and mixing time are 7 g and 2 minutes , respectively. The measurements are undertaken at temperatures of 10 , 23 and 30°C to investigate the effects of curing temperature on heat of hydration and the accuracy of hydration heat models in capturing this effect. The duration of the experiments is between 3 and 6 days.

3.4 Results and discussion

3.4.1 The effect of SCMs and retarders on hydration curves

- **Fly Ash**

Figure 3- 1a demonstrates the effect of the variation in FA content on the hydration heat. When comparing the cement mix containing 20% FA with the reference mix, the results indicate 22% decrease in the peak heat flow value. Similarly, at FA replacement levels of 40% and 50%, the peak heat flow is reduced by 39% and 51% compared to the reference sample, respectively. Figure 3- 1a reveals that the addition of FA significantly affects the early age hydration kinetics, especially in the first 48 hours, while having minimal effect on heat of hydration after 3 days. The replacement level of FA can also be shown to have an impact upon the initiation time of the acceleration phase and the duration of the acceleration and deceleration phases.

Table 3- 1 Chemical compositions for OPC, Class F FA and GGBFS (%)

Oxide	OPC	Class F FA	GGBFS
Sodium oxide (Na ₂ O)	0.30	0.68	0.44
Magnesium oxide (MgO)	1.03	0.70	5.57
Aluminum oxide (Al ₂ O ₃)	4.96	22.36	13.79
Silicon dioxide (SiO ₂)	18.8	66.06	0.44
Phosphorus oxide (P ₂ O ₅)	0.10	-	0.02
Sulphur trioxide (SO ₃)	3.00	0.09	2.45
Potassium oxide (K ₂ O)	0.66	1.82	0.28
Calcium oxide (CaO)	63.8	1.65	41.49
Titanium oxide (TiO ₂)	0.26	0.89	1.349
Vanadium pentoxide (V ₂ O ₅)	0.01	-	-
Manganese oxide (Mn ₃ O ₄)	0.15	0.07	0.41
Iron oxide (Fe ₂ O)	2.84	3.45	0.55
Loss of ignition (LOI)	4.45	1.34	0.13

Table 3- 2 Technical data for retarders

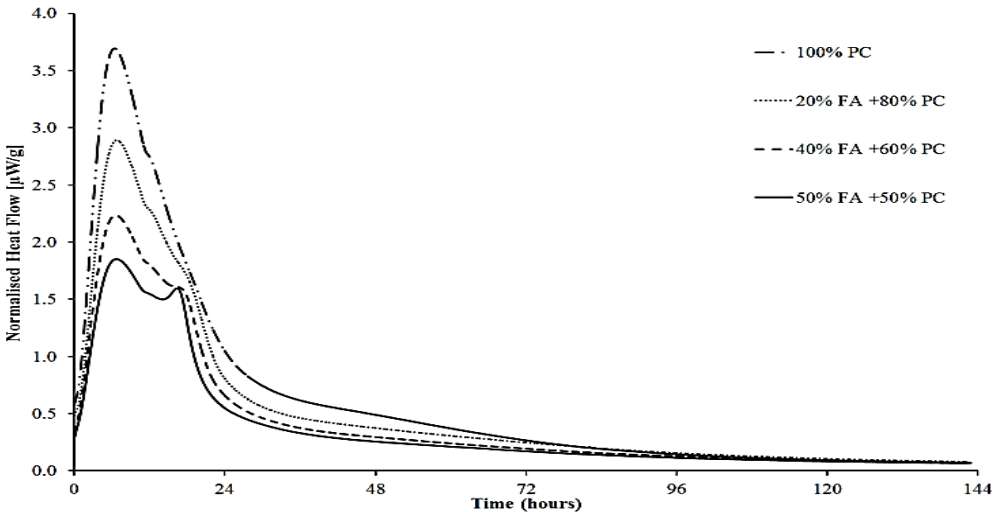
Retarder	Form	Empirical Formula	pH value	Other Characteristics
Retarder N	Liquid-selected carbohydrates	-	Approx. 7.5-9.5	-
Citrate (Tri-sodium dihydrate)	White crystalline granules	$\text{Na}_3\text{C}_6\text{H}_5\text{O}_7 \cdot 2\text{H}_2\text{O}$	7.5-9 (5% Solution)	Soluble in H_2O , clear, colorless
Sucrose	Granules	$\text{C}_{11}\text{H}_{22}\text{O}_{11}$	5.5-7 (1M in H_2O)	Soluble in H_2O , clear, colorless

The results particularly indicate that the dormant period is prolonged with increasing replacement levels of FA. Therefore, the initiation of the acceleration phase is retarded with time at higher replacement levels. The combined effect of delaying the acceleration phase and prolonging the peak of the hydration curve signifies that the reaction is being slowed. This is in accordance with previous works showing that higher replacement levels of FA contribute to minimize the peak heat evolution of a cement paste [16].

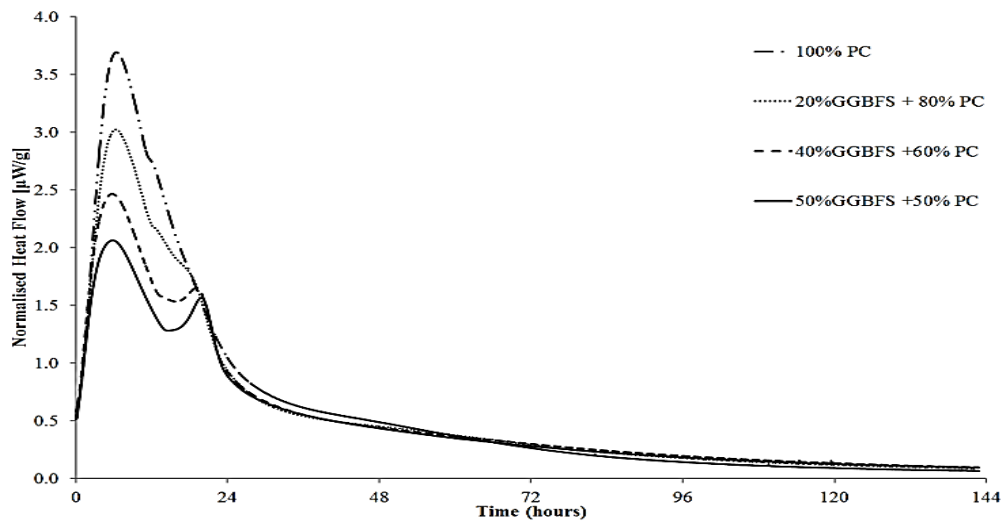
- **Ground granulated blast furnace slag**

Figure 3- 1b demonstrates that an increase in the GGBFS content in cement results in a relatively proportional decrease in the peak heat evolution of the hydration process. The results indicate that 20% cement replacement with GGBFS results in about 19% decrease in the peak heat flow. This difference is 34% and 43% for replacement levels of 40% and 50%, respectively. The occurrence of the peak flow

follows a dissimilar pattern compared with FA, with the peak occurring slightly earlier at higher GGBFS content. In addition, the initiation of the acceleration phase occurs almost simultaneously for each replacement level. It can also be seen in Figure 3- 1b that the hydration curves for each replacement level follow a consistently linear pattern for the first half of the acceleration phase. The curves deviate from the linear acceleration period preceding the peak heat flow. This indicates that the rate of heat evolution is consistent for the early age hydration, up to 4 hours, for each replacement level. However, following the initial linear acceleration, the hydration curves differ with changing replacement levels. Figure 3- 1b illustrates that after 3 days the rate of heat evolution of the reference mix becomes comparable to that of the cement pastes that incorporate GGBFS. Moreover, considering Figure 3- 1a and 3- 1b it can be seen that increasing the amount of cement replacement causes a second peak in the heat evolution curve. This can be the result of the hydration of C_3A or aluminate phase in the system due to the presence of FA and GGBFS [94].



a.



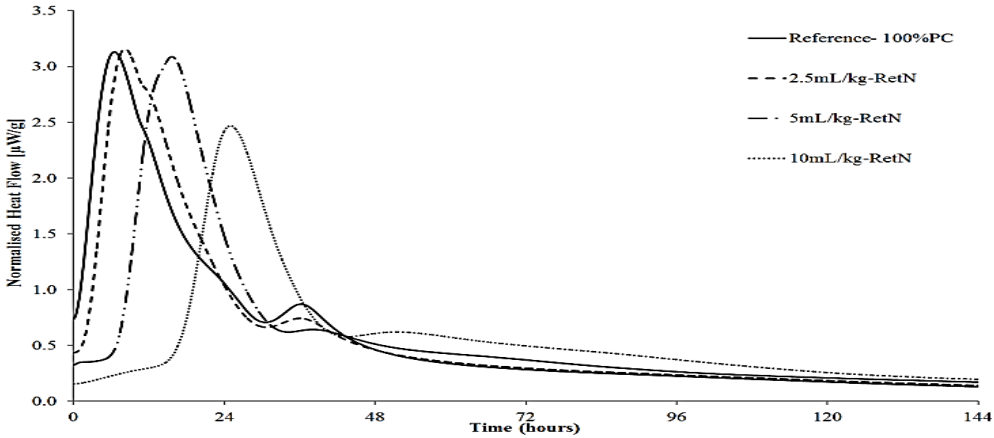
b.

Figure 3- 1 Heat evolution for OPC pastes with different levels of a. Class F FA and b. GGBFS

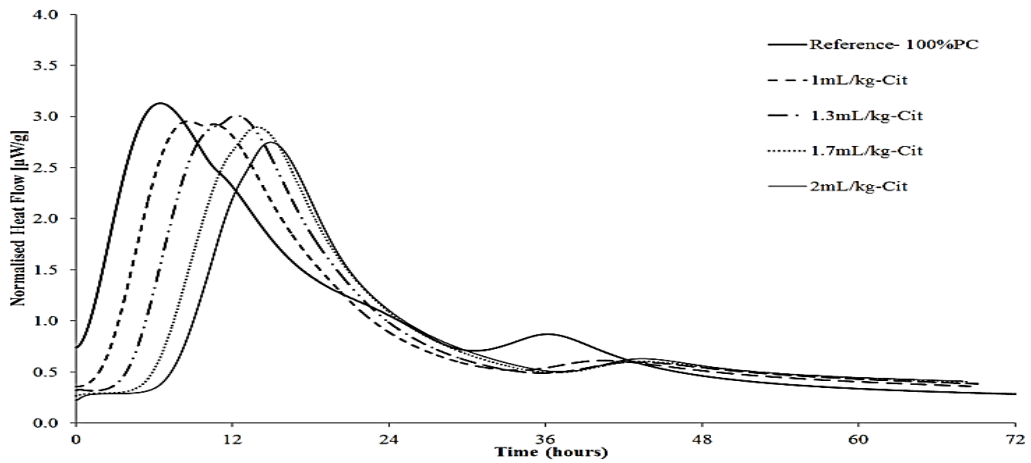
• Retarders

Figures 3- 2a, b and c show the variations in the rate of heat evolution of cement after addition of various dosages of Retarder N, Citrate and Sucrose retarders, respectively. Figure 3- 2a shows that for the small incremental dosages of Retarder N, the peak heat evolution is gradually retarded. In particular, about 24% decrease in the heat peak (from 3.2 $\mu\text{W/g}$ to 2.45 $\mu\text{W/g}$) is observed at the maximum studied Retarder N dosage of 10 mL/kg. Figure 3- 2b indicates that the end of the dormant period is retarded near proportionally with an increase in the dosage of Citrate. At Citrate concentrations of 1, 1.3, 1.7 and 2 mL/kg, the end of the dormant period is retarded by 3, 4.5, 6.5 and 8 hours, respectively. Furthermore, the magnitude of the peak heat evolution is gradually reduced by about 16%, compared to the reference (from 3.2 $\mu\text{W/g}$ to 2.7 $\mu\text{W/g}$) at the maximum considered Citrate dosage of 2mL/kg. On one hand, Figure 3- 2c shows that an increase in the level of Sucrose concentration has a

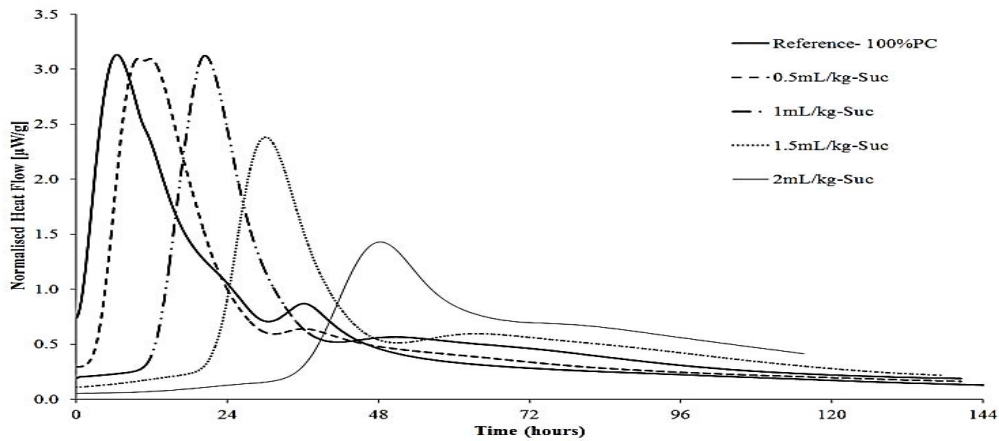
significant effect on delaying the peak heat occurrence time. On the other hand, while having a minimal impact on the magnitude of the heat peak at small concentrations, higher concentrations of Sucrose appear to significantly reduce the heat peak magnitude. In particular, results indicate 55% reduction in the heat peak magnitude, compared to the reference sample, at Sucrose concentration of 2 mL/kg. Comparing the effectiveness of different retarders for cases leading to a maximum of 20 hours retardation highlights that Citrate shows the best performance in terms of reducing the peak heat evolution for an acceptable extent of retardation. Citrate dosages of 1.7 mL/kg and 2mL/kg reduce the peak heat flow by 8% and 16%, respectively. The peak heat flows for Retarder N and Sucrose are only reduced for high concentrations that retarded the peak beyond 24 hours.



a.



b.



c.

Figure 3- 2 Heat evolution for OPC pastes with different dosages of a. Retarder N, b. Citrate and c. Sucrose

3.4.2 The effect of curing temperature on hydration curves

• General Portland cement

The results of isothermal calorimeter tests illustrate that curing temperature has a significant influence over the heat release of a hydrating cement paste. Figure 3- 3 demonstrates the hydration heat curves of the reference mix, 100% OPC, at three different curing temperatures of 10°C, 23°C, and 30°C. It is evident that at higher temperatures the normalized peak heat flow is increased and the time to peak is reduced. The extent of the retardation of the peak heat flow is presented in Table 3-3.

The peak heat flow of the acceleration phase occurred after 5.3, 7.2 and 17.4 hours for curing temperatures of 30°C, 23°C and 10°C, respectively. This signifies that reducing the curing temperature plays a significant role in prolonging the dormant period and delaying the initiation of the acceleration phase of a cement paste. In addition, the duration of the acceleration phase and the deceleration phase are increased with decreasing temperature, which is evidenced by the width of the peak heat evolution.

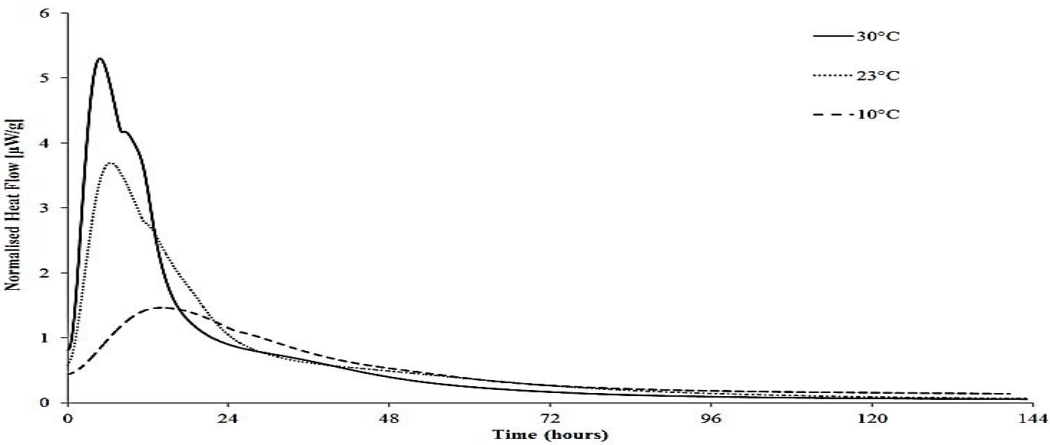


Figure 3- 3 Heat evolution for OPC at various curing temperatures

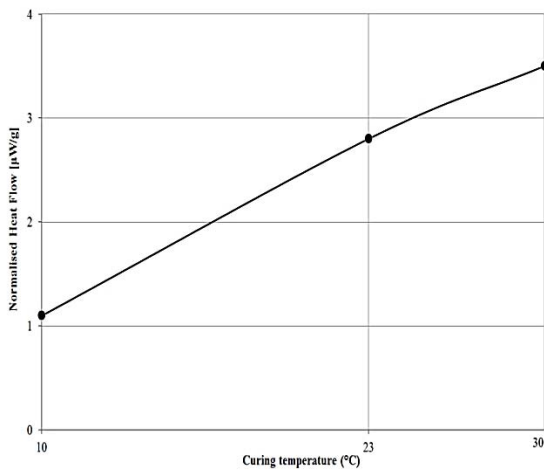


Figure 3- 4 Relationship between curing temperature and peak heat flow

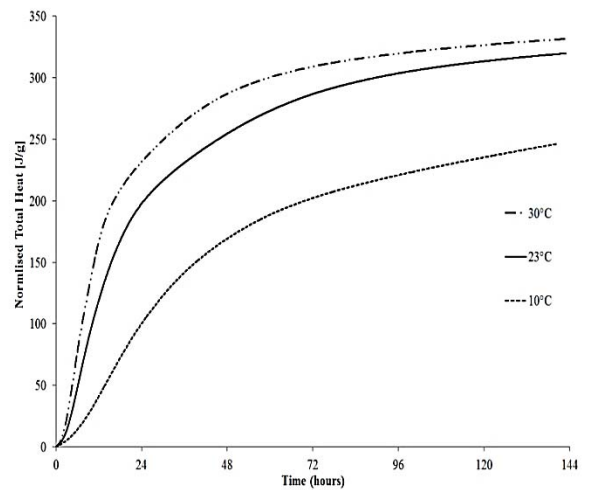


Figure 3- 5 Normalized cumulative heat for OPC at various curing temperatures

It is clear that reducing the curing temperature has a significant effect on lowering the peak heat evolution. As can be seen in Figure 3- 3, after approximately 96 hours, the difference in heat flow of each curve is only marginal. Figure 3- 4 shows the variations in the normalized peak heat flow of the reference cement mix with variations in the curing temperature, highlighting a directly proportional relationship between the two parameters. Accordingly, Table 3-3 demonstrates a 30% reduction in peak heat flow between 30°C and 23°C and a 60% reduction between 23°C and 10°C. Figure 3- 5 shows the effect of the curing temperature on the cumulative released heat [J/g] of the 100% GP cement mix in the first six days. The results indicate that the cumulative heat of hydration released at early ages increases with an increase in curing temperature.

Table 3- 3 Comparison of peak heat flow for OPC at various curing temperatures

Curing Temperature [°C]	Time at end of dormant phase [hr]	Time of peak heat flow [hr]	Magnitude of peak heat flow [μ W/g]	Change in peak heat flow (%)
30	0.80	4.80	5.30	Reference
23	0.90	6.41	3.70	-30%
10	3.80	14.17	1.50	-60%

• **Pastes containing SCMs**

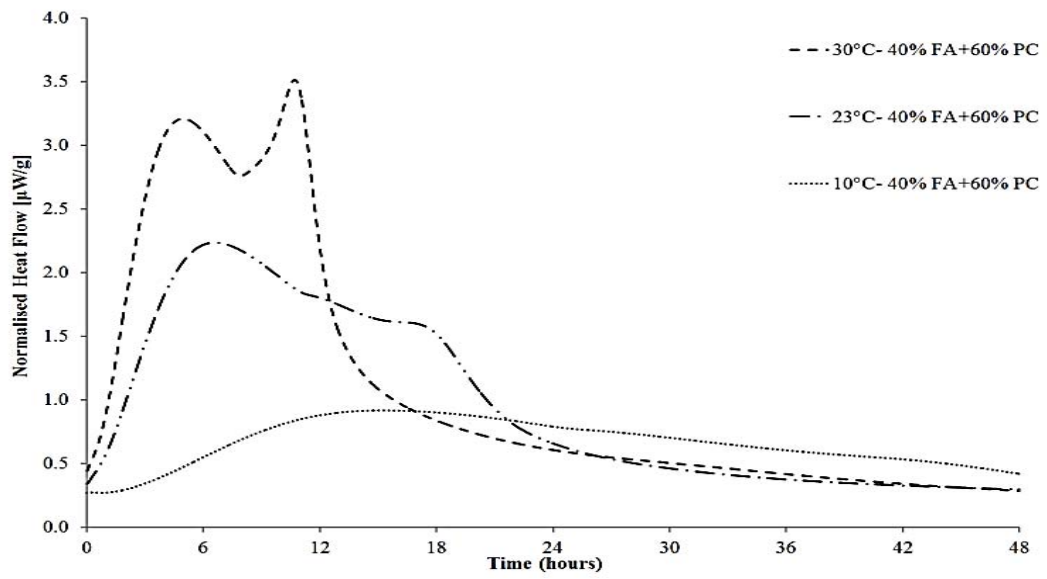
Figures 3- 6a and 3- 6b demonstrate the hydration curves of OPC paste samples with 40% replacement of FA and GGBFS, respectively, at three different curing temperatures of 10°C, 23°C and 30°C. It can be seen that the shape of the hydration curve is strongly impacted by the curing temperature. Figures 3- 7a, 3- 7b and 3- 7c compare the hydration curves of the cement pastes with either 40% FA or 40% GGBFS with that of the reference sample containing 100% OPC at different curing temperatures. The results clearly highlight that the curing temperature is the most dominant factor impacting upon the shape of the hydration curve. Similar to the trend observed for reference cement mixes, the peak heat evolution is retarded with time and reduced in magnitude as the temperature is reduced. At 10°C, the peak heat flow is retarded by approximately 16-19 hours from the time of first contact with water. This indicates that the hydration reaction is slowed down at lower temperatures, as expected. It can be seen for all temperatures that the peak heat flow for GGBFS systems is larger compared to FA systems considering the replacement level of 40% FA or GGBFS. Figure 3- 8 plots the variations in the normalized peak heat flow due to different curing

temperatures. As can be seen, for a given mix a relatively linear relationship exists between the curing temperature and peak heat flow. Comparing the results presented in Figures 3-7a to 3-7b and Table 3-4 highlights a number of general trends. In particular, the tendency for GGBFS to generate a higher peak heat flow than FA is consistently observed at all curing temperatures. In addition, the delay in the initiation period of the acceleration phase, and the time of peak heat flow is observed to be greater for FA compared with GGBFS.

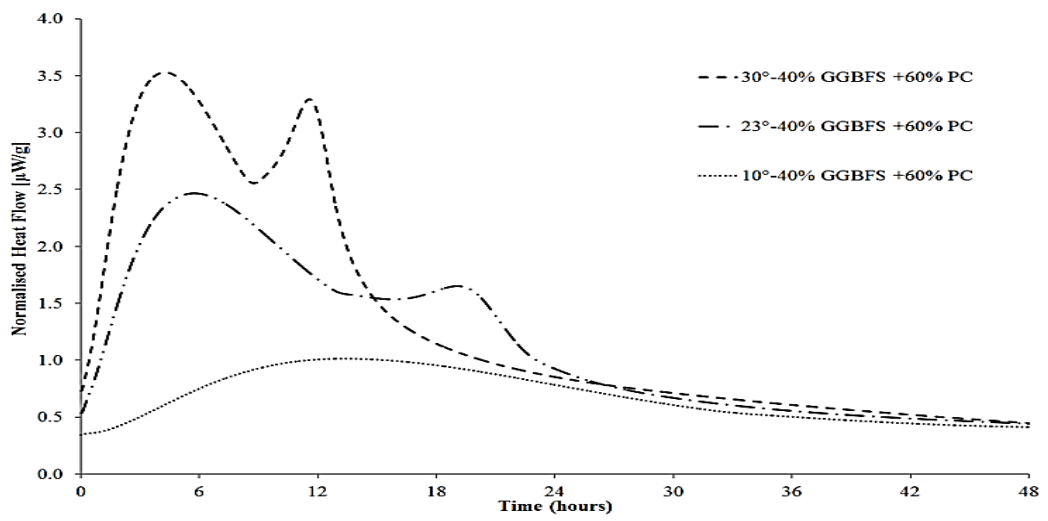
3.4.3 Comparing the experimental results with hydration heat prediction models

The two commonly used cement hydration heat models proposed by the Bogue model [18] and Schindler and Folliard [16] were reviewed in Section 2. Schindler and Folliard's model considers the effects of fly ash, slag and the curing temperature, while Bogue's model considers the effect of fly ash, slag, curing temperature and chemical retarders. The values of the key input parameters used in these models including Bogue values, as reported by cement manufacturer (Boral Cement Ltd) are summarized in Tables 3-1 and 3-5. Figures 3-9a, 3-9b and 3-10 compare the predictions of the Schindler and Folliard's model for the cementitious systems containing different percentages of FA, GGBFS and Portland cement with the experimental measurements. The test results show that the delay in heat peak at high FA or GGBFS replacements is not matched by the predictions. Furthermore, the effect of SCM's on decreasing the rate of the hydration as indicated by experimental results is not precisely reflected in the prediction of Schindler and Folliard's model. Table 3-7 summarizes the level of errors in the estimations of Schindler and Folliard's model for the time of occurrence and magnitude of the peak heat flow. The errors in estimating the time of peak heat are

found to increase with an increase in curing temperature. In particular, the error increases from 48% to 58% by increasing the curing temperature from 10 to 30°C for the mixes containing 100% OPC. Moreover, it can be seen that the inaccuracy of the results of this model for the samples containing GGBFS is generally less than the samples containing Fly ash. The predictions of Schindler and Folliard's model indicate a relatively longer retardation for cements containing FA than GGBFS, which is consistent with the trend observed in the experimental measurements. The results however indicate a good accuracy for Schindler and Folliard's model in terms of predicting the value of heat peak flow. As shown in Table 3-7, Schindler and Folliard's model accurately predicts the peak heat flow of the reference cement mix (100% OPC); with a maximum error of only 5.5%. The accuracy of the model in estimating the magnitude of the peak heat flow of the reference sample is found to be considerably higher at the lower temperatures considered, overestimating the heat peak flow by only 2% and 2.2% at curing temperatures of 10°C and 23°C, respectively. The results presented in Table 3-7 highlight generally a relatively similar range for the errors in peak heat and peak heat time estimations of Schindler's model for mixes with different FA and GGBFS content. This indicates that estimation errors are likely to be systematic rather than random errors, thus, highlighting re-calibrations as a possible strategy to minimize such errors.

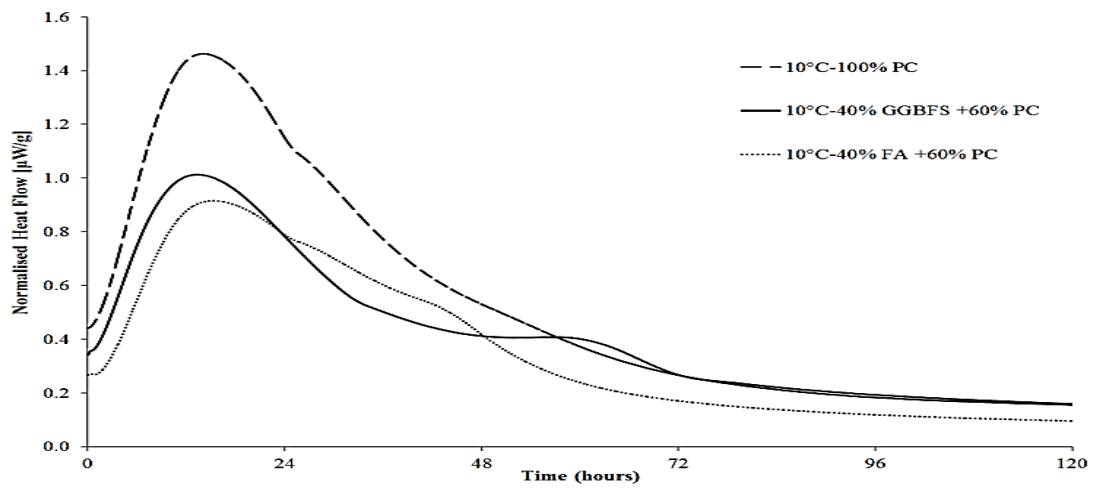


a.

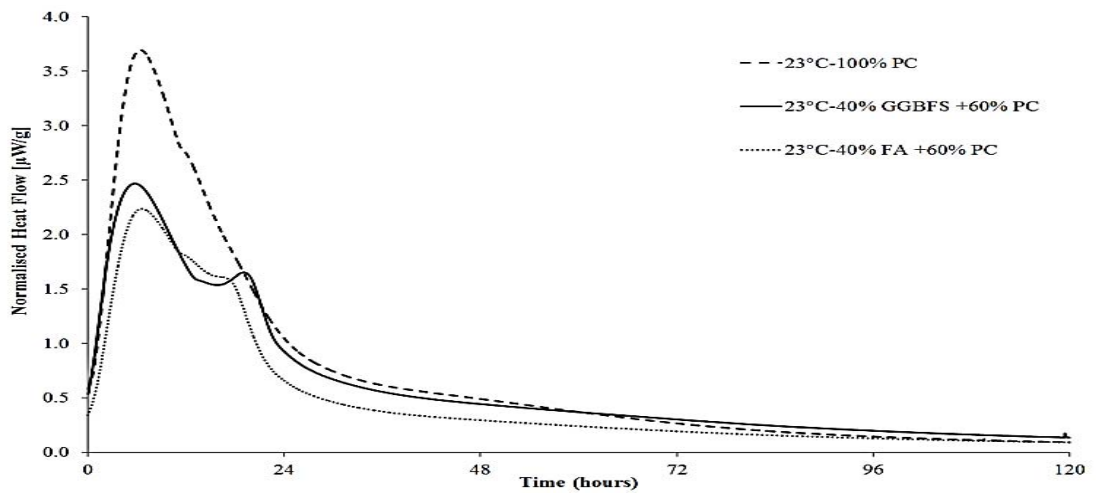


b.

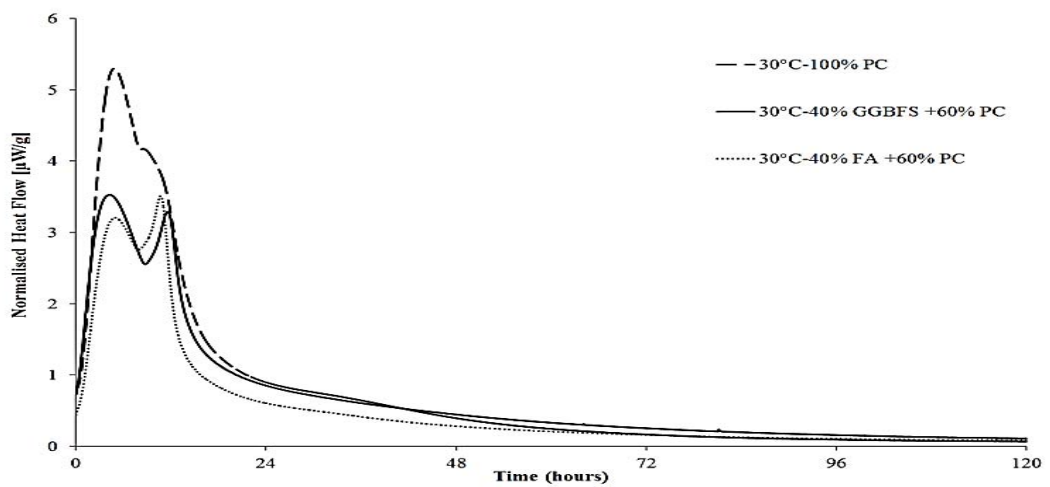
Figure 3- 6 Heat evolution for OPC pastes at various temperatures with a. 40% FA and
b. 40% GGBFS



a.



b.



c.

Figure 3- 7 Comparison of heat evolution for cement pastes with 40% FA or GGBFS at a) 10 °C, b) 23°C and c) 30°C

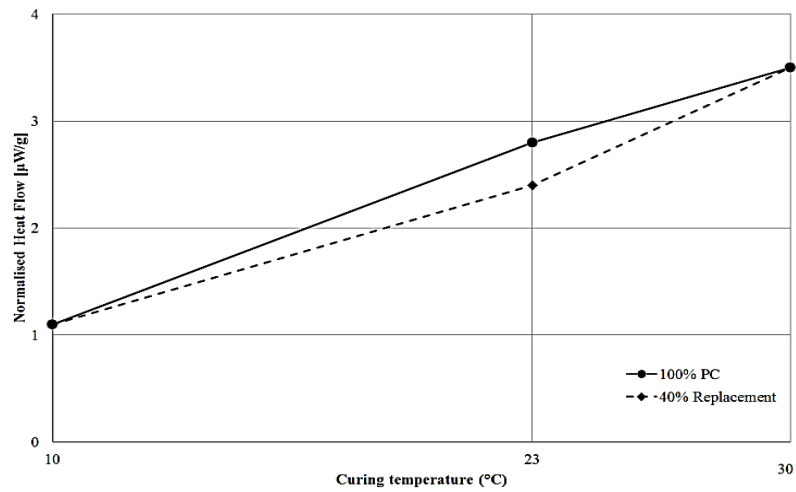


Figure 3- 8 Relationship between curing temperature and peak heat flow for 40% replacement

Table 3- 4 Comparison of selected hydration curve parameters for cement pastes with 40% FA or 40% GGBFS at various curing temperatures

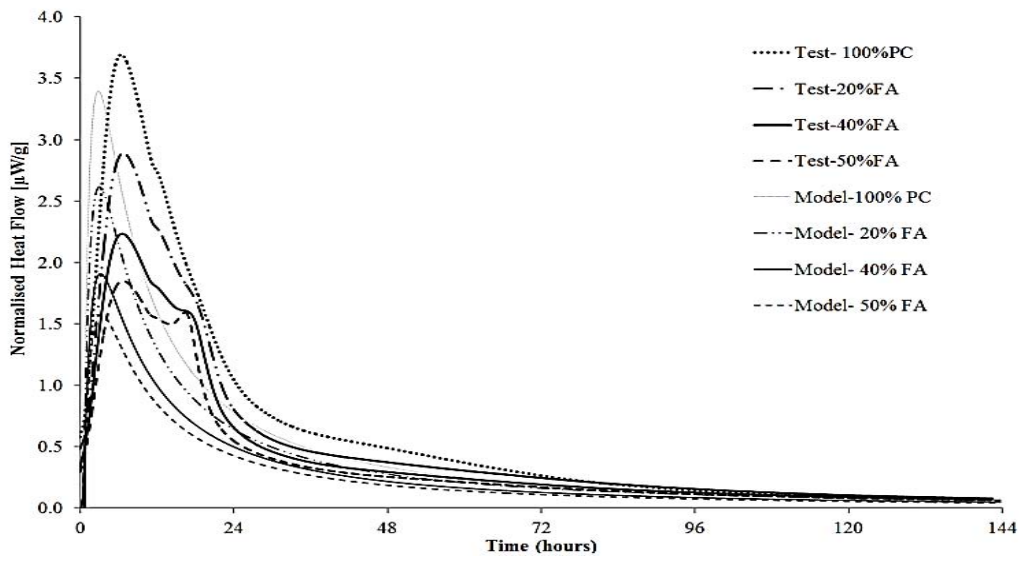
Curing Temperature [°C]	SCM	Time at end of dormant phase [hr]	Time of peak heat flow [hr]	Magnitude of peak heat flow [µW/g]
30	GGBFS	1.0	4.3	3.5
30	FA	1.4	10.7	3.5
23	GGBFS	1.2	5.8	2.5
23	FA	1.6	6.6	2.2
10	GGBFS	2.5	13.2	1.0
10	FA	3.7	15.3	0.9

Table 3- 5 Input parameters for existing hydration models

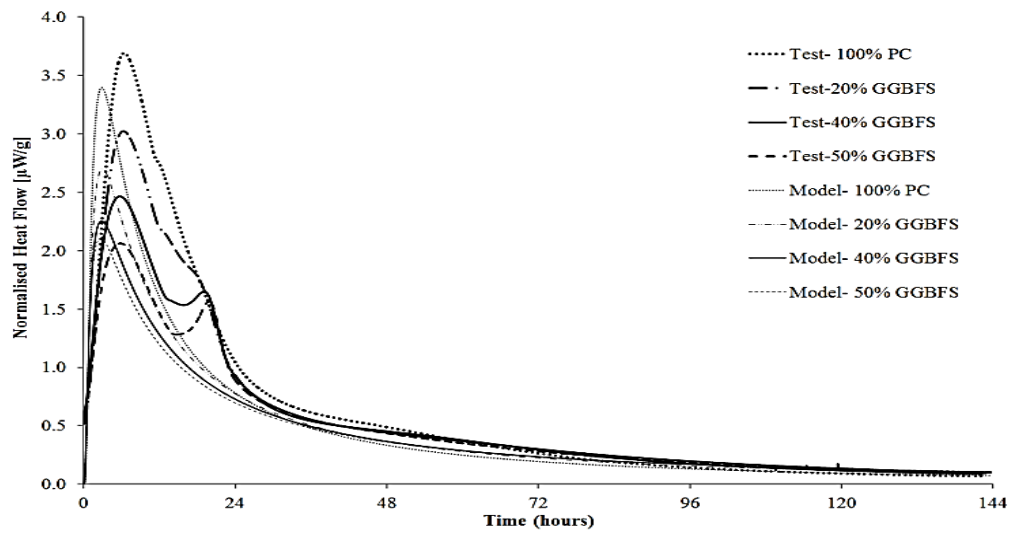
Alite, C3S	51.1%
Belite, C2S	15.5%
Aluminate, C3A	8.9%
Ferrite, C4AF	8.4%
Blaine (m ² /kg)	380
W/b	0.45
Reference Temperature	21°C

Table 3- 6 Output parameters of existing hydration models

Mix	Hu [J/g]	Au			Ea		
	Schindler & Bogue	Schindler	Bogue	Δ (%)	Schindler	Bogue	Δ (%)
Reference	449	0.720	0.758	5%	46753	35543	-24
20% FA	365	0.722	0.779	8	37340	35173	-6
40% FA	281	0.724	0.812	12	27927	34804	25
50% FA	239	0.725	0.835	15	23220	34619	49
20% GGBFS	451	0.781	0.781	0	50494	35206	-30
40% GGBFS	454	0.840	0.819	-3	54234	34868	-36
50%GGBFS	455	0.871	0.845	-3	56104	34700	-38



a.



b.

Figure 3- 9 Comparison of heat evolution between test results and Schindler and Folliard's model for an OPC system containing a. FA and b. GGBFS

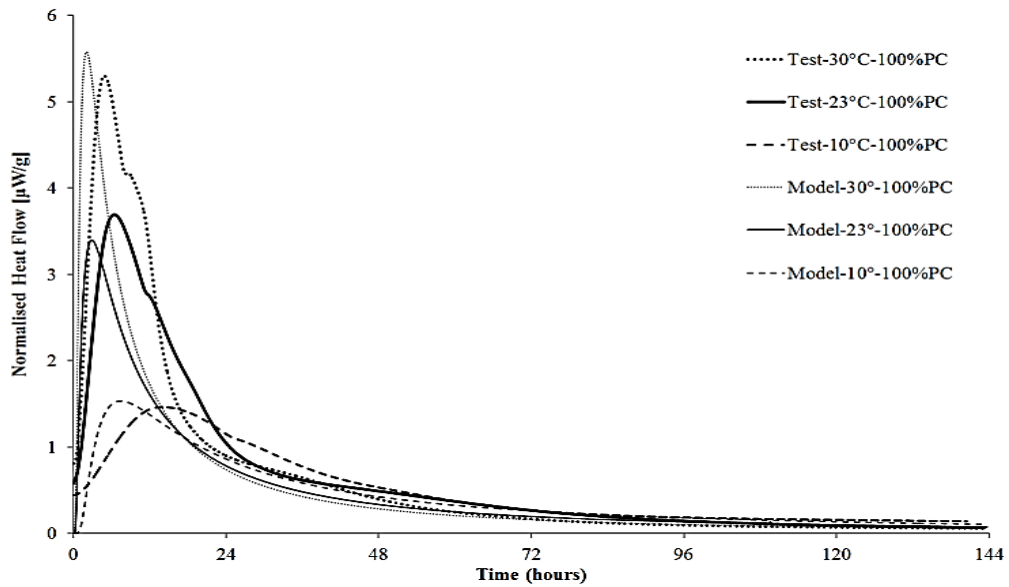


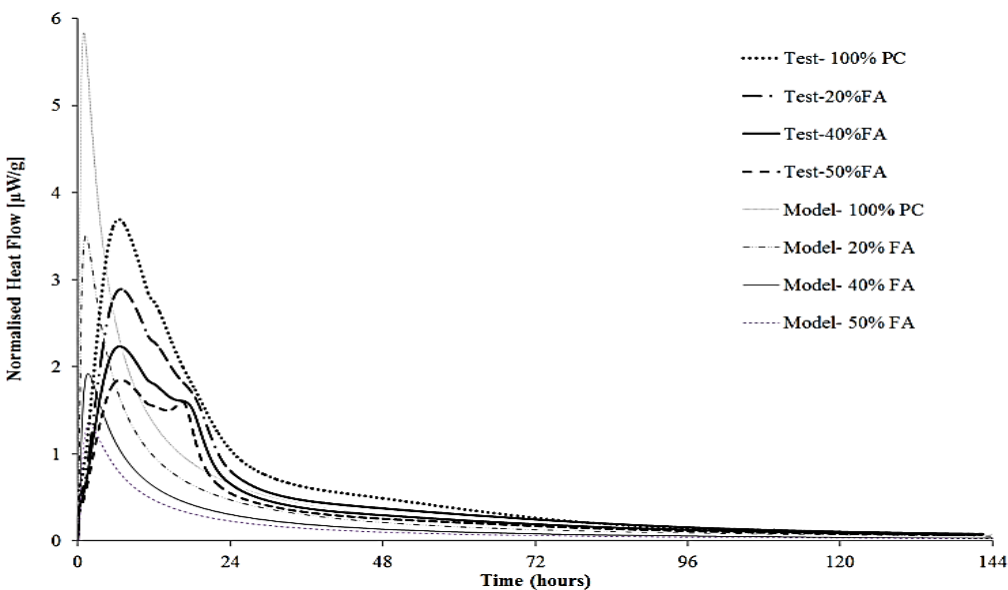
Figure 3- 10 Heat evolution of test results and Schindler and Folliard's Model for a 100% OPC system at varying curing temperatures

Figures 3-11a, 3-11b and 3-12 compare the Bogue model predictions for the samples containing FA, GGBFS and 100% Portland cement with the corresponding calorimetry measurements. Several significant inaccuracies are observed with the most pronounced being duration of the acceleration and deceleration phases. It is evident in Figures 3-11a, 3-11b that the time of occurrence of the peak heat in the hydration curve is severely underestimated by the Bogue model. The inaccuracy of the model in predicting the peak heat flow is amplified when decreasing the temperature. Figure 3-12 shows that an increase in ambient temperature results in a decrease in the time taken until stabilization of heat profiles to a common value. As shown, at 30°C the heat flow stabilizes to a common value after 60 hours, while a considerably longer duration of about 84 and 95 hours is observed for this to happen at 23°C and 10°C ambient temperatures, respectively.

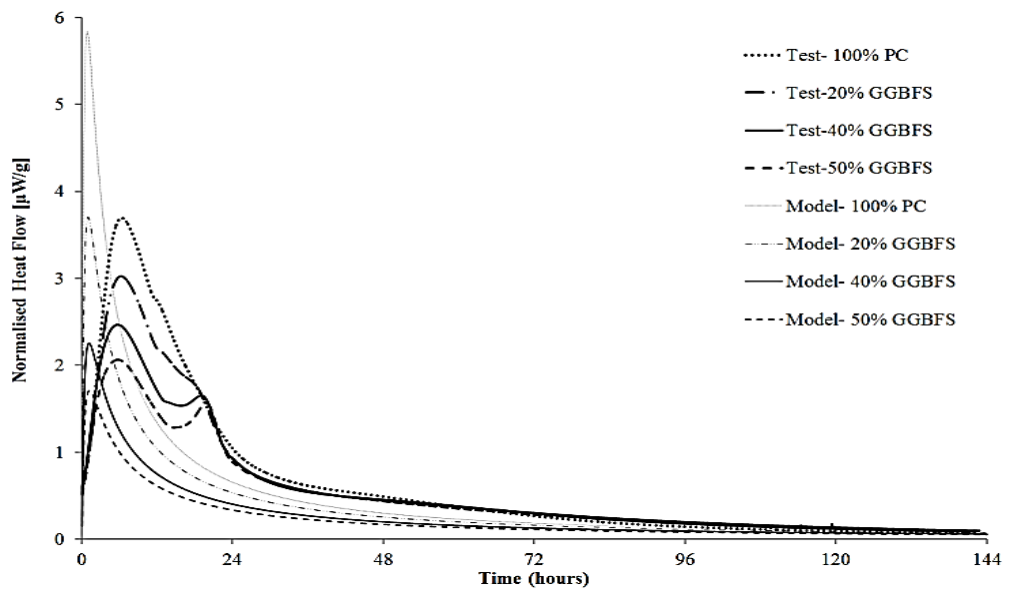
Table 3- 7 Comparison of peak heat flow time and magnitude between test results and Schindler and Folliard’s Model

10 DegC	100% PC		20% FA		40% FA		50% FA		20% GGBFS		40% GGBFS		50% GGBFS	
	Peak time	Peak Magnitude												
Test	14.17	1.50	14.17	0.96	15.05	0.92	16.11	0.88	12.13	1.46	13.45	1.01	13.75	0.91
Model	7.40	1.53	6.60	1.40	5.90	1.21	5.50	1.100	8.50	1.10	9.40	0.833	9.40	0.73
Δ (%)	-47.8	2.00	-53.40	45.8	-60.80	31.5	-65.9	25.0	-29.90	-24.5	-30.10	-17.7	-31.60	-19.40
23 DegC	100% PC		20% FA		40% FA		50% FA		20% GGBFS		40% GGBFS		50% GGBFS	
	Peak time	Peak Magnitude												
Test	6.41	3.71	6.75	2.89	6.60	2.20	6.71	1.85	6.29	3.02	5.70	2.50	5.85	2.32
Model	3.11	3.62	3.40	2.79	3.60	2.03	3.60	1.68	3.40	2.79	3.40	2.25	3.30	2.06
Δ (%)	-51.60	-2.21	-49.61	-3.61	-45.50	-7.60	-46.30	-9.00	-45.90	-7.50	-40.40	-10.00	-43.60	-11.30
30 DegC	100% PC		20% FA		40% FA		50% FA		20% GGBFS		40% GGBFS		50% GGBFS	
	Peak time	Peak Magnitude												
Test	4.80	5.29	4.90	3.38	10.70	3.21	11.12	2.98	4.89	4.77	4.27	3.53	4.71	3.41
Model	2.00	5.58	2.30	3.94	2.70	2.63	2.90	2.09	2.10	4.56	2.00	3.46	2.50	3.15
Δ (%)	-58.30	5.40	-53.10	16.51	-74.80	-18.00	-73.90	-29.90	-57.12	-4.51	-53.20	-2.00	-46.90	-7.60

Figure 3-12 also indicates a considerable lack of accuracy in the Bogue model's predictions in terms of capturing the effect of temperature on hydration heat profile. The errors of the Bogue model's predictions of the peak heat flow and peak heat time for different mixes are reported in Table 3-8. As can be seen, the error in estimating the time of the peak heat varies from 70% to 80% in all cases and it is not much affected by curing temperature. The results indicate that the peak heat magnitude estimation error for the reference sample (100% PC) and samples including 20% FA decreases with an increase in the curing temperature while in all other cases an increase in curing temperature leads to higher errors in predicting the peak heat magnitude. Furthermore, the error in estimating the peak heat magnitude tends to be higher at higher levels of SCM replacements. For instance, for the samples containing 50% GGBFS at 30°C this error alters from 13% to 42.5%. Based on the test results presented in Table 3-7 and 3-8, Bogue's model predictions of the peak heat magnitude and time for the reference sample (100% PC) show considerably higher deviations from measurements when compared to predictions of Schindler's model.



a.



b.

Figure 3- 11 Comparison of heat evolution between test results and Bogue’s model for an OPC system containing a. FA and b. GGBFS

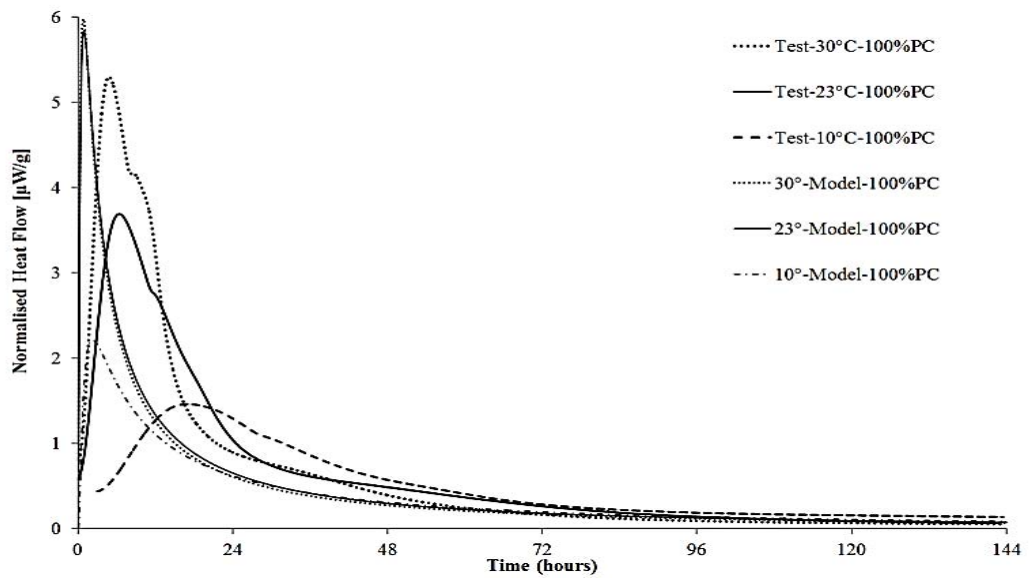


Figure 3- 12 Heat evolution of test results and Bogue’s Model for a 100% OPC system at varying curing temperatures

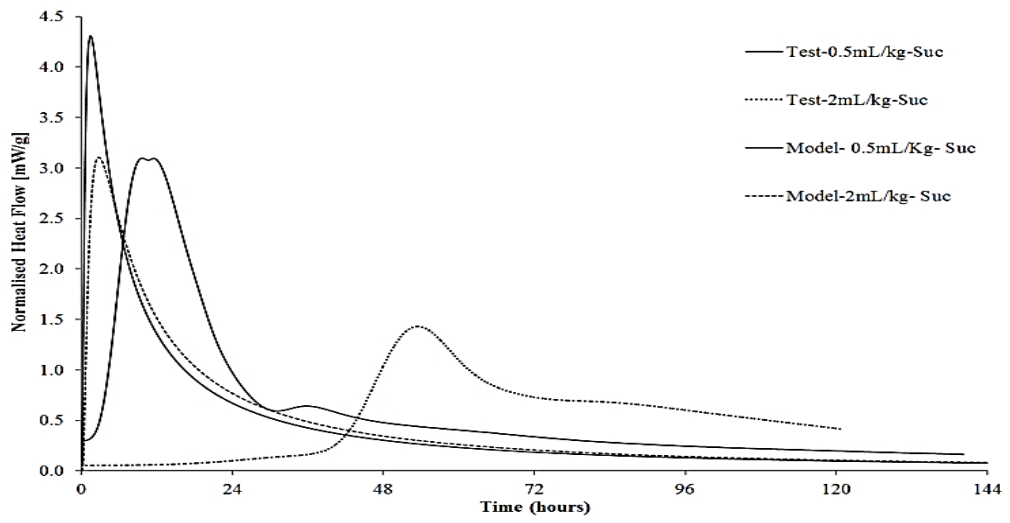
Table 3- 8 Comparison of peak heat flow between test results and Bogue’s Model for a 100% OPC system

10 DegC	100% PC		20% FA		40% FA		50% FA		20% GGBFS		40% GGBFS		50% GGBFS	
	Peak time	Peak Magnitude												
Test	14.17	1.50	14.17	0.96	15.05	0.92	16.11	0.88	12.13	1.46	13.45	1.01	13.75	0.91
Model	2.31	2.21	2.90	1.40	3.50	0.81	3.90	0.58	2.50	1.48	2.70	0.95	2.80	0.74
Δ (%)	-83.80	47.30	-79.50	45.80	-76.70	-12.00	-75.80	-34.10	-79.40	1.40	-79.90	-6.10	-79.60	-18.71
23 DegC	100% PC		20% FA		40% FA		50% FA		20% GGBFS		40% GGBFS		50% GGBFS	
	Peak time	Peak Magnitude												
Test	6.41	3.70	6.75	2.89	6.60	2.20	6.71	1.85	6.29	3.02	5.70	2.50	5.85	2.32
Model	1.20	4.29	1.50	2.70	1.80	1.55	2.00	1.11	2.00	2.70	1.40	1.81	1.70	1.70
Δ (%)	-81.30	15.90	-77.80	-6.60	-72.70	-29.50	-70.20	-40.00	-68.21	-10.61	-75.41	-27.60	-70.90	-26.70
30 DegC	100% PC		20% FA		40% FA		50% FA		20% GGBFS		40% GGBFS		50% GGBFS	
	Peak time	Peak Magnitude												
Test	4.80	5.29	4.90	3.38	10.70	3.21	11.12	2.98	4.89	4.77	4.27	3.53	4.71	3.41
Model	0.90	5.98	1.10	3.75	1.30	2.15	1.50	1.54	0.90	3.95	1.00	2.52	1.10	1.96
Δ (%)	-81.30	13.00	-77.60	10.90	-87.90	-33.00	-86.50	-48.30	-81.60	-17.20	-76.60	-28.60	-76.60	-42.50

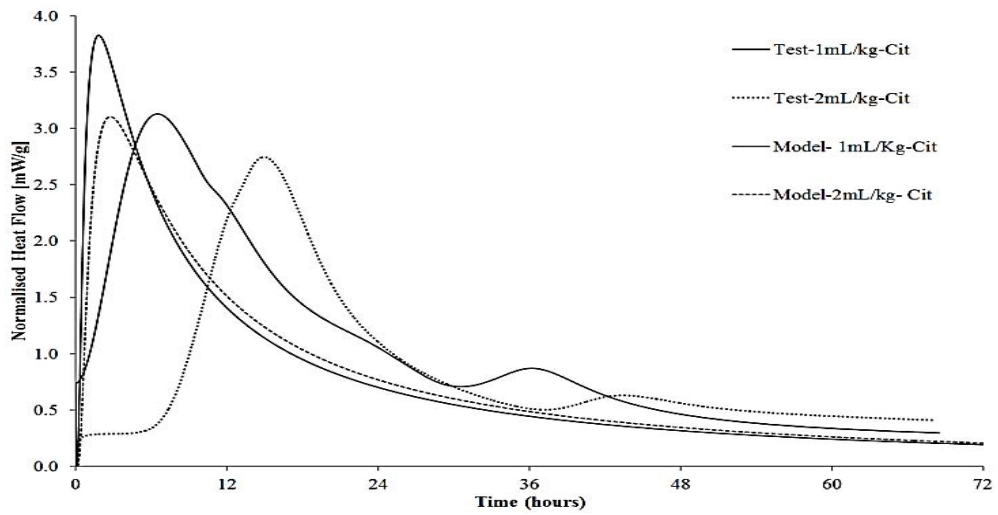
Schindler and Folliard's model does not consider the effect of chemical retarders. Therefore, the precision in capturing the effect of retarders is only investigated for the Bogue model. The Bogue method does not account for differences in the type of the retarders. Table 3-9 shows the errors of the Bogue model in estimating the magnitude and time of the peak heat flow for systems containing 100% OPC and various dosages of three types of retarders used in this chapter. Figure 3-13 compares the experimental and modeled heat development curves for pastes containing 100% OPC and mentioned retarders at their minimum and maximum dosages. It can be seen that the Bogue model overestimates the peak heat magnitude by 39% to 54% and underestimates the time of peak heat flow by up to 95% when using Sucrose. Table 3-9 also shows that using the Bogue model for cementitious systems containing different dosages of Citrate leads to a 12 to 31% error in estimating the peak heat magnitude and up to an 87% error in estimating the time of the peak heat flow. Moreover, the Bogue model underestimates the magnitude and the time of the peak heat flow of the systems containing Retarder N up to 36% and 60%, respectively.

Table 3- 9 Comparison of peak heat flow between test results and Bogue's model for
100% OPC with chemical retarders

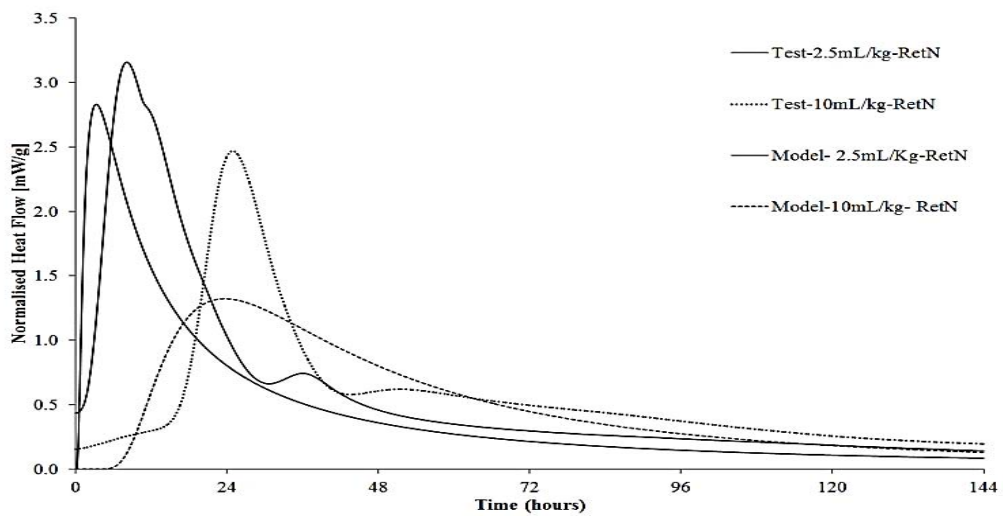
Retarder Type	Concentration	Magnitude of peak heat flow			Time of peak heat flow		
	[mL/kg]	Test [μ W/kg]	Model [μ W/kg]	Δ (%)	Test [μ W/kg]	Model [μ W/kg]	Δ (%)
Sucrose	0	3.70	4.29	-16%	6.41	1.20	81%
	0.5	3.10	4.31	-39%	12.3	1.50	88%
	1	3.12	3.83	-23%	20.45	1.80	91%
	1.5	2.38	3.43	-44%	30.12	2.20	93%
	2	1.43	3.11	-54%	53.30	2.70	95%
Citrate	1	2.92	3.83	-31%	10.60	1.80	83%
	1.3	3.01	3.80	-26%	14.03	2.10	85%
	1.7	2.90	3.60	-24%	14.90	20	87%
	2	2.75	3.11	-12%	14.93	2.70	82%
Retarder N	2.5	3.16	2.83	10%	8.15	3.30	60%
	5	3.09	1.97	36%	15.63	7.50	52%
	10	2.47	1.3	47%	24.95	23.70	5%



a. Minimum and Maximum concentration of Sucrose



b. Minimum and Maximum concentration of Citrate



c. Minimum and Maximum concentration of Retarder N

Figure 3- 13 Comparison of heat evolution between test results and Bogue's Model for a General-Purpose cement system containing retarders.

Overall, the results presented above show that while the existing models, especially Schindler's model, provide valuable input in terms of predicting the heat of hydration of cements with different chemical compositions, significant errors may occur when using such models for predicting the heat profile of cementitious mixes containing fly ash, GGBFS and retarders. The lack of adequate precision in capturing the effects of SCMs and retarders may considerably affect the finite element model predictions used to estimate the risk of thermal cracking in concrete and evaluate the effectiveness of various strategies for minimizing the risk of early age thermal cracking. This signifies the need for a comprehensive study to improve the predictions of existing models. The results however suggest that the errors in predictions are most likely systematic, rather than random errors as evidenced by the close range of errors in the models' predictions for different mixes. Therefore, the results highlight the possibility of minimizing the prediction errors by re-calibrating such models for locally

used cementitious materials. This is particularly true for Schindler's model which shows a considerably good level of accuracy in predicting the peak hydration heat for mixes without SCMs and retarders.

3.5 Conclusions

The results of an experimental study conducted to investigate the effects of fly ash, GGBFS, retarders and curing temperature on the heat of hydration profiles as well as the ability of existing models in capturing these effects were presented. The results indicate that addition of fly ash and GGBFS is an effective method to reduce the peak heat, with a relatively proportional relationship between the heat reduction achievable and cement's SCM content. About 51% and 43% decreases in the peak heat flow are observed at 50% fly ash and GGBFS content, respectively. Furthermore, results show that the use of retarders at optimal level can be an effective method in controlling the risk of thermal cracking. The use of retarders is observed to not only delay the peak heat but also reduce its magnitude, especially at higher concentrations. The type and concentration of retarder are found to play a major role in determining the extent of retardation and the peak heat flow. Citrate is found to offer the highest level of reduction in the peak heat for an acceptable extent of retardation, i.e. maximum 20 hours. Moreover, results reveal that lowering the curing temperature decreases peak heat flow. The results also illustrate significant inaccuracies in the predictions of existing hydration heat models for pastes containing fly ash, GGBFS and retarders. A common error in both models considered in this chapter is apparent in the modelling of the duration and occurrence of the acceleration and deceleration phases of hydration. Schindler and Folliard's model proved to be significantly more accurate for systems containing FA and GGBFS, in terms of predicting the magnitude and occurrence of the

peak heat flow. However, Schindler and Folliard's model is unable to predict the effect of chemical retarders. A key issue in using the Bogue method for analysing retarded cement systems is found to be the model's inability to account for the type of retarder used. The systematic prediction errors can be reduced by recalibrating the mentioned models for locally used cementitious materials, especially for Schindler's model which shows a considerably good level of accuracy in predicting the peak hydration heat for mixes without SCMs and retarders. Moreover, a practical and more reliable approach in terms of reducing the modelling errors is the use of calorimetry measurement as input directly into finite element models particularly in mixes containing SCMs and retarders.

Chapter 4: A Three-Dimensional Customizable Model to Simulate Thermal Cracking of Concrete at Early Ages

4.1 Introduction

Early age cracking occurs when the tensile strain due to temperature gradient or thermal contractions increases and exceeds the tensile strain capacity of the concrete [3, 22, 103, 104]. Therefore, predicting the variations in temperature gradient and thermal stresses over time is critical identifying the risk of thermal cracking in a particular concrete element. With this in mind, several efforts have been made in available literature to develop numerical simulation models, mainly based on finite element and finite difference methods, to evaluate the temperature rise and risk of thermal cracking in concrete [103–105]. The input into such models include usually the geometry of the element, the properties of the concrete constituent materials, the mix proportions, ambient conditions as well as the boundary conditions including the type of formworks. The output on the other hand, is typically the variations in the temperature of concrete at selected points of a simplified 2D geometry, and a cracking risk potential measure defined based on the ratio of thermal stresses and thermal strength of concrete [105, 106]. However, the existing models have a number of drawbacks rendering them unsuitable for use in the present study: i) the existing models provide only a limited number of pre-defined geometries, which may not represent the full range of complicated geometries encountered in practice. In cases that the geometry of the element does not fit within predefined geometries, it needs to be simplified; ii) existing modelling packages provide limited flexibility in terms of customizing the input parameters into the model and making modification to the formulations used to predict heat of hydration, maturity development, etc.; iii) the existing models are in 2D and

would require considerable simplifications when dealing with asymmetric geometries; iv) the existing models provide a limited post processing options to present the results of the analysis; this is mainly limited to 2D graphs of variations in the temperature in a given point; v) a majority of existing models tend to use hydration heat equations developed in the literature to predict heat generation; however, such models have been created mainly through regression on numerous data sets of cements produced in the US and as highlighted in Chapter 3 tend to be highly erroneous in presence of Australian supplementary cementitious materials and admixtures. vi) the existing models tend to overlook the effect of reinforcement on the temperature rise in concrete elements. However, given the significantly higher thermal conductivity of steel compared to concrete, this can lead to considerable errors in predicting the temperature in heavily reinforced concrete elements. In this chapter a numerical simulation model is developed to predict the increase in temperature, and temperature gradient in a concrete element, as well as the resulting thermal stresses, and cracking potential; vi) designed mainly for typical materials and boundary conditions experienced in the US, the existing models tend to show considerable errors in predating the temperature rise in concrete elements cast in Australia and therefore, there is significant room for improvement in precision of modelling through incorporation of local data and practices in the model formulation and parameters.

To address the above gaps, in this chapter a 3D numerical model is developed to allow complete flexibility to modifying the formulation and parameters used to predict temperature and thermal stresses in concrete elements. The model is developed in COMSOL Multiphysics to allow considerable flexibility in defining different geometries, material properties, and different types of thermal and structural boundary conditions. The latter would in turn allow practitioners to evaluate the comparative

performance of various mixes used by the Australian Construction industry by updating the mechanical and thermal properties of the materials used in Australia. To address the inadequate precision of hydration heat prediction equations, as demonstrated in Chapter 3, the model presented in this chapter is designed to accept direct calorimetry measurement as the thermal load imposed on the elements. An innovative approach involving interpolation between calorimeter inputs at several temperatures is used to improve the accuracy of the predictions. While a variety of curing methods and boundary conditions are pre-defined in the model, the design of the model allows customisation of new curing methods and boundary conditions experienced in practice. In addition, the proposed methods are designed to account for the effect of highly conductive reinforcing bars on temperature rise in concrete, which has not been previously considered.

The model is developed through coupling of heat transfer and solid mechanics finite element modules in COMSOL Multiphysics, where the variables and parameters are defined to represent the thermal load developed due to hydration. The heat transfer and solid mechanics models are developed by incorporating the concept of equivalent age to model maturity development rate and thus the rate of development of thermal and mechanical properties, including thermal conductivity, thermal capacity, modulus of elasticity, compressive strength and tensile strength. The proposed model is validated through an actual case study on a full-scale thick in-situ wall in Queensland, Australia, where the temperature development was measured through wireless temperature sensors.

4.2 Features of proposed model

The developed numerical model is a comprehensive three-dimensional model comprising of three main modules: Heat transfer model, Solid mechanics model, and Coupled Heat transfer- Solid mechanic model in COMSOL Multiphysics. Moreover, to integrate the time-dependant variable during the calculations, the model is coupled with time-dependant Ordinary Differential Equation (ODEs) interface. Figure 4-1 shows the framework of the proposed numerical model.

As shown in Figure 4-1, the initial step of the simulation is defining the input parameters needed for the analysis such as concrete mix design, placement temperature, time step, analysis duration, geometry of the element under study, etc. The geometry of the concrete element and the surrounding conditions can significantly affect the generated heat and thermal stress. For instance, increasing the thickness of the element can be directly attributed to a higher temperature rise [3]. The proposed model uses the Graphical User Interface (GUI) in COMSOL Multiphysics to create different geometries. This powerful tool enables the users to simulate different three-dimensional geometries with no/little limitations. As can be seen in Figure 4-1, Heat Transfer model is used to predict the thermal properties of hardening concrete and temperature development. Also, the Solid Mechanics model is utilized to predict the development of mechanical properties of concrete. Coupling of the Heat Transfer and Solid Mechanics models gives the numerical model the ability to predict the thermal expansion, thermal stress and thermal cracking ratio of the concrete element under study. Ordinary differential equations are used for the analysis as shown in Figure 4-1.

Since the developed numerical simulation is time-dependent, preferred time step of the analysis as well as the duration of analysis must be defined as an input to the model.

It should be noted that smaller time steps lead to more accurate results but in expense of a longer analysis duration and therefore a trade-off between level of required precision and duration of analysis may be required, when modelling relatively large 3D elements [107].

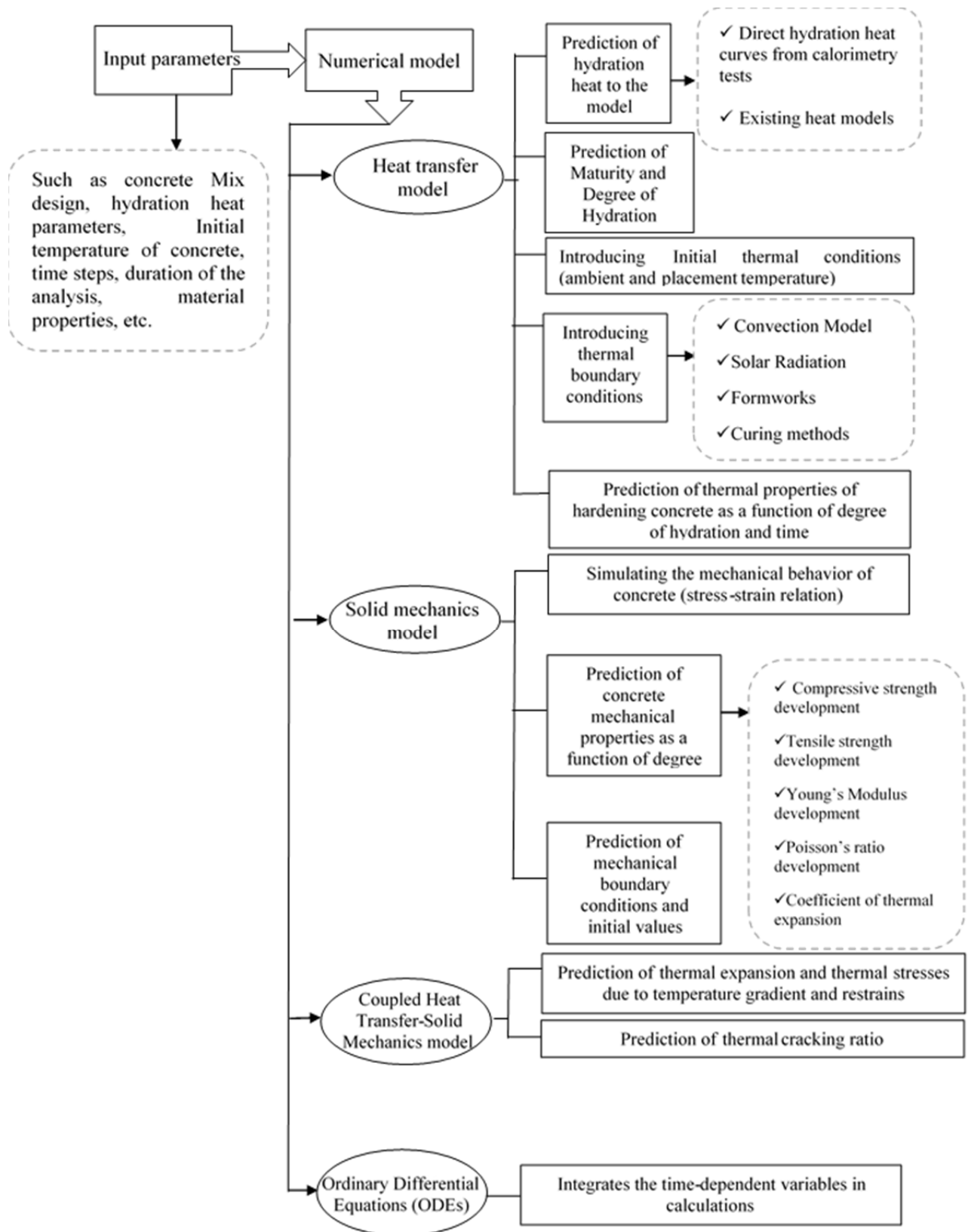


Figure 4- 1 the framework of the numerical model

Moreover, the time of formwork removal should be introduced based on the construction plan for each project. This is important since formworks affect the radiation and the heat exchange between the concrete and the surrounding environment. The radiation emitted by the formwork and reflected radiation act as heat sinks [106].

Thermal and mechanical behaviour as well as durability performance of concrete elements are significantly dependent on concrete mix design [3]. In the current numerical model, the effect of concrete mix design on thermal behaviour of concrete is introduced to the model through defining the heat function presented in Chapters 2 and 3. Furthermore, mix design affects the thermal properties of concrete such as thermal conductivity and heat capacity which will be discussed later in section 4-2-1-2. Concrete mix design also influences the mechanical properties of concrete. Accordingly, the relationship between mix variables and mechanical properties of concrete has been widely investigated in the literature [58, 108–110]. In this model, the previously verified models, described in detail in Section 4-2-2-2, are adopted to predict mechanical properties of a particular mix design and the development rate of these properties over time. With this in mind, concrete mix design is the most remarkable factor affecting the early age thermal cracking of concrete via influencing the heat generation alongside with thermal and mechanical properties of concrete. The amounts of cementitious materials, water, coarse and fine aggregate as well as density should be entered to the model as the basic information about the mix design of the element under study.

4.2.1 Heat Transfer model

The methodology for defining hydration heat as heat source is presented in the following section. In modelling early age thermal cracking of concrete, all types of heat

transfer including conduction, convection and radiation are incorporated in the model through formulation of heat transfer equation as well as defining relevant boundary conditions, which are described in detail in the following sections.

4.2.1.1 Heat Source

The proposed model is designed to provide two alternative approaches for estimating the variations in the heat input to the model. These include i) the use of hydration heat equations used widely in the literature, where the heat generation is estimated as a function of quantity of different concrete ingredients, and ii) the direct use of isothermal calorimetry measurements for a particular mix. The methodology adopted for each of these approaches is described in detail in the following:

Modelling the heat source using hydration heat models

As discussed in detail in Chapter 3, available literature includes several models to predict the heat of hydration of different concrete mixes. In the present study, Arrhenius equation, which defines the rate of heat generation as a given function of the degree of hydration, is used as the heat source in the heat transfer equations[13].

$$Q_h(t) = H_u \times C_c \times \left(\frac{\tau}{t_e}\right)^\beta \times \left(\frac{\beta}{t_e}\right) \times \alpha_u \times \exp\left(-\left[\frac{\tau}{t_e}\right]^\beta\right) \times \exp\left(\frac{E}{R}\left(\frac{1}{273+T_r} - \frac{1}{273+T_c}\right)\right)$$

Equation 4- 1

where Q_h is the rate of heat generation (J/h/m³); H_u is the total amount of heat generated at 100% hydration (J/kg); C_c is the total amount of cementitious materials (kg/m³); τ is the hydration time parameter, in hours; t_e is the concrete equivalent age at the reference temperature, in hours; β is the hydration slope parameter; α_u is the ultimate degree of hydration; E is the activation energy (J/mol); R is the universal gas

constant (J/mol/K); T_r is the reference temperature (°C); and T_c is the concrete temperature (°C). It should be noted that the rate and magnitude of heat generation of the concrete can vary significantly by variations in the concrete mix proportions, cement compositions, and the properties of the supplementary cementing materials and chemical admixtures used. If this option is selected for calculating the heat source in the developed numerical model in this study, Bogue method, described in Chapter 3, is employed to calculate the concrete heat of hydration parameters [28].

Direct use of calorimetry measurements

As demonstrated in Chapter 3, the predictions of existing hydration heat models may be erroneous in presence of admixtures and supplementary cementitious materials. With this in mind, the proposed model is designed with the option to model heat source directly using calorimetry measurements obtained for the actual concrete mix. Given the important effect of curing temperature on the rate of hydration and the rate of hydration heat generation, the direct heat modelling functionality defined in our model requires access to calorimetry measurements obtained at the temperatures experienced by concrete [3]. However, due to time consuming nature of calorimetry tests and resource limitations, measuring the hydration heat curves at all temperatures is not usually practical. To address this issue, the proposed numerical model is embedded with an interpolation model which allows measurements at only several selected temperatures covering the roughly the expected temperature range experienced by concrete. To achieve an acceptable interpolation accuracy however it is recommended to limit the temperature intervals to a maximum of 10°C. The interpolation between each of the two measured heat flows under different curing temperatures is performed using:

$$H(t) = \frac{T-T_1}{T_2-T_1}(H_2 - H_1) + H_1 \quad \text{Equation 4- 2}$$

where T , is the concrete temperature at each point of the element at each time step, T_1 and T_2 are curing temperatures of the first and second calorimetry experiments, respectively and H_1 and H_2 are the heat of hydrations measured through two different calorimetry tests for each time step.

4.2.1.2 Thermal properties of hardening concrete

Thermal properties such as thermal conductivity, heat capacity and the coefficient of thermal expansion are vital for calculating heat transfer and conduction between the concrete particles. Thermal properties of hardening concrete change as the concrete hydrates. Therefore, the proposed model is designed to account for time dependency of key material properties used by the heat transfer module. This is achieved through adoption of the concept of degree of hydration which quantifies the magnitude of hydration as a function of time, by relying on the assumption that the growth or dissolution is controlled by the diffusion because of a liquid mass transfer layer [58, 59]. The degree of hydration at time t is defined as the ratio of the quantity of hydrated cementitious materials at time t to the total amount of cementitious materials. The degree of hydration can also be introduced as the ratio of the chemically bounded water at time t to the chemically bounded water at ideal complete hydration [58, 59]. Mathematically, the degree of hydration can be represented by the ratio of heat released to total heat available as below[16].

$$\alpha(t) = \frac{\Sigma H(t)}{H_T} \quad \text{Equation 4- 3}$$

where $\alpha(t)$ is the degree of hydration at time t , $\Sigma H(t)$ is the cumulative heat of hydration released at time t (J/m³) and H_T is the ultimate heat of hydration of concrete (J/m³).

The formulation adopted by our proposed model to account for time dependency of key thermal properties of concrete, by relying on the concept of degree of hydration, are described in the following.

- **Thermal conductivity**

In this study, the equations recommended by Schilder et al. [16] are used to calculate thermal conductivity of concrete. As shown by Equation 4-4, the selected formulation assumes that thermal conductivity decreases linearly with an increase in the degree of hydration [16]:

$$k_c(\alpha) = k_{ult} \times (1.33 - 0.33\alpha) \quad \text{Equation 4- 4}$$

where k_c is the thermal conductivity of the hardening concrete, (W/m/K), α is the degree of hydration, and k_{ult} is the ultimate thermal conductivity of the hardened concrete. The ultimate thermal conductivity is a function of mixture properties and should be introduced as an input parameter.

- **Specific heat**

Several methods have been proposed in previous studies to estimate the specific heat of concrete as a function of mixture proportions, degree of hydration, and temperature [114, 115]. Reinhardt proposed a linear function of the degree of hydration to obtain the specific heat of hardening concrete, [116]:

$$C_c(\alpha) = C_{ult} \times (1.25 - 0.25\alpha) \quad \text{Equation 4- 5}$$

where C_c is the specific heat of hardening concrete, (J/kg.m/K), α is the degree of hydration (Chapter 3), and C_{ult} is the ultimate specific heat of hardened concrete. The ultimate specific heat is a function of mixture properties and should be introduced as an input parameter.

- **Coefficient of thermal expansion of concrete**

The coefficient of thermal expansion of concrete utilizing in this study is calculated using Equation 4- 6 which relies on concrete mix proportions and properties of aggregates as input data[117].

$$CTE_c = \frac{CTE_{ca}V_{ca}+CTE_{fa}V_{fa}+CTE_pV_p}{V_{ca}+V_{fa}+V_p} \quad \text{Equation 4- 6}$$

In Equation 4-6, CTE_c , CTE_{ca} , CTE_{fa} , and CTE_p are the coefficient of thermal expansion of concrete mix, coarse aggregates, fine aggregates, and cement paste, respectively ($\mu\epsilon/^\circ\text{C}$) and V_{ca} , V_{fa} , and V_p are the volume of coarse aggregates, fine aggregates, and cement paste (kg/m^3).

- **Initial values and boundary conditions**

Initial temperature of concrete which has been shown to significantly affect the maximum temperature of the concrete element, as well as the temperature of the adjacent surfaces, and ambient temperature for the duration of the analysis which could impact the temperature gradient within the concrete element and consequently the risk of early age thermal cracking must be introduced [3]. Apart from their initial temperature, the type and thermal properties of adjacent contact surfaces can also considerably affect the transfer of heat inside and outside the concrete element. The effects of such contact surfaces including soil, water, or air are taken into account through defining appropriate convection and conduction boundary conditions on different external surfaces of concrete elements, as elaborated in the following sections.

4.2.1.3 Thermal boundary conditions

The convection boundary condition is imposed on the interface between the concrete element and the surrounding media including air, water or soil. Furthermore,

thermal radiation boundary condition is considered to account for radiation heat loss from concrete surfaces which are exposed to the ambient. The developed numerical model considers convection (ambient temperature, wind speed, and surface roughness), and solar radiation to account for the known effects of such parameters on the rate of thermal convection [3]. Furthermore, the effect of the type and color of the material used for the formworks, the use of other curing methods such as blankets, and contact with soil and water are taken into account in defining the heat flow in and out of the concrete element using the methodology presented in the following. Due to the 3-D nature of our proposed model, boundary conditions are defined for all top, bottom and side surfaces.

- Convection Model

Convection is the energy transfer from a surface to a surrounding fluid by diffusion (random fluid particle motion contacting the surface) and bulk motion of the fluid. In this study, Newton's law of cooling (Equation 4-7) explains the model of convection heat transfer [112].

$$q_{cv} = h(T_s - T_\infty) \quad \text{Equation 4- 7}$$

In Equation 4-7, q_{cv} is the convection heat flux (W/m^2), h is the convection coefficient ($\text{W}/\text{m}^2 \cdot \text{K}$), T_s is the surface temperature (K), and T_∞ is the fluid temperature (K), which can be approximated as T_a , viz. the ambient temperature (K). Convection heat transfer consists of two parts: free convection and forced convection. Free convection is caused by buoyancy forces from differences in local fluid density. On the contrary, the fluid motion in forced convection is caused by an external source of fluid motion [118]. In the case of mass concrete, convection is a combination of free and forced convection. As explained by Riding et al. [106], if the boundary layer air is heated by the concrete

surface, the air's density will be decreased and the air will travel up the surface (free convection). Moreover, forced convection is created by wind moving the air around the surfaces. In this study, the convection coefficient due to forced and free convections is [118]:

$$h = C \times 0.2782 \times \left[\frac{1}{T_{avg} + 17.8} \right]^{0.181} \times |T_s - T_a|^{0.266} \times \sqrt{1 + 2.8566 \times w}$$

Equation 4- 8

where T_{avg} is the average air film temperature (°C) which can be approximated by the average of T_a (ambient temperature) and T_s (surface temperature); C is a heat flow constant which is equal to 10.15, 15.89, and 20.4 for bottom, vertical, and top surfaces, respectively; and w is the wind speed (m/s). Equation 4-8 is for relatively smooth surfaces. In order to consider the surface roughness, the convection coefficient h should be multiplied by a roughness multiplier R_f . According to Clear et al. (2003), concrete has a roughness multiplier of 1.52 which is considered in the model once the formworks are removed [119]. The wind speed used in Equation 4-8 is obtained from the available weather data reported by Bureau of meteorology. The maximum wind speed is defined as a user input parameter.

In this study, ambient temperature considered in each simulation is acquired from the weather forecast provided by Weather Underground. In the absence of reliable forecasts on time variation of temperature during a day, the diurnal variation of the ambient air temperature is calculated using:

$$T_{air} = - \sin \left[\frac{2\pi(t_d + t_m)}{24} \right] \left[\frac{T_{max} - T_{min}}{2} \right] + \left[\frac{T_{max} + T_{min}}{2} \right]$$

Equation4-9

in which T_{max} and T_{min} are the maximum and minimum daily ambient temperatures, t_d is the time of the day at which the prediction is being made (0 to 24 hours) and t_m is the time of the occurrence of the minimum temperature overnight.

- Solar Radiation

Direct exposure to solar radiation may considerably affect the temperature development in the concrete element [120]. In this study, solar radiation is considered using a linear relationship between cloud cover and solar radiation as:

$$EH = (0.91 - (0.7 \times C)) \times ETOA \quad \text{Equation 4-10}$$

where EH is the surface horizontal solar radiation (W/m^2), C is the cloud cover fraction, and $ETOA$ is the extra-terrestrial horizontal solar radiation (W/m^2) [120].

- Irradiation from Concrete Surface

The Stefan-Boltzmann law, is used to calculate the radiation heat loss from the concrete surface [112]:

$$qc = \varepsilon_c \sigma T_c^4 \quad \text{Equation 4- 11}$$

where qc is the heat lost from the column (W/m^2); ε_c is the surface emissivity and it assumed to be equal to 0.92 for concrete, wood formworks and red steel formworks, while it is considered to be equal to 0.95 for yellow steel formworks [106]. σ is the Stefan-Boltzmann constant with a suggested value of 5.67×10^{-8} ($\text{W/m}^2 \cdot \text{K}^4$); and T_c (K) is the temperature of the concrete surface [112].

4.2.1.4 Curing methods

After formwork removal, concrete can be in contact with air, subsoil or water. Contact with air is modelled using the convection boundary condition explained

above. Furthermore, the heat conduction between the concrete mass and the surrounding environment such as soil or water is considered on the boundaries of the developed model. Accordingly, in case of defining soil or water in the boundaries, the thermal properties and user defined average soil/water temperature are considered in the thermal boundary conditions.

The choice of curing method to minimise excessive evaporation of water may considerably affect the heat transfer and should be considered in numerical simulation of early age thermal cracking of concrete. In this study, the common curing methods used in practice are incorporated through defining appropriate boundary conditions. These curing methods include covering the surface with plastic sheets, thermal blankets, or cure compounds [55]. To implement appropriate boundary conditions, a function is defined to modify the abrasion and emissivity values of each surface of concrete based on the type of the material that comes in contact with concrete during the curing process [106, 121]. When thermal blanket is used, boundary condition on top and side boundaries is implemented by using R -value and blanket thickness to estimate the equivalent thermal conductivity- k_{bl} - of the interface through the following:

$$k_{bl} = \frac{T_{bl}}{R_{bl}} \quad \text{Equation 4- 12}$$

where T_{bl} is the blanket thickness (m), and R_{bl} is the blanket R -value ((m²*k)/W). The default values of thickness and R -value are set as 0.025 (m) and 0.04 ((m²*k)/W) [122]. However, these values can be modified by the user for different cases.

4.2.2 Solid Mechanics model

Solid mechanics model in COMSOL Multiphysics software is employed to enable prediction of thermal stresses developed in concrete and therefore the early age

thermal cracking potential of a concrete element. The methodology adopted by the solid mechanics model is described in the following sections.

4.2.2.1 Stress-Strain Relationship in Early Age Concrete

De Schutter [103] suggests a linear elastic stress–strain relationship for short-term loading of concrete; and states that compressive stresses, in hardening concrete, are usually much smaller than compressive strength. This makes the proposed linear relationship accurate enough to use for early age concrete. Therefore, in the current model, the linear relationship is adopted to relate strains and stresses in concrete mass as shown in Equation 4-13 [123].

$$\sigma = \sigma_{ex} + C : \varepsilon_{el} = \sigma_{ex} + C : (\varepsilon - \varepsilon_{inel}) \quad \text{Equation 4- 13}$$

where σ and σ_{ex} are total and extra stress contribution tensors, respectively, C is the 4th order elasticity tensor, “:” stands for the double-dot tensor product or double contraction, ε_{el} , ε and ε_{inel} show elastic, total and inelastic strains, respectively. As discussed in Chapter 2, the mechanical properties of an early age concrete including compressive strength, tensile strength and Young’s modulus tend to vary as a function of concrete’s maturity. Concrete maturity is itself a function of degree of hydration which varies with time and with location inside the element. Therefore, in this study, the elastic modulus and Poisson ratio for each element are defined as a function of maturity and degree of hydration in every time step which will be defined in the next section.

4.2.2.2 Mechanical properties of hardening concrete

Given the early age nature of the analysis performed in this study, concrete properties evolve rapidly with time as cement hydrates. The rate of variations in

properties of concrete is influenced significantly by the rate of hydration of cement and therefore the parameters affecting the latter [122]. Failure to account for variations in the mechanical properties of concrete with time could lead to significant errors in estimation of stress, strain and consequently cracking potential of concrete. To account for variations in the mechanical properties, the present study adopts a dynamic approach in which all material properties are defined as a function of time. Some of the most important mechanical properties of concrete that should be defined for stress, strain and early age cracking predictions include compressive strength, tensile strength, Young's modulus, and Poisson's ratio. The proposed numerical model calculates all the mentioned properties as time dependent functions which consist of pre-defined constants. These assumed constants must be defined as inputs. Maturity method and degree of hydration concepts are the two competitive approaches commonly used to estimate the early age mechanical properties of hardening concrete [115]. As shown by Schindler [115], both methods principally yield the same results and conclusions, which can be used as valid tools for calculating the properties of the early age concrete. The formulations to predict the variations in different mechanical properties used in the proposed model are described in the following.

- **Compressive Strength development**

Compressive strength is a key property used by the solid mechanics modules to predict potential cracking under compressive load developed during restrained/unrestrained shrinkage and expansion of concrete. Several models have been proposed in previous studies to estimate the development of compressive strength in concrete [15, 122, 124]. In the present study, the maturity model concept is adopted to predict the variations in the compressive strength as shown by:

$$f_c(t_e) = f_{cult} \times \exp\left(-\left(\frac{\tau_s}{t_e}\right)^{\beta_s}\right) \quad \text{Equation 4- 14}$$

Where f_c is the compressive strength development (MPa), f_{cult} is the ultimate compressive strength of concrete from the compressive strength tests (MPa), τ_s and β_s are fitting parameters, and t_e is the equivalent age maturity (described in detail in Chapter 3). In the proposed numerical mode, the fitting parameters- τ_s and β_s - are considered as 27.8 (hour) and 0.721, respectively as suggested by Riding [122].

- **Young's modulus development**

Modulus of elasticity is used for calculating the shear modulus and shrinkage. A common method to estimate the elastic modulus development of the hardening concrete is to link its development rate to the development rate of compressive strength. Equation 4-15 shows the adopted method to estimate the elastic modulus development of concrete [125].

$$E = k \times (f_c)^n \quad \text{Equation 4- 15}$$

where E is the elastic modulus development (MPa), f_c is the compressive strength development (MPa), and n and k are fitting parameters; n is assumed to be equal to 0.5 and k is calculated using Equation 4-16.

$$k = 0.043 \times w_c^{1.5} \quad \text{Equation 4- 16}$$

where w_c is the density of fresh concrete.

- **Tensile Strength development**

Early age thermal cracking occurs when the tensile stresses developed in concrete exceeds its tensile strength. Therefore, the accuracy of cracking predictions can be significantly influenced by the level of accuracy in estimating the tensile

strength development of concrete. The tensile strength has been found to develop faster than compressive strength, but slower than the elastic modulus [126]. Equation 4-17 is used to estimate the tensile strength development by correlating its development rate to that of compressive strength that is [126]:

$$f_t = l \times (f_c)^m \quad \text{Equation 4- 17}$$

where f_t is the tensile strength development (MPa), and l and m are fitting parameters. Based on the results of the extensive studies conducted by Raphael [126], in this study we consider the values of l and m to be 0.3 and 0.66, respectively.

- **Poisson's ratio**

Estimating the Poisson's ratio of concrete is essential for predicting its shear modulus. As long as the concrete is in its liquid state, the Poisson's ratio is equal or close to that of water and is considered equal to 0.5. After setting, however, the hydration process transforms the concrete mix from a suspended liquid to a rigid skeleton; and therefore the Poisson's ratio of concrete tends to decrease gradually to reach commonly a value between 0.15 and 0.2 [27]. In our proposed model, Equation 4-18 is used to estimate the changes in Poisson's ratio as a function of the degree of hydration [108].

$$v(\alpha) = 0.18 \times \sin\left(\frac{\pi \times \alpha}{2}\right) + 0.5 \times \exp(-10\alpha) \quad \text{Equation 4- 18}$$

It should be noted that the aforementioned formulas and constants are suggested for normal concrete and may not be used for all concrete types especially concretes subject to especial curing methods. In such cases, the constants should be calculated for each case considering the specification of the concrete under study.

4.2.2.3 Mechanical boundary conditions

Adopting appropriate mechanical boundary conditions is essential for accurate prediction of tensile strain and the risk of early age thermal cracking of concrete. As discussed in ACI207.2R-07, all concrete elements are restrained to some degree by volume because there is typically some restraint provided either by the supporting elements or by different parts of the element itself [2]. Two types of restraints can be categorised: external and internal restraints [127]. Both types are interrelated and usually exist to some degree in all concrete elements. Internal restraint exists due to non-uniform volume change in the concrete mass while the external restraint exists along the constant surfaces and boundaries of the concrete mass [3]. In our numerical model, internal restraints are embedded in formulation of the solid mechanics module of COMSOL Multiphysics while the external restraints should be accurately defined using the appropriate mechanical boundary conditions. No shear resistance between the formworks and the concrete surface is assumed. In the bottom boundary, where the concrete mass is in contact with the foundation, high degree of resistant in both normal and shear directions are present which is mainly a function of foundation rigidity. Therefore, the bottom boundary condition is defined as a spring foundation with spring constant relevant to foundation rigidity as:

$$k = \begin{bmatrix} GT & 0 & 0 \\ 0 & GT & 0 \\ 0 & 0 & 2.1e^{10} \end{bmatrix} \quad \text{Equation 4- 19}$$

where, k is the sprig constant per unit area, GT is the modulus of rigidity of hardening concrete defined as Equation 4-20 (Pa) and $2.1e^{10}$ is the modulus of rigidity for hardened concrete (Pa) which is related to the foundation in contact with the bottom surface of the wall.

$$GT(t) = \frac{E(t)}{2(1+\nu(t))} \quad \text{Equation 4- 20}$$

where $E(t)$ and $\nu(t)$ are modulus of elasticity and Poisson's ratio of hardening concrete, respectively, and are calculated using the methodology described in Section 4-2-2-2.

In the developed numerical model, the characteristics of the mechanical boundary conditions are defined in accordance with ACI207.2R-07 [2]. The initial values for the displacement field and velocity field are set to zero.

4.2.3 Numerical simulation of reinforcement

Reinforcing steel bars are commonly used in a majority of structural concrete elements to improve tensile behaviour and limit the growth of cracks [128]. The reinforcing bars generally possess a considerably higher thermal conductivity compared to concrete and the presence of significant amount of steel bars in heavily reinforced concrete may affect the transfer of heat within the concrete element [128]. Despite this the presence of reinforcing bar is commonly overlooked as a simplifying assumption in a majority of previously developed early age thermal cracking simulation models and software.

In our proposed model, the effect of reinforcing bars on heat transfer and development of temperature in concrete is accounted for using a predefined geometrical module that allows defining the sizing and spacing of the bars for the elements under study. In particular, truss interface in COMSOL Multiphysics, as shown in Figure 4-2, is used to eliminate the necessity of using small meshes to model the bars resulting in the considerable save in computational time. Since the steel reinforcements are relatively thin compared to the concrete section, it is assumed that steel reinforcements

are only transmitting axial forces, and the bending stiffness of each bar does not contribute much to the overall total bending stiffness of the section. The developed numerical model is capable of simulating common reinforcement configurations in the cross-section by assigning the covers, space between bars, number of layers, and diameter of bars in the bottom, side, and top boundaries of the three-dimensional numerical model. The material properties of the reinforcing steel bars are used by the model are listed in Table 4-1.

4.2.4 Coupling Heat transfer and Solid mechanics models

To numerically simulate the thermal expansion in concrete and the resulting thermal stresses, the heat transfer and solid mechanics models are coupled, so that the temperature and displacement fields will be analysed simultaneously. Accordingly, thermal expansion of concrete is calculated using the following equation:

$$\varepsilon_{th} = CTE_c \times \Delta T \quad \text{Equation 4- 21}$$

where, ε_{th} is the thermal strain, ΔT is the change of temperature (K), and CTE_c is the coefficient of thermal expansion of hardening concrete (1/K) which can be obtained from Equation 4-6.

Table 4- 1 properties of structural steel

Density	7850 [kg/m ³]
Young's modulus	200 e9 [Pa]
Heat capacity at constant pressure	475 [J/(kg*K)]
Poisson's ratio	0.33
Thermal conductivity	44.5 [W/(m*K)]
Electrical conductivity	4.032 e6 [S/m]
Coefficient of thermal expansion	12.3 e-6 [1/K]

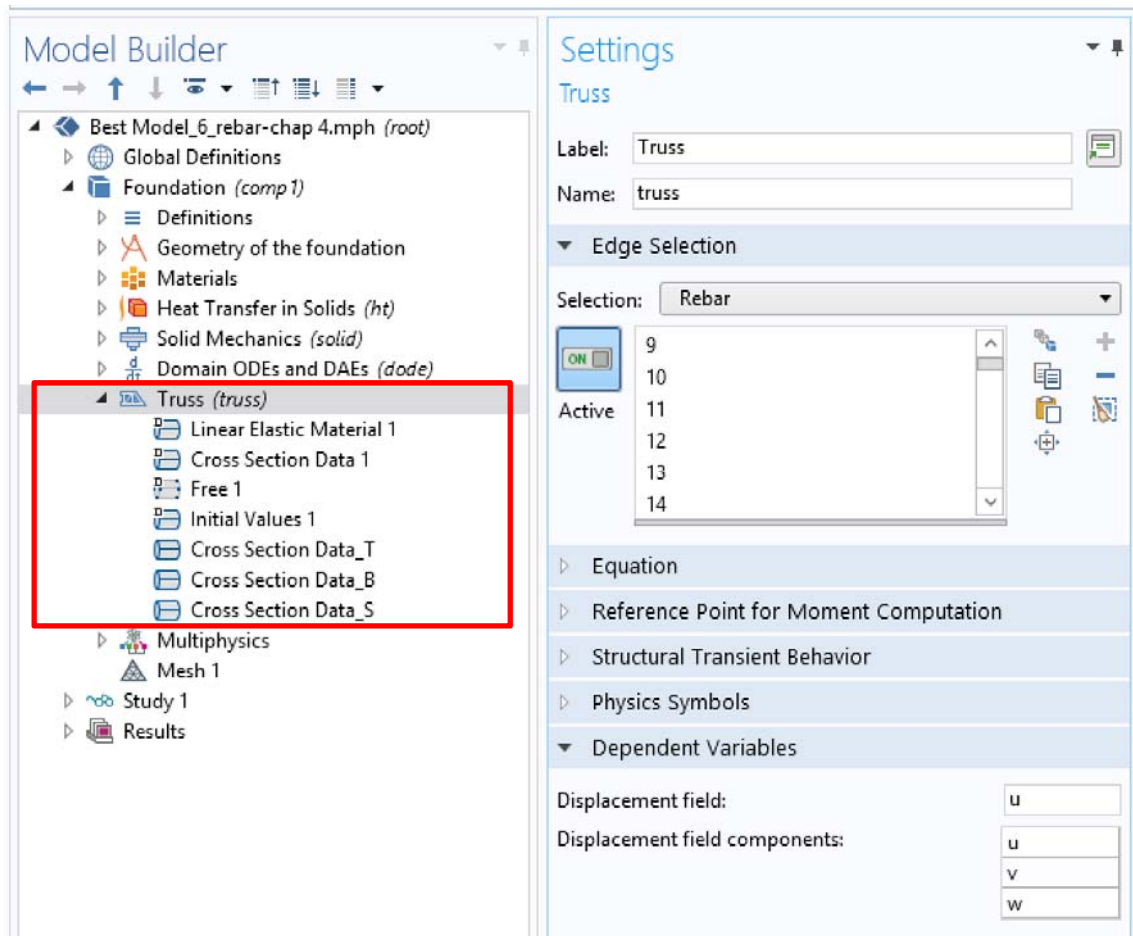


Figure 4- 2 Truss interface

Moreover, the numerical model developed in this study estimates the risk of early age cracking by relying on the commonly used assumption that cracking occurs when the highest principal tensile stress reaches the actual and local tensile strength [103]. Cracking ratio is used as a measure of risk of cracking and is defined as the ratio of developed tensile stress to tensile strength in the early age concrete [105, 122]. The estimated cracking ration is linked with a cracking probability using the cracking probability density function proposed by Riding (Figure 4-3) based on the results of extensive experiments [122]. The adopted probability density function follows a lognormal distribution and is divided into four risk regions as defined below:

- Low risk: 25% or lower cracking probability (cracking ratio<0.6)

- Moderate risk: 25% to 50% cracking probability ($0.6 < \text{cracking ratio} < 0.66$)
- High risk: 50% to 75% cracking probability ($0.66 < \text{cracking ratio} < 0.73$)
- Very High risk: more than 75% cracking probability ($0.73 < \text{cracking ratio}$)

4.2.5 Ordinary Differential Equation (ODEs)

As explained, all the properties of hardening concrete vary with time. It is necessary to undertake time-integration for each zone in every time-step in order to calculate the accumulative values such as concrete maturity, and the degree of hydration in the developed numerical model. As such, the model is coupled with time-dependant Ordinary Differential Equation (ODEs) interface. Accordingly, the defined ODEs in COMSOL Multiphysics calculates the time-integration of the required parameters. The developed ODE is fully coupled with the concrete heat transfer model by sharing the dependable variables.

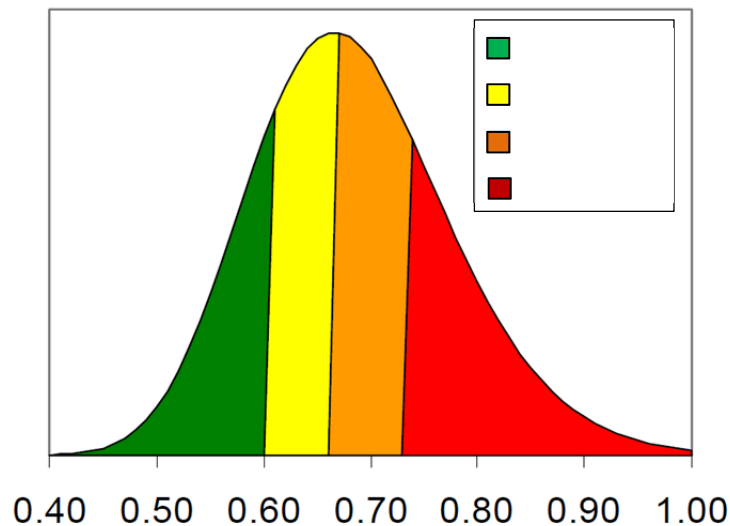


Figure 4- 3 Cracking probability density [122]

4.3 Case study

A case study involving modelling and monitoring the temperature development of a concrete wall section is presented to validate the proposed model and demonstrate its applications. Furthermore, apart from temperature, other results including the development of different properties, as well as resulting thermal stresses and cracking potential of concrete are presented to demonstrate the benefits of our model. The dimensions of the concrete wall were $13.07(L) \times 2.1(H) \times 1.2(T)$ (m); and it was built in one of Boral Quarries in Queensland, Australia. The planned mix design for this wall is presented in Table 4-2. Furthermore, the composition of the Portland cement used in this project is shown in Table 4-3.

The heat parameters were calculated using the data shown in Table 4-3 and Equations presented in Chapter 3 to use in the hydration heat calculation presented also in Chapter 3; The heat parameters were calculated using the data shown in Table 4-3 and

Table 4- 2 Mix design of the concrete wall

Material	Mass (Kg/m ³)
Cement	260
Slag	173
Water	199
W/CM	0.46
West Burleigh 10 mm	828
Zannows Coarse sand	501
Lytton Fine sand	401

Table 4- 3 Composition of Portland cement

Cement composition	Weight (%)
C ₃ S	64.07
C ₂ S	8.18
C ₃ A	9.36
C ₄ AF	8.49
CaO	0.64
K ₂ O	0.41
SO ₃	2.78
MgO	1.41
Na ₂ O	0.26
Blaine	367 (m ² /Kg)

equations presented in Chapter 3 to use in the hydration heat calculation presented also in Chapter 3; and the results are presented in Table 4-4. Furthermore, the values of other input parameters assumed for this case study are presented in Table 4-5. In order to evaluate the effect of using direct calorimetry measurements, rather than hydration heat equations, on accuracy of predictions, the simulation was repeated once by varying the heat source estimation methodology from one method to another. To direct calorimetry measurements were obtained using isothermal calorimetry of the binder mix used in this project at three different temperatures of 25, 30 and 40°C and the results are shown in Figure 4-4.

Table 4- 4 Heat parameters for the concrete mix design based on Bogue model

Heat Parameters	Values
Activation Energy	38244.85 (J/mol)
τ	26.465 (hrs)
β	0.3589
α	0.827
H_u	479.356 (kJ/kg)

Table 4- 5 Input parameters

Input parameters	Values
Time step	0.05 (hrs)
Analysis duration	100 (hrs)
Time of formwork removal	100 (hrs)
k_{ult}	2.5 (W/m/K)
Cp_{ult}	800 (J/kg/K)
f_{ult}	40 (MPa)
Initial temperature of concrete	25 (□)
Formwork type	Yellow steel
Curing	Normal curing

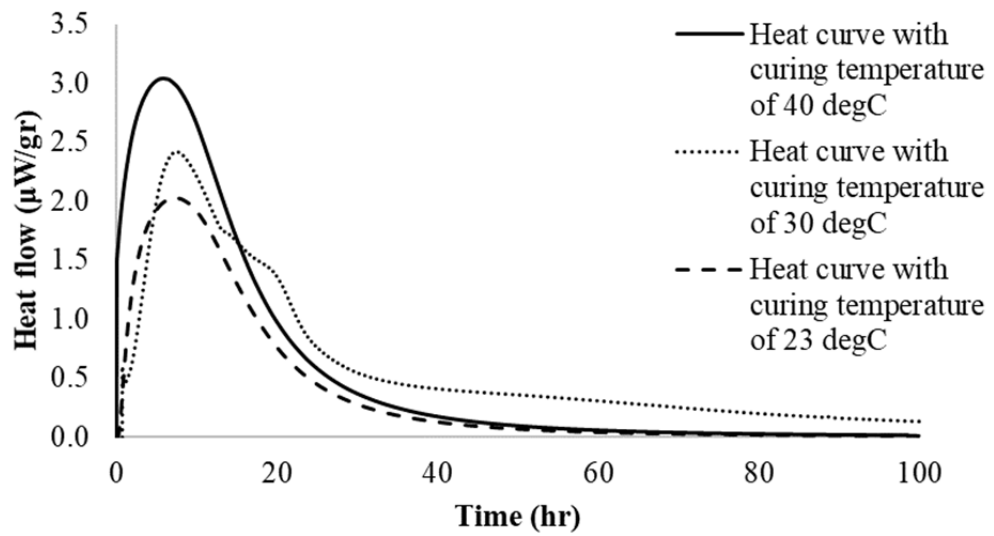


Figure 4- 4 Measured heat data under three different curing temperatures

In order to verify the results of our proposed numerical model, in-situ measurement of temperature at 15 points inside the concrete wall were carried SmartRock2 wireless temperature sensors. Moreover, one temperature sensor was installed outside the wall to record ambient temperature. The location of the installed sensors is shown in Figures 4-5 and 4-6. The measured temperatures were extracted from sensors four days after concrete placement.

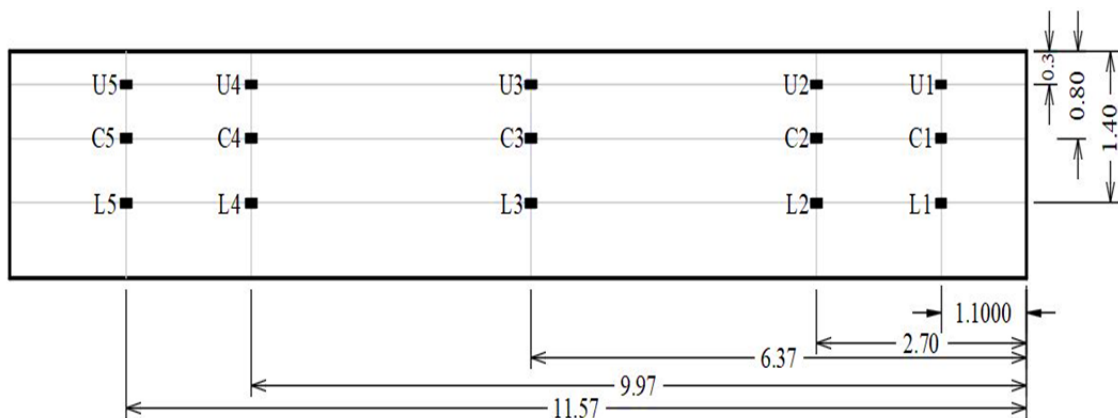


Figure 4- 5 Embedded sensor locations (in meter)

The concrete wall was modelled numerically using the proposed numerical model. Since the wall was exposed to ambient, convection and solar radiation boundary conditions were imposed on all side surfaces as well as the top surface of the wall, while conduction with the concrete foundation was considered as thermal boundary condition for the bottom surface. Furthermore, all side surfaces and the top surface were defined unrestrained, whereas the bottom surface which was in contact with the foundation was defined as a spring foundation based on Equation 4-19. The temperature, thermal stresses and resulting cracking ratios were numerically obtained. In particular, the temperature predictions at the coordinates corresponding to the exact location of embedded temperature sensors were used to validate the model (Figure 4-7).





Figure 4- 6 Sensor Installation and data collection

Moreover, in order to consider the impacts of the reinforcing bars on hydration heat development, a 30cm×30cm reinforcement mesh at the top and side surfaces of the concrete wall is simulated numerically (Figure 4-8). $\varnothing 16$ steel bars are selected for reinforcement; and a concrete cover of 500 mm is considered for the outer surface of the concrete element

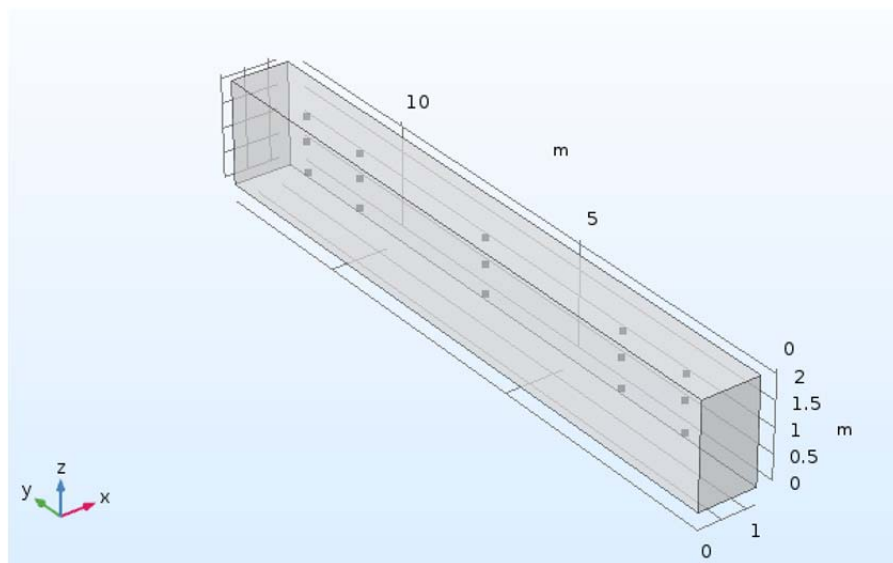


Figure 4- 7 Numerical model of the concrete wall

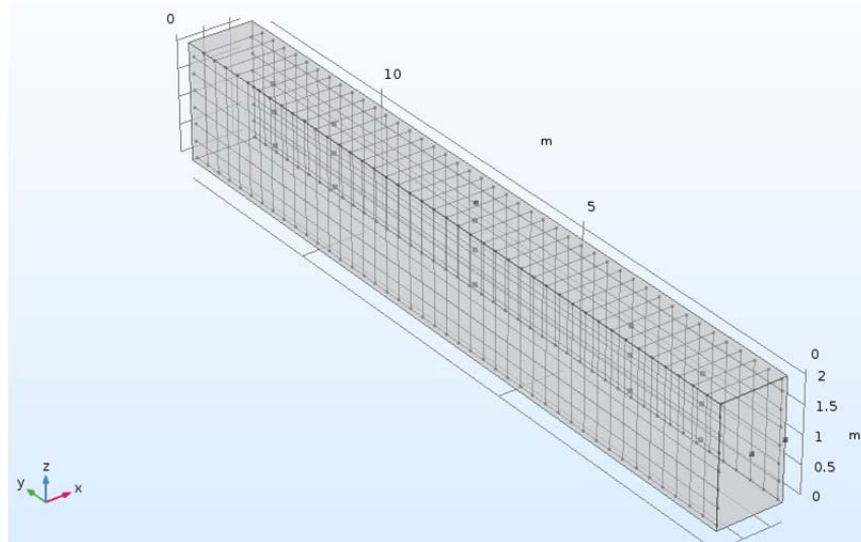


Figure 4- 8 Reinforced element simulation

4.3.1.1 Results and discussion

Figure 4-9 shows the variations in the ambient temperature as recorded by temperature sensor installed outside in close vicinity of the concrete wall. As can be seen, the variations in the ambient temperature during a day may vary considerably from one day to another; and the range of variations may be significant. This highlights the importance of a realistic ambient temperature input to the model using reliable forecasts. Table 4-6 compares the measured and predicted maximum peak temperatures for all the points highlighted in Figure 4-7.

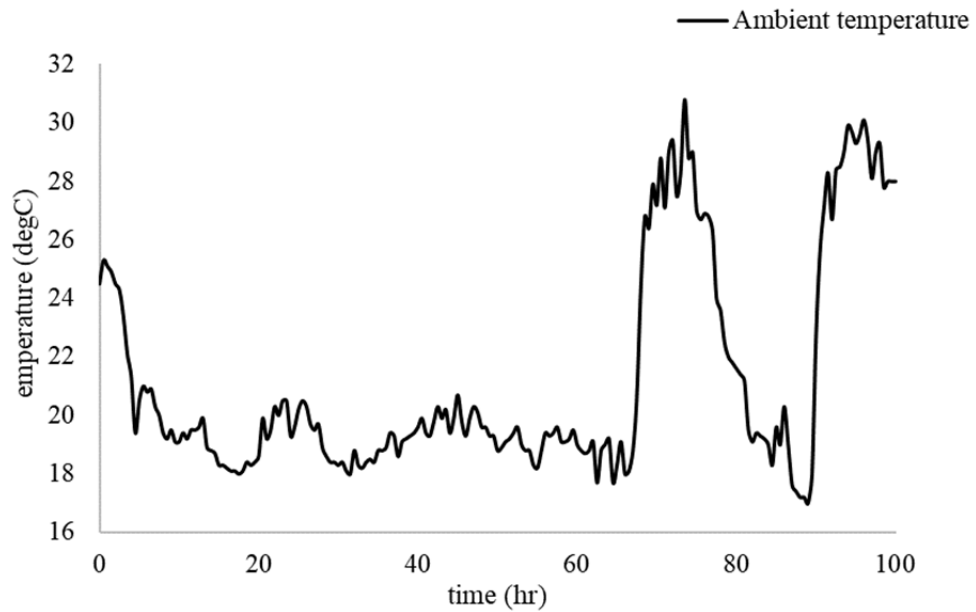


Figure 4- 9 Recorded ambient temperature

Furthermore, Figures 4-10 to 4-12 show the variations in the temperature with time at three random selected points. As can be seen, comparing the results shows insignificant errors in predicting the maximum temperature as well as predicting the variations in temperature with time. Therefore, the results confirm the acceptable precision of the numerical simulation model in predicting the temperature profile and thus the reliability of the numerical model to compare different mixes.

Figure 4-13 and Table 4-7 compare the temperature prediction results obtained through numerical simulation runs performed using direct calorimetry data with those obtained by using Equation 4-2 as heat source. As can be seen, direct use of calorimetry measurement as heat source in heat transfer model led to noticeable improvements in the accuracy of temperature predictions. Use of direct calorimetry data in particular led to about 3% decrease in the overall error of temperature prediction, which significantly improves the overall precision of the model.

Table 4- 6 Comparing the numerical model results and temperature sensor measurements

Point	Max. measured temperature (DegC)	Max. Predicted Temperature (DegC)	Error (%)
U1	77.5	70.34	9.24%
L1	79.5	82.50	3.77%
U2	70.4	70.67	0.38%
C2	77.2	82.7	7.12%
L2	76.7	82.9	8.08%
U3	71.3	70.81	0.69%
C3	81.0	82.86	2.30%
L3	77.9	82.86	6.37%
U4	68.1	70.74	3.88%
C4	80.5	82.79	2.84%
L4	78.3	82.89	5.86%
U5	67.7	70.76	4.52%
L5	77.7	82.76	6.51%

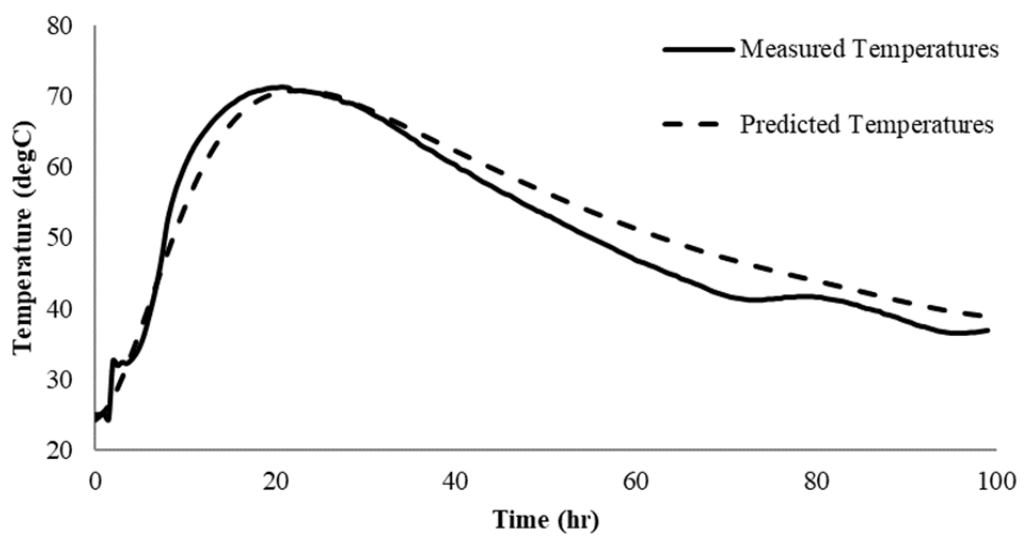


Figure 4- 10 Comparison between numerical results and site measurements for point U3

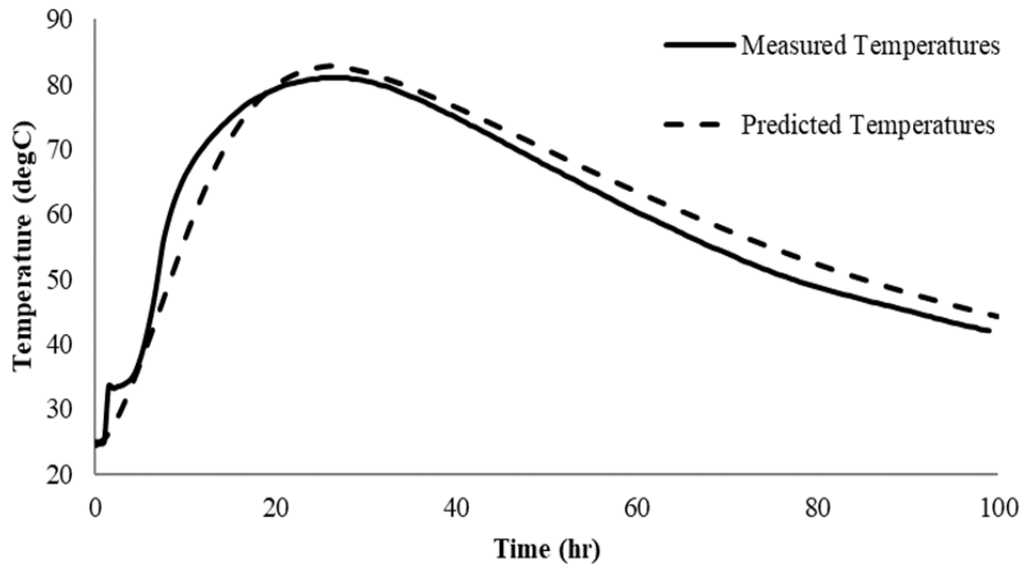


Figure 4- 11 Comparison between numerical results and site measurements for point C3

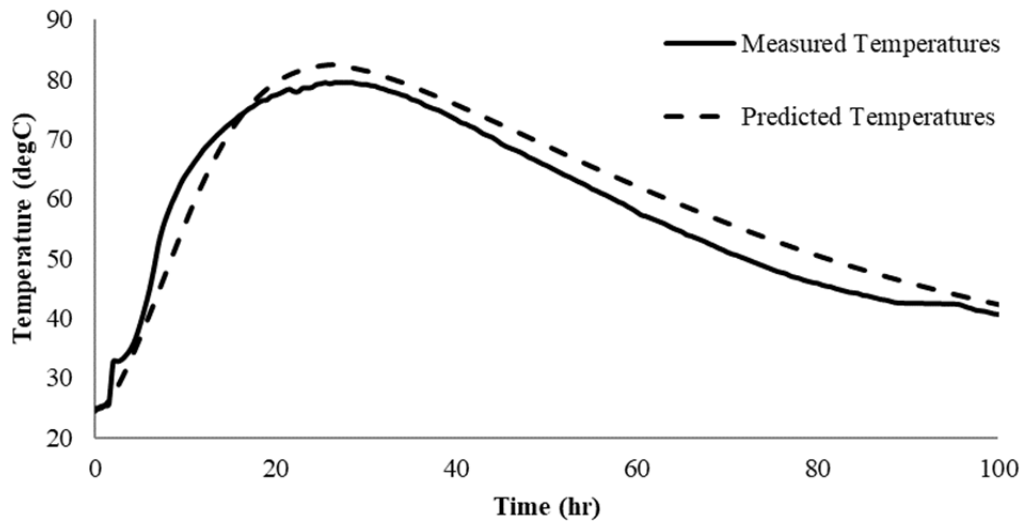


Figure 4- 12 Comparison between numerical results and site measurements for point L1

The level of improvements is expected to be significantly higher when dealing with concrete mixes with high SCM content and/or retarders, due to significant errors in predictions of hydration heat models reported for such mixes, as discussed in Chapter 3.

Table 4- 7 Comparing the numerical model results when using the direct calorimetry results and heat prediction model with temperature sensor measurements

Point	Max. measured temperature (degC)	Max. Predicted Temperature when using the heat prediction model (degC)	Error when using the heat prediction model (%)	Max. Predicted Temperature when using the calorimetry data (degC)	Error when using the calorimetry data (%)
U1	77.5	70.3	9.24%	71.92	7.19%
L1	79.5	82.5	3.77%	80.17	0.84%
U2	70.4	70.7	0.38%	70.73	0.47%
C2	77.2	82.7	7.12%	81.30	5.31%
L2	76.7	82.9	8.08%	80.19	4.55%
U3	71.3	70.8	0.69%	70.49	1.14%
C3	81.0	82.9	2.30%	81.08	0.10%
L3	77.9	82.9	6.37%	80.08	2.79%
U4	68.1	70.7	3.88%	70.20	3.08%
C4	80.5	82.8	2.84%	80.82	0.39%
L4	78.3	82.9	5.86%	79.97	2.13%
U5	67.7	70.8	4.52%	70.56	4.22%
L5	77.7	82.8	6.51%	79.89	2.82%

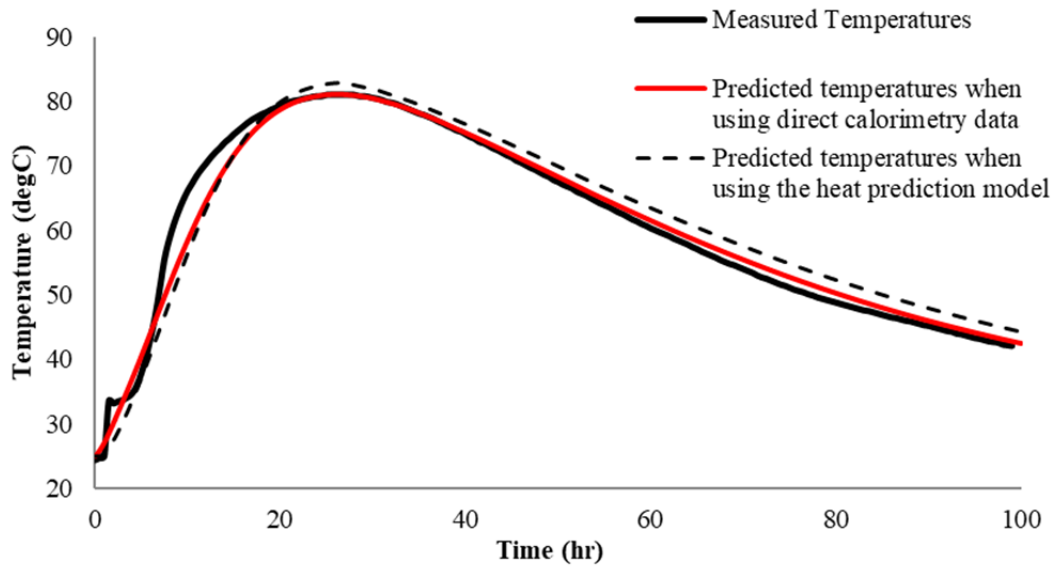


Figure 4- 13 Comparing the numerical model results when using the direct calorimetry results and heat prediction model with temperature sensor measurements for point C3

One of the main advantages of proposed model compared previous models and commercially available software is its 3D nature and its extensive post processing capability. The latter enables a thorough analysis of distribution of temperature, stresses and cracking risk across a concrete element, rather than only at specified points. This is illustrated in Figures 4-14 to 4-18 which provide different slice views of temperature development in the wall modelled in this study at different times.

Due to the direct relationship between the risk of early age thermal cracking and the level of tensile stresses, four different points with the highest and the lowest risk of cracking are defined in the model as shown in Figure 4-19 to study.

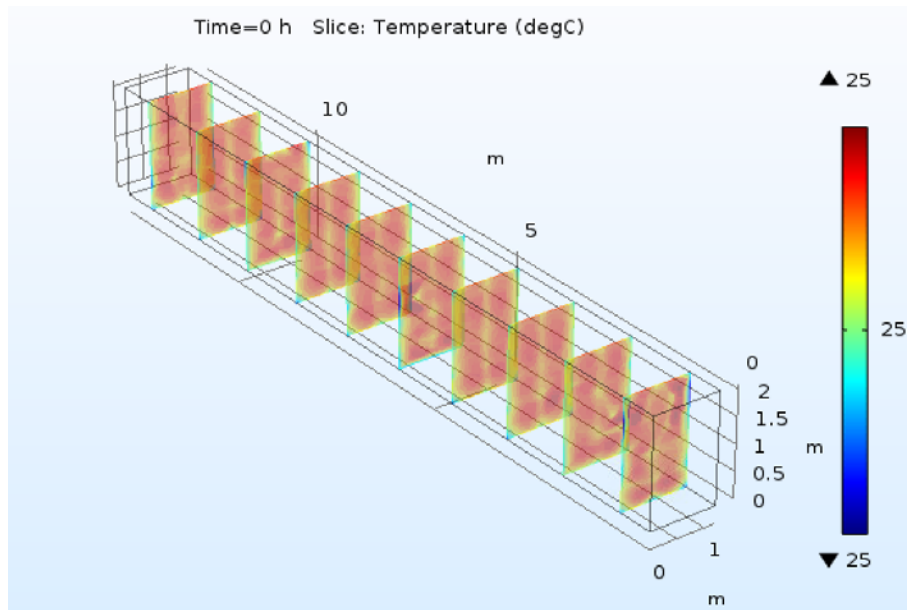


Figure 4- 14 2D presentation of temperature results at t=0 (hr)

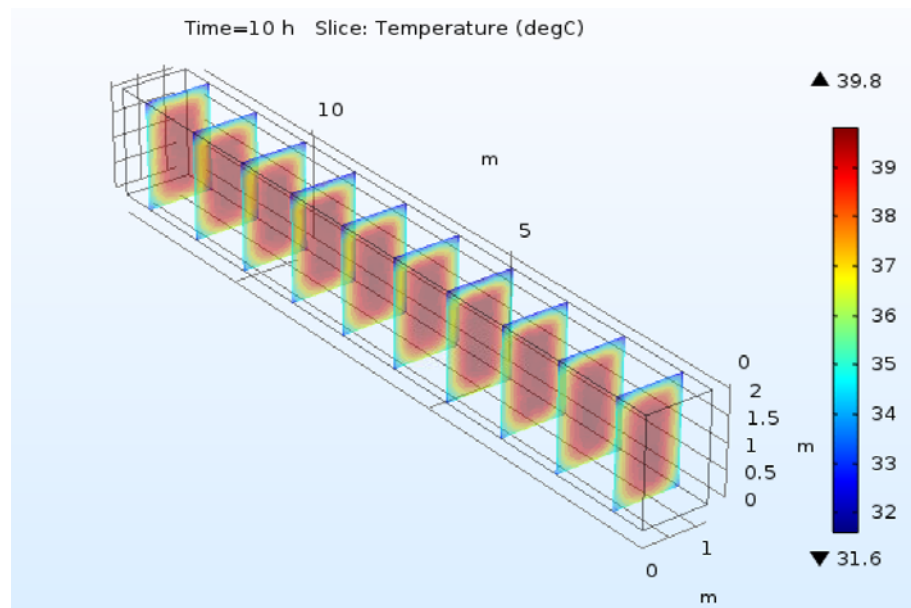


Figure 4- 15 2D presentation of temperature results s at t=10 (hr)

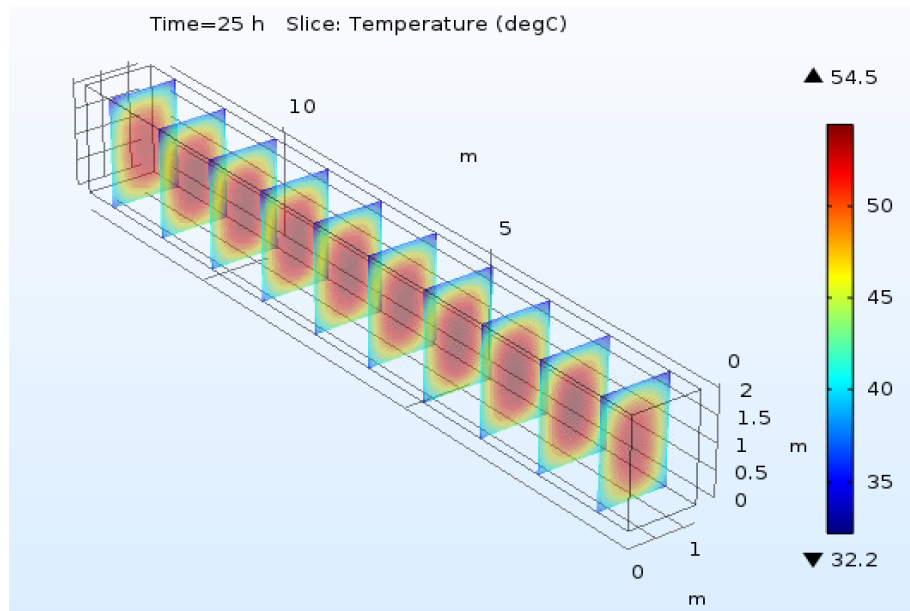


Figure 4- 16 2D presentation of temperature results at t=25 (hr)

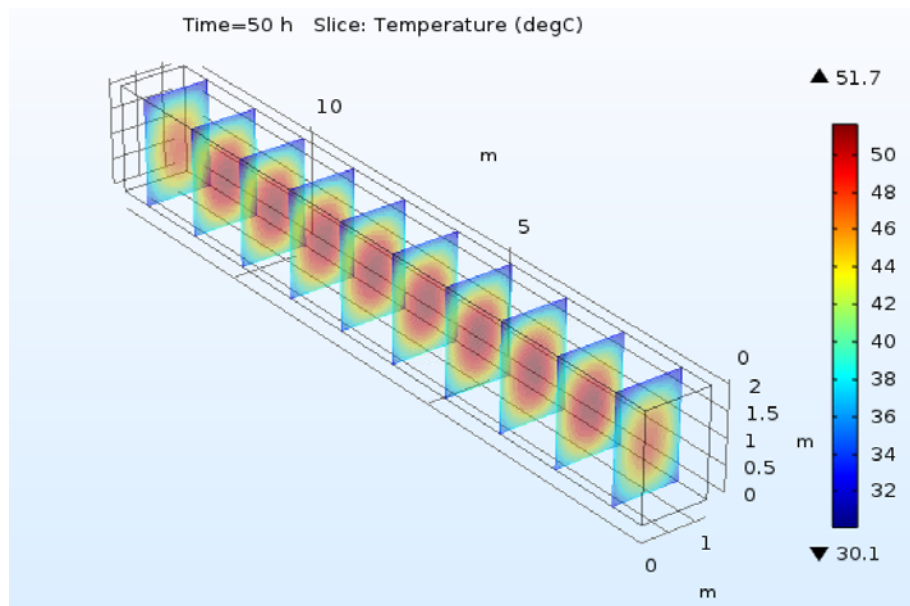


Figure 4- 17 2D presentation of temperature results at t=50 (hr)

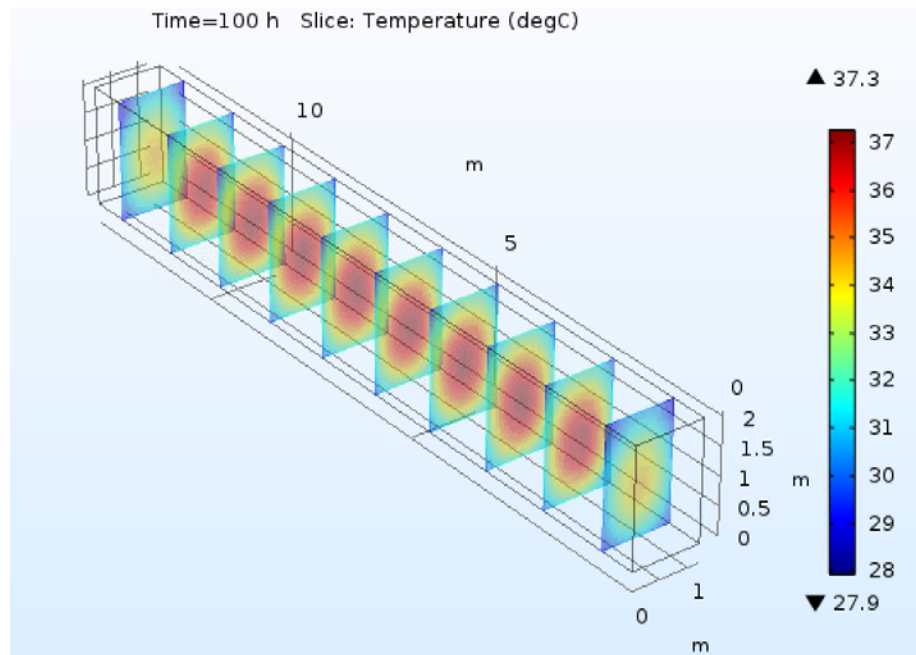


Figure 4- 18 2D presentation of temperature results at t=100 (hr)

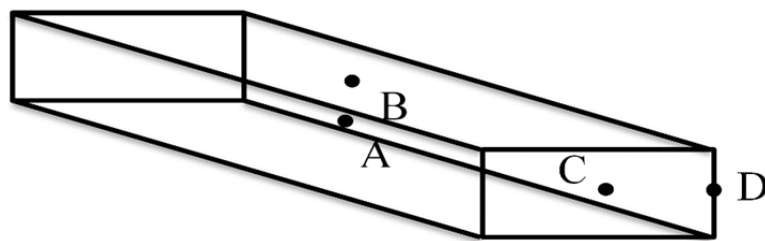


Figure 4- 19 The studied points on the raft

Figures 4-20 and 4-21 illustrate the thermal stress development in the mentioned points. As can be seen, the compressive stress is higher in the middle point while the tensile stress is higher at the surface points. Moreover, Figure 4-22 shows the cracking ratio at the selected points. As can be seen, the cracking ratio is the highest at Point D which is a corner point and the least cracking ratio occurs in the middle point of the element. Based on section 4-2-4, the probability of cracking for this element is very high as the cracking ratio reaches 1 at the surface point.

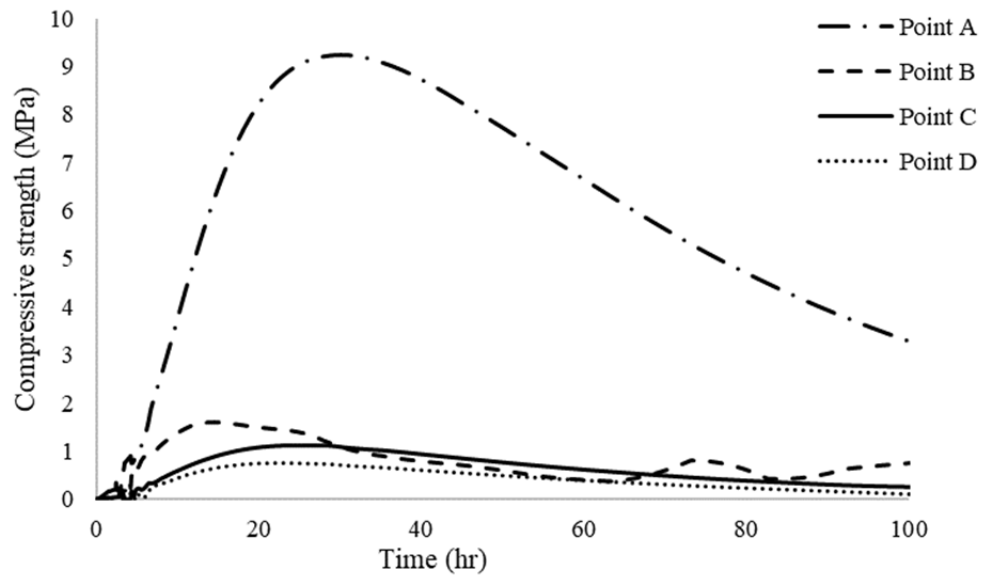


Figure 4- 20 Thermal (compressive) stress development

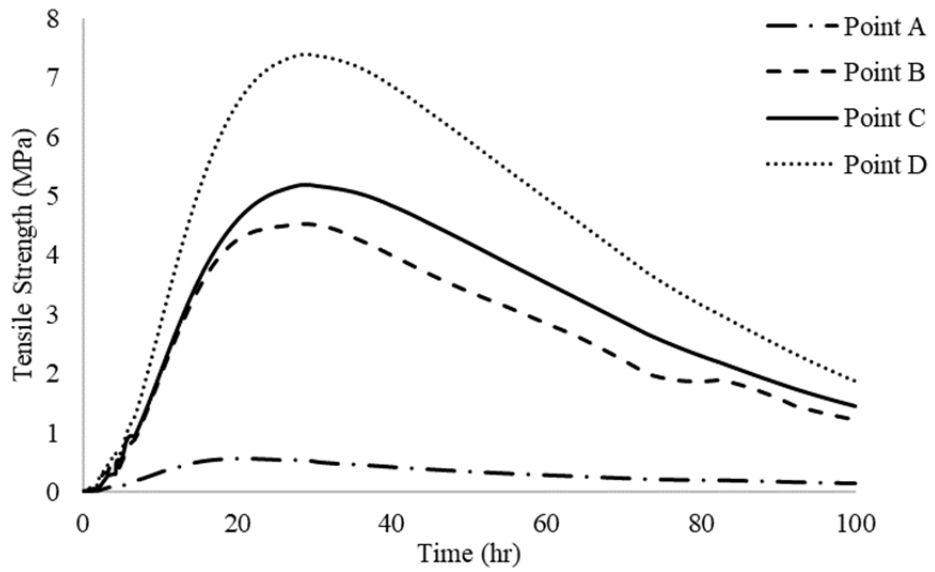


Figure 4- 21 Thermal (tensile) stress development

Figures 4-23 to 4-26 shows the crack formation pattern. As can be seen the cracking ratio is higher mostly on the surfaces.

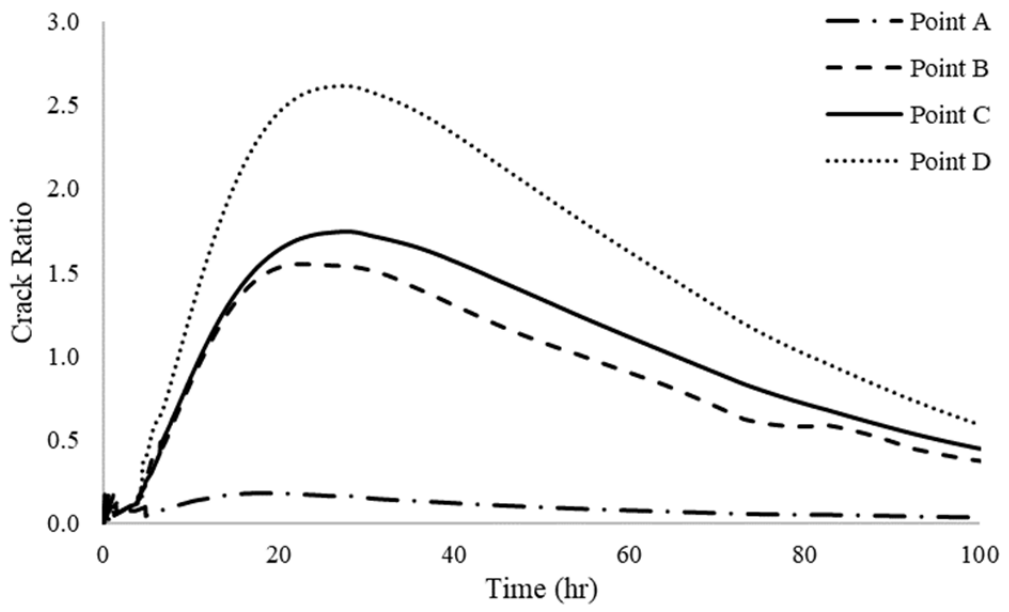


Figure 4- 22 Cracking ratio development

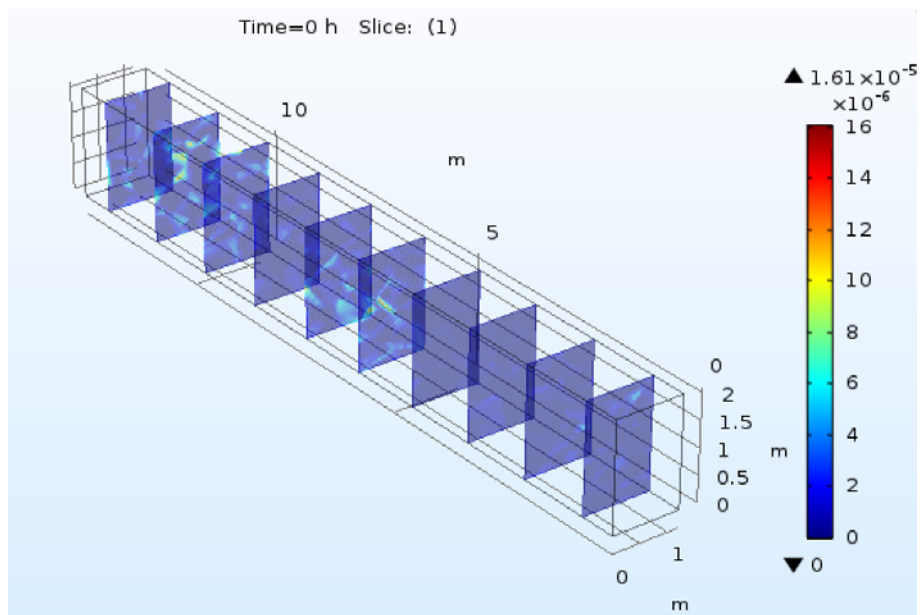


Figure 4- 23 Cracking ratio pattern at $t=0$ (hr)

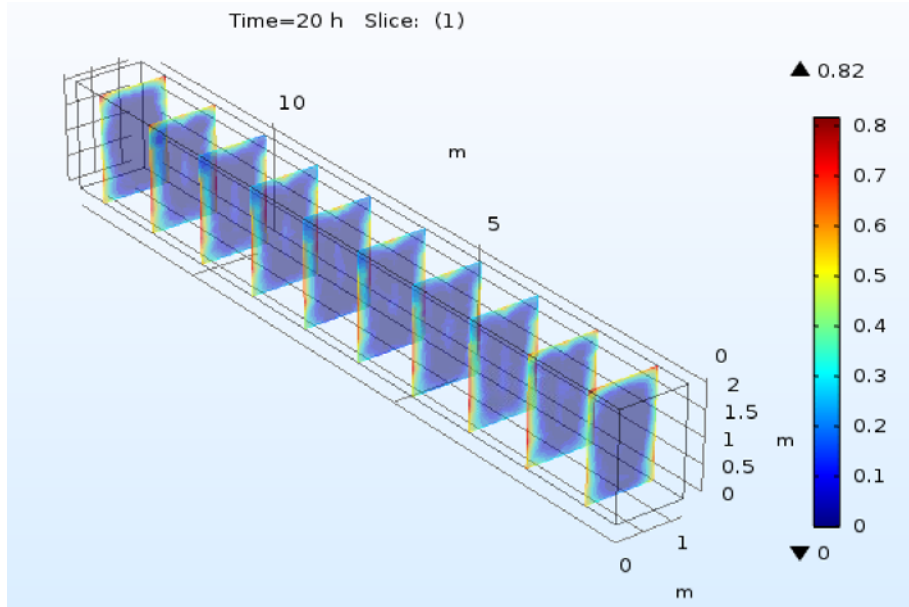


Figure 4- 24 Cracking ratio pattern at $t=20$ (hr)

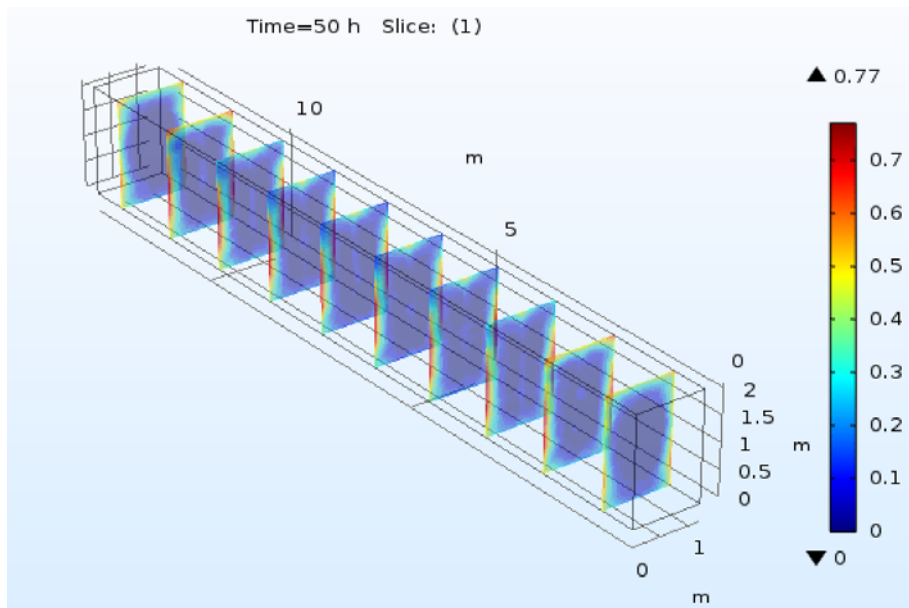


Figure 4- 25 Cracking ratio pattern at $t=50$ (hr)

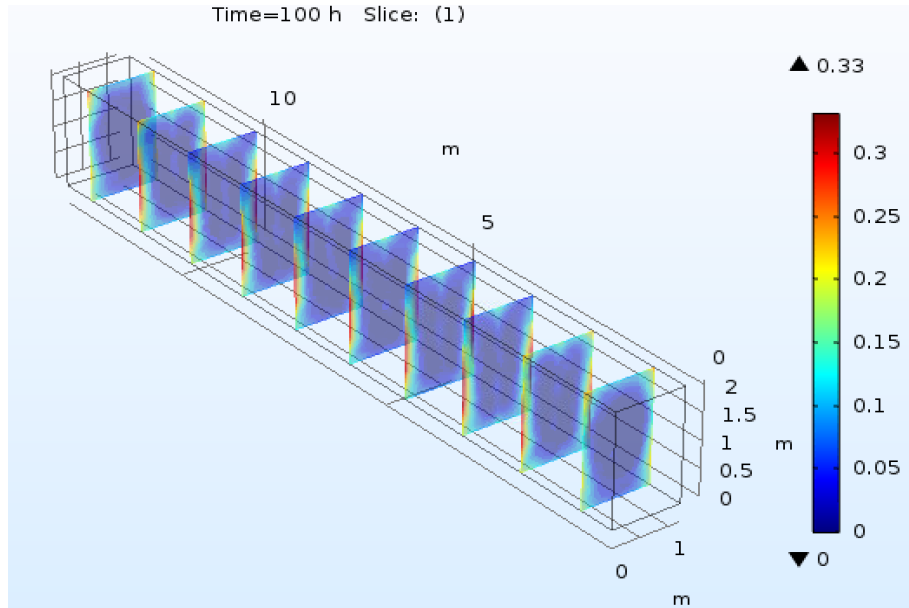


Figure 4- 26 Cracking ratio pattern at t=100 (hr)

Reinforcement simulation

As discussed earlier, in order to consider the impact of reinforcement on the analysis, reinforced concrete wall was modelled as well. After analysing the reinforced concrete wall, temperature development at point A in Figure 4-19 as well as the cracking ratio at the points highlighted in Figure 4-19 are compared to those obtained when modelling the wall without reinforcement. The temperature development pattern for the reinforced concrete is shown in Figure 4-27. Figure 4-28 displays the effect of reinforcement on temperature development. As can be seen in Figure 4-29, the cracking ratio is slightly reduced due to adding the reinforcements. The reinforcement impact can be more significant for cases containing more and closer spaced reinforcing bars.

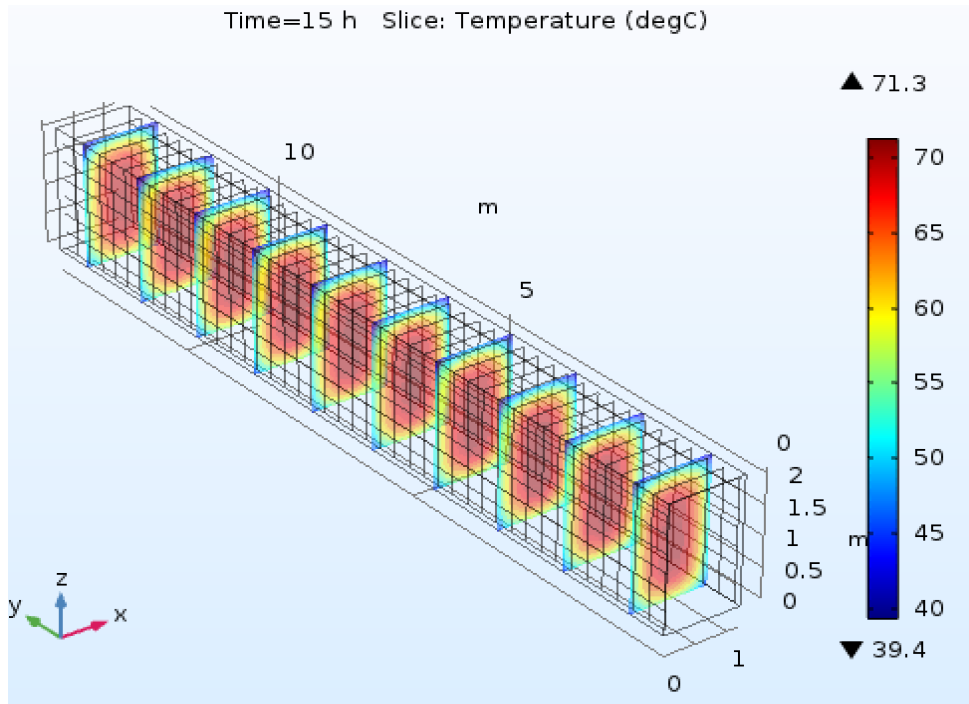


Figure 4- 27 Temperature development pattern at t=100 (hr)

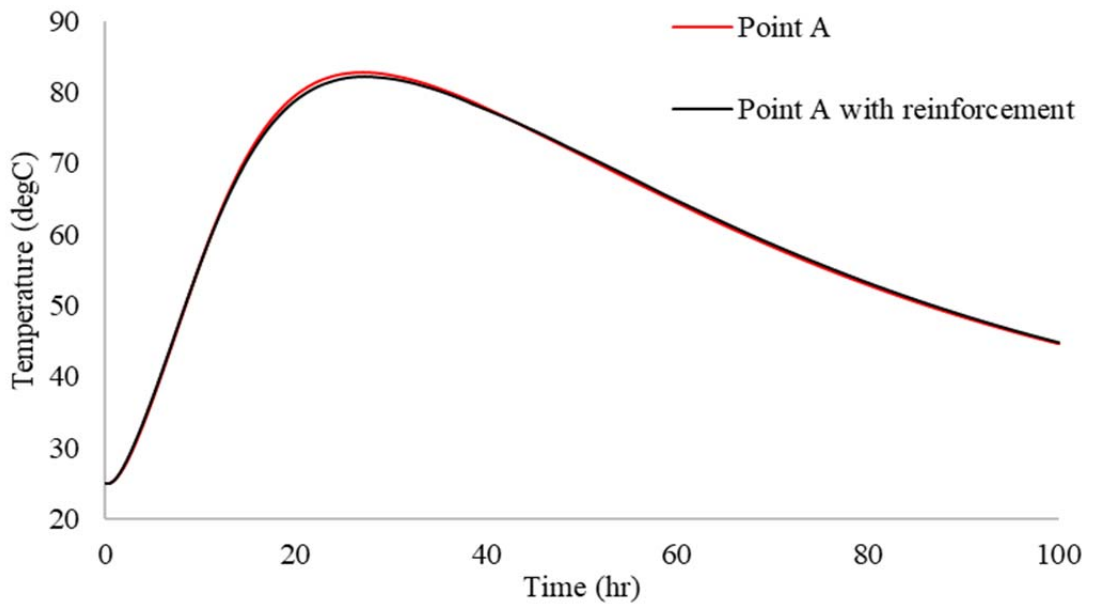


Figure 4- 28 Temperature development of Point A for the wall with or without reinforcement

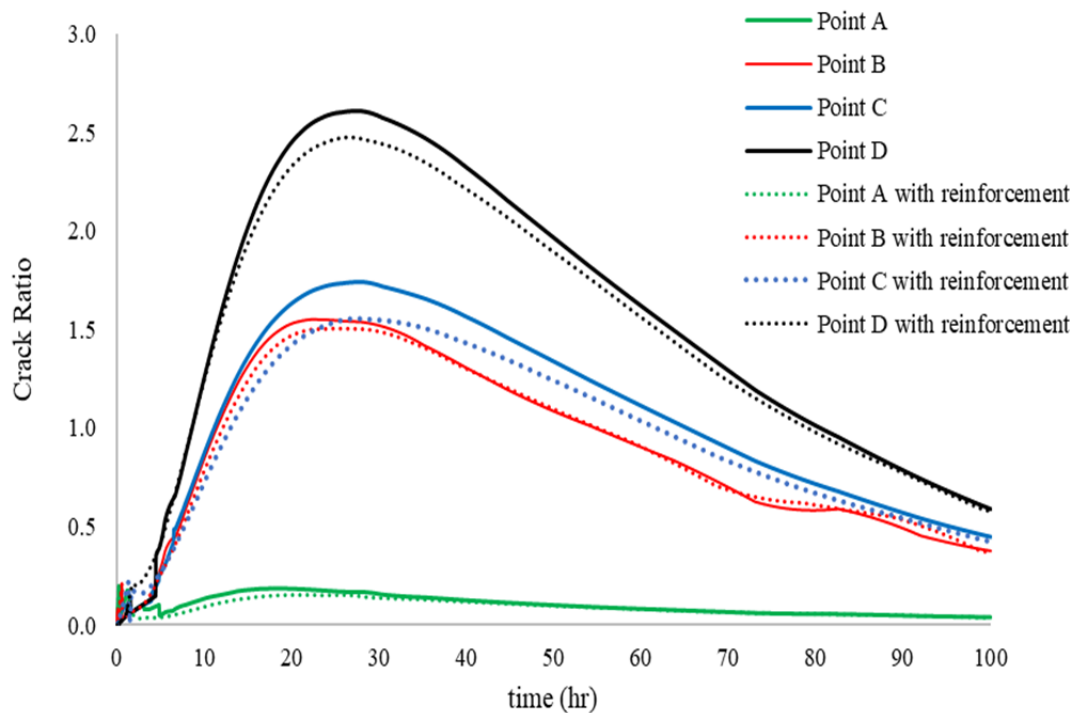


Figure 4- 29 Cracking ratio pattern at t=100 (hr)

4.4 Conclusions

A reliable simulation model to estimate the development of temperature gradient, thermal stresses and cracking ratio in a concrete element is crucial to detect and minimise the risk of early age thermal cracking in the design stage. However, the models developed in previous studies have a number of major drawbacks; these include i) a lack of precision of hydration heat models employed in previous simulation models, and ii) their 2D nature, and iii) the limited range of geometries that can be modelled, In this chapter, a finite element 3D numerical simulation model was developed using COMSOL Multiphysics to study thermal and mechanical behaviours of hardening concrete with the objective of estimating the risk of early age thermal cracking. The proposed model utilizes combined heat transfer and solid mechanics models to estimate temperature and strain development in a concrete element, while using a broad range of thermal and mechanical boundary conditions to simulate the

effect of the surrounding environment and the curing methods used. In order to verify the precision of the model, a real-world case study was conducted, and the predicted temperatures by the model were compared with the actual temperature measurement obtained on site using wireless temperature sensors. The results indicated the promising level of precision in predictions of the model. Furthermore, the proposed model was used to estimate the thermal stresses and cracking ratio in the wall, which were then used to estimate the risk of early age thermal cracking using the probability density function used by the model. The risk of early age thermal cracking was found to be very high.

Chapter 5: A mix design optimisation algorithm method to minimize risk of early age thermal cracking of concrete

5.1 Introduction

As discussed in previous chapters, the mismatch between the rate of heat generation due to cement hydration and the rate of heat dissipation through conduction and convection may result in considerable temperature gradient within mass concrete and concrete elements with high cement content. This temperature gradient can, in turn, lead to considerable thermal stresses in concrete at its early age when it has not achieved its full tensile strength, leading to early age thermal cracking. Among various measures investigated to minimize the risk of early age thermal cracking, optimising the concrete mixes and the use of supplementary cementitious materials are usually favored by industry mainly because these methods do not affect the methodology construction. However, regulating the internal heat generation in conjunction with increasing the tensile strength to reduce the risk of thermal cracking is not considered as an objective in existing mix design approaches.

In this chapter, a mathematical optimisation model based on genetic algorithms is developed to identify the optimal mix for typical concrete elements subject to risk of early age thermal cracking. The multi-objective optimisation model is designed to reduce the temperature gradient while maximizing the tensile strength development rate. Since the Bogue's model presented in Chapter 3 is able to consider different dosages and types of admixtures and is more universal, it is used for calculating the heat source. For calculating temperature development and tensile strength at different points within a concrete element, a finite difference simulation model is developed and

used for optimisation. The proposed optimisation method is applied to a real-world case study to identify optimal mix design for a concrete raft in Botany, NSW, Australia. Following mix design optimisation, the raft is simulated numerically using the previously verified numerical model presented in Chapter 4 with both optimised mix and the originally planned mix to investigate potential reduction in risk of early age thermal cracking as a result of mix optimisation.

5.2 Proposed Framework

The proposed optimisation model, the risk of early age thermal cracking of concrete is minimised through minimizing temperature gradient while maximising tensile strength developed in concrete. The proposed methods rely on genetic algorithm. Different steps undertaken by GA to identify the optimal mix design are shown in Figure 5-1 and described in detail in the following sections.

5.2.1 Genetic algorithm optimisation

As discussed in Chapter 2, Genetic Algorithms (GA) are heuristic problem-solving methods that are able to consider different constraints based on natural selection and natural genetics [60].

- **Initial population**

In this study the first generation can be generated randomly within the range of the lower and upper bounds that are defined for each variable satisfying all constraints or the concrete mix design that has been designed originally for each case.

- **Selection**

Among all the methods introduced in Chapter 2, the selection method used in this study is Tournament Selection since it is one of the most popular selection methods due to its efficiency and simple implementation [65].

- **Crossover**

As presented in Chapter 2, crossover is an operation which mixes the genetic information of two parents to produce the new offspring and there are several crossover methods in the literature. Considering the conditions of the optimisation problem in this study, Intermediate Crossover which is a weighted average of the parents for recombination is utilized.

- **Mutation**

Mutation is a genetic operator that aims to preserve diversity between different generations. Since the optimisation problem in this study is a constrained optimisation problem, adaptive feasible mutation which considers the previous successful or unsuccessful generations and generates a random direction accordingly that satisfies the constraints is used as the mutation method [63, 74].

- **Fitness function**

This study aims to control the early age thermal cracking. Therefore, the fitness function is defined as function that quantifies the effect of mix design on a direct measure of risk of early age thermal cracking. Given the direct relationship between temperature gradient and risk of early age thermal cracking [3, 22, 103, 104], temperature gradient between the surface and center of an element is used to define the fitness function, as shown in Equation 5.8.

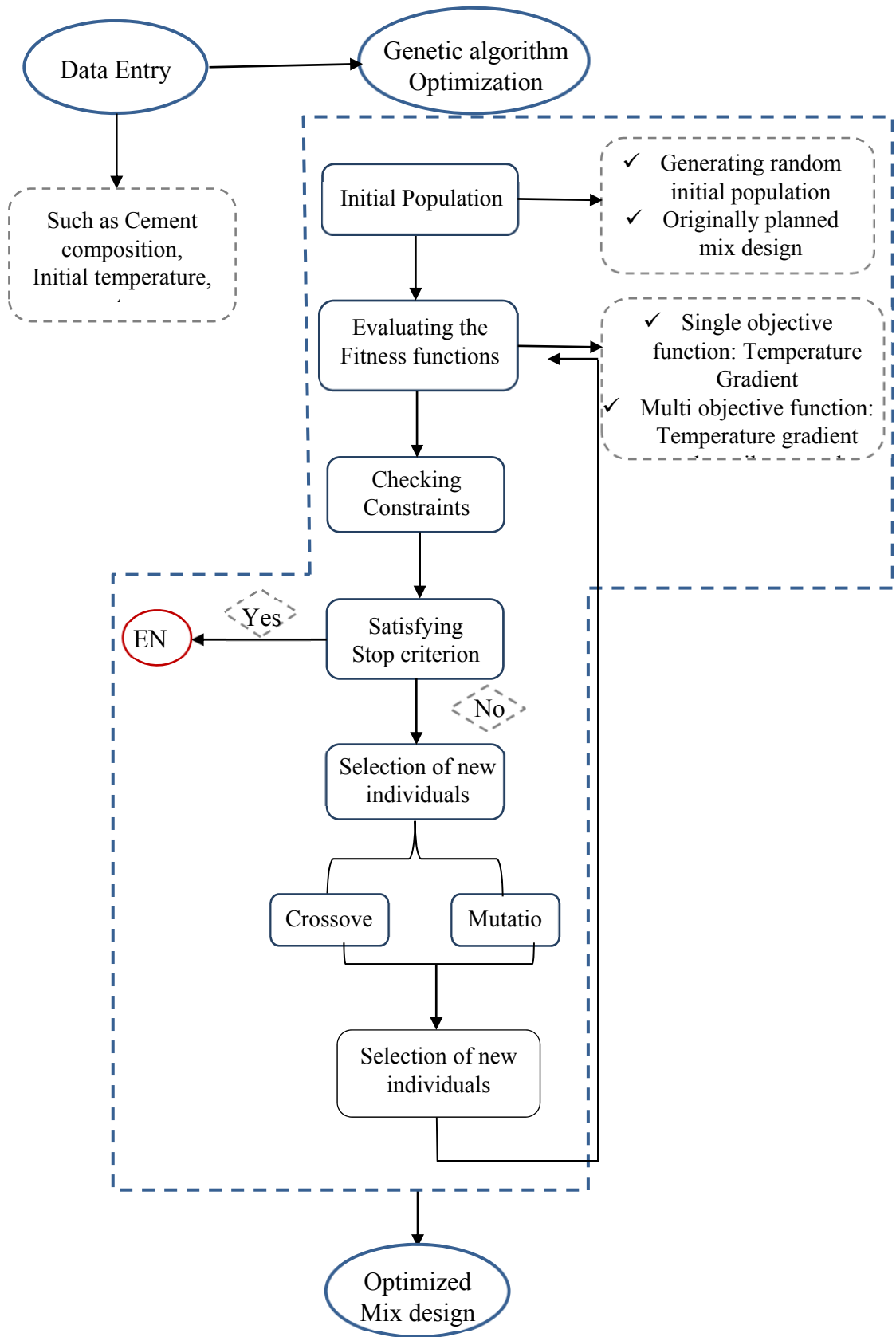


Figure 5- 1 Flowchart of the proposed framework

$$Fitness\ function = \begin{cases} Min(\frac{T_{center}-T_{surface}}{h}) \\ Max\ F_t \end{cases} \quad \text{Equation 5-1}$$

where, T_{center} and $T_{surface}$ are the temperatures of the middle and surface points of the concrete section ($^{\circ}C$), respectively, h is the distance between the two points (m) and F_t is the concrete tensile strength (MPa). The methodology for calculating the fitness function is discussed later.

- **Decision variables**

Six mix design variables are considered as decision variables as below:

$\frac{W}{CM}$: water to cementitious materials ratio,

P_c : percentage of Portland cement in cementitious materials,

P_{FA} : percentage of Fly Ash in cementitious materials,

P_{SF} : percentage of Silica Fume in cementitious materials,

P_{GGBFS} : percentage of Ground granulated blast-furnace slag in cementitious materials,

CM : total cementitious material content ($\frac{kg}{m^3}$).

- **Constraints**

In practice, the design of concrete mixes is subject to meeting several practical constraints specified by standards and common practice. These generally include the lower and upper bounds for different mix design variables, constraints on availability of local materials, and required limits for particular properties including workability, strength development, etc. With is in mind, to produce a realistic solution, an optimisation problem should be defined with mathematical constraints to ensure such practical limits and requirements are incorporated into the model. The constraints

defined in this study are described by Equations 5-2 to 5-10. Equation 5-2 ensures that the fraction ratios of different cementitious materials add up to 1. Equation 5-3 defines an acceptable range for the water to binder ratio as per requirements of the user and workability requirement. Equation 5-4 expresses that the ultimate degree of hydration should be less than 1. Equations 5-6 to 5-8 define the practical ranges of the amount of different cementitious materials in the mix based on practice. Equation 5-9 limits the total amount of the binder used in the mix within a practical range. Equation 5-10 is considered to ensure the or target compressive strength at a given age is achieved. The latter is important to ensure that the optimal solution is identified without compromising the strength development rate of concrete beyond acceptable limits.

$$P_c + P_{FA} + P_{SF} + P_{GGBFS} = 1 \quad \text{Equation 5-2}$$

$$\left(\frac{W}{CM}\right)_{min} \leq \frac{W}{CM} \leq \left(\frac{W}{CM}\right)_{max} \quad \text{Equation 5-3}$$

$$\alpha_u \leq 1 \quad \text{Equation 5-4}$$

$$0 \leq P_c \leq 1 \quad \text{Equation 5-5}$$

$$0 \leq P_{FA} \leq (P_{FA})_{max} \quad \text{Equation 5-6}$$

$$0 \leq P_{SF} \leq (P_{SF})_{max} \quad \text{Equation 5-7}$$

$$0 \leq P_{GGBFS} \leq (P_{GGBFS})_{max} \quad \text{Equation 5-8}$$

$$(CM)_{min} < CM < (CM)_{max} \quad \text{Equation 5-9}$$

$$F_c(t = n \text{ days}) \leq \text{required } F_c(\text{at } n \text{ days}) \quad \text{Equation 5-10}$$

In Equations 5-2 to 5-10, α_u is the ultimate degree of hydration which is defined in Chapter 3, F_c is the compressive strength development (MPa) and *required Fc* is the minimum required compressive strength at different ages. For instance, the compressive strength at the ages of 3 and 7 days can be approximately considered to gain at least 40% and 65% of the compressive strength at the age of 28 days [129].

5.2.2 Numerical heat prediction model

Assuming a homogenous and isotropic material, concrete thermal behavior can be considered as a transient heat transfer problem that can be formatted using Equation 5-11 (based on Fourier's law of conduction) [112, 130].

$$\frac{\partial}{\partial x} \left(k \frac{\partial T}{\partial x} \right) + \frac{\partial}{\partial y} \left(k \frac{\partial T}{\partial y} \right) + \frac{\partial}{\partial z} \left(k \frac{\partial T}{\partial z} \right) + q' = \rho c_p \frac{\partial T}{\partial t} \quad \text{Equation 5-11}$$

where k is the thermal conductivity of concrete ($\frac{W}{mK}$), x , y and z are element coordinates, T is the temperature of each element ($^{\circ}C$), q' is the rate of internal heat generation (W), ρ is the concrete density ($\frac{kg}{m^3}$), c_p is the specific heat of concrete ($\frac{kJ}{kg^{\circ}K}$) and t is the time (hour). The left-hand side of this equation represents the net heat conduction and heat generation in a solid material while the right-hand side stands for the accumulated internal energy. The solution of this differential equation calculates the heat flow in solids. However, because most of the real-world cases are complex due to different geometric shapes, boundary conditions, etc., the direct solution of this equation is not always possible; and an approximate numerical approach such as finite difference is commonly applied. Finite difference uses approximately equivalent partial difference quotients instead of derivative expressions [130]. To implement the finite difference method, a control volume is considered around each grid point as can be seen in Figure 5-2.

The concept of conservation of energy is applied to consider all the changes in thermal energy in the control volume, as shown in Equation 5-12 [131].

$$E_{in} + E_{generated} = E_{out} + \Delta U \quad \text{Equation 5-12}$$

where, E_{in} is the thermal energy entering the control volume (W), $E_{generated}$ is the thermal energy generated in the control volume (W), E_{out} is the thermal energy leaving the control volume (W) and ΔU is the change in stored thermal energy (W).

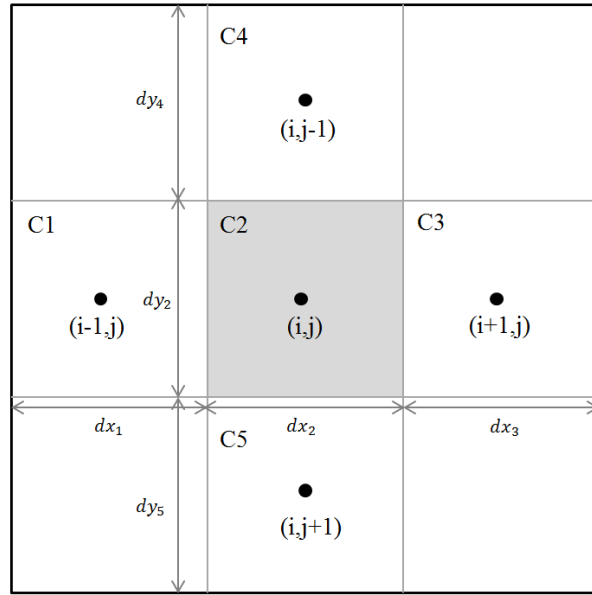


Figure 5- 2 2D control volume

By using an explicit time discretization, Equation 5-12 is applied to the control volume C2 shown in Figure 5- 2 as follows.

$$E_{in} = T_{C1} \cdot a_{1-2} + T_{C3} \cdot a_{2-3} + T_{C4} \cdot a_{4-2} + T_{C5} \cdot a_{2-5} \quad \text{Equation 5-13}$$

$$E_{out} = T_{C2} (a_{1-2} + a_{2-3} + a_{4-2} + a_{2-5}) \quad \text{Equation 5-14}$$

where, T_{C1} , T_{C2} , T_{C3} , T_{C4} and T_{C5} are the temperatures at the nodes in control volumes C1 to C5, respectively for the current time step ($^{\circ}C$), The terms a_{i-j} are the heat transfer coefficients between control volumes i and j [132] as defined by:

$$a_{1-2} = \left[\frac{dx_{1/2}}{k_1} + \frac{dx_{2/2}}{k_2} \right]^{-1} \cdot dy_2 \quad \text{Equation 5-15}$$

$$a_{2-3} = \left[\frac{dx_{2/2}}{k_2} + \frac{dx_{3/2}}{k_3} \right]^{-1} \cdot dy_2 \quad \text{Equation 5-16}$$

$$a_{4-2} = \left[\frac{dy_{4/2}}{k_4} + \frac{dy_{2/2}}{k_2} \right]^{-1} \cdot dx_2 \quad \text{Equation 5-17}$$

$$a_{2-5} = \left[\frac{dy_{2/2}}{k_2} + \frac{dy_{5/2}}{k_5} \right]^{-1} \cdot dx_2 \quad \text{Equation 5-18}$$

where, k_i is the thermal conductivity and dx_i and dy_i are the dimensions of the i th control volume shown in Figure 5- 2.

The term ΔU in Equation 5-19 which is the change in the stored thermal energy of control volume C2, is calculated by Equation 5-19.

$$\Delta U = \frac{\rho_{C2} \cdot c_{pC2} \cdot dx_2 \cdot dy_2 \cdot (T_{C2}^{n+1} - T_{C2}^n)}{\Delta t} \quad \text{Equation 5-19}$$

where, ρ_{C2} and c_{pC2} are the density and specific heat of the concrete in control volume C2. T_{C2}^n and T_{C2}^{n+1} are the temperatures of C2 in the current and the next time step ($^{\circ}C$), respectively, and Δt is the time step (hours). The generated thermal energy in a concrete element is due to the hydration of cementitious materials. Thus, the generated thermal energy of control volume C2 can be defined by:

$$E_{\text{generated}} = Q \cdot dx_2 \cdot dy_2 \quad \text{Equation 5-20}$$

where, Q is the generated heat per unit mass of cementitious materials (W) calculated by Equation 5-21 [133] as discussed in Chapter 3.

$$Q(t_e) = H_u \cdot C_c \cdot \left(\frac{\tau}{t_e} \right)^{\beta} \cdot \left(\frac{\beta}{t_e} \right) \cdot \alpha_u \cdot \exp \left(- \left(\frac{\tau}{t_e} \right)^{\beta} \right) \cdot \exp \left(\frac{E_a}{R} \left(\frac{1}{273+T_r} - \frac{1}{273+T_{C2}} \right) \right) \cdot \left(\frac{1}{3600} \right)$$

$$\text{Equation 5-21}$$

where, t_e is the equivalent age at the reference curing temperature (hours), H_u is the total heat available for reaction ($\frac{J}{kg}$), C_c is the amount of cementitious materials ($\frac{kg}{m^3}$), τ is the

hydration time parameter (hours), β is the slope of the S-shaped curve, α_u is the ultimate degree of hydration, E_a is the activation energy ($\frac{J}{mol}$), R is the universal gas constant ($\frac{J}{mol \cdot ^\circ K}$), T_{C2} is the temperature of control volume C2 at the current time step and Δt is the time step (hours). The calculation of heat of hydration parameters τ , β , α_u , E_a and H_u are discussed in Chapter 3.

Since this method is fully explicit, the results may be unstable, so its stability must be checked. The stability criterion for this problem is:

$$E_{out} < \frac{\rho_{C2} \cdot c_{pC2} \cdot dx_2 \cdot dy_2 \cdot T_{C2}^n}{\Delta t} \quad \text{Equation 5-22}$$

Also, thermal properties of concrete such as thermal conductivity and specific heat are used in the calculations. Concrete thermal properties are used as shown in Equations 23 and 24 based on the recommendation of Schindler [134]:

$$k(\alpha) = k_u \cdot (1.33 - 0.33\alpha) \quad \text{Equation 5-23}$$

$$C_p(\alpha) = C_{pu} \cdot (1.25 - 0.25\alpha) \quad \text{Equation 5-24}$$

where, k and k_u are the concrete thermal conductivity and the ultimate hardened concrete thermal conductivity ($\frac{W}{mK}$), respectively, C_p and C_{pu} are the specific heat and the ultimate specific heat of hardened concrete ($\frac{J/kg}{K}$), respectively, and α is the degree of hydration calculated from:

$$\alpha(t_e) = \alpha_u \cdot \exp(-[\frac{\tau}{t_e}]^\beta) \quad \text{Equation 5-25}$$

Using the above method, the temperature of each point of the concrete element can be predicted at each time step. The temperature of each point at different times is used to calculate the temperature gradient as one of the objective functions of this study as presented in Equation 5-1. To determine the risk of early age thermal cracking,

estimation of tensile strength development of concrete is crucial; the tensile strength of concrete to its compressive strength by [126]:

$$F_t(t) = l \times (F_c(t))^m \quad \text{Equation 5-26}$$

where, F_t is the tensile strength development (MPa) and F_c is the compressive strength development, l and m are equal to 0.303 and 0.66, respectively, as suggested by Raphael [126] and t is time (hours). This equation is used to calculate the second objective function in this study (Equation 5-1) that is to maximize using this method.

5.3 Case study

5.3.1 General information

To demonstrate its effectiveness, the proposed genetic algorithm method is applied to identify the optimal concrete mix for a 30m × 30m × 1m thick concrete raft in Sydney, Australia with the algorithms programmed in MATLAB. The plan view of this foundation is shown in Figure 5- 3. The originally planned mix design is presented in Table 5-1; the composition of the Portland cement used in the calculations for this case study is reported by the provider (Boral Cement Ltd.) as can be seen in Table 5-2.

The proposed optimisation model was applied to identify the optimal mix to minimize temperature gradient and maximize the tensile strength. The relative performance of optimised and originally planned mixes is compared using a verified numerical simulation model developed in COMSOL Multiphysics. The numerical model (Figure 5-4) used for verifying the effectiveness of proposed mix optimisation approach is a multi-physics model relying on heat transfer and solid mechanics modules in COMSOL Multiphysics. The accuracy of the numerical model is demonstrated by applying it to predict the temperature development in the actual raft considered in the case study, which was also measured on site using embedded SmartRock2™ sensors.

Fourteen sensors were embedded at different locations of the raft as shown in Figures 5-5 and 5-6 and Table 5- 4. Having the mix design and the compositions of cementitious materials, the heat parameters that are used in the numerical model can be found in Table 5- 3. The ambient conditions measured by a SmartRock2™ wireless temperature sensor were imposed on the model by defining convection boundary condition. The initial concrete temperature of 20°C and placement time as 10 am reported by the contractor were input into the model. Temperature of each point was recorded continuously for four days while the temperature development of same points was predicted using the numerical model.

As discussed in Chapter 3, the numerical model is capable of calculating thermal and mechanical properties of concrete elements including temperature, tensile, compressive strength, etc. Having these outputs, the effectiveness of the implication of the proposed framework on this case study in reducing the risk of thermal cracking is presented in the next section.

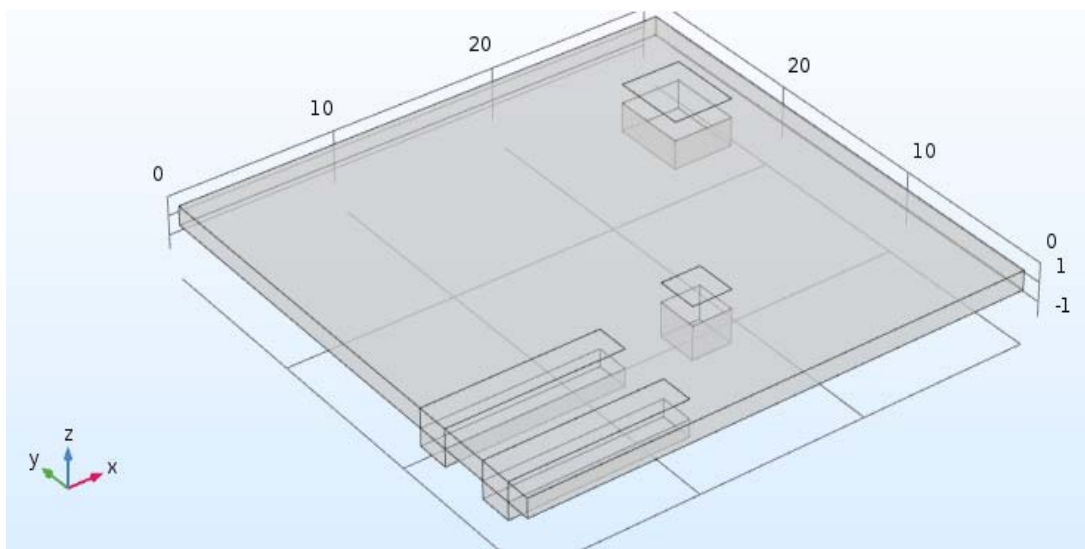


Figure 5- 4 Numerical model of the raft in COMSOL Multiphysics

Table 5- 1 Originally planned mix design

Material	Amount
Portland Cement	252 (Kg/m ³)
Portland Cement percentage in total cementitious materials	70%
GGBFS	108 (Kg/m ³)
GGBFS percentage in total cementitious materials	30%
Total Cementitious Material content (CM)	360 (Kg/m ³)
Water	183 (Kg/m ³)
Water/CM	0.51

Table 5- 2 Composition of Portland cement

Cement composition	Weight (%)
C ₃ S	64.07
C ₂ S	8.18
C ₃ A	9.36
C ₄ AF	8.49
CaO	0.64
K ₂ O	0.41
SO ₃	2.78
MgO	1.41
Na ₂ O	0.26
Blaine	367 (m ² /Kg)

Table 5- 3 Heat parameters for the original mix design based on Bogue model

Heat Parameters	Values
Activation Energy	38244.85 (J/mol)
τ	26.465 (hrs)
β	0.3589
α	0.827
H_u	479.356 (kJ/kg)

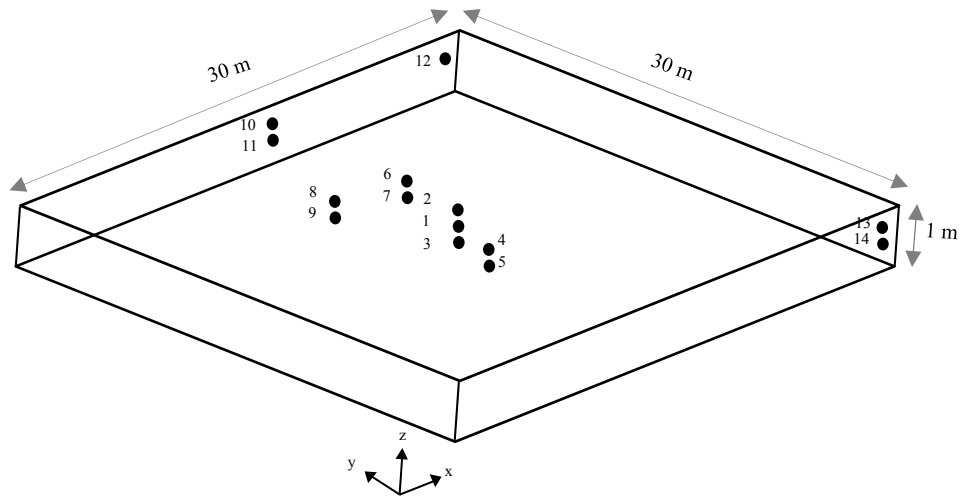


Figure 5- 5 Embedded sensor locations (in meters)

Table 5- 4 Sensor coordinates

Point	x	y	z
1	14.7	15.5	0.48
2	14.7	15.5	1.00
3	14.7	15.5	0.00
4	13.0	11.5	1.00
5	13.0	11.5	0.56
6	14.4	21.2	1.00
7	14.4	21.2	0.50
8	10.5	21.8	1.00
9	10.5	21.8	0.50
10	12.9	29.4	1.00
11	12.9	29.4	0.55
12	29.6	29.4	0.60
13	29.3	0.5	1.00
14	29.3	0.5	0.45

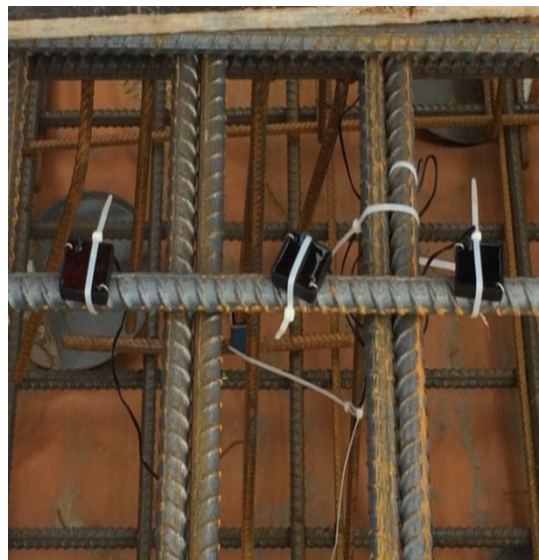


Figure 5- 6 Sensor installation

5.3.2 Constraints

As outlined in Section 5-2-1, the constraints of the optimisation problems may vary due to different circumstances of each case study. All the selected chromosomes must meet the constraint requirements, and the fitness value is assigned to them based on Equation 5-1 afterwards. The constraints of this case study are defined based on the required characteristics asked by the provider (Boral Ltd.). The minimum and maximum amount of water to cementitious materials ratio are considered as 0.25 and 0.6, respectively (see Equation 5-3). The percentage of Fly Ash and GGBFS are assumed to be less than 60%, while the maximum allowed Silica fume is 10% (Equation 5-6 to Equation 5-8). Also, Portland cement contribution in total cementitious materials can differ from 0 to 100% (see Equation 5-5). Moreover, the amount of total cementitious materials content is considered to be between 250 (kg/m³) and 700 (kg/m³). In order to monitor the compressive strength development, Equation 5-10 is calculated for concrete at the ages of 3 and 7 days. In this case, the required compressive strength at the ages of 3 and 7 days are defined as 40% and 65% of the final compressive strength of the concrete element at the age of 28 days.

5.3.3 Results and discussion

- **Numerical model verification**

As discussed in the previous section, the numerical model for this case study is verified through comparing its results with in-situ measurements. Figure 5- 7 and Table 5- 5 show the variations in the temperature with time at point 1 and the maximum measured and predicted temperatures for different points, respectively. It is noted that some of the embedded sensors were damaged during pouring of the concrete and unable to record data. As shown in Figure 5- 7 and Table 5- 5 the numerical results illustrate

insignificant errors in predicting the maximum temperature as well as predicting the variations in temperature with time and the results confirm the acceptable precision of the numerical simulation model in predicting the temperature profile and thus the reliability of the numerical model in comparing different mixes.

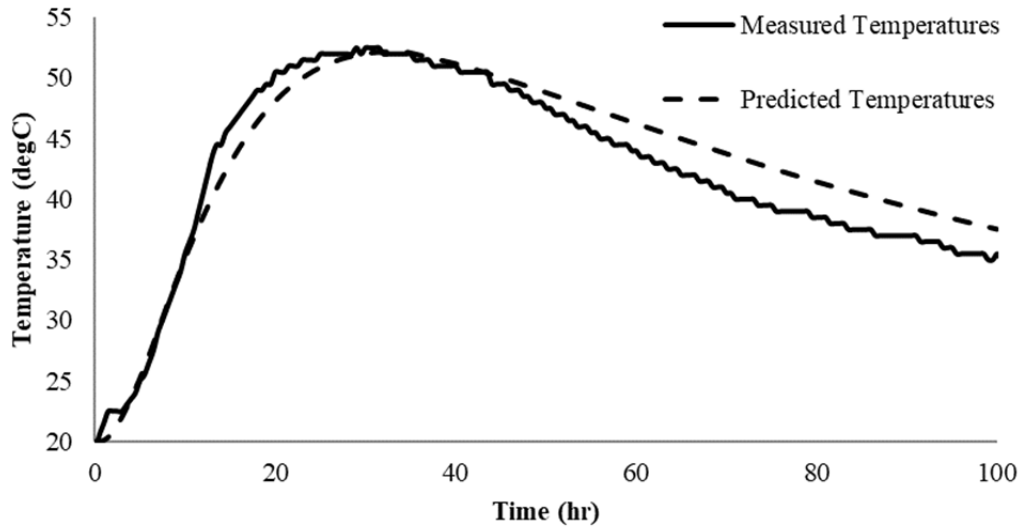


Figure 5- 7 Comparison between numerical results and site measurements for point 1

Table 5- 5 Comparing the numerical model results and temperature sensor measurements

Point	Max. temperature (Site measurements) (DegC)	Max. Predicted Temperature (DegC)	Error (%)
1	52.5	53.4	1.7%
2	36.0	38.6	7.2%
3	43.0	45.7	6.3%
4	42.0	38.6	8.1%
5	-	52.5	-
6	42.5	38.6	9.2%
7	51.5	53.2	3.3%
8	-	38.5	-
9	-	53.3	-
10	-	37.4	-
11	-	50.7	-
12	-	46.2	-
13	32.0	36.2	13.1%
14	-	49.7	-

- **Results of the applied framework**

The multi- Objective Genetic algorithm framework was applied to this case study. The time step and maximum mesh size are chosen as 0.01 (hr) and 0.01 (m), respectively. The GA was run for 200 generations. As can be seen in the formulations for calculating the objective function, optimising the functions is conflicting. For instance, to maximize tensile strength, it is necessary to increase the cement content, while this increases the temperature gradient. Figure 5- 8 is the pareto front curve which is a trade-off between two components of the objective function for different generations.

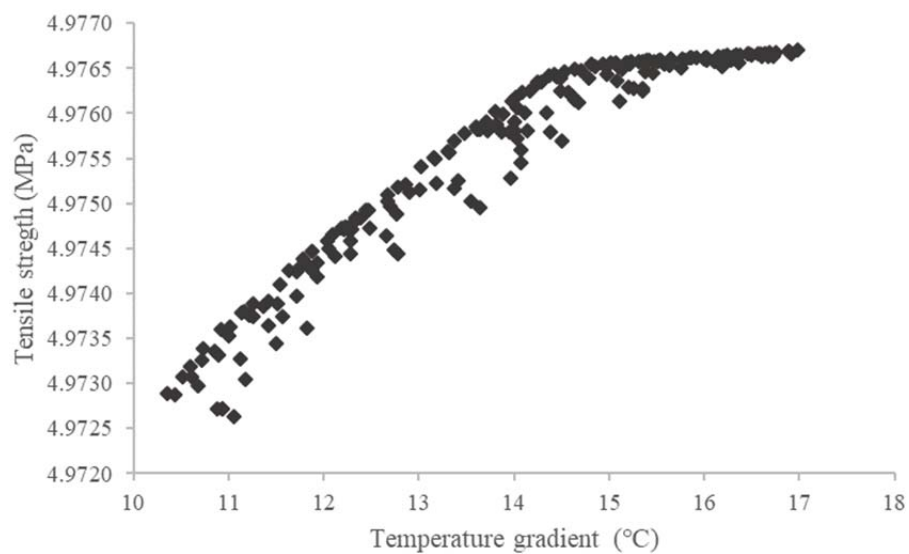


Figure 5- 8 Pareto front curve

Table 5- 6 shows the optimised mix design obtained by the proposed method. Comparing the optimised mix with the original mix in Figure 5- 9 indicates that the amount of total cementitious materials is decreased from $360 \left(\frac{Kg}{m^3}\right)$ to $355 \left(\frac{Kg}{m^3}\right)$. Moreover, Portland cement content is reduced from $252 \left(\frac{Kg}{m^3}\right)$ to $220 \left(\frac{Kg}{m^3}\right)$, that is an 8%

reduction in the percentage of Portland cement. Comparison between the two mixes also shows that the amount of Slag is 86.7 kg less in the optimised mix while the values of Fly Ash and Silica fume are increased to 110 kg and 3.55 kg, respectively. As noted, the amount of GGBFS is decreased by optimising the mix design while the amount of fly ash is significantly increased. This can be explained by Equation 3-3 (Calculating H_u). In this formula the constants for fly ash and Slag are suggested as 342 and 550, respectively. This means that using more Slag leads to higher heat of hydration compared to using Fly Ash and that can be the reason for the reduction in GGBFS content when optimising the mix. Furthermore, the ratio of water to cementitious materials and water content is decreased from 0.51 to 0.3 and $183 \left(\frac{Kg}{m^3}\right)$ to $107 \left(\frac{Kg}{m^3}\right)$, respectively. It should be mentioned that the aggregate types and content are the same for both mix designs.

To observe the effectiveness of using the optimised mix design in reducing the risk of early age thermal cracking, numerical modelling is carried out for both mixes by COMSOL Multiphysics. Three different points shown in Figure 5- 10 are studied. Points A and B are chosen because it is assumed that the temperature gradient between these two points is the maximum temperature gradient of the raft, and point C is selected as a surface point since the amount of tensile stress is higher on the surface. Temperature development, maximum temperature gradient, and tensile stress (due to temperature) are calculated for these points. Moreover, to control the early age thermal cracking, monitoring the cracking ratio is suggested in the literature [105, 122]. Cracking ratio is defined as the ratio of developed tensile stress to tensile strength in the early age concrete mass. When the cracking ratio is equal to 1, it shows that the tensile stress is equal to the tensile capacity of concrete and this means the initiation of cracking.

Table 5- 6 Optimised mix design

Material	Amount
Portland Cement	220.1 (Kg/m ³)
Portland Cement percentage in total cementitious materials	62%
Fly Ash	110.05 (Kg/m ³)
Fly Ash percentage in total cementitious materials	31%
Silica fume	3.55 (Kg/m ³)
Silica fume percentage in total cementitious materials	1%
GGBFS	21.3 (Kg/m ³)
GGBFS percentage in total cementitious materials	6%
Total Cementitious Material content (CM)	355 (Kg/m ³)
Water	106.5 (Kg/m ³)
Water/CM	0.3

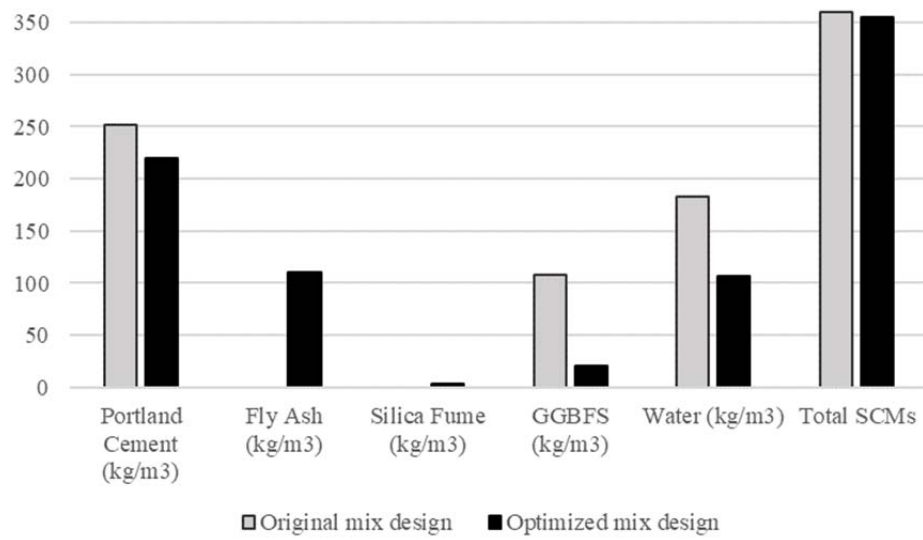


Figure 5- 9 Comparing the original and optimised mix designs

Figure 5- 11 shows the numerically predicted temperature development of the centre point (point A in Figure 5- 10) and the surface point (point B in Figure 5- 10) of the raft for original and optimised mixes.

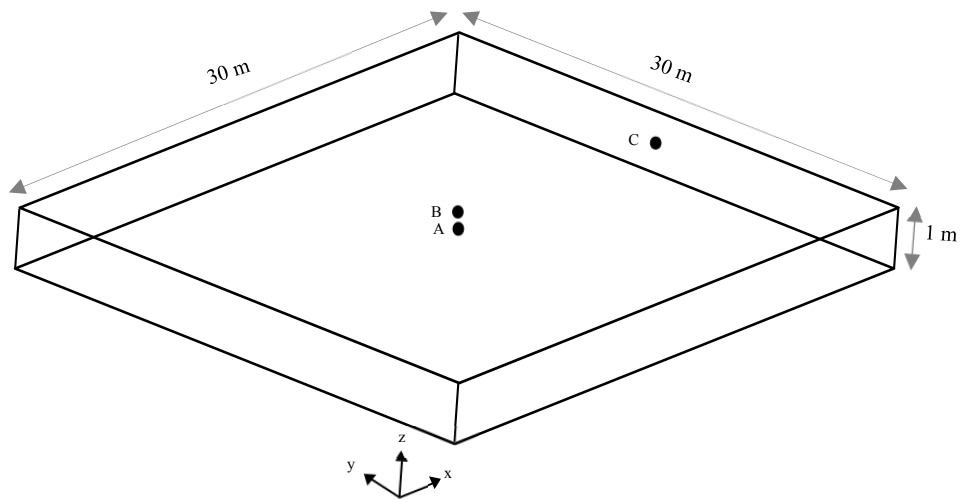


Figure 5- 10 The studied points on the raft

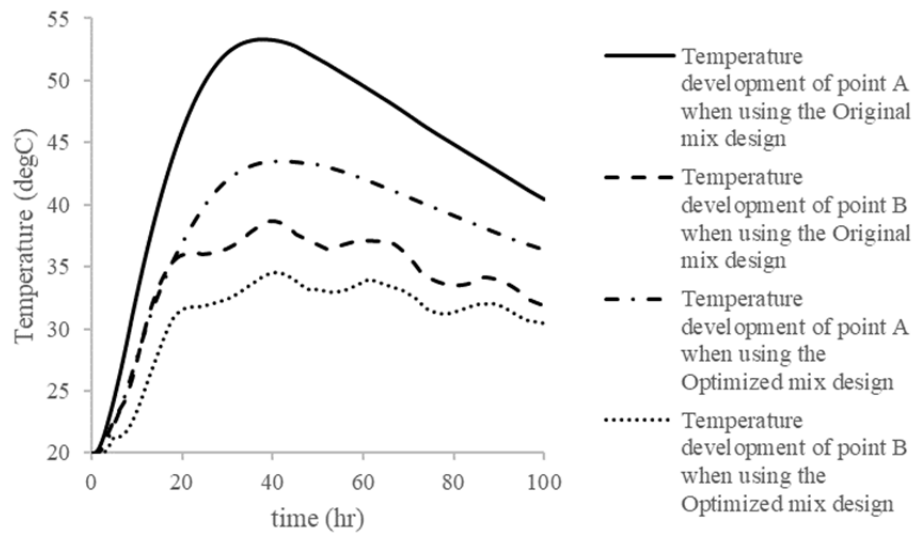


Figure 5- 11 Temperature development of points A and B for both mix designs

Figure 5- 11 shows that optimising the mix design leads to a considerable reduction in overall temperature development of points A and B. The maximum temperature of point A and B was found to decrease from 53.3 °C to 43.5 °C and from 38.7 °C to 33.5 °C, respectively, giving a 15% reduction of the maximum temperature of this raft foundation. Furthermore, this was accompanied by 36% reduction in the maximum temperature gradient between points A and B from 31.7 °C/m to 20.2 °C/m. Given the direct relationship between the risk of early age thermal cracking and the level of thermal tensile stresses due to the temperature gradient, the reduction in the temperature gradient achieved through applying the proposed optimisation method can lead to considerable reductions in the risk of early age thermal cracking. Furthermore, Figures 5- 12 and 5- 13 show the thermal stress developments. The generation of compressive stress is dominant in the centre of the concrete element, while tensile stress generates mainly in the side and top surfaces; a similar trend was observed by Klemczak and Wrobel [135]. As shown in Figures 5- 12 and 5- 13, the thermal stresses are reduced by about 40% for all the points which means a great reduction in the chance of

cracking. Figures 5- 14 and 5- 15 show the cracking ratio of the concrete raft when using the originally planned mix and optimised mix design, respectively. The analysis results (Figures 5-14 and 5-15) show that surface point C (Figure 5- 10) is more likely to crack. The maximum cracking ratio of point C is reduced from 0.68 to 0.39 when using the optimised mix. This shows about 42% reduction of the maximum cracking ratio for these points. A similar reduction pattern can be found in the figures for points A and B (Figure 5- 10).

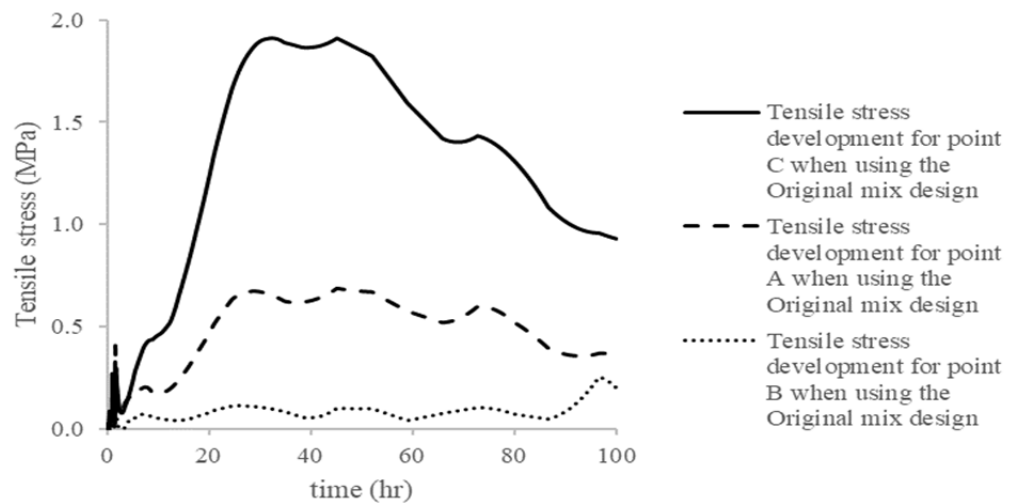


Figure 5- 12 Thermal (tensile) stress development using the originally planned mix design

The compressive strength of this concrete foundation is 35 MPa at 28 days. The constraints related to compressive strength after 3 and 7 days are considered to be at least 45% and 65% of the maximum compressive strength which are equal to 16 MPa and 23 MPa. Figure 5- 16 shows the compressive strength development of this raft. As can be seen the compressive strength at the ages of 3 and 7 days are in the acceptable range which means that the optimised mix design meets the required compressive strength development as specified by the client. This highlights the importance of

identifying the optimal trade-off between strength development objective and cracking risk minimization objective as achieved by the proposed model.

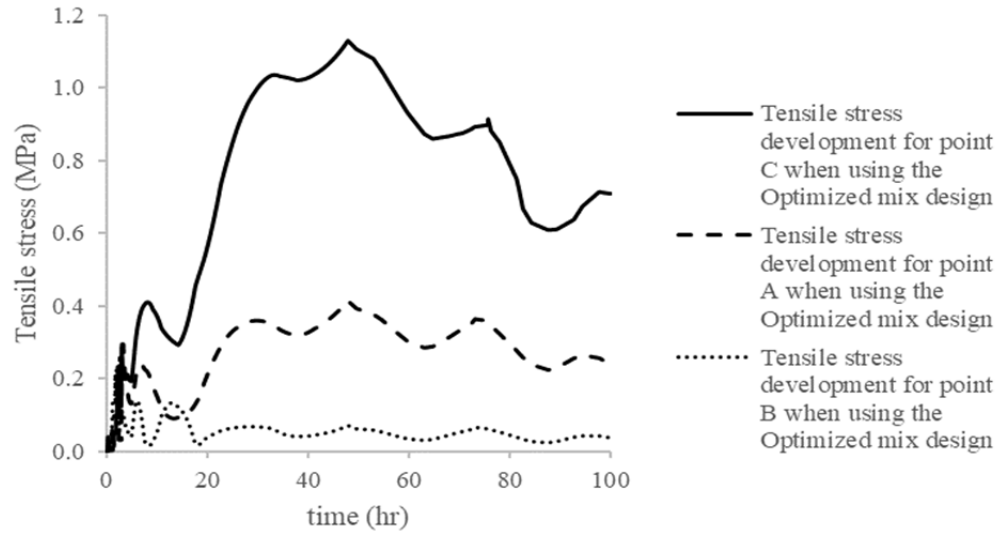


Figure 5- 13 Thermal (tensile) stress development using the optimised mix design

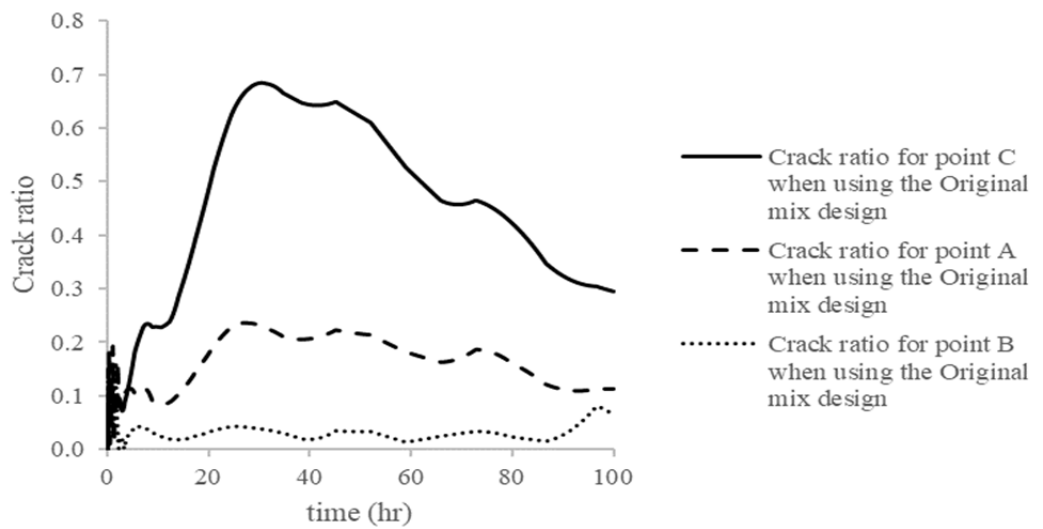


Figure 5- 14 Cracking ratios using the originally planned mix design

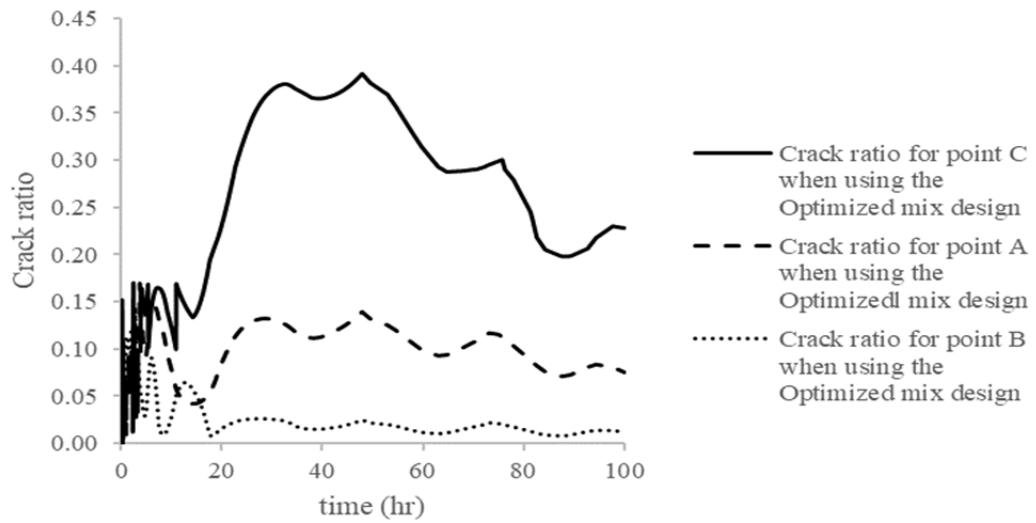


Figure 5- 15 Cracking ratios using the optimised mix design

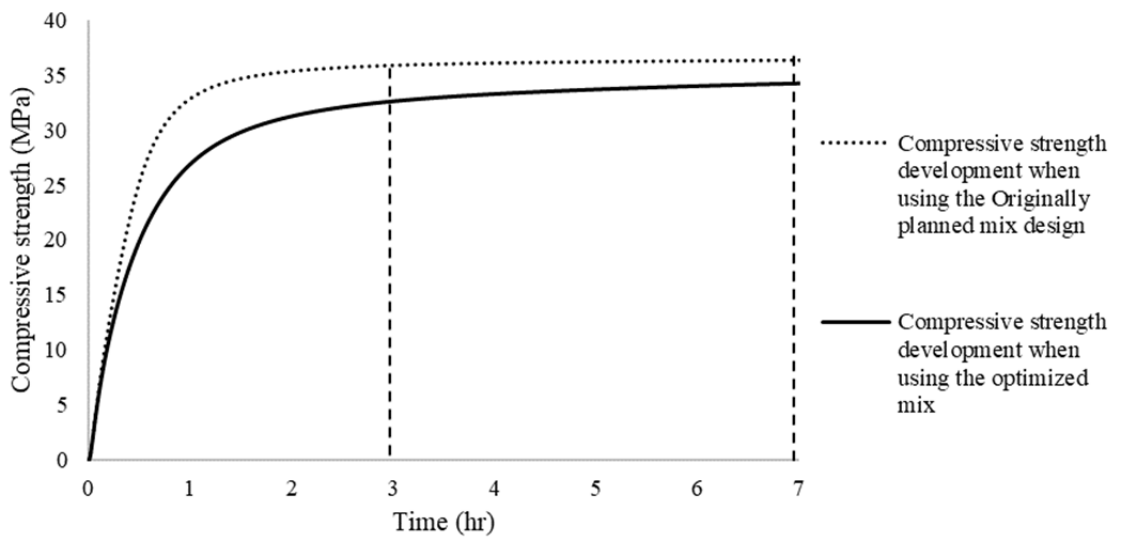


Figure 5- 16 Compressive strength development for both mixes

5.4 Conclusions

Reducing the risk of early age thermal cracking by optimising the concrete mix design and using SCMs in concrete are usually favoured by the industry due to minimal changes to the construction methods and procedures required by these strategies. In this chapter, a mathematical optimisation model based on genetic algorithms was

developed to identify the optimal mix for a typical concrete element subject to a risk of early age thermal cracking. This was achieved through minimizing the temperature gradient and maximizing the tensile strength in the concrete without compromising the development of the compressive strength of concrete. A genetic algorithm coupled with a finite difference heat transfer model, both developed in MATLAB, was used to implement the proposed methodology. A numerical model which was separately verified with site measurements was used to evaluate the comparative effectiveness of the optimised mix in terms of reducing the risk of early age thermal cracking. The results showed that a considerable reduction in temperature gradient, maximum temperature, thermal stresses and cracking ratio was achievable through adoption of the proposed optimisation model. The results also highlighted the effectiveness of the model in meeting the cracking risk minimization objective without compromising the ability to meet the required compressive development rate. In this case, a slight relaxation of the strength development rate within the permissible limit was utilized by the model to minimize the risk of early age thermal cracking. This chapter contributes to the body of knowledge by opening a new class of concrete mix optimisation models to achieve durability objectives, in particular a crack minimization objective. While the results provide reliable evidence of the effectiveness of the proposed model, it should be noted that the proposed model, similar to any other model, is sensitive to provision of accurate input data including ambient temperature, initial concrete temperature, and cement composition. The proposed model in its current form does not consider the addition of admixtures which are commonly used in practice, which needs to be addressed in future work. Furthermore, the proposed model can be extended to optimise other variables including the type of the aggregate as well as time placement.

In addition, further site testing and laboratory validation is required to evaluate the effectiveness of the optimised mixes proposed by the model.

Chapter 6: Numerical investigation of construction strategies for mitigating the risk of early age thermal cracking

6.1 Introduction

As discussed in previous chapters, the main two strategies to reduce the risk of early age thermal cracking include i) reducing heat of hydration generation and the resulting temperature rise and peak temperature in concrete and ii) increasing the overall tensile strength and the development rate of tensile strength of concrete to increase the concrete's ability to resist developing tensile stresses. To reduce the peak temperature and the rate of temperature development in concrete, the literature proposes a variety of methods ranging from mix design optimisation to construction related methods [3, 11]. A Genetic algorithm numerical optimisation method was introduced in Chapter 5 to minimize the risk of early age thermal cracking with a focus on mix design. The proposed method presents a significant improvement in the state of the art concrete mix optimisation methodology for minimizing the risk of early age thermal cracking, which is mainly limited to try and error, supported by laboratory testing, by following a number of generic guidelines and/or based on previous experience of the concrete design team [20, 76, 78, 81, 96, 136]. Mix design optimisation is commonly considered as a more desired strategy over other construction phase focused strategies to reduce the risk of early age cracking. This is mainly because changing the mix design does not require any significant effort on a construction site and can be usually implemented at minimal extra costs to the contractors. However, when dealing with massive concrete elements or being obliged to meet stringent strength development requirements, mix design optimisation may not sufficiently lower the temperature differential and the resulting risk of early age thermal cracking [3,

137]; and other construction strategies may be required in conjunction with mix design optimisation to achieve the best results.

The common construction strategies to reduce the risk of early age cracking include lowering the initial concrete temperature, sequential concrete pouring, use of internal cooling pipes, and using lower thermal expansion aggregates [3, 23]. Adoption of such methods in practice is costly and therefore careful consideration is required to identify the optimum strategy to achieve the required reduction in cracking risk level at minimum costs. However, there is currently a lack of robust numerical models to evaluate the effectiveness of different construction strategies in reducing the risk of early age cracking in a particular structural element; and the decision to adopt a particular strategy is made solely by relying on the judgement and experience of concrete specialists.

This chapter presents a numerical modelling approach for evaluating the effectiveness of common risk mitigation methods for early age thermal cracking of concrete. Furthermore, several case studies involving real-world concrete placement operations are used to demonstrate how numerical simulation can be used to effectively optimise the variables associated with the risk mitigation strategies. The variables include time interval between placement of each layer in sequential placement strategy, the number of cooling pipes in internal cooling strategy, and the maximum initial temperature in placement temperature lowering strategy.

6.2 Sequential concrete placement

For a given mix design, an increase in the thickness of the concrete element results in slower heat dissipation and thus a higher temperature development rate [1, 138]. With this in mind, placement of concrete in multiple thinner layers is a common

strategy to reduce the risk of early age thermal cracking of thick concrete elements [3]. The delay between placement of each subsequent layer depends on the level of cracking risk [3, 139]. This allows the release of a portion of the generated heat before placement of subsequent layer and prevents to some extent the exponential increase in the rate of heat generation due to higher rates of hydration at higher starting temperatures [87]. Delaying the placement of the succeeding concrete layers may however adversely affect the bond between the layers [88]. Moreover, sequential placement of concrete increases the total duration of concreting operation and therefore the total construction time, negatively affecting the overall cost of the project. Due to the significant costs associated with each day of delay in completion of concrete placement, minimizing the delay between castings of different layers, while minimizing the risk of cracking, is a major objective of sequential placement strategy. In order to identify the minimum required time interval between placements of different layers which meets the risk mitigation objectives, the numerical model presented in Chapter 4 is modified to model the sequential concrete placement strategy. The developed sequential placement numerical model allows a detailed evaluation of the effect of variations in the time intervals and thickness of concrete layers on the risk of early age thermal cracking, thereby providing concrete specialists with a reliable decision support tool for optimising sequential placement decisions.

6.2.1 Numerical modelling methodology

The numerical model presented in Chapter 4 was modified to account for sequential concrete pouring. The approach adopted in this study involves defining each layer, i.e. each pour, as a separate object with its own properties, heat function and boundary conditions. The latter is critical to model the fact that at a given time, the

concrete of each layer is at a different stage of hydration. The heat of hydration generation model is defined as a time dependent model to ensure that hydration of cement in each layer starts only after the time of placement of the layer rather than the start of the analysis. This is achieved through defining the equivalent age at the reference curing temperature (hours or days) for each layer by:

$$t_e(T_r) = \sum_n^t \exp\left(\frac{E}{R}\left(\frac{1}{273+T_r} - \frac{1}{273+T_c}\right)\right) \cdot \Delta t \quad \text{Equation 6-1}$$

where n is the placement time of the n^{th} layer. For each layer, the time dependent function enforces a convection boundary condition on the exposed surfaces before they are covered by the next layer. Thermal and mechanical boundary conditions on the side and bottom surfaces are defined for each layer individually based on the methodology discussed in Chapter 4 (Section 4-2-1-3). Since all the layers are defined in the geometry from the beginning of the analysis, the time dependent function in Equation 6-2 is used to impose the boundary temperature of the top surface of each layer at a given time:

$$\begin{cases} \text{if } (dt(n-1) < t < dt(n)), & T_{topsurface(n)} = T_{ambient}(t) \\ \text{otherwise,} & T_{topsurface(n)} = T_c(t) \end{cases} \quad \text{Equation 6-2}$$

where, dt is the time interval between placement of each layer, n is the number of the layer under study, $T_{topsurface(n)}$ is the temperature of the top surface of the n^{th} layer, $T_{ambient}$ is the ambient temperature at time t , and $T_c(t)$ is the concrete temperature at time t . The boundary conditions between adjacent layers is defined so that the hydration heat is transmitted by conduction between the layers. The external mechanical restraints are defined for all surfaces by considering its surrounding environment. The spring foundations are defined as the boundary condition on the bottom surface of each layer. The mechanical boundary condition between the first layer and the ground or

foundation is defined by a spring constant, Equation 4-19 in Chapter 4. The mechanical boundary conditions between subsequent layers is defined using a time dependent spring constant, presented by Equation 6-3 where the time GT is the time dependent modulus for the hardening concrete.

$$k = \begin{bmatrix} GT & 0 & 0 \\ 0 & GT & 0 \\ 0 & 0 & GT \text{ (previous layer)} \end{bmatrix} \quad \text{Equation 6-3}$$

The modulus GT can be calculated using Equation 4-20 in Chapter 4.

6.2.2 Case study

The sequential placement model described above is used to simulate temperature development in a dam foundation on Lake Macdonald in Queensland, Australia. The geometry of the dam base is shown in Figures 6-1 and 6-2. The objective of modelling is to identify the minimum required time interval between placements of each layer to minimize the risk of early age thermal cracking. The thickness of each layer is one metre, leading to fifteen concrete placement rounds. The dimension of each resulting layer is $14.9\text{m} \times 18.5\text{m} \times 1\text{m}$ thick, as shown in Figure 6-3. The external mechanical restraints are defined as free on side surfaces while the boundary condition of the bottom surface is defined using Equation 6-1. The required compressive strength of this mix is 40 MPa.

The mix design used in this project is shown in Table 6-1. Moreover, the composition of Portland cement composition and the heat parameters used to calculate the heat source are summarized in Tables 6-2 and 6-3. The initial concrete temperature is considered to be 20°C . The numerical simulation is run to study three different placement time interval scenarios, viz. 1, 2 and 3 days delay between placements of

each subsequent layer. The analysis is conducted for approximately 45 days (1,100 hours).

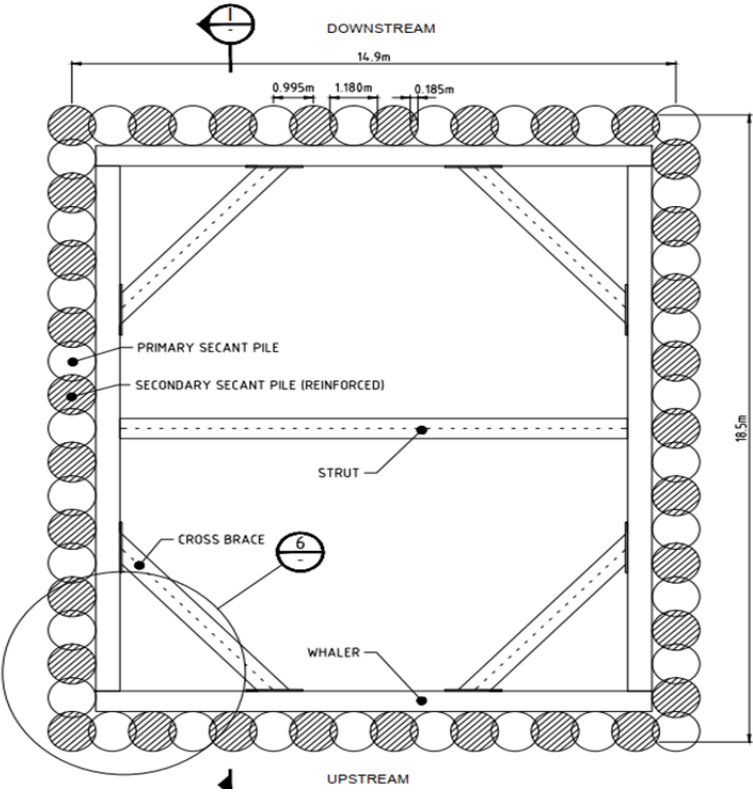


Figure 6- 1 Plan view of the dam base

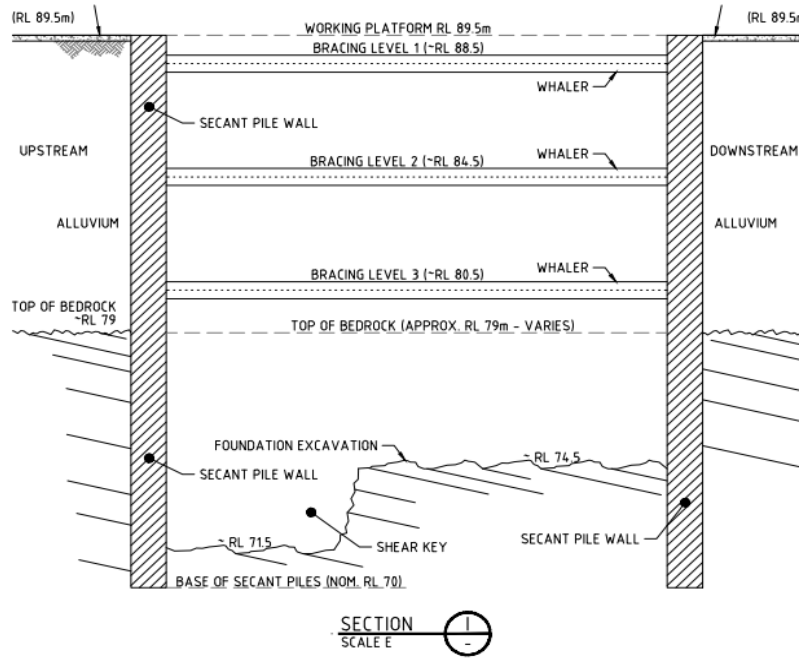


Figure 6- 2 Section view of the dam base

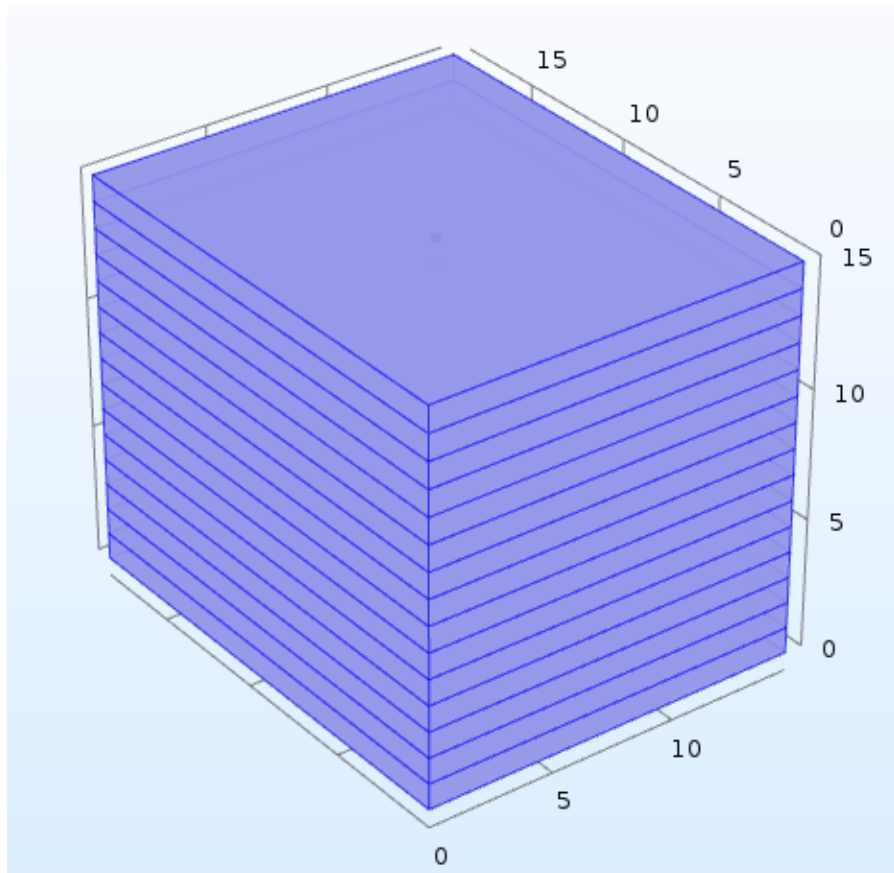


Figure 6- 3 Numerical model of the dam base

Table 6- 1 Mix design of the dam base

Material	Mass (Kg/m ³)
Portland cement	200
Fly Ash	90
Water	188.5
W/CM	0.65
Coarse aggregate	1022
Fine aggregate	830

Table 6- 2 Composition of Portland cement

Cement composition	Weight (%)
C ₃ S	64.07
C ₂ S	8.18
C ₃ A	9.36
C ₄ AF	8.49
CaO	0.64
K ₂ O	0.41
SO ₃	2.78
MgO	1.41
Na ₂ O	0.26
Blaine	367 (m ² /Kg)

Table 6- 3 Heat parameters for the concrete mix design based on Bogue model

Heat parameters	Values
Activation Energy	35228.83 (J/mol)
τ	15.82 (hrs)
β	0.48
α	0.78
H_u	377.79 (kJ/kg)

6.2.3 Results and discussion

The results of temperature development for each of the three placement scenarios considered in this case study are presented in Figures 6-4 to 6-7. The results are shown for 16 different points in the element, including one point on the surface of the foundation and 15 points in the middle sections of the layers. As shown in Figures 6-4 to 6-6, the results indicate that the heat dissipation rate in the first layer increases with an increase in time interval of sequential placement. As can be seen, the temperature at the middle point of the first layer, i.e. Point 1, at 1,100 hours reaches 29.0, 27.2 and 26.3°C when considering the casting intervals of 1, 2 and 3 days, respectively. Furthermore, the slopes of the cooling section of the temperature curve for this point are -0.008, -0.013 and -0.017, respectively. This indicates that increasing the delay between placing second layer from 1 to 3 days leads to an increase in the cooling rate of first layer by 52%. The results presented in Figure 6-4 indicate that at the minimum time interval scenario, i.e. one day delay between placements of layers, the short duration of exposure of the top surface of placed concrete layers to air results in little opportunity to dissipate the heat. This leads to difficulties in identifying a distinct

cooling phase in the temperature profile curves for this scenario (Figure 6-4). However, when the new layer is placed every 3 days, the initiation of the cooling phase for each layer is apparent in the results. This in turn reduces the cumulative heat transmitted to upper layers and consequently the maximum temperature heat. Therefore, as illustrated in Figure 6-7, the maximum temperature reached within the concrete section is 44.2, 42.4 and 39.0°C for the concrete pouring in 1, 2 and 3 days. This indicates an approximately 12% reduction in the maximum temperature of the foundation when increasing the time interval between placement of layer from 1 day to 3 days. The maximum temperature gradient between the middle point and the surface point of the foundation for 1, 2 and 3 days placement delay scenarios are found to be 3.3, 2.9 and 2.5 ($\frac{^{\circ}\text{C}}{\text{m}}$), as shown in Figure 6-8. As can be seen, the maximum temperature gradient is decreased by 25% when the sequential placement delay increases from 1 day to 3 days.

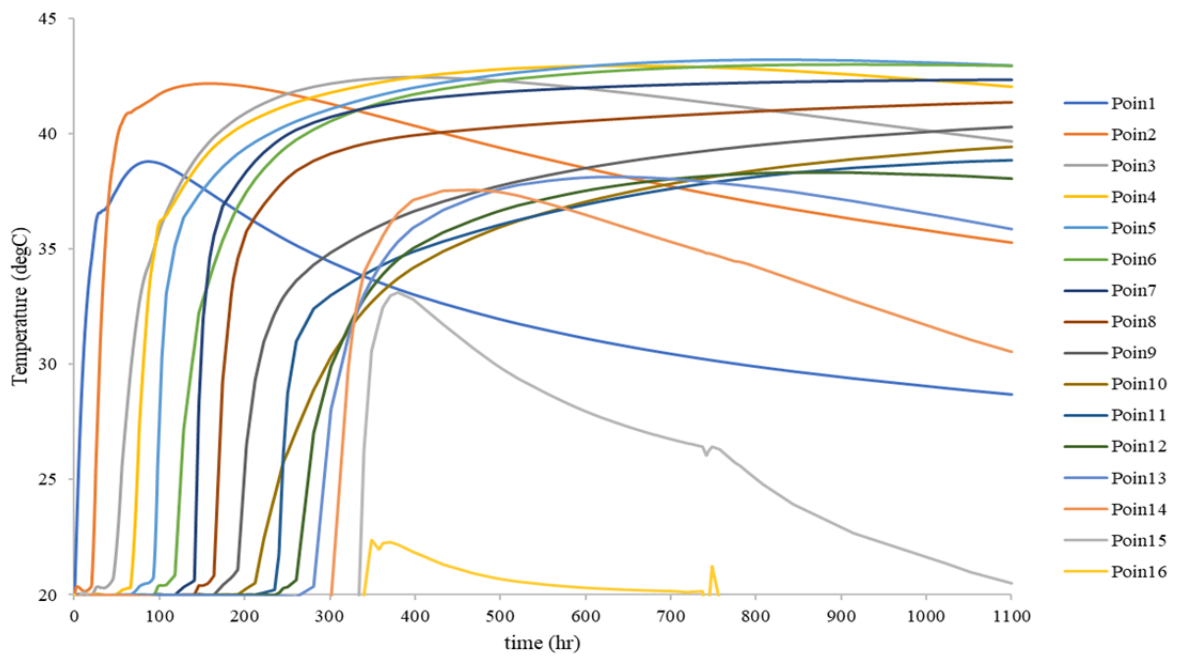


Figure 6- 4 Temperature curves for different points of the foundation for the time interval of 1 day

Figures 6-9 to 6-14 show the 3D results highlighting heat development over time for a representative scenario, i.e. 3 days delay between placements of different layers. As shown, the heat generation at each layer starts after concrete placement of that layer while the heat generation of the previous layers continues and is transferred via conduction. Furthermore, the initiation of the cooling phase, starting from the bottom layer, is apparent in time dependent 3D results presented in Figures 6-13 and 6-14. This highlights the effective implementation of the time-dependent heat generation models considered in this study.

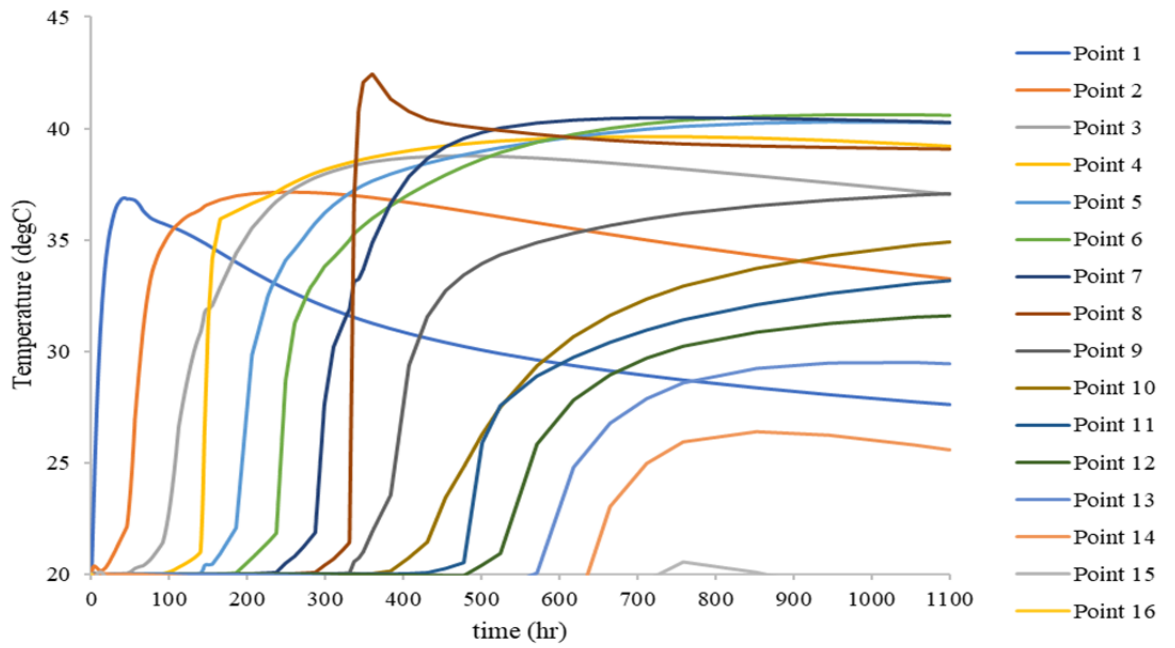


Figure 6- 5 Temperature curves for different points of the foundation for the time interval of 2 days

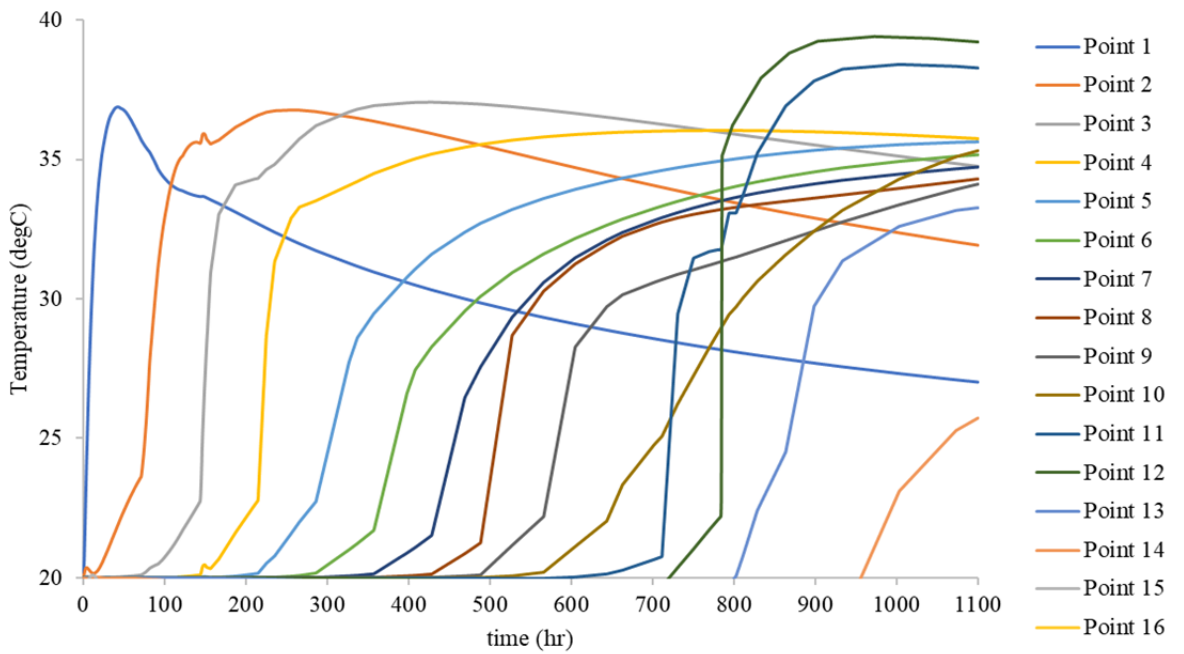


Figure 6- 6 Temperature curves for different points of the foundation for the time interval of 3 days

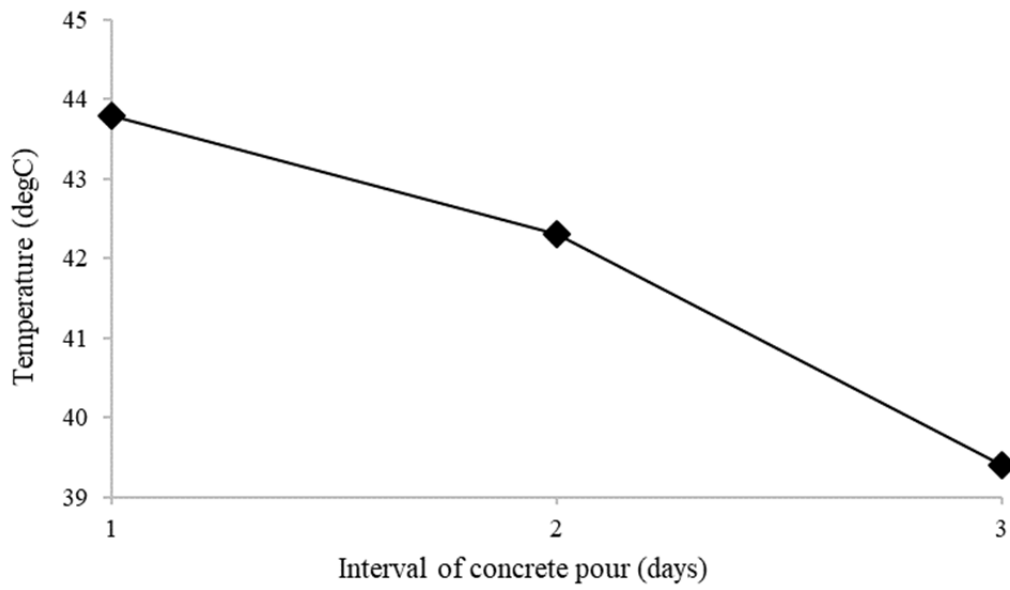


Figure 6- 7 Maximum temperature within the foundation

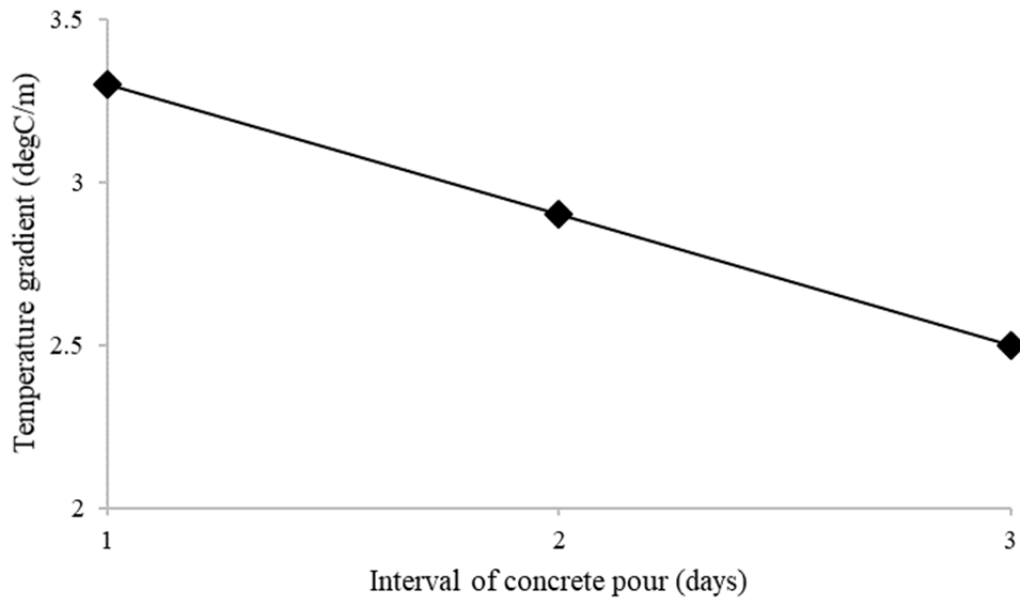


Figure 6- 8 Maximum temperature gradient within the foundation

Figure 6-15 illustrates the effectiveness of the concrete placement scenario in reducing the maximum cracking ratio within the concrete foundation. As shown, at one day placement delay scenario, the maximum cracking ratio reaches 6.35, while it

significantly drops to 2.9 and 2.5, when increasing the sequential placement delay to 2 and 3 days, respectively. It can be noted that increasing the delay between placement of layers from 1 to 3 days leads to about 60% decrease in the cracking ratio. Despite the significant reduction in the overall risk of cracking, the results indicate an early age thermal cracking ratio of higher than 1, which indicates concrete will crack almost certainly. With this in mind, further investigate alternative scenarios is advised, including reducing the thickness of each layer or increasing the delay between placement of each later.

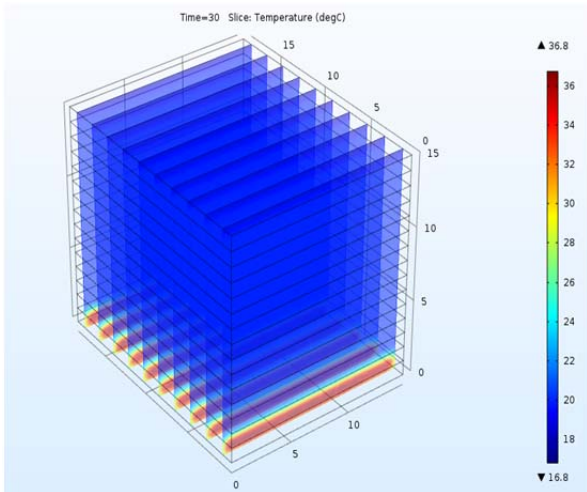


Figure 6- 9 Heat transfer in the foundation after pouring the first layer at time= 30 hrs

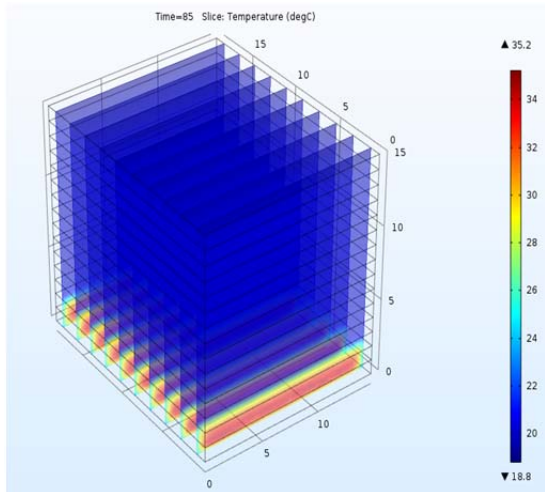


Figure 6- 10 Heat transfer in the foundation after pouring the 2nd layer at time= 85 hrs

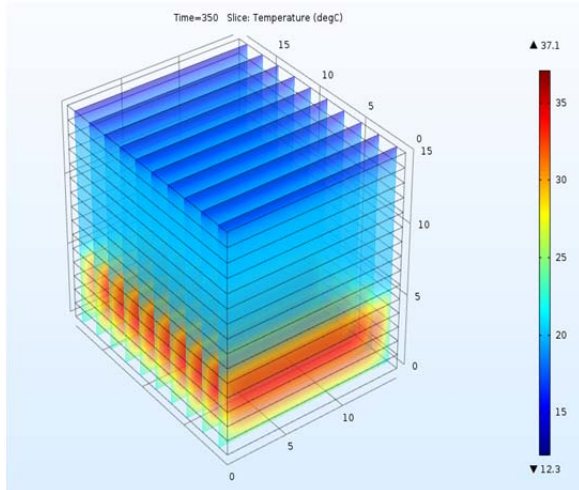


Figure 6- 11 Heat transfer in the foundation at time= 350 hrs

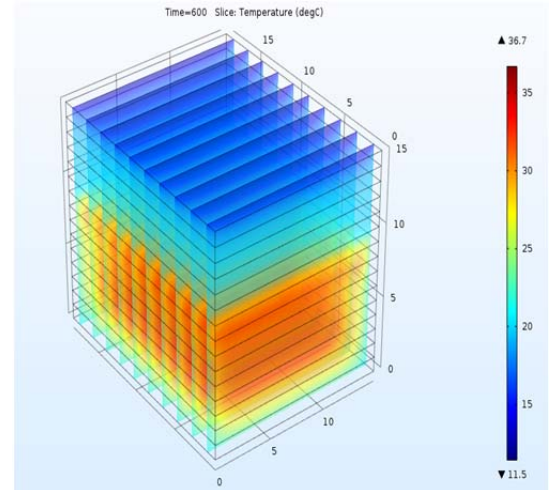


Figure 6- 12 Heat transfer in the foundation at time= 600 hrs

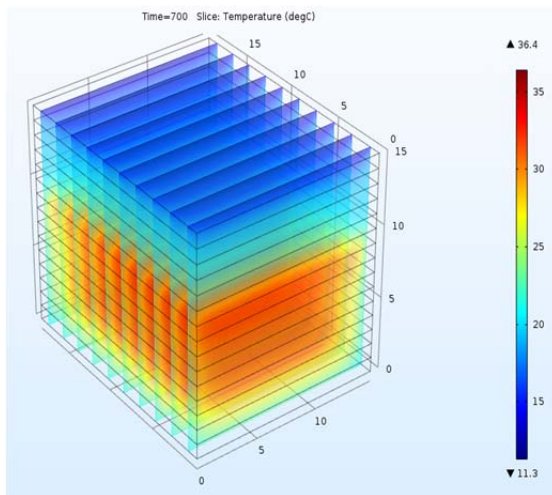


Figure 6- 13 Heat transfer in the foundation at time= 700 hrs

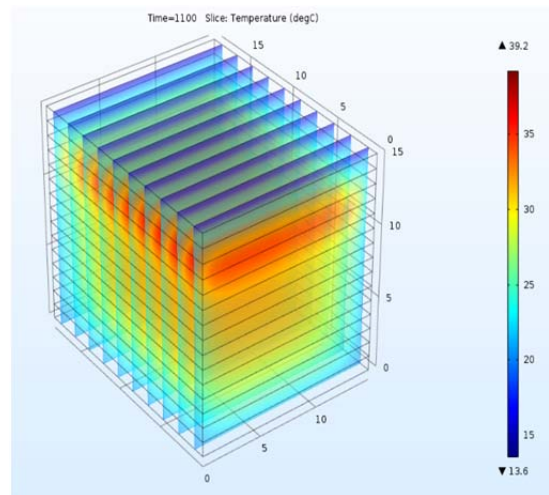


Figure 6- 14 Heat transfer in the foundation at time= 1100 hrs

It should be noted that further increase in the delay between the concrete pouring of the layers may not be possible as it increases the total construction time and has a negative impact on the finance of the project. Also, too much delay may cause bonding problems between different layers [3]. Therefore, in such cases, other crack controlling methods such as mix design optimisation which was discussed in Chapter 5 or other methods which will be discussed in the subsequent sections can be used in

conjunction with sequential concrete placement for further reduction in the risk of early age thermal cracking.

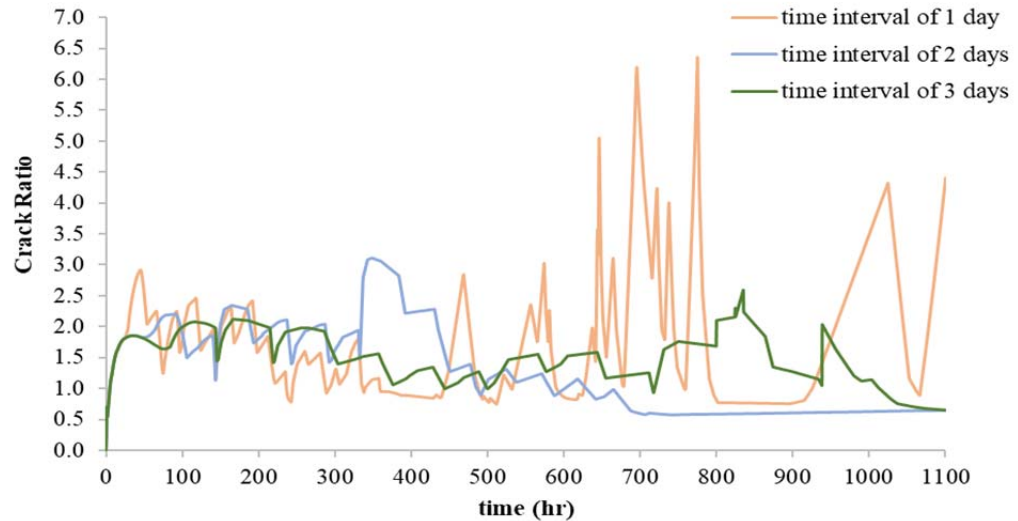


Figure 6- 15 Maximum crack ratio within the foundation

6.3 Lowering placement temperature

Concrete placement temperature is a key factor affecting the rate of temperature rise and the maximum temperature reached in concrete [3, 23, 87]. Figure 6- 16 shows the effect of initial temperature on the temperature profile of a typical concrete as highlighted in CIRI C660 guiltiness [3]. A number of construction strategies are commonly used to decrease the initial temperature of concrete as an effective risk mitigation strategy for early age thermal cracking. These include shading, sprinkling of aggregate piles, using chilled mixing water, substitution of mixing water with ice, covering the concrete trucks when transporting concrete, and using liquid nitrogen injection before placing for highly specialized mass concrete pouring [87, 88]. The numerical model presented in Chapter 4 could be adopted in order to evaluate the influence of changing the initial temperature for each case.

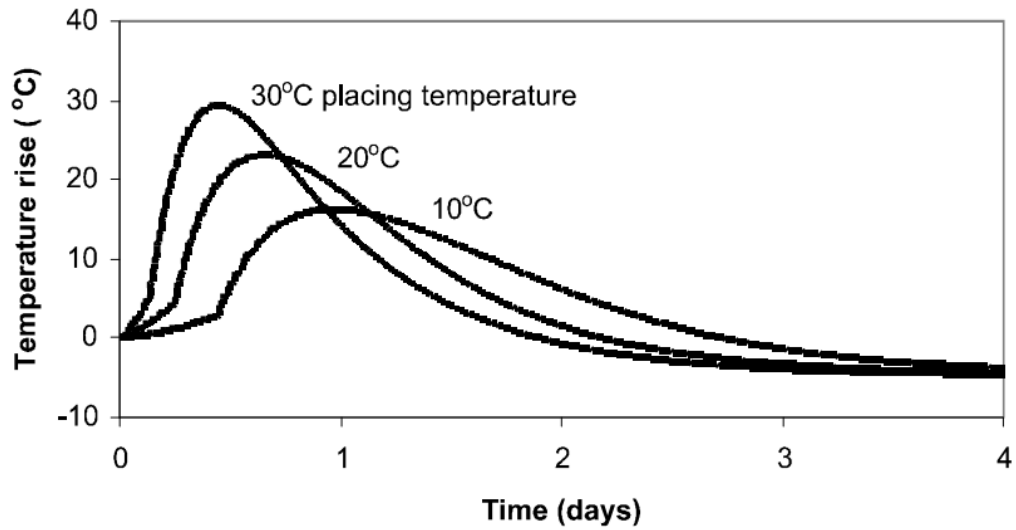


Figure 6- 16 The effect of placing temperature on the temperature rise in a 500 mm thick wall using concrete with 350 kg/m³ CEM I cast in steel formwork [3]

6.3.1 Case study

To investigate the effects of placement temperature on maximum temperature and risk of thermal cracking, a real-world concrete pile with the dimensions of 2.4 m diameter×15 m high is modelled (Figure 6- 17). The original placement temperature reported to be 32 °C. The mix design used for this pile and calculated heat parameter are shown in Tables 6-4 and 6-5. To study the effect that lowering the placement temperature has on risk of early age thermal cracking, numerical simulation is repeated three times by varying the initial concrete temperature to 20 °C, 25°C and 32 °C degrees. The target compressive strength of the mix is 40 MPa and the mix design is shown in Table 6-4.

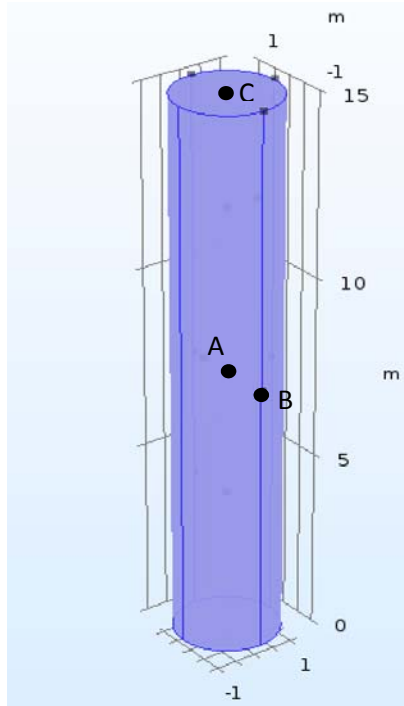


Figure 6- 17 Numerical model of the concrete pile

Table 6- 4 Mix design for the concrete pile

Material	Mass (Kg/m ³)
Portland cement	290
Fly Ash	120
GGBFS	140
Water	170
W/CM	0.31
Coarse aggregate	980
Fine aggregate	700

Table 6- 5 Heat parameters for the concrete mix design based on Bogue model

Heat parameters	Values
Activation Energy	35228.83 (J/mol)
τ	28.1 (hrs)
β	0.6
α	0.782
H_u	475.75 (kJ/kg)

6.3.2 Results and discussion

Figure 6- 18 shows the variations in the temperature of concrete at the center point of the pile (point A in Figure 6-17) and the effect of variations in the initial temperature of concrete on the latter. As can be seen, the peak temperature is decreased by approximately 9.5 °C from 107.4 °C to 97.8 °C by decreasing the initial placement temperature from 32 °C to 25 °C. Moreover, further decrease in the initial temperature to 20 °C is found to reduce the concrete's maximum temperature to 91.6°C, indicating about 15% reduction in peak temperature compared to the original placement temperature. Moreover, the time of the peak temperature is delayed for approximately 13 hours by reducing the placement temperature to 20°C. This will provide concrete with more time to gain tensile strength and consequently lowers the risk of early age thermal cracking. Figure 6- 19 shows the effect on initial temperature on the maximum temperature gradient within the concrete element. As can be seen, the maximum temperature gradient is decreased almost linearly from 8.5°C /m to 7°C /m when the initial temperature is decreased from 32 °C to 20 °C. Figure 6- 20 illustrates that the compressive strength is slightly affected by changing the placement

temperature in the first days. This is due to a higher rate of hydration caused by higher placement temperatures. It should be noted that the final compressive strength reaches the same value for all different initial temperature options.

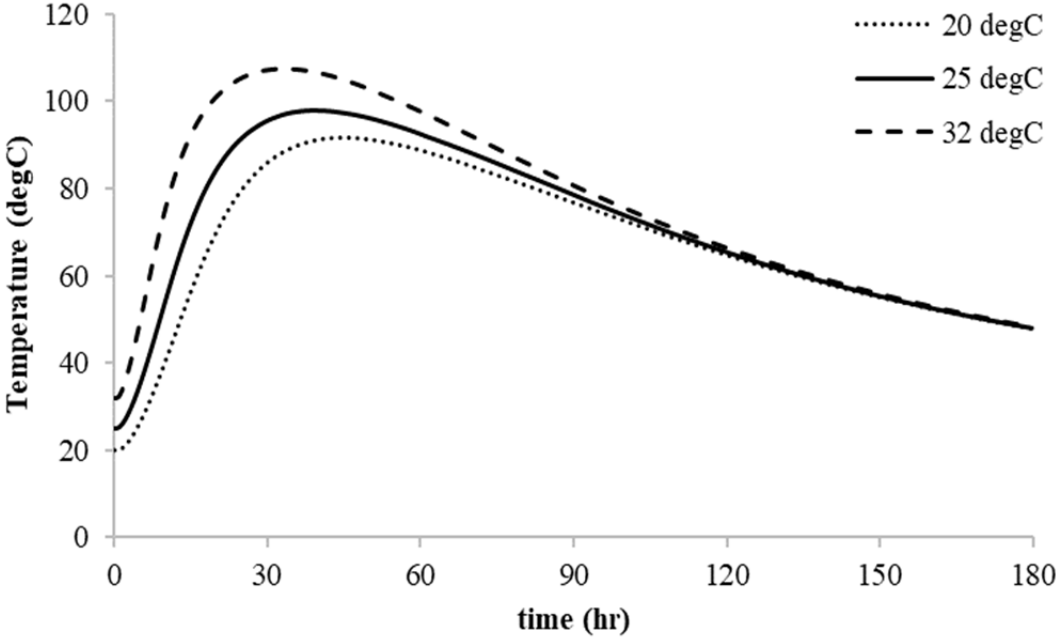


Figure 6- 18 Temperature development of point A for different initial temperatures

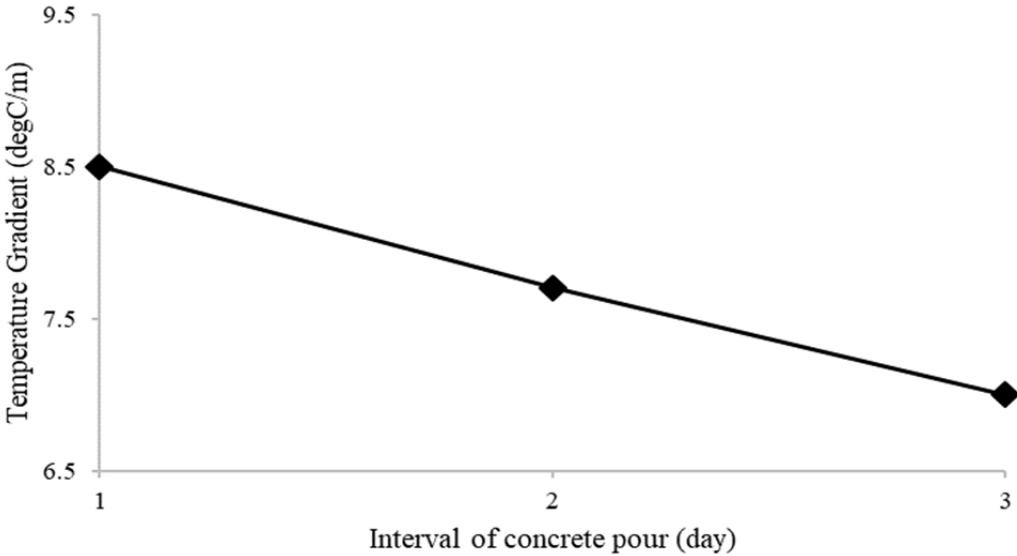


Figure 6- 19 Maximum temperature gradient within the pile

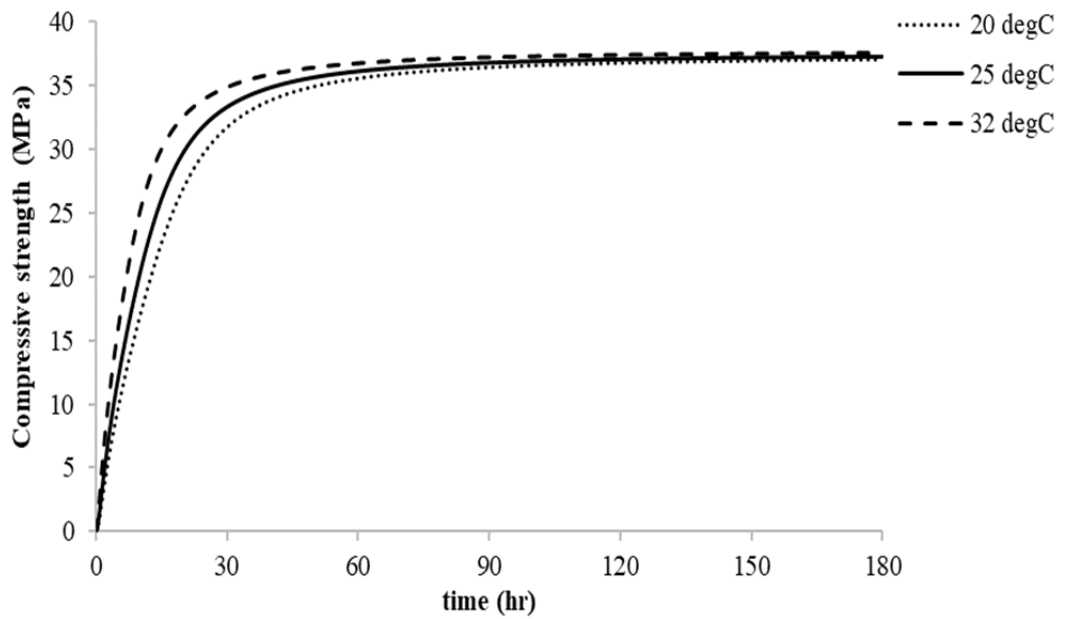


Figure 6- 20 Compressive strength development of point A for different initial temperatures

To investigate the effects of placement temperature on the risk of early age thermal cracking, the maximum cracking ratio within the concrete pile over the analysis time is drawn in Figure 6- 21. This figure shows 25% reduction in the maximum cracking ratio when lowering the placement temperature to 20 °C. Figure 6- 22 shows an approximately linear relationship between the maximum cracking ratio of the pile and the placement temperature. However, the risk of early age thermal cracking is found to remain high and use of supplementary strategies should be considered to further lower the risk of cracking to an acceptable level. These are described below.

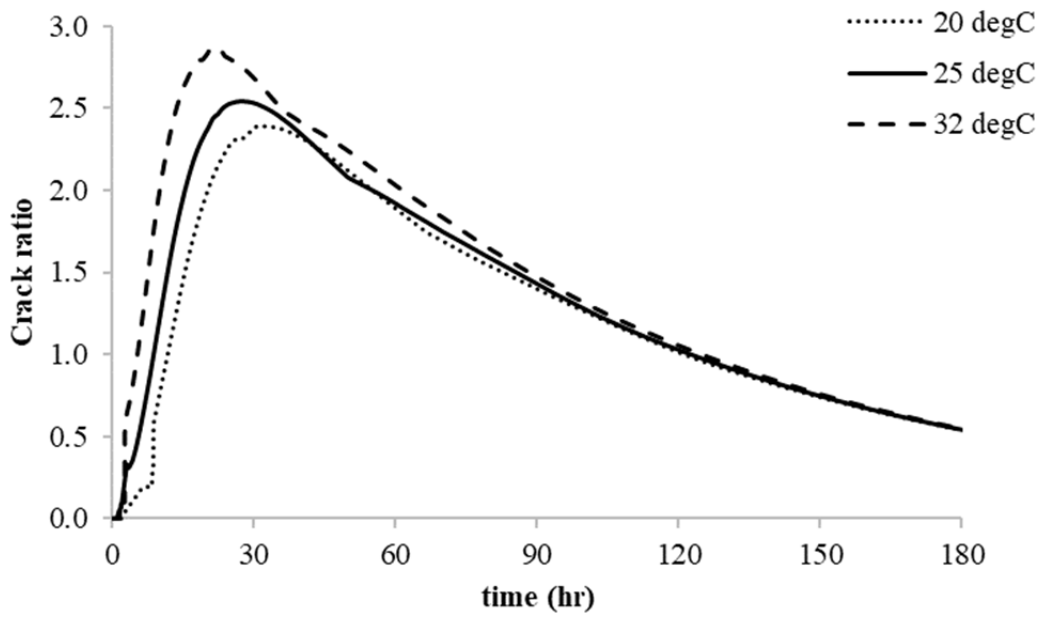


Figure 6- 21 Maximum Cracking ratio development within the concrete pile

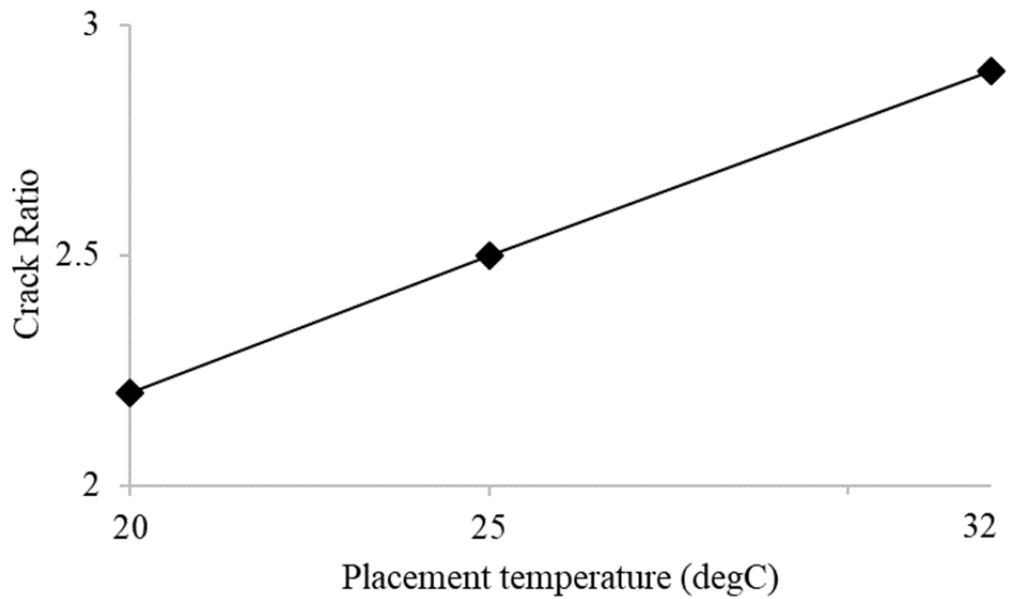


Figure 6- 22 Maximum Cracking ratio within the concrete pile for different placement temperatures

6.4 Using aggregates with lower thermal expansion coefficient

As shown previously, differential internal heating of concrete due to hydration tends to lead to differential expansion within the concrete element. Since all concrete elements are internally and/or externally restrained, expansion results in development of tensile stress and consequent cracking. An important concrete property affecting the level of tensile stresses developed in concrete is the coefficient of thermal expansion (CTE). Bamford suggests that lowering the coefficient of thermal expansion of concrete can significantly reduce the risk of early-age thermal cracking [3]. Thermal expansion of concrete is highly dependent on the thermal expansion of the aggregates used in casting since the amount of aggregate is dominant in a concrete mix [140]. This section aims to demonstrate how numerical modelling can be utilized to understand the effect of aggregate type on the thermal expansion and the risk of early age thermal cracking of concrete, thereby providing concrete specialists with decision support data to select the most suitable aggregate type for a particular mix.

6.4.1 Thermal Expansion of aggregates- Case study

To study the effect of changing the aggregate type on the risk of early age thermal cracking, of the same placing a concrete pile element, described in Section 6-2-2-2, is adopted as case study. The initial temperature of the concrete is assumed to be 32 °C. Same mix design was considered for the pile as in Section 6-2-2-2. The type of aggregate is varied between sandstone, Basalt and Limestone to investigate the effect of variations in the type of aggregate and the resulting variation in the coefficient of expansion of concrete on the risk of early age thermal cracking. The coefficient of thermal expansion for these aggregates are presented in Table 6- 6 [140]. The type of the aggregates is presumed to be the same for both coarse and fine aggregates in each

mix design. As shown in Table 6-6, Sandstone has the highest thermal expansion coefficient while Limestone's thermal expansion coefficient is the lowest among all the aggregate types under study.

Table 6- 6 Coefficient of thermal expansion of different aggregate types

Aggregate type	CTE×10 ⁻⁶ , ($\frac{1}{k}$)
Sandstone	12.6
Basalt	8.1
Limestone	4.5

6.4.2 Results and discussion

Figures 6-23 to 6-25 indicate the variation in maximum temperature, the tensile stress and early age thermal cracking ratio within the concrete pile when using three different aggregate types, respectively. It can be seen that although changing the aggregate type does not affect the temperature development significantly, it has a noticeable impact on the thermal stress and cracking ratio of the pile. Since aggregate occupies most of the volume of the concrete, the thermal expansion coefficient of the concrete element is directly related to the thermal expansion coefficient of the aggregate. As shown in the Figures 6-23 and 6-24 for the same temperature in all three different models, the higher the thermal expansion coefficient of the aggregates is, the more the volume change of the element will be which causes higher amount of stress. Therefore, as shown in Figure 6-25, using Sandstone with the highest thermal expansion coefficient results in higher cracking ratio while using limestone decreases the thermal cracking ratio by about 40%. This indicates how changing the aggregate

type in the same mix design can reduce the risk of early age thermal cracking in a concrete element.

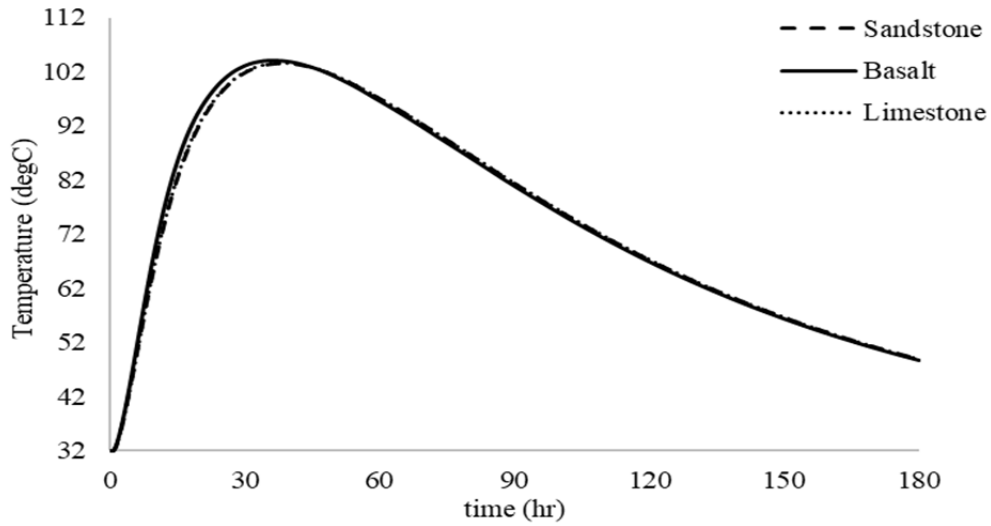


Figure 6- 23 Maximum temperature development within the concrete pile using different aggregate types in the mix design

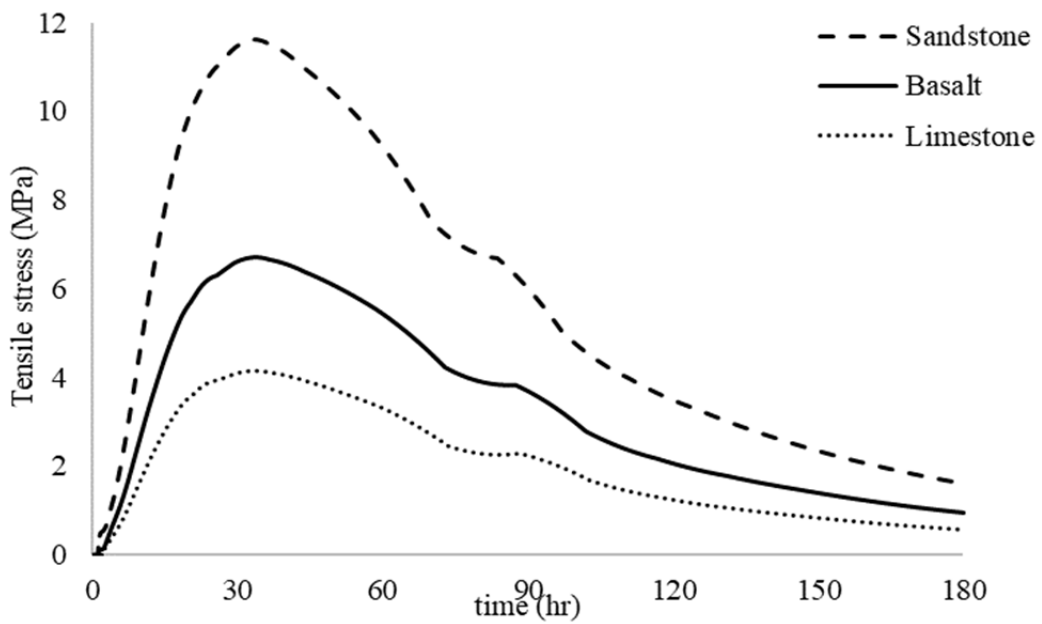


Figure 6- 24 Maximum tensile stress within the concrete pile using different aggregate types in the mix design

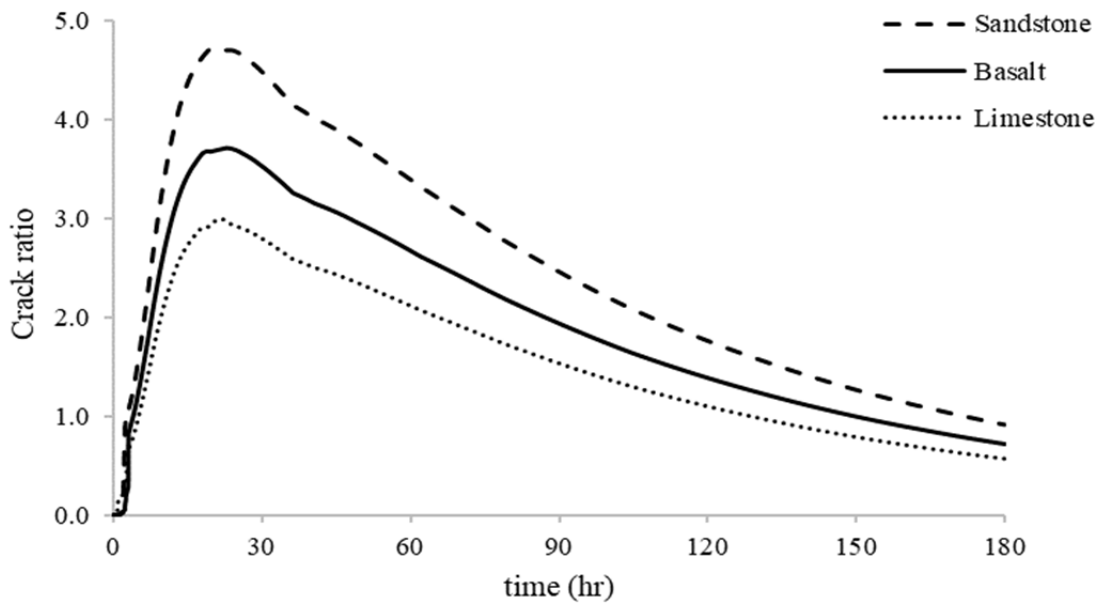


Figure 6- 25 Maximum cracking ratio development within the concrete pile using different aggregate types in the mix design with placement temperature of 32 °C

6.5 Internal water cooling

Internal cooling of concrete through a network of embedded water pipes is a common risk mitigation strategy for elements subject to high risk of early age thermal cracking including dams, foundations, and pumping stations [92]. In such cases, large-scale mass concrete structures are constructed with embedded pipes which circulate cold water to help with preventing excessive heat build-up in the structure[91]. An important decision to make in implementing the internal cooling strategy is selecting the location of the water pipes. Depending on level of risk and the location of the high risk regions in a concrete element, the internal cooling pipes can be localized at foundation proximity or other sections of the element subject to high risk of cracking, or can be uniformly distributed throughout the structure as required [87]. Given the costs associated with implementation of this strategy, minimizing the size of the internal cooling network by optimising its location and spacing of pipes is a crucial.

This section uses a case study to demonstrate how numerical simulation can be used to evaluate the effectiveness of internal cooling strategy and its selected implementation methodology in reducing the risk of early age thermal cracking.

6.5.1 Numerical modelling

The numerical model presented in Chapter 4 was modified to model the embedded water-cooling pipes. In this numerical model, the pipe material can be chosen along with water flow which is introduced as a laminar flow. The Navier-Stokes equation is defined as below for laminar flows.

$$\begin{cases} \rho \left(\frac{\partial u}{\partial t} + u \cdot \nabla u \right) = -\nabla p + \nabla \cdot \left(\mu \left(\nabla u + (\nabla u)^T - \frac{2}{3} \mu (\nabla \cdot u) I \right) \right) + F \\ \rho \nabla \cdot u = 0 \end{cases}$$

Equation 6- 4

where u is the fluid velocity, p is the fluid pressure, ρ is the fluid density, μ is the fluid dynamic viscosity and F is the external forces applied to the fluid [141]. After defining the geometry and location of the pipes in the structure, the water temperature is introduced to the model. It is assumed that heat transfer occurs through conduction between the liquid flow, the pipe, and the concrete surrounding the pipe. The concrete element generates heat due to hydration. The heat transfer in the water is modelled using [90]:

$$\rho_w c_w \left(\frac{\partial T_w}{\partial t} + u \cdot \nabla T_w \right) = k_w \nabla^2 T_w$$

Equation 6- 5

where T_w is the temperature of water in the pipe, ρ_w , c_w and k_w are the density, specific heat and conductivity of water, respectively. The mechanical and thermal boundary conditions of the concrete element under study are defined using the same as methodology as discussed in Chapter 4.

6.5.2 Embedded water-cooling pipes- Case study

In order to investigate the influence of the embedded water pipes on the peak temperature, a water piping system is modelled for a part of the concrete pile introduced in section 6-2-2-1, as shown in Figure 6-26. The dimensions of the pile are 2.4m diameter× 2.0m high. To consider this pile as the middle part of the original pile, convection boundary condition is imposed only defined on side surfaces, while the top and bottom surface are defined as insulated surfaces. This means that no heat flux is considered across these two surfaces. Also, the mechanical boundary condition of the top and bottom surface is imposed using Equation 6-6. This means that the rigidity of the concrete at these two surfaces is calculated based on the rigidity of the hardening concrete:

$$k = \begin{bmatrix} GT & 0 & 0 \\ 0 & GT & 0 \\ 0 & 0 & GT \end{bmatrix} \quad \text{Equation 6- 6}$$

GT can be calculated using Equation 4-20 in Chapter 4.

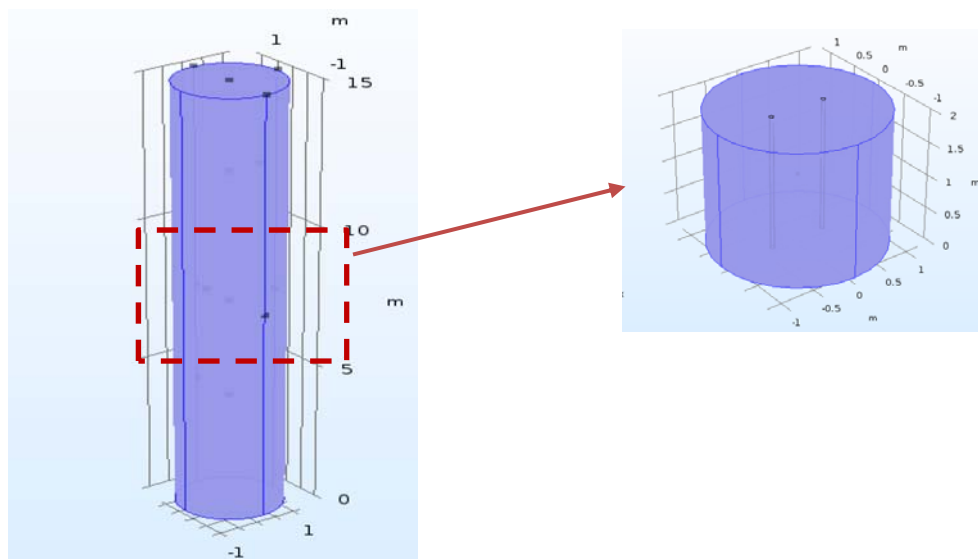


Figure 6- 26 Numerical model of the embedded water piping system

The mix design and the thermal properties of this case study are presented in Tables 6-4 and 6-5. Two water pipes with the inner and outer diameters of 0.03m and 0.035m are modelled inside the pile as shown in Figure 6-27. The pipe material is defined as cast iron and its thermal and mechanical properties are presented in Table 6-7. The initial temperature of the concrete is assumed to be 32 °C, while the temperature of water is defined to be 20 °C. The simulation is performed for the pile with and without internal cooling system and the results are compared. Moreover, to investigate the impact of the number of the pipes in reducing the cracking ratio, the pile is also modelled with four embedded pipes (Figure 6-28) and the results are compared to the pile containing two pipes and the pile with no embedded pipes.

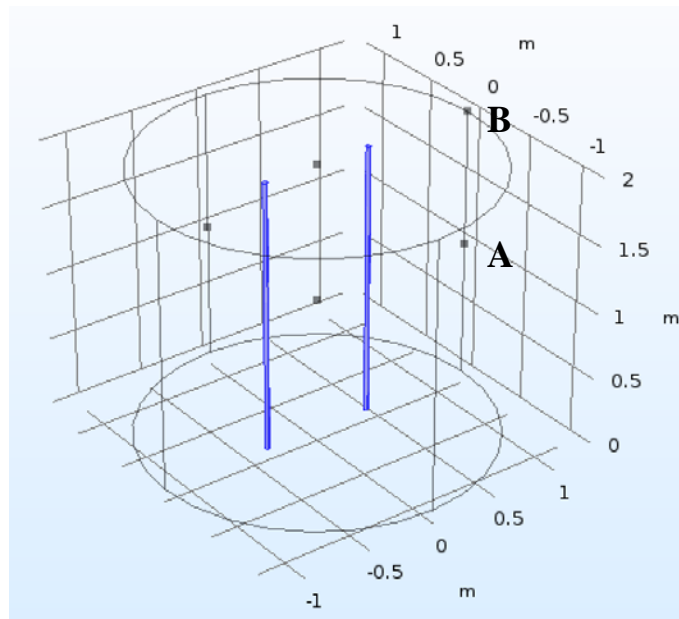


Figure 6- 27 Pile containing 2 embedded water pipes and the points under study

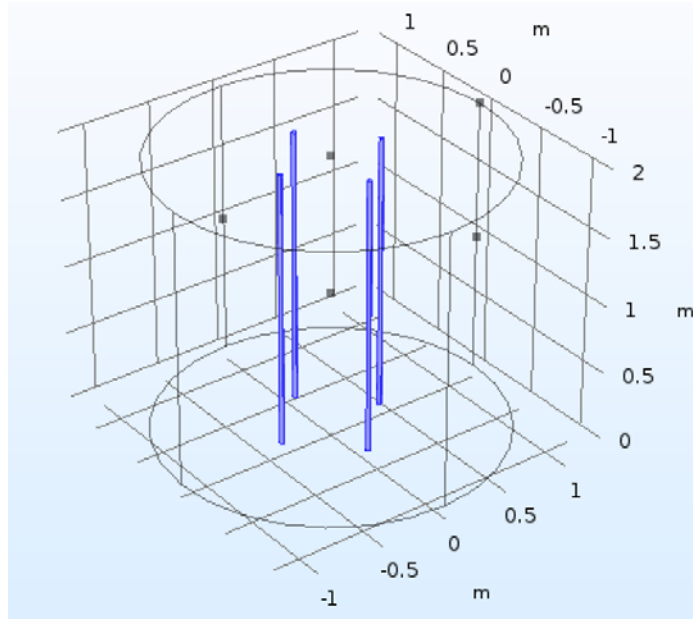


Figure 6- 28 Pile containing 4 embedded water pipes

Table 6- 7 Thermal properties of the pipes

Density	7000 [kg/m ³]
Heat capacity	420 [J/(kg*K)]
Thermal conductivity	50 [W/(m*K)]
Young's Modulus	140e9 [Pa]

6.5.3 Results and discussion

Temperature development within the concrete pile with two embedded water pipes is shown in Figures 6-29 to 6-32. As can be seen, water pipes prevent the extreme temperature rise within the concrete pile. The effect of embedded cooling system on the maximum temperature within the pile is shown in Figure 6-33. As shown, the maximum temperature within the pile is reduced from 107.1 °C to 84.6 °C when two water pipes are embedded. This amount is decreased to 68.6 °C when the number of the

embedded pipes is increased to 4. This indicates about 21% and 35% reduction in the maximum temperature when adding two and four embedded cooling pipes, respectively. It also shows that embedding two more water pipes in the pile reduces the maximum temperature by about 19%.

Figures 6-34 and 6-35 show the variations in the cracking ratio of the pile at two surface points, viz points A and B in Figure 6-27. The surface points are selected, due to the higher risk of early age thermal cracking at the surface of concrete [108]. It is seen in Figure 6-34 that the maximum cracking ratio at point A is decreased from 2.03 to 1.23 and 0.91 when two and four water pipes are embedded in the pile, respectively. This indicates about 40% and 55% reduction in the maximum cracking ratio when the cooling pipes are used in the pile.

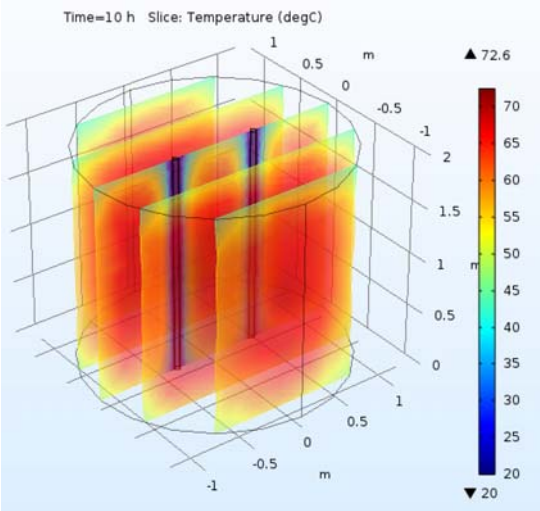
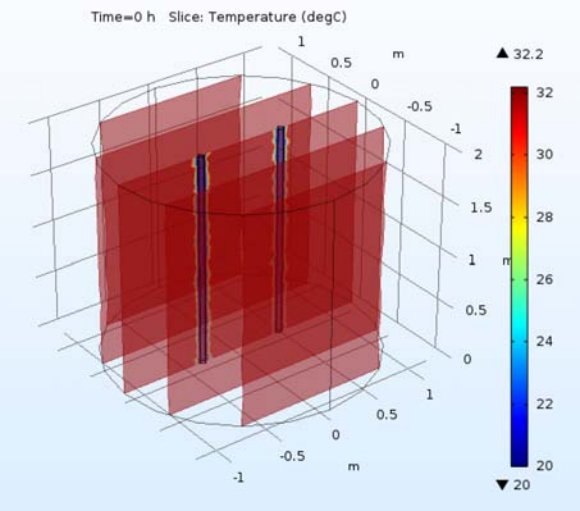


Figure 6- 29 Temperature distribution of the pile with piping system at t=0 hours

Figure 6- 30 Temperature distribution of the pile with piping system at t=10 hours

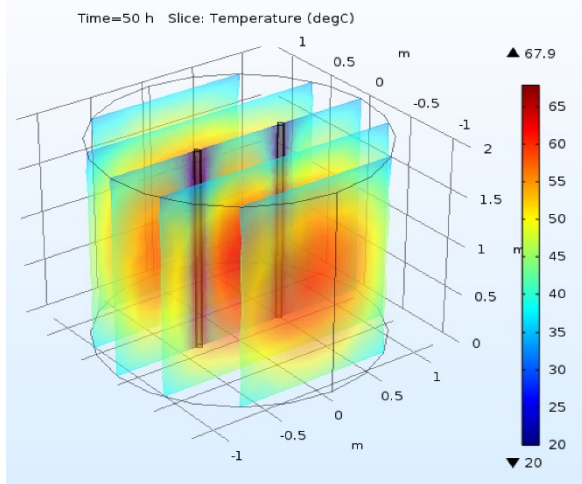


Figure 6- 31 Temperature distribution of the pile with piping system at t=50 hours

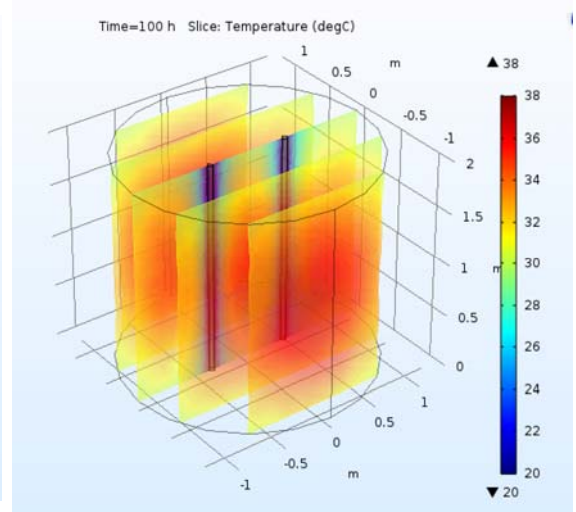


Figure 6- 32 Temperature distribution of the pile with piping system at t=100 hours

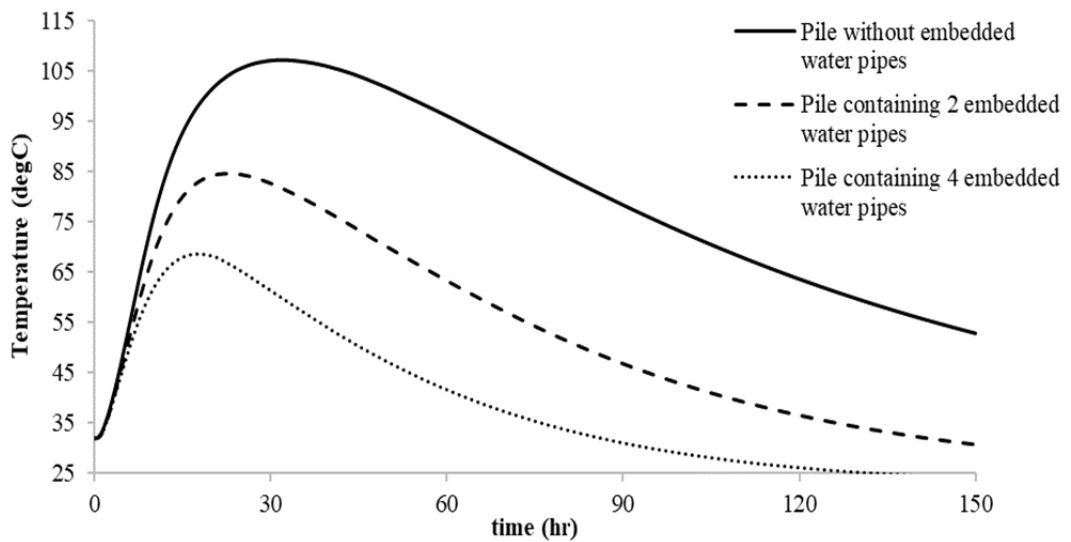


Figure 6- 33 Maximum temperature of the piles with and without water piping system

Also, Figure 6-35 shows that the maximum cracking ratio of point B is decreased from 0.76 to 0.2 and 0.09 by using 2 and 4 cooling pipes, respectively. Therefore, the results highlight the effectiveness of internal cooling strategy as an effective method to reduce the risk of early age thermal cracking. It is seen that increasing the number of embedded cooling pipes improves the performance of the cooling pipe system and reduces the cracking ratio more. This highlights the need to

fine tuning the internal cooling strategy through measures such as increasing the number or diameter of the pipes or the temperature of the circulating water in concrete.

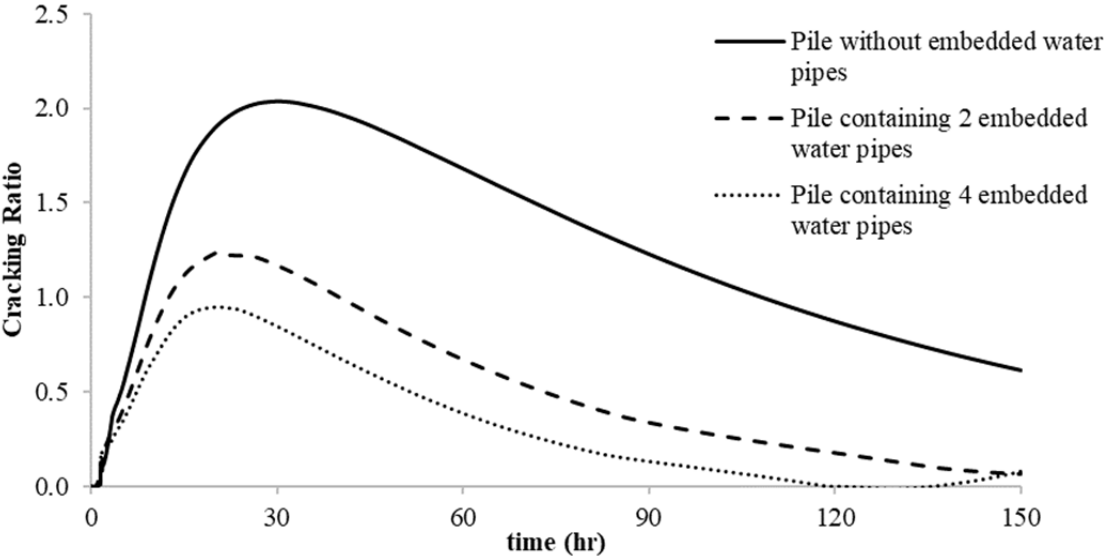


Figure 6- 34 Cracking ratio of point A for the pile with and without internal cooling system

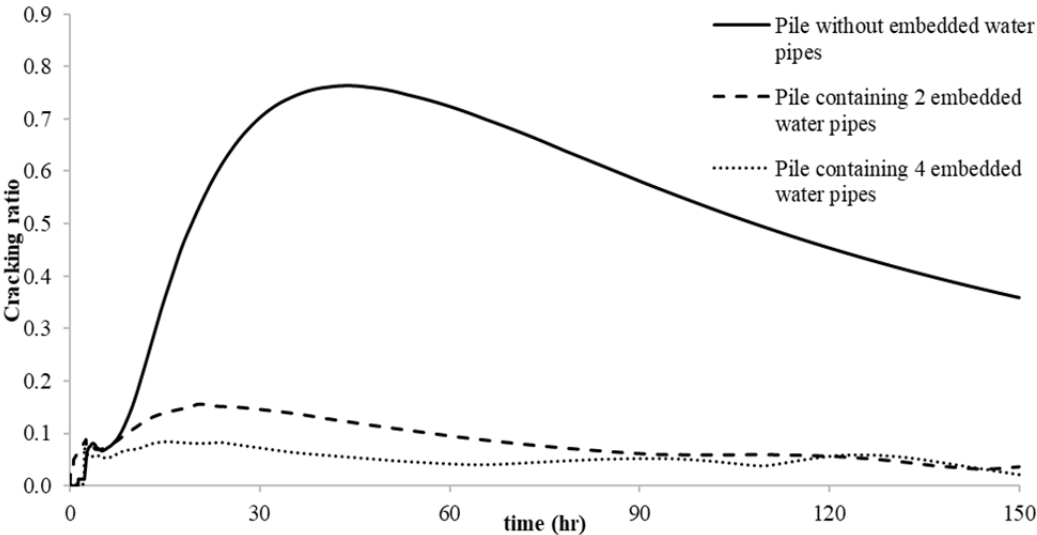


Figure 6- 35 Cracking ratio of point B for the pile with and without internal cooling system

6.6 Conclusions

This chapter presented a numerical simulation approach for investigating the effectiveness of construction strategies available to mitigate the risk of early age thermal cracking of concrete. The numerical model developed previously in Chapter 4 was modified to enable modelling four common risk mitigation strategies including sequential placement of concrete, using aggregates with low thermal expansion coefficient, lowering the initial temperature of concrete, and internal cooling through embedded water pipes. As these numerical simulation models can easily be used by the engineers when using the strategies mentioned above, case studies involving actual concrete placement projects undertaken were used to investigate the effectiveness of each of the above strategies and how numerical simulation can provide the required decision support data to assist concrete specialist in optimising the selected strategy. All four strategies were found to be effective in achieving significant reduction in the level of cracking risk. It was shown, however, that when dealing with elements subject to high risk of early age thermal cracking, a single strategy may not be adequate to achieve the required level of risk mitigation and a combination of strategies may be required.

Chapter 7: Conclusions

7.1 Concluding remarks

This thesis presents the results of a comprehensive study conducted to develop a decision support tool to assist concrete specialists in i) evaluating the risk of early age thermal concrete for a particular concrete element, ii) identifying the optimal concrete mix design to reduce the risk of early age thermal cracking, iii) evaluating the effectiveness of construction strategies, including sequential placement and internal cooling using embedded pipes, in reducing the risk of early age thermal cracking.

In Chapter 2, the major issues affecting the ability of existing models to meet the above objectives were discussed. The key issues and gaps in the available literature were found to be i) a lack of evidence on precision of existing hydration heat and temperature rise prediction models for Australian concrete, ii) a lack of verified 3D simulation model for early age thermal cracking with the ability to model different geometries and different construction scenarios as well as the ability to use direct calorimetry data as heat source, iii) a lack of mix optimisation method to minimize the risk of early age thermal cracking without compromising concrete's ability to meet strength development requirements.

In Chapter 3, an experimental study was conducted to address the first gap by evaluating the precision of existing hydration heat models. The results of extensive calorimetry measurements showed that while existing hydration heat models are relatively accurate for mixes containing only Portland Cement as binder, the level of precision deteriorates significantly when supplementary cementitious materials and retarders are used. The results indicated that Schindler and Follaird's model with

reasonable accuracy predicted the peak heat flow of the reference cement mix (100% OPC); a maximum error of 5.5% was found. The prediction error of both models was found, however, to increase with an increase in the amount of supplementary cementitious materials. For instance, increasing the fly ash component from 0% to 50% at a curing temperature of 30°C led to an increase in estimation error from 5% to about 30%. Furthermore, it was shown that the errors in estimating the time of peak heat increase with an increase in curing temperature. The trend was shown when using the Bogue method. It was shown that the estimation error of this method increased from 13% to about 40% with an increase in amount of GGBFS from 0 to 50% at the curing temperature of 30°C. Moreover, the prediction of both models for time of the occurrence of the peak heat was found to be significantly in error. The estimation error of these models for mixes containing retarders including Sucrose, Citrate and Retardant N was noticeable. The results errors when using 2 [mL/kg] Sucrose and Citrate and 10 [mL/kg] Retardant N were found to be about 52%, 20% and 47%, respectively. All in all, the findings of this chapter have several practical implications. First, the significant errors in predicting the heat of hydration using the existing models highlights the potential for error in estimating the risk of early age thermal cracking when using the existing commercial software, which commonly adopt these hydration models as heat source. Therefore, the results of this chapter highlight the need to recalibrate the hydration models or develop new models that are capable of capturing the effects of SCMs and retarders. Alternatively, in the absence of such models, using direct calorimetry measurements as heat source may appear as a practical approach to improve the accuracy of predictions. However, there are several challenges associated with this approach including the time-consuming nature of calorimetry measurements

and lack of numerical simulation models capable of accepting a limited number of calorimetry data as heat source in the heat transfer module.

To address the drawbacks associated with numerical simulation of early age thermal cracking, in Chapter 4 an advanced three-dimensional numerical simulation model was developed and verified using site measurements. The developed numerical model used a combination of heat transfer and solid mechanics modules in COMSOL Multiphysics to develop a 3D simulation environment capable of modelling all practical geometries. The model addresses the drawbacks of existing hydration heat models by allowing the use of calorimetry data as heat source, modelling the effect of reinforcement, considering different thermal and mechanical boundary conditions, and modelling different concrete pouring strategies, etc. The precision of developed model was verified using a large-scale test study. A concrete wall built (and monitored) in one of Boral's Quarries in Queensland, Australia with the dimensions of 13.07m × 2.1m × 1.2m thick was simulated numerically. The temperature development at different points inside the concrete wall was monitored using SmartRock2 wireless temperature sensors. Comparing numerical results and site measurements verified the acceptable precision of model's predictions for temperature development, with a maximum of 10% error. The developed tool provides concrete specialists with a reliable approach to gain an insight into risk of early age thermal cracking for a particular concrete element. By providing a 3D representation of distribution of stresses and cracking potential, the proposed model makes available a unique tool for design of crack control rebars throughout the element. Furthermore, in practice, the model provides a robust tool for optimising design and planning decisions affecting the risk of early age thermal cracking; these include mix design of concrete, choice of aggregate (due to its effect on

thermal and mechanical properties), choice of formwork and curing method (due to their effects on boundary conditions), etc.

The developed numerical simulation model (Chapter 4) makes available a means of evaluating the effect of different mixes on the risk of early age thermal cracking through comparison for different concrete mix designs. However, relying on this approach to identify the optimal mix design that minimizes the risk of early age thermal cracking can be time consuming, if practical at all, due to nearly infinite number of mix design alternatives. To address this, in Chapter 5 a genetic algorithm based multi-objective mix design optimisation method was developed to mathematically identify the optimal mix design that minimizes the risk of early age thermal cracking in a particular element, while considering the practical constraints. The proposed optimisation algorithm was developed in MATLAB code and was designed to include an embedded finite difference model to allow its use as a stand-alone tool. Cracking occurs when tensile stress exceeds the tensile strength of the concrete. The direct impact of temperature gradient on tensile stress, minimizing the temperature gradient within a concrete section and maximizing the tensile strength of concrete, simultaneously, was adopted as the mix optimisation methodology to minimize the risk of early age thermal cracking. In order to maintain the compressive strength development within an acceptable range, two constraints were introduced to define the acceptable limits for compressive strength at 3 and 7 days.

The effectiveness of the proposed mix optimisation method in reducing the risk of thermal cracking was validated through a real-world case study. The concrete element considered in the case study was numerically simulated using the previously verified numerical model, presented in Chapter 4. The numerical simulation was

performed once with the originally intended mix design proposed by concrete specialists and once with the mix designs identified using proposed mix optimisation method. The results indicated about 40% decrease in thermal stresses as well as about 36% decrease in peak temperature when using the optimised mix design. Furthermore, it was shown that the maximum crack ratio was decreased by about 42%. The proposed optimisation model makes available a unique tool to mathematically identify an optimal mix design, among thousands of possible variations that can lead to minimizing the risk of early age thermal cracking in a particular element. Furthermore, the proposed optimisation methodology leads a paradigm shift in the focus of mix design methods, which has been thus far focused solely on meeting the mechanical-performance objectives of concrete without accounting for other important durability objectives including minimizing the risk of early age thermal cracking.

As illustrated through the case study presented in Chapter 5, mix design optimisation can be an effective approach to reduce the risk of early age thermal cracking. When dealing with high risk elements such as mass concrete, however, mix optimisation alone may prove inadequate and additional risk mitigation strategies may be required to reduce the risk of early age thermal cracking to an acceptable limit. However, despite availability of several construction methods including sequential placement and internal cooling using embedded water pipes, there is currently a lack of reliable methods to evaluate the effectiveness of such methods in practice before implementation. To address this issue, in Chapter 6 of this thesis, the numerical model presented earlier in Chapter 4 was modified to simulate common risk mitigation strategies. These include sequential concrete placement, use of embedded water-cooling pipes, reducing placement temperature and using aggregates with lower thermal expansion coefficient. These methods were applied to two different real-world

case studies, including a dam foundation with the dimensions of $14.9\text{m} \times 18.5\text{m} \times 15\text{m}$ thick and a concrete pile with the dimensions of 2.4m diameter $\times 15\text{m}$ high. Sequential concrete pouring was considered for the dam foundation. A total of 15 layers with the dimensions of $14.9\text{m} \times 18.5\text{m} \times 1\text{m}$ thick were modelled and the delay time between pouring each layer was varied between 1, 2 and 3 days. The results showed that at one day placement delay scenario, the maximum cracking ratio reached 6.35, while it significantly dropped to 2.9 and 2.5, when increasing the sequential placement delayed to 2 and 3 days, respectively. Accordingly, the maximum cracking ratio decreased by about 60% with an increase in the pouring delay from 1 to 3 days. Furthermore, the maximum temperatures reached within the concrete section were 44.2, 42.4 and 39.0 °C for the concrete pouring in 1, 2 and 3 days which indicated approximately 12% reduction in the maximum temperature of the foundation when increasing the pouring delay time between layers from 1 day to 3 days. The impact of the reducing the initial temperature of concrete on the risk of early age thermal cracking was studied using the concrete pile case study presented earlier. The temperature of the pile was decreased from 32°C to 25 and 20°C. The results of the numerical simulation revealed that the peak temperature of the pile decreased from 107.4 °C to 97.8 °C and 91.6°C by decreasing the initial placement temperature from 32 °C to 25 °C and 20°C, respectively. Moreover, occurrence time of the peak temperature was delayed for approximately 13 hours by reducing the placement temperature to 20°C. The results also indicated about 25% reduction in the maximum cracking ratio of the pile when changing the placement temperature from 32 °C to 20 °C.

The effect of the aggregate type on early age thermal cracking was also studied by modelling the concrete pile described above while varying the type of aggregate between Sandstone, Basalt and Limestone. The results showed that although having

minimal effect on temperature development, variations in type of aggregate can significantly affect thermal stresses and cracking ratio. Using Sandstone, which has the highest thermal expansion coefficient compared to other aggregates considered, led to the most notable increase in cracking ratio while using limestone instead of Sandstone decreased the thermal cracking ratio by about 40%.

The effect of embedded cooling pipe system was also modelled using the concrete pile case study. Two and four water pipes with the inner and outer diameters of 0.03m and 0.035m were modelled inside the pile by considering a constant temperature of 20°C for the circulating water. The results showed that water pipes can effectively prevent extreme temperature rise within the concrete pile. The use of 2 and 4 water pipes resulted in about 21% and 35% reduction in the maximum temperature of the pile, respectively. Moreover, it was shown that the maximum cracking ratio within the pile decreased by about 40% and 55% when 2 and 4 embedded cooling pipes were simulated.

The results presented in Chapter 6 demonstrate that numerical simulation can provide a robust tool to evaluate the effectiveness of risk mitigation strategies for early age thermal cracking and optimising the implementation parameters related to each method. This can have significant practical implication by allowing concrete specialist to identify the most cost-effective approach to deal with risk of early age thermal cracking while ensuring satisfactory outcome. The results may also then be simulated using the refined model of Chapter 4 to validate the predicted outcomes.

7.2 Limitations and Future Work Recommendations

While providing efficient methods to estimate and minimize the risk of early age thermal cracking of concrete, this study has a number of limitations that should be

taken into consideration when interpreting its findings. First, while direct use of calorimetry measurements was proposed to reduce hydration heat prediction errors, calorimetry measurements are time consuming and may not be always practical within the short time frame allocated typically to design concrete mixes. Therefore, further studies involving developing an extensive database of calorimetry measurement for local cement, supplementary cementitious materials and admixture can be highly beneficial. Alternatively, the use of data science approaches including artificial intelligence may be explored to predict more reliable predictions using limited empirical data.

Second, in addition to development of models for reliable estimates of hydration heat, the accuracy of numerical model presented in this study is highly dependent on accuracy of the thermal properties of concrete, including heat capacity, thermal conductivity and thermal expansion coefficient. However, due to lack of availability of local data on these properties, the values obtained from available literature were adopted and may affect the accuracy of predictions. Developing an extensive database of thermal properties of local concrete and aggregates can be highly beneficial in improving the accuracy of proposed numerical simulation and optimisation models.

Third, due to instrumentation challenges, the verification attempts in this study were limited to monitoring temperature development. Further studies are needed to fully validate stress development predictions of the models.

Fourth, due to lack of reliable hydration heat models that account for effect of admixtures, including retarders, the optimisation model develop in this study does not account for effect of admixtures on hydration heat parameters. While the effects of this

on overall optimisation results may be minimal (due to focus of optimisation on relative performance of mixes), the temperature and stress prediction obtained using finite difference module embedded in the optimisation model may be affected. Therefore, further studies are recommended on developing mathematical models for heat of hydration which account for the effects of different types of admixtures. These would be highly valuable and contribute significantly to improving the accuracy of proposed optimisation model.

Fifth, the optimisation model developed in this study can be extended to include more variables including the type of the aggregate as well as placement temperature. In addition, further site testing and laboratory validation is required to evaluate the effectiveness of the optimised mixes proposed by the model.

Sixth, the cracking ratio values are not validated since there is currently a lack of experimental testing methodologies to experimentally quantify the cracking ratio in a particular structure. While several equipment, such as cracking frame discussed in the literature review Chapter 2, are available to monitor the relative cracking risk of different mixes, such frames do not provide absolute values for cracking ratio as the latter can be affected significantly by the actual degree of restraint. Therefore, further studies on experimental methods for quantifying cracking ratio are suggested.

References

- [1] D.P. Bentz, W.J. Weiss, REACT : Reducing Early-Age Cracking Today, (2008).
- [2] ACI207.2R, Report on Thermal and Volume Change Effects on Cracking of Mass Concrete, Am. Concr. Institute, Wwww.Concrete.Org. (2007).
- [3] P. Bamford, Early-Age thermal crack control in concrete, Constr. Ind. Res. Inf. Assoc. (2007) 23.
- [4] Portland Cement Association, Portland Cement, Concrete, and Heat of Hydration, Old Orchard Road Skokie, Illinois, 1997. <http://cement.org/tech/pdfs/pl972.pdf>.
- [5] A. Akbarnezhad, K. Ong, Thermal stress and pore pressure development in microwave heated concrete, Comput. Concr. (2011).
- [6] M. Ghareh Chaei, R. Lloyd, L. Keyte, A. Akbarnezhad, S. Foster, Precision of cement hydration heat models in capturing the effects of SCMs and retarders, (2017) 1–15.
- [7] A. Castel, R. Francois, G. Arliguie, Effect of loading on carbonation penetration in reinforced concrete elements, Cem. Concr. Res. (1999).
- [8] A. Castel, R. François, Modeling of steel and concrete strains between primary cracks for the prediction of cover-controlled cracking in RC-beams, Eng. Struct. (2011).
- [9] M. Briffaut, F. Benboudjema, Effects of early-age thermal behaviour on damage risks in massive concrete structures, J. Eur. J. Environ. Civ. Eng. (2012) 589–605.
- [10] M. Safiuddin, A. Kaish, C.-O. Woon, S. Raman, M. Safiuddin, A.B.M.A. Kaish, C.-O. Woon, S.N. Raman, Early-Age Cracking in Concrete: Causes, Consequences, Remedial Measures, and Recommendations, Appl. Sci. 8 (2018) 1730. doi:10.3390/app8101730.
- [11] P. Groth, H. Hedlund, Air cooling of concrete by means of embedded cooling pipes—Part II: Application in design, Mater. Struct. 31 (2006) 387–392. doi:10.1007/bf02480711.
- [12] Y. Yuan, Z.L. Wan, Prediction of cracking within early-age concrete due to thermal, drying and creep behavior, Cem. Concr. Res. 32 (2002) 1053–1059. doi:10.1016/S0008-8846(02)00743-3.
- [13] Z.P. Bazant, J.K. Kim, S.E. Jeon, Cohesive fracturing and stresses caused by hydration heat in massive concrete wall, J. Eng. Mech. 129 (2003) 21–30. doi:10.1061/(ASCE)0733-9399(2003)129:1(21).
- [14] Z. Najafi, K. Ahangari, The Prediction of Concrete Temperature during Curing Using Regression and Artificial Neural Network, J. Eng. 2013 (2013) 1–5. doi:10.1155/2013/946829.
- [15] E. Martinelli, E.A.B. Koenders, A. Caggiano, A numerical recipe for modelling hydration and heat flow in hardening concrete, Cem. Concr. Compos. 40 (2013)

- 48–58. doi:10.1016/j.cemconcomp.2013.04.004.
- [16] A.K. Schindler, K.J. Folliard, K. Schindler, A. and Folliard, Heat of hydration models for cementitious materials, *ACI Mater. J.* 102 (2005) 24–33. doi:10.1680/adcr.11.00007.
- [17] J.F. Unger, S. Eckardt, Multiscale Modeling of Concrete, *Arch. Comput. Methods Eng.* 18 (2011) 341–393. doi:10.1007/s11831-011-9063-8.
- [18] R.H. Bogue, *The chemistry of portland cement*, Reinhold Publishing Corporation, New York, 1947.
- [19] S. Ahmad, S.A. Alghamdi, S. Ahmad, S.A. Alghamdi, A Statistical Approach to Optimizing Concrete Mixture Design, *A Statistical Approach to Optimizing Concrete Mixture Design*, *Sci. World Journal*, *Sci. World J.* 2014, 2014 (2014) e561539. doi:10.1155/2014/561539, 10.1155/2014/561539.
- [20] A. Chaboki-Khiabani, M. Bastami, M. Baghbadrani, M. Kordi, Optimization of the Concrete Mix Proportions Centered on Performance after Exposure to High Temperature, *Adv. Mater. Res.* 268–270 (2011) 372–376. doi:10.4028/www.scientific.net/AMR.268-270.372.
- [21] X.S. Xie, D.J. Yan, Y.Z. Zheng, Optimization Design of High-Performance Concrete Based on Genetic Algorithm Toolbox of Matlab, *Adv. Mater. Res.* 250–253 (2011) 2672–2677. doi:10.4028/www.scientific.net/AMR.250-253.2672.
- [22] H. Mihashi, J.P. de B. Leite, State-of-the-Art Report on Control of Cracking in Early Age Concrete, *J. Adv. Concr. Technol.* 2 (2004) 141–154. doi:10.3151/jact.2.141.
- [23] A.C.I. Committee, *Report on Thermal and Volume Change Effects*, n.d.
- [24] A.S.M.A. Awal, I.A. Shehu, Evaluation of heat of hydration of concrete containing high volume palm oil fuel ash, *Fuel.* 105 (2013) 728–731. doi:10.1016/j.fuel.2012.10.020.
- [25] T. Kishi, T. Shimomura, K. M., Thermal crack control design of high performance concrete, in: *Int. Conf. “Concrete 2000”* Dundee, Scotland. London E&FN Spon, 1993.
- [26] D.J. Thomas, D.H. Jennings, *The science of concrete*, Northwestern University, 2014.
- [27] S. Mindess, J.F. Young, D. Darwin, *Concrete*, 2nd ed., Prentice Hall, Pearson Education, Inc., Upper Saddle River, NJ 07458, U.S.A., 2003.
- [28] R.H. Bogue, *The chemistry of Portland Cement*, Reinhold Publishing Corp, New York, 1947.
- [29] B.W. Lerch, R.H. Bogue, *Heat of hydration of portland cement pastes*, (1934).
- [30] *Concrete Manual*, 8th ed., United States Bureau of Reclamation, Water Resources Technical Publication, 1975.
- [31] K. Schindler, A. and Folliard, Heat of hydration models for cementitious materials, *AC I Mater. J.* 102-M04 (2005).

- [32] S. Mindess, J.F. Young, *Concrete*, Prentice-Hall Inc., 1981.
- [33] P. Termkhajornkit, R. Barbarulo, Modeling the coupled effects of temperature and fineness of Portland cement on the hydration kinetics in cement paste, *Cem. Concr. Res.* 42 (2012) 526–538. doi:10.1016/j.cemconres.2011.11.016.
- [34] F. Lin, C. Meyer, Hydration kinetics modeling of portland cement considering the effects of curing temperature and applied pressure, *Cem. Concr. Res.* 39 (2009) 255–265.
- [35] D.P. Bentz, C.J. Haecker, An argument for using coarse cements in high-performance concretes, *Cem. Concr. Res.* 29 (1999) 615–318.
- [36] American Concrete Institute, ACI207.2R, Report on Thermal and Volume Change Effects on Cracking of Mass Concrete, 2007.
- [37] Portland Cement Association, Portland cement, concrete, and heat of Hydration, *Concr. Technol. Today.* 18 (1997) 1–4.
- [38] L.E. Copeland, D.L. Kantro, G. Verbeck, Chemistry of hydration of Portland cement, *Natl. Bur. Stand. (U.S. Dep. Commer. I)* (1960) 429–465.
- [39] F. Lin, C. Meyer, Hydration kinetics modeling of Portland cement considering the effects of curing temperature and applied pressure, *Cem. Concr. Res.* 39 (2009) 255–265. doi:10.1016/j.cemconres.2009.01.014.
- [40] P. Siler, J. Kratky, N.D. Belie, Isothermal and solution calorimetry to assess the effect of superplasticizers and mineral admixtures on cement hydration isothermal and solution calorimetry to assess the effect of superplasticizers and mineral admixtures on cement hydration isothermal an, *J. Therm. Anal. Calorim.* 107 (2011).
- [41] I.K. Labarca, R.D. Foley, S.M. Cramer, Wisconsin Highway Research Program Effects of Ground Granulated Blast Furnace Slag in Portland Cement Concrete (PCC) - Expanded Study, (2007) 1–75.
- [42] P. Bamforth, in Situ Measurement of the Effect of Partial Portland Cement Replacement Using Either Fly Ash or Ground Granulated Blast-, *ICE Proc.* (1980) 777–800. <http://www.icevirtuallibrary.com/content/article/10.1680/iicep.1980.2377>.
- [43] B. Lothenbach, K. Scrivener, R.D. Hooton, Supplementary cementitious materials, *Cem. Concr. Res.* 41 (2011) 1244–1256. doi:10.1016/j.cemconres.2010.12.001.
- [44] National Ready Mixed Association (NRMCA), CIP 15 - Chemical Admixtures for Concrete, (2014) 1–2. doi:10.4103/0976-7800.66988.
- [45] W. Nocuń-Wczelik, P. Czapik, Use of calorimetry and other methods in the studies of water reducers and set retarders interaction with hydrating cement paste, *Constr. Build. Mater.* 38 (2013) 980–986. doi:10.1016/j.conbuildmat.2012.09.048.
- [46] ASTM C186- 05, Standard Test Method for Heat of Hydration of Hydraulic Cement, *Chem. Anal.* 95 (2005) 1–2. doi:10.1520/C0187-10.2.

- [47] RILEM Technical Committee 119-TCE, Avoidance of Thermal Cracking in Concrete At Early Ages, *Mater. Struct.* 30 (1998) 451–464. doi:10.1007/BF02524773.
- [48] P. Fjellström, Heat Loss Compensation for Semi-Adiabatic Calorimetric Tests, (n.d.) 1–22.
- [49] Thermometric AB, Handbook TAM Air Calorimeter, (2011) 63.
- [50] ASTM International, ASTM C1702 - 17 Standard Test Method for Measurement of Heat of Hydration of Hydraulic Cementitious Materials Using Isothermal Conduction Calorimetry, West Conshohocken, PA, 2017.
- [51] N.J. Carino, H.S. Lew, The Maturity Method: From Theory to Application, *Struct. 2001.* (2001) 1–19. doi:10.1061/40558(2001)17.
- [52] S.A. Wade, A.K. Schindler, R.W. Barnes, EVALUATION OF THE MATURITY METHOD TO, (2006).
- [53] C. Concrete, M. Cabinets, M. Rooms, A. Curing, T. Concrete, C. Test, H. Concrete, P.L. Strength, Standard Practice for Estimating Concrete Strength by the Maturity Method 1, (2011) 1–10. doi:10.1520/C1074-11.2.
- [54] V.M. Malhotra, N.J. Carino, TESTING, (2015).
- [55] D. Ye, Early-age concrete temperature and moisture relative to curing effectiveness and projected effects on selected aspects of slab behavior, (2008). <http://gradworks.umi.com/32/81/3281186.html>.
- [56] K. Folliard, M. Juenger, A. Schindler, J. Whigham, J. Meadows, FHWA/TX-08/0-4563-1 Prediction Model for Concrete Behavior., 7 (2008) 77.
- [57] K.A. Riding, J.L. Poole, A.K. Schindler, M.C.G. Juenger, K.J. Folliard, Evaluation of temperature prediction methods for mass concrete members, *ACI Mater. J.* 103 (2006) 357–365.
- [58] M. Cervera, R. Faria, J. Oliver, T. Prato, Numerical modelling of concrete curing, regarding hydration and temperature phenomena, *Reforma y Democr.* 80 (2002) 1511–1521. doi:10.1016/S0045-7949(02)00104-9.
- [59] B. Kuriakose, B.N. Rao, G.R. Dodagoudar, V. Venkatachalapathy, Modelling of heat of hydration for thick concrete constructions - A note, *J. Struct. Eng.* 42 (2015) 348–357.
- [60] D. Sundar, B. Umadevi, D.K. Alagarsamy, Multi Objective Genetic Algorithm for the optimized Resource usage and the Prioritization of the Constraints in the Software project planning, *Int. J. Comput. Appl.* 3 (2010) 1–4. doi:10.5120/718-1010.
- [61] D. Beasley, D.R. Bull, R.R. Martin, An Overview of Genetic Algorithms : Part 1, Fundamentals, *Univ. Comput.* 2 (1993) 1–16. doi:10.1017/CBO9781107415324.004.
- [62] E. Goldberg, david, Genetic algorithm in search, optimization and machine learning, Addison-Wesley Publishing Company. Inc., 1989.

- [63] H. Iba, C.C. Aranha, Introduction to genetic algorithms, 2012. doi:10.1007/978-3-642-27648-4_1.
- [64] N.M. Razali, J. Geraghty, Genetic algorithm performance with different selection strategies in solving TSP, Proc. World Congr. Eng. 2011. 2 (2011) 1134–1139. doi:10.1053/joms.2000.16615.
- [65] D.E. Goldberg, K. Deb, A Comparative Analysis of Selection Schemes Used in Genetic Algorithms, (1991) 69–93. doi:10.1016/B978-0-08-050684-5.50008-2.
- [66] C.R. Reeves, J.E. Rowe, A Guide to GA Theory, 2003.
- [67] B. Lassalle-Kaiser, S. Gul, J. Kern, V.K. Yachandra, J. Yano, In situ/Operando studies of electrocatalysts using hard X-ray spectroscopy, J. Electron Spectros. Relat. Phenomena. 221 (2017) 18–27. doi:10.1016/j.elspec.2017.05.001.
- [68] C.H. Lim, Y.S. Yoon, J.H. Kim, Genetic algorithm in mix proportioning of high-performance concrete, Cem. Concr. Res. 34 (2004) 409–420. doi:10.1016/j.cemconres.2003.08.018.
- [69] N. Soni, T. Kumar, Study of Various Crossover Operators in Genetic Algorithms, Int. J. Comput. Sci. Inf. Technol. 5 (2014) 7235–7238.
- [70] Y. Kaya, M. Uyar, R. Tek{\D{j}}n, A Novel Crossover Operator for Genetic Algorithms: Ring Crossover, (2011) 1–4. <http://arxiv.org/abs/1105.0355>.
- [71] J. Ackora-Prah, S.A. Gyamerah, P.S. Andam, A heuristic crossover for portfolio selection, Appl. Math. Sci. 8 (2014) 3215–3227. doi:10.12988/ams.2014.43203.
- [72] A.C. Koenig, KOENIG: A STUDY OF MUTATION METHODS FOR EVOLUTIONARY COMPUTING A Study of Mutation Methods for Evolutionary Algorithms CS 447 -Advanced Topics in Artificial Intelligence, (2002) 1–8. <https://pdfs.semanticscholar.org/6972/29e60758b411bcb7f4b0b2c2aeb54d2c9ba4.pdf>.
- [73] O. Abdoun, J. Abouchabaka, C. Tajani, Analyzing the Performance of Mutation Operators to Solve the Travelling Salesman Problem, (2012). <http://arxiv.org/abs/1203.3099>.
- [74] N. Soni, T. Kumar, Study of Various Mutation Operators in Genetic Algorithms, Int. J. Comput. Sci. Inf. Technol. 5 (2014) 4519–4521. doi:10.1016/j.elspec.2017.05.001.
- [75] R.L. Haupt, S.E. Haupt, a J. Wiley, Algorithms Practical Genetic Algorithms, 2004. doi:10.1198/jasa.2005.s45.
- [76] M.J. Simon, Concrete Mixture Optimization Using Statistical Methods, (2003) 168.
- [77] M.A. Jayaram, M.C. Nataraja, C.N. Ravikumar, Elitist genetic algorithm models: Optimization of high performance concrete mixes, Mater. Manuf. Process. 24 (2009) 225–229. doi:10.1080/10426910802612387.
- [78] T. Ji, T. Lin, X. Lin, A concrete mix proportion design algorithm based on artificial neural networks, Cem. Concr. Res. 36 (2006) 1399–1408.

doi:10.1016/j.cemconres.2006.01.009.

- [79] E. Ozbay, M. Gesoglu, E. Guneyisi, Transport properties based multi-objective mix proportioning optimization of high performance concretes, *Mater. Struct.* 44 (2010) 139–154. doi:10.1617/s11527-010-9615-7.
- [80] B. Ahmadi-Nedushan, An optimized instance based learning algorithm for estimation of compressive strength of concrete, *Eng. Appl. Artif. Intell.* 25 (2012) 1073–1081. doi:10.1016/j.engappai.2012.01.012.
- [81] W. Park, Genetic-algorithm-based mix proportion design method for recycled aggregate concrete, *Trans. Can. Soc. Mech. Eng.* 37 (2013) 345–354.
- [82] H. Rahmani, Packing degree optimization of arbitrary circle arrangements by genetic algorithm, *Granul. Matter.* 16 (2014) 751–760. doi:10.1007/s10035-014-0513-5.
- [83] X. Wang, K. Wang, P. Taylor, G. Morcou, Assessing particle packing based self-consolidating concrete mix design method, *Constr. Build. Mater.* 70 (2014) 439–452. doi:10.1016/j.conbuildmat.2014.08.002.
- [84] A.R. Marí, Numerical simulation of the segmental construction of three dimensional concrete frames, *Eng. Struct.* 22 (2000) 585–596. doi:10.1016/S0141-0296(99)00009-7.
- [85] H.G. Kwak, Y.J. Seo, C.M. Jung, Effects of the slab casting sequences and the drying shrinkage of concrete slabs on the short-term and long-term behavior of composite steel box girder bridges. Part 1, *Eng. Struct.* 22 (2000) 1453–1466. doi:10.1016/S0141-0296(99)00095-4.
- [86] L. Dezi, F. Gara, G. Leoni, Construction sequence modelling of continuous steel-concrete composite bridge decks, *Steel Compos. Struct.* 6 (2006) 123–138. doi:10.12989/scs.2006.6.2.123.
- [87] N. E-c, *Control of Cracking in Concrete*, (2006).
- [88] T. Carpark, S. Development, C.I.N. Situ, *CONCRETE IN SITU*, (2003) 218–242.
- [89] T.R. Naik, F. Asce, R.N. Kraus, M. Asce, R. Kumar, Influence of Types of Coarse Aggregates on the Coefficient of Thermal Expansion Influence of Types of Coarse Aggregates on the Coefficient of Thermal Expansion of Concrete, (2015). doi:10.1061/(ASCE)MT.1943-5533.0000198.
- [90] J. Charpin, T. Myers, A.D. Fitt, N. Fowkes, Y. Ballim, A.P. Patini, *PIPED WATER COOLING OF CONCRETE DAMS*, (n.d.) 69–85.
- [91] S. Qiang, Z. Xie, R. Zhong, A p-version embedded model for simulation of concrete temperature fields with cooling pipes, *Water Sci. Eng.* 8 (2015) 248–256. doi:10.1016/j.wse.2015.08.001.
- [92] Y. Hong, W. Chen, J. Lin, J. Gong, H. Cheng, Thermal field in water pipe cooling concrete hydrostructures simulated with singular boundary method, *Water Sci. Eng.* 10 (2017) 107–114. doi:10.1016/j.wse.2017.06.004.
- [93] Portland Cement Association, P.C. Association, Portland Cement, Concrete, and

- Heat of Hydration, Old Orchard Road Skokie, Illinois, 1997. <http://cement.org/tech/pdfs/pl972.pdf>.
- [94] J.L. Poole, Modeling Temperature Sensitivity and Heat Evolution of Concrete, The University of Texas at Austin, 2007.
- [95] Australian Standard, General purpose and blended cements, AS 3972, 2010.
- [96] M. Thomas, Optimizing the Use of Fly Ash in Concrete, Portl. Cem. Assoc. (2007) 24.
- [97] R. Siddique, D. Kaur, Properties of concrete containing ground granulated blast furnace slag (GGBFS) at elevated temperatures, *J. Adv. Res.* 3 (2012) 45–51. doi:10.1016/j.jare.2011.03.004.
- [98] N. Bouzoubaa, S. Foo, Use of fly ash and slag in concrete: A Best Practice Guide, 2004 <http://www.circainfo.ca/documents/UseofFAandSlaginConcrete-ICONPWGSCJan2005.pdf>.
- [99] Sika Australia, Safety Data Sheet, 2010.
- [100] M.C. Garci Juenger, H.M. Jennings, New insights into the effects of sugar on the hydration and microstructure of cement pastes, *Cem. Concr. Res.* 32 (2002) 393–399. doi:10.1016/S0008-8846(01)00689-5.
- [101] M. Bishop, A.R. Barron, Cement hydration inhibition with sucrose, tartaric acid, and lignosulfonate: Analytical and spectroscopic study, *Ind. Eng. Chem. Res.* 45 (2006) 7042–7049. doi:10.1021/ie060806t.
- [102] TA Instruments, TAM Assistant Software Getting Started Guide, 2012.
- [103] G. De Schutter, Finite element simulation of thermal cracking in massive hardening concrete elements using degree of hydration based material laws, *Comput. Struct.* 80 (2002) 2035–2042. doi:10.1016/S0045-7949(02)00270-5.
- [104] N.J. Carino, J.R. Clifton, NISTIR 5634 Prediction of Cracking in Reinforced Concrete Structures, *Fire Res.* (1995).
- [105] Y. Tian, X. Jin, N. Jin, Thermal cracking analysis of concrete with cement hydration model and equivalent age method, *Comput. Concr.* 11 (2013) 271–289. doi:10.12989/cac.2013.11.4.271.
- [106] K.A. Riding, J.L. Poole, A.K. Schindler, M.C.G. Juenger, K.J. Folliard, Temperature boundary condition models for concrete bridge members, *ACI Mater. J.* 104 (2007) 379–387. doi:10.14359/18827.
- [107] K. Van Breugel, Prediction of Temperature Development in Hardening Concrete, 1998.
- [108] G. De Schutter, L. Taerwe, Degree of hydration-based description of mechanical properties of early age concrete, *Mater. Struct.* 29 (1996) 335–344. doi:10.1007/BF02486341.
- [109] A. Naaman, F. Alkhairi, H. Hammoud, High Early Strength Fiber Reinforced Concrete, Mechanical Behavior of High Performance Concretes, Volume 6, Contract. (1993). <http://onlinepubs.trb.org/onlinepubs/shrp/SHRP-C-366.pdf>.

- [110] B. Klemczak, A. Knoppik-Wrobel, Early age thermal and shrinkage cracks in concrete structures, influence of curing conditions, *Arch. Civ. Mech. Eng.* 4 (2011) 47–58.
- [111] F.P. Incropera, D.P. DeWitt, *Introduction to heat transfer*, Wiley, New York, 1985.
- [112] L.T. Bergman, S.A. Lavine, P.F. Incropera, P.D. DeWitt, *Fundamentals of Heat and Mass Transfer*, John Wiley & Sons, Inc., New York, 2011.
- [113] L. Theodore, *Heat Transfer Applications for the Practicing Engineer*, 2011. doi:10.1002/9780470937228.
- [114] K. Van Breugel, S. Lokhorst, Stress-based crack criterion as a basis for prevention of through-cracks in concrete structures at early ages, ... RILEM Conf. (2003).
- [115] A.K. Schindler, Effect of Temperature and Curing on the Early Hydration of cementitious materials, *ACI Mater. J.* 101 (2004) 72–81.
- [116] H. Reinhardt, J. Blaauwendraad, J. Jongedijk, Temperature development in concrete structures taking account of state dependent properties, *Int. Conf. Concr. Early Ages.* (1982).
- [117] J.H. Emanuel, J.L. Hulse, No Prediction of the Thermal Expansion Coefficient of Concrete., *J. Am. Concr. Inst.* 74 (1977) 149–155.
- [118] Ashrae, *ASHRAE Handbook*, Atlanta, 1993.
- [119] R.D. Clear, L. Gartland, F.C. Winkelmann, An empirical correlation for the outside convective air-film coefficient for horizontal roofs, *Energy Build.* 35 (2003) 797–811. doi:10.1016/S0378-7788(02)00240-2.
- [120] G.S. WOJCIK, Effects of Atmospheric and Construction Conditions on Concrete Equivalent Ages, *Mater. J.* 101 (2004) 374–384.
- [121] Final Report 2001-06, (2001).
- [122] K. a Riding, *Early Age Concrete Thermal Stress Measurement and Modeling*, PhD Diss. (2007).
- [123] Comsol, *Comsol Multiphysics User's Guide, Equation-Based Model.* (2012) 803–879, *Equation-Based Modeling.* doi:10.1016/S0260-8774(99)00111-9.
- [124] K. a. Riding, J.L. Poole, A.K. Schindler, M.C.G. Juenger, K.J. Folliard, Statistical Determination of Cracking Probability for Mass Concrete, *ASCE J. Mater. Civ. Eng.* 26 (2013) 04014058. doi:10.1061/(ASCE)MT.1943-5533.0000947.
- [125] ACI207.2R-95, *Effect of Restraint, Volume Change, and Reinforcement on Cracking of Mass Concrete.*, 1995.
- [126] J.M. Raphael, Tensile strength of concrete, *ACI Mater. J.* 81 (1984) 158–165.
- [127] P. Bamforth, J. Shave, S. Denton, *DESIGN FOR EARLY AGE THERMAL CRACKING*, *Bridg. Des. to Eurocodes UK Implement.* (2007) 239–249. doi:10.1680/bdte.41509.239.

- [128] E.A. Abdun-Nur, F.A. Anderson, H.L. Boggs, D.A. Bonikowsky, R.A. Bradshaw, E.G.W. Bush, L.H. Diaz, T.P. Dolen, K.D. Hansen, G.R. Mass, A.T. McCarthy, J.E. Oliverson, R.F. Oury, J.M. Raphael, E.K. Schrader, S.B. Tatro, Effect of restraint, volume change, and reinforcement on cracking of mass concrete, *ACI Mater. J.* 87 (1990) 271–295.
- [129] A.M.M. Neville, J.J.J. Brooks, *Concrete Technology*, *Build. Environ.* 11 (2010) 442. doi:10.1016/0360-1323(76)90009-3.
- [130] M. Othuman, Modeling of transient heat transfer in foamed concrete slab, *J. Eng. Sci. Technol.* 8 (2013) 331–349.
- [131] K. Folliard, A. Schindler, P. Pesek, *ConcreteWorks V3 Training / User Manual ConcreteWorks Software (P2)*, (2017).
- [132] V.S. Patankar, *Numerical heat transfer and fluid flow*, McGraw-Hill Book Company, New York, 1980.
- [133] K.A. Riding, J.L. Poole, K.J. Folliard, M.C.G. Juenger, A.K. Schindler, Modeling hydration of cementitious systems, *ACI Mater. J.* 109 (2012) 225–234. doi:10.14359/51683709.
- [134] A.K. Schindler, *Concrete Hydration, Temperature Development, and Setting at Early- Ages*, The University of Texas at Austin, 2002.
- [135] B. Klemczak, A. Knoppik-wróbel, Early Age Thermal and Shrinkage Cracks in Concrete Structures – Influence of Curing Conditions, *c* (2011) 47–58.
- [136] S. Rajasekaran, Optimal mix for high performance concrete by evolution strategies combined with neural networks, *Indian J. Eng. Mater. Sci.* 13 (2006) 7–17.
- [137] D.P. Bentz, *EARLY-AGE CRACKING REVIEW: MECHANISMS , MATERIAL PROPERTIES , AND MITIGATION STRATEGIES*, (2009).
- [138] B.Y.J. Gajda, M. Vangeem, *Temperatures in Mass Concrete*, (2002) 59–62.
- [139] M.Y. Riad, S.N. Shoukry, E.M. Sosa, G.W. William, Concrete mix pouring sequence for uniform setting and curing of bridge decks, *Constr. Build. Mater.* 25 (2011) 1653–1662. doi:10.1016/j.conbuildmat.2010.10.006.
- [140] B. Sc, D. Ph, *ENGINEERING RESEARCa " The Thermal Expansion of*, (n.d.) 320–330.
- [141] H. Nguyen, T. Hoang, Numerical Simulation of Laminar Flow Through a Pipe using COMSOL Multiphysics, *Int. J. Sci. Eng. Res.* 8 (2017) 290–295. <http://www.ijser.org>.